Evaluation of Full Structural and Optimized Weld Overlays As Mitigation Strategies for Primary Water Stress Corrosion Cracking in Pressurized Water Reactors

Lee Fredette and Paul Scott

Battelle Columbus

April 2010

Disclaimer

ABSTRACT

The full structural weld overlay (FSWOL) and optimized weld overlay (OWOL) are being proposed by the nuclear power industry in the United States as mitigation strategies for dealing with primary water stress corrosion cracking (PWSCC) in dissimilar metal welds (DMWs) in the PWR fleet. Primary water stress corrosion cracking is a temperature-dependent phenomenon that attacks inconel-based dissimilar metal welds, specifically Inconel 82/182 welds. Previously, the FSWOL was used successfully to mitigate intergranular stress corrosion cracking (IGSCC) in BWRs. The scope and objective of the study described in this report was to investigate the effectiveness of the FSWOL as a mitigation strategy for PWSCC. OWOL is proposed for larger nozzles were FSWOL application times become excessive, exceeding the time available in a standard refueling outage. OWOL is investigated for these geometries. Of specific concern is the question of whether the technical basis for the FSWOL and OWOL as mitigation strategies for PWSCC is sufficient.

As a result of this study it was shown that the FSWOL is an effective method to reduce weld residual stresses at the pipe weld inside surface which can lead to PWSCC in DMWs in PWR piping systems. In addition to creating a more favorable weld residual stress state at the inside surface to mitigate PWSCC initiation and growth, the FSWOL is also beneficial from the standpoint of providing additional structural reinforcement and an additional leak barrier of a more resistant material to PWSCC (i.e., Alloy 52M). In addition, there is the potential side benefit that the FSWOL may provide a geometry more favorable for inspection.

It is important to note that changes in weld sequencing in the field from that which was analyzed can negate any claimed weld residual stress benefit predicted for the weld overlay. Several sensitivity studies were conducted to evaluate the effect of weld overlay weld sequencing on the resulting weld residual stress field. Some sequence changes evaluated created large changes in the resulting weld residual stress field. In designing a full structural weld overlay or an optimized weld overlay for a certain geometry it is crucial that the design that is evaluated and approved is the design that is actually created in the field.

Finally, the results for the geometries considered herein tend to indicate that the OWOL design is an effective mitigation strategy for dealing with PWSCC in PWRs. For the cases considered herein, i.e., the cold leg/RCP outlet nozzle geometry, the stresses post-OWOL application were at, or in some cases, below those for the post-FSWOL application. Note, it must be emphasized that this conclusion is based solely on our assessment of this one geometry, i.e., the cold leg/RCP outlet nozzle geometry considered herein. If other licensees chose to apply optimized weld overlays to other geometries, additional confirmatory analyses will be needed to confirm the effectiveness of the OWOL design for those applications.

Table of Contents

List of Figures

List of Tables

EXECUTIVE SUMMARY

With the recent occurrences of primary water stress corrosion cracking (PWSCC) at inconel-based dissimilar metal welds (DMWs), specifically Inconel 82/182 welds, in the nation's pressurized water reactors (PWRs), the commercial nuclear power industry has been proposing a number of mitigation strategies for dealing with the problem. The weld overlay (WOL) is one of those strategies. The full structural weld overlay (FSWOL) has been successfully used in the past as a mitigation strategy for intergranular stress corrosion cracking (IGSCC) in the BWR fleet. Prior to its use in the BWRs, it was evaluated extensively by the industry through the Electric Power Research Institute (EPRI) and the NRC at Battelle. The scope and objective of the study described in this report was to investigate the effectiveness of weld overlays as a mitigation strategy for PWSCC in the PWRs, thus addressing the question as to whether the technical basis for weld overlays (both full structural and optimized) as a mitigation strategy for PWSCC is sufficient. As part of the sensitivity studies conducted during this effort, the effect of the overlay thickness on the effectiveness of a weld overlay was investigated. By considering thinner overlays in comparison to FSWOLs, some assessment of the industry-proposed optimized weld overlays (OWOL) can be made. As part of this effort an evaluation of the OWOL was made for the two larger diameter, cold leg geometries, i.e., the cold leg/reactor pressure vessel (RPV) nozzle geometry for a stainless steel primary piping system and the cold leg/reactor coolant pump (RCP) outlet nozzle geometry incorporated in a ferritic primary piping system.

Four dissimilar metal weld pipe/nozzle geometries were considered as part of this effort: (1) two large diameter cold-leg sized components; the reactor pressure vessel (RPV) nozzle weld and the reactor coolant pump (RCP) outlet nozzle weld, (2) a medium diameter pressurizer surge nozzle weld, and (3) a small diameter pressurizer safety nozzle weld. In each case the weld residual stresses, both before and after the application of the WOL, were estimated in order to evaluate the effectiveness of the WOL as a mitigation strategy for PWSCC in PWRs. As part of these assessments, cracks were introduced into the weld butter region in order to assess how the WOL affects the crack openings and stress intensity factors, and ultimately the crack growth of a crack in this region.

In this study 2-D, axi-symmetric weld residual stress analyses using the ABAQUS finite element code were conducted. In modeling the welds, the application of the butter to the ferritic material was modeled along with the post weld heat treatment (PWHT) of the butter material. In addition, the weld root passes at the inside surface were ground out and re-welded as part of the analyses to simulate this common practice in the field. This full-circumference grind out/re-welding resulted in a residual stress field similar to that for a full 360 degree inside surface repair weld. For the two cold leg geometries considered, more extensive repair welds, 25 and 50 percent of the wall thickness in depth were also considered.

Both hoop and axial weld residual stresses were estimated. However, the primary focus of this study was on the axial stresses which cause circumferential crack initiation and growth. The hoop stresses were thought to be of less concern since the axial cracks which are driven by the hoop stresses are thought to be limited in length to the width of the circumferential girth weld in seamless pipe typically used in nuclear power plants. Due to their limited length, any axial cracks which may break through the wall thickness should leak and not rupture. Even so, the hoop stress results are of interest. Contrary to the axial stress results where there are typically significant areas of compression through the wall thickness, the hoop stress results indicate that the conditions may exist (before applying the WOL) for an axial crack to grow completely through the wall thickness, i.e., the hoop stresses were tensile thought the entire wall thickness. This finding is supported by field experience, e.g., the axial through wall crack growth at V. C. Summer. The good news is that the FSWOL significantly reduced these hoop stresses; see Figure 59 for

the cold leg/RCP outlet nozzle geometry. This FSWOL-induced compressive stress field should mitigate any possibility of axial through-wall crack growth.

The axial weld residual stress results were plotted both through the thickness and along the length of the pipe (spanning the weld) on the inside surface. In examining the axial stress results for the four geometries considered, one sees some similarity in the results. One sees high tensile stresses at the inside surface of the dissimilar metal weld which tend to be mitigated by the presence of the secondary stainless steel weld if one is in close proximity to the DMW. For example, the surge nozzle inside surface axial stresses after fabricating the Inconel dissimilar metal weld, which joins the ferritic nozzle to the stainless steel safe end, are in the range of 550 MPa (80 ksi) tensile. However, after fabricating the secondary stainless steel weld, joining the stainless steel safe end to the stainless steel pipe, the axial stress at the inside surface drops to 140 MPa (20 ksi) tensile. The application of the FSWOL in turn reduces these stresses to near zero at this location, see Figure 23. A similar set of results are evident for the safety nozzle (Figure 36) and the cold leg/RPV nozzle (Figure 47).

In addition to enhancing the inside surface residual stress field, a FSWOL also adds an element of structural reinforcement to the DMW. Prior full-scale pipe experiments conducted at Battelle for the NRC for which through-wall cracked pipe sections were repaired with weld overlays demonstrated this contention. Furthermore, the addition of the Alloy 52M material over top the DMW adds a layer of crack resistant material (i.e., resistant to PWSCC) to the pressure boundary. In addition, the overlay may enhance the quality of the ultrasonic inspection by providing a flatter, more conducive to inspection surface for the ultrasonic inspections.

A series of sensitivity analyses were conducted. As part of these analyses the effect of the FSWOL weld sequence (left to right versus right to left), the effect of the secondary stainless steel safe end weld, the effect of overlay thickness, and the effect of the ID repair depth were considered. The major findings from these sensitivity analyses were:

- The effect of weld sequencing, i.e., left-to-right versus right-to-left weld deposition had a minimal effect on the resultant weld residual stresses (Figure 69 and Figure 70). However, the resultant weld residual stresses for the case where two weld heads were used (Figure 73 and Figure 74) were higher than when a single head was used, as is typically the case.
- The secondary stainless steel weld had a significant effect on the axial weld residual stresses at the DMW. The secondary stainless steel weld tends to add an element of radial constraint to the adjacent dissimilar metal weld which reduces the axial stresses on the inside surface of the dissimilar metal weld. (Note, the hoop stresses remain tensile through much of the wall thickness, see Figure 25.) In fact, for the safety nozzle geometry considered, the FSWOL was found to be of limited benefit from a weld residual stress perspective since the presence of the secondary stainless steel weld for this small diameter safety nozzle geometry created a situation where the inside surface axial stresses were already compressive throughout the region of the dissimilar metal weld before the application of the FSWOL (see Figure 36). However, in those cases where there was no secondary stainless steel weld, such as the hot leg geometry at V. C. Summer, or where the secondary stainless steel weld was not in close proximity to the DMW, such as the cold leg/RCP outlet nozzle weld evaluated herein, the sensitivity analyses conducted as part of this effort indicated that the FSWOL would cause the DMW residual stresses to be as compressive as were the post-FSWOL stresses for those cases where there was a secondary stainless steel weld in close proximity to the DMW. As such, while the FSWOL is still effective, it is of most benefit in those cases where no secondary weld existed (e.g., for the V. C. Summer hot leg geometry) in that the pre-FSWOL stress state was already lower, i.e., compressive or less tensile, for the case where there is a secondary stainless steel weld in close proximity.
- In looking at the results for the repair size sensitivity analyses, it was found that peak stresses were comparable for each of the repair sizes considered, i.e., 0, 25, and 50 percent of the wall thickness. However, the extent of the affected area was much more pronounced for the deeper

repairs. For the deeper repairs, the axial extent of the tensile stresses along the ID surface (Figure 106) and the through thickness extent of those stresses (remain tensile for more of the wall thickness, see Figure 107) were both much more pronounced.

- The effect of overlay thickness was also considered. For the surge nozzle geometry considered the number of weld overlay passes had a minimal effect on the through thickness axial stresses near the weld centerline, see Figure 77. There was some effect on the ID axial stresses at the butter/ferritic steel interface, i.e., more layers of weld overlay resulted in a greater reduction in stress, see Figure 78, but that effect tended to saturate after about 3 layers of overlay. For the hoop stress case, Figure 80 and Figure 81, the effect was more pronounced with each successive layer further reducing the stresses. For the cold leg/RPV nozzle, there was a similar effect as found for the surge nozzle in that both the ID stress along the length of the nozzle as well as the through-thickness stresses near the weld centerline tended to reach a point of saturation, where further layers of overlay resulted in a minimal change in stress, after about half the layers of the FSWOL were deposited, see Figure 91and Figure 92. For the cold leg/RCP outlet nozzle geometry, this saturation effect was even more pronounced. For this geometry, the OWOL induced axial stresses were even more compressive in the vicinity of the DMW than they were for the FSWOL case, see Figure 95.

It is important to note that changes in weld sequencing in the field from that which was analyzed can negate any claimed weld residual stress benefit predicted for the weld overlay. Several sensitivity studies were conducted to evaluate the effect of weld overlay weld sequencing on the resulting weld residual stress field. Some sequence changes evaluated created large changes in the resulting weld residual stress field. In designing a full structural weld overlay or an optimized weld overlay for a certain geometry it is crucial that the design that is evaluated and approved is the design that is actually created in the field.

The results for the analyses where circumferential cracks were introduced were also consistent for the geometries considered. In each case the stress intensity factors (K) after applying the FSWOL were less than what they would have been if no FSWOL had been applied. Contrast this to what was found in a prior study on the mechanical stress improvement process (MSIP), where the results demonstrated that if a deep crack (i.e., greater than approximately 60 percent of the wall thickness) existed in the weld prior to the application of the MSIP, the MSIP made matters worse. For the case of these pre-existing cracks, the MSIP increased the stress intensity factors (K), such that the time required for the circumferential crack to grow through the remaining wall thickness of the treated weld (post-MSIP) is very short (estimated to be on the order of a few years or less). Conversely, for the untreated cases (no MSIP applied), the time required to grow these 75 percent deep circumferential cracks through the remaining wall thickness was estimated to be on the order decades or longer.

This finding that the FSWOL improves the residual stress field, even for the case of very deep pre-existing cracks (> ~60 percent of the wall thickness), lends credence to the lack of a requirement for a pre-overlay through thickness examination using ultrasonics in the pertinent ASME Code Cases (N-504-4 and N-740-2). The only pre-overlay inspections required are surface examinations using liquid penetrant. (This is in contrast to inspection requirements for MSIP in Code Case N-770 which does stipulate a through-thickness examination prior to implementing a MSIP in almost all cases. Code Case N-770 does grant an exception to this pre-MSIP inspection for the cold leg/reactor pressure vessel welds.) The one concern with the lack of a requirement for a pre-overlay inspection is that pre-existing cracks may be more difficult to detect after the application of the overlay due to the fact that the compressive stresses caused by the overlay may force the crack faces to close upon themselves, therefore reducing their ultrasonic specular and tip responses. This is a similar concern to that previously expressed for the MSIP. Prior NDE studies have shown that crack responses that were evident by ultrasonic testing prior to MSIP were significantly reduced, and in some cases, not detectable, after MSIP. The question then becomes will the compressive stresses caused by the FSWOL affect the NDE response in the same manner. In the coming months a series of FSWOL/NDE mockup studies will be conducted during which this issue will

be examined. One potential advantage that the FSWOL may have in this regard is that the post-overlay surface geometry may enhance the quality of the ultrasonic inspection.

In conclusion, based on the evaluations conducted, the FSWOL appears to be an effective method to reduce inside surface weld residual tension stresses which can lead to PWSCC in dissimilar metal welds in PWR piping systems. The process was found to be most beneficial for the larger diameter cold leg/RCP outlet nozzle geometry considered where there was no pre-existing benefit from the secondary stainless steel safe end weld. Also, the process was found to be more beneficial for the intermediate diameter pressurizer surge line nozzle than the smaller diameter safety nozzle geometry considered. For the safety nozzle geometry considered, the FSWOL was found to be of limited benefit from a weld residual stress perspective since the presence of the secondary stainless steel weld for the small diameter safety nozzle geometry created a situation where the inside surface axial stresses were already compressive throughout the region of the dissimilar metal weld before the application of the FSWOL. Note, even though the weld overlay provided limited benefit to this safety nozzle geometry from a stress reduction perspective, it was still beneficial since it adds additional structural reinforcement and additional layers of crack resistant material (Alloy 52M) over top the DMW. In addition, it was found that if a deep crack were present prior to the application of the FSWOL, the overlay would act to lower the stress intensity factor of that crack, thus increasing the time required for that crack to potentially grow through the remaining wall thickness.

Finally, the results for the geometries considered herein tend to indicate that the OWOL design can be an effective mitigation strategy for dealing with PWSCC in PWRs. For the cases considered herein, i.e., the cold leg/RCP outlet nozzle geometry, the stresses post-OWOL application were at, or in some cases, below those for the post-FSWOL application, see Figure 95 and Figure 96. Note, it must be emphasized that this conclusion is based solely on our assessment of this one geometry, i.e., the cold leg/RCP outlet nozzle geometry considered herein. If other licensees chose to apply optimized weld overlays to other geometries, additional confirmatory analyses will be needed to assess the effectiveness of the OWOL design for those applications.

1. INTRODUCTION

With the occurrence of primary water stress corrosion cracking (PWSCC) in the nation's pressurized water reactors (PWRs), the commercial nuclear power industry has been proposing a number of mitigation strategies for dealing with the problem. One of those strategies is the the application of weld overlays that were successfully used in the past in mitigating intergranular stress corrosion cracking (IGSCC) in the boiling water reactor (BWR) fleet. Primary water stress corrosion cracking is a temperature dependent degradation mechanism that attacks dissimilar metal welds (DMWs) fabricated from Inconel 82/182 weld metal. The driving force behind the initiation and growth of these cracks is residual stress caused by the welding process. Weld overlays mitigate PWSCC by introducing a compressive residual stress field on the inside wetted-surface of the dissimilar metal nozzle/pipe weld. The scope and objective of this study was to investigate the effectiveness of weld overlays (both full structural [FSWOL] and optimized [OWOL]) as a mitigation strategy for PWSCC. Of specific concern is the question as to whether the technical basis for the both the FSWOL and OWOL as a mitigation strategy for PWSCC is sufficient.

As part of this effort the effectiveness of the FSWOL and OWOL at mitigating the detrimental effects of PWSCC in LBB systems was investigated. While this report focuses on weld overlays, there is a separate report prepared to address the effectiveness of the mechanical stress improvement process (MSIP) as a mitigation strategy [1]. Ultimately, the Battelle efforts examining these mitigation strategies will be coupled with ongoing work at Pacific Northwest National Laboratories (PNNL) focusing on non-destructive testing of DMWs and in-house work at the NRC studying the possible benefits of modifying the environment as a mitigation strategy, along with the NRC's xLPR (eXtremely Low Probability of Rupture) initiative, to develop a comprehensive strategy for addressing PWSCC in LBB systems in the nation's PWR fleet.

Note, the main focus of this report is to address the effectiveness of the FSWOL, OWOL designs were also of interest to the NRC as more and more applications for using OWOLs are expected to be forthcoming. Optimized weld overlays (OWOL), a subset of the FSWOL, have been proposed for larger geometries (hot and cold leg nozzles) where FSWOL application becomes too time consuming for a typical refueling outage. The effectiveness of OWOL as a mitigating strategy for these geometries was studied for a reactor coolant pump outlet nozzle (RCP) and for a cold leg reactor pressure vessel (RPV) nozzle geometry. The effect of reduced thickness overlays on the smaller pressurizer nozzles was also examined in sensitivity studies for those geometries.

2. DISCUSSION OF THE WELD OVERLAY PROCESS

The FSWOL and mechanical stress improvement process (MSIP) have been used for many years to mitigate IGSCC found in boiling water reactors (BWRs) which have austenitic stainless steel piping and welds. Whereas the effectiveness of the MSIP is solely dependent on altering the inside surface residual stress field as a mitigation strategy for dealing with stress corrosion cracking, the application of the FSWOL offers other potential benefits. In addition to creating a more favorable weld residual stress field, the FSWOL also provides additional structural reinforcement and an additional layer of crack resistant material, i.e., Inconel 52M, to the pressure boundary. In this regard, the thought being is that if a crack were to grow and penetrate the original pipe weld outer surface, it would stop growing once it reached the more resistant (i.e., resistant to PWSCC growth) Inconel 52M overlay material.

The FSWOL method has been the subject of extensive research in the past as documented in a number of Electric Power Research Institute (EPRI) reports referenced in the non-propritary version of MRP-169 (Technical Basis for Preemptive Weld Overlays for Alloy 82/182 Butt Welds in PWRs – MRP-169) [2]. Much of this research focused on the effectiveness of a weld overlay at mitigating the IGSCC concern in BWRs in the 1980's. In one of the referenced reports [3], large diameter (28-inch diameter) Type 316 stainless steel pipes that contained machined notches in the weld region on the inside diameter of the pipe were repaired with a weld overlay and tested in a boiling magnesium chloride solution to demonstrate the effectiveness of the overlay at creating a compressive residual stress field at the tip of the notch. Destructive metallographic examination of the tips of moderately deep circumferential notches that were exposed to the chloride solution, both prior to and after the application of a weld overlay, indicated that extensive cracking at the tip of the notch occurred for the unrepaired case while no cracking was observed for the repaired case.

In addition to these studies sponsored by the industry through EPRI, which demonstrated the effectiveness of a FSWOL to create a compressive weld residual stress field on the inside pipe surface, Battelle conducted a number of full-scale weld overlay repaired pipe experiments as part of the Degraded Piping Program [4] for the US NRC. This Battelle/NRC work demonstrated that a FSWOL provides significant structural reinforcement to a cracked pipe section.

Figure 1 shows the schematic of the application of the FSWOL on the surge nozzle geometry evaluated in this study. The nozzle on the left is shown prior to the application of the FSWOL and the nozzle on the right shows the profile after the weld overlay application.

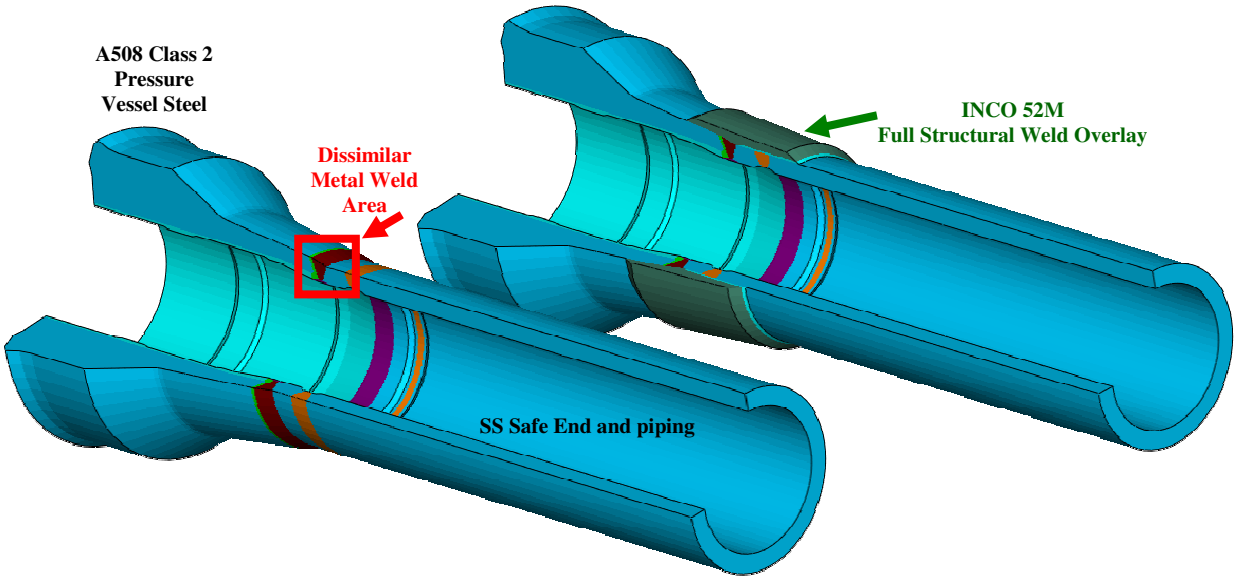

Figure 1 Schematic of a FSWOL applied to a surge nozzle geometry

The minimum acceptable FSWOL thickness is equal to 1/3 the original pipe wall thickness as specified in MRP-169 [2] and ASME Boiler and Pressure Vessel Code Case N-504-4 [5]. The minimum length is $0.75\sqrt{(Rt)}$ on either side of the dissimilar metal weld to be treated, where R is the outer radius of the item and t is the nominal thickness of the item. The total minimum length of the FSWOL is therefore $1.50\sqrt{(Rt)}$ plus the length of the dissimilar metal weld to be treated. The total length of the FSWOL used for the surge nozzle geometry in this study was 10.5".

Optimized weld overlays (OWOL), a subset of the FSWOL, have been proposed for larger geometries (hot and cold leg nozzles) where FSWOL application becomes too time consuming for a typical refueling outage. The optimized weld overlay thickness is less than that of a full structural weld overlay in order allow completion in the time available in a typical refueling outage for the larger geometries. The required minimum axial length of the OWOL is defined in ASME Code Case N-754 [6] and is the same as that required for a FSWOL. The code case also says that the thickness must be sufficient to provide compressive residual stresses to preclude SCC growth. Industry has proposed that an OWOL design is sufficient if it reduces tensile stresses in the dissimilar metal weld area to less than 69MPa (10ksi) with operating temperature and loads applied. Each OWOL must be designed for a specific geometry and application and must be evaluated on a case-by-case basis to prove that the overlay is sufficient to mitigate the possibility of PWSCC.

3. TECHNICAL APPROACH

Two-dimensional axi-symmetric models were used to calculate the weld residual stresses to evaluate the effectiveness of a FSWOL and the behavior of postulated cracks in the treated weld. The use of axi-symmetric models allowed for finer mesh refinement and computational efficiency in running the multiple load cases and sensitivity studies that were conducted for each geometry.

Early evaluations of the FSWOL process have been conducted using physical test specimens and axi-symmetric finite element models [Refs. 2 and 3]. Figure 2 shows the typical mesh density used in the axi-symmetric weld residual stress development model.

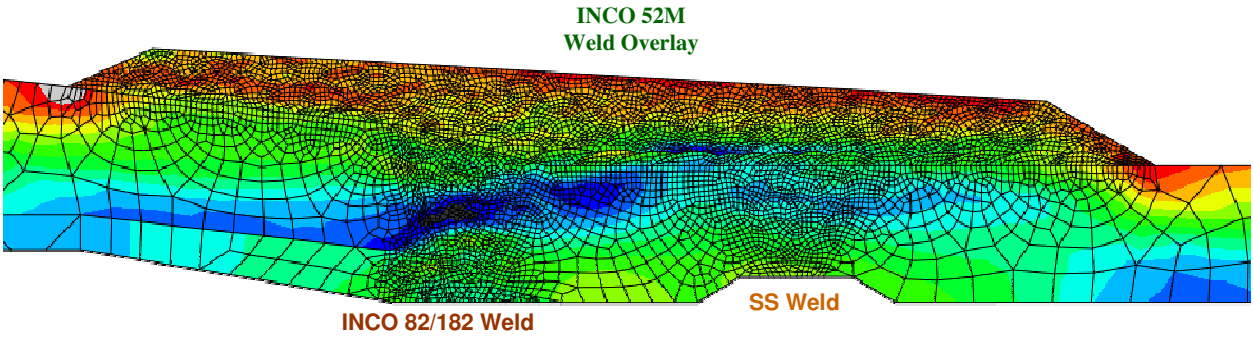

Figure 2 Typical Mesh Density used in Two-Dimensional Axi-symmetric Analyses

3.1 Material Data

The material properties used for the thermal and structural analysis for the Inconel 82/182 weld metal, the A508 Grade 2 steel nozzle material, and the Type 300 series stainless steels are shown in Tables 1 to 4. Figure 3 through Figure 6 illustrate the temperature dependent elastic plastic properties for these materials. The ABAQUS isotropic material hardening laws were followed using the material true stress-strain data presented here. The tensile properties for Inconel 182 were developed in a prior program by Oak Ridge National Laboratory (ORNL). The elastic-plastic properties for the A508 Grade 2 steel were obtained from the literature, and the stainless steel properties were developed from prior work done at Battelle. It is important to note that stress relieved and annealed weld material must be used to develop elastic-plastic tensile properties of the weld material. The welding simulation process subsequently creates work hardening of the material. Finally, Table 5 shows creep properties used to model stress relaxation during the post weld heat treatment.

Inconel 82/182 properties were used in lieu of Alloy 52 properties for the weld overlay material in all of the analyses presented in this report. When this work began, no data for Alloy 52 were available. Since that time Alloy 52 data have been developed although the differences between the new Alloy 52 data and the existing Alloy 82/182 data were found to be minor and the effect on the resultant weld residual stresses were thought to be small. As such, the previously existing Alloy 82/182 data were used throughout.

Table 1 Material Properties for Inconel 182 Weld Material

T	C_p	k	E	ν	σ_y	α
°F	BTU/lbm-F	BTU/sec-inch-F	ksi		ksi	10^{-6}/°F
70	0.095	0.00013	22674	0.3	38.5	6.50
200	0.110	0.000145	22023	0.3	36.2	6.73
400	0.120	0.000162	21022	0.3	33.5	7.09
600	0.125	0.000185	20021	0.3	30.0	7.44
800	0.130	0.000206	19051	0.3	28.3	7.62
1000	0.135	0.000226	18081	0.3	26.6	7.80
1200	0.140	0.000247	17987	0.3	26.2	8.10
1400	0.150	0.000273	17893	0.3	25.7	8.40
1600	0.160	0.000298	15621	0.3	19.0	8.70
1800	0.165	0.000324	13350	0.3	12.1	9.00
2000	0.170	0.000354	10000	0.3	3.70	9.20
2550	0.170	0.000354	200	0.3	0.40	9.20

T = Temperature
C_p = Specific heat
k = Conductivity
E = Elastic Modulus
ν = Poisson's constant
σ_y = Yield stress
α = thermal expansion

Table 2 Temperature Dependent Material Properties for A508 Class 2

T	C_p	T	k	T	E	ν	σ_y	α
°F	BTU/lbm-F	°F	BTU/sec-inch-F	°F	ksi		ksi	10^{-6}/°F
70	0.11	32	0.000694	71.6	30784	0.3	54.5	7.67
122	0.116	212	0.00067	600	28807	0.3	43.8	7.67
302	0.124	392	0.000647	1000	25633	0.3	29.5	8.33
392	0.127	572	0.000617	1400	14540	0.3	9.78	8.61
482	0.133	752	0.000571	1800	10243	0.3	2.78	8.89
572	0.137	932	0.000527	2732	203	0.3	0.44	8.89
662	0.143	1112	0.000476					
842	0.158	1292	0.000425					
1022	0.179	1472	0.000348					
1202	0.202	1832	0.000364					
1292	0.342	2192	0.000397					
1382	0.227							
1562	0.215							
1832	0.202							
2192	0.201							

T = Temperature
C_p = Specific heat
k= Conductivity
E = Elastic Modulus
ν = Poisson's constant
σ_y = Yield stress
α = thermal expansion

Table 3 Temperature Dependent Material Properties for Type 316 Stainless Steel and Type 309 Stainless Steel Weld Materials

T	C_p	T	k	T	E	ν	σ_y	α
°F	BTU/lbm-F	°F	BTU/sec-inch-F	°F	ksi		ksi	10^{-6}/°F
74	0.1079	70	0.000173	75	28400	0.3	38.0	8.09
165	0.1132	200	0.000186	300	27500	0.3	30.0	8.77
191	0.1143	400	0.000207	550	25950	0.3	23.4	9.33
400	0.1229	623	0.000231	700	24900	0.3	23.0	9.57
603	0.1291	800	0.000248	900	23500	0.3	22.0	9.84
794	0.132	1011	0.000269	1100	22200	0.3	20.5	10.09
1020	0.136	1195	0.000288	1300	20820	0.3	20.0	10.21
1204	0.1398	1391	0.000308	1500	19100	0.3	17.0	10.43
1410	0.145	1583	0.000327	1652	16900	0.3	14.1	10.60
1595	0.1505	1783	0.000348	1832	14500	0.3	8.46	10.70
1784	0.1556	1996	0.000369	2012	14500.	0.3	3.77	10.90
1996	0.1622			2732	203	0.3	0.44	11.20

T = Temperature
C_p = Specific heat
k= Conductivity
E = Elastic Modulus
ν = Poisson's constant
σ_y = Yield stress
α = thermal expansion

Table 4 Temperature Dependent Material Properties for Type 304 Stainless Steel

\

T	C_p	T	k	T	E	ν	σ_y	α
°F	BTU/lbm-F	°F	BTU/sec-inch-F	°F	ksi		ksi	10^{-6}/°F
74	0.1079	70	0.000173	75	28400	0.3	36.9	8.09
165	0.1132	200	0.000186	300	27500	0.3	27.7	8.77
191	0.1143	400	0.000207	550	25950	0.3	23.2	9.33
400	0.1229	623	0.000231	700	24900	0.3	21.8	9.57
603	0.1291	800	0.000248	900	23500	0.3	19.9	9.84
794	0.132	1011	0.000269	1100	22200	0.3	18.1	10.09
1020	0.136	1195	0.000288	1300	20820	0.3	16.2	10.21
1204	0.1398	1391	0.000308	1500	19100	0.3	11.4	10.43
1410	0.145	1583	0.000327	1652	16900	0.3	10.1	10.60
1595	0.1505	1783	0.000348	1832	14500	0.3	8.46	10.70
1784	0.1556	1996	0.000369	2012	14500	0.3	3.77	10.90
1996	0.1622			2732	203	0.3	0.44	11.20

T = Temperature
C_p = Specific heat
k= Conductivity
E = Elastic Modulus

ν = Poisson's constant
σ_y = Yield stress
α = thermal expansion

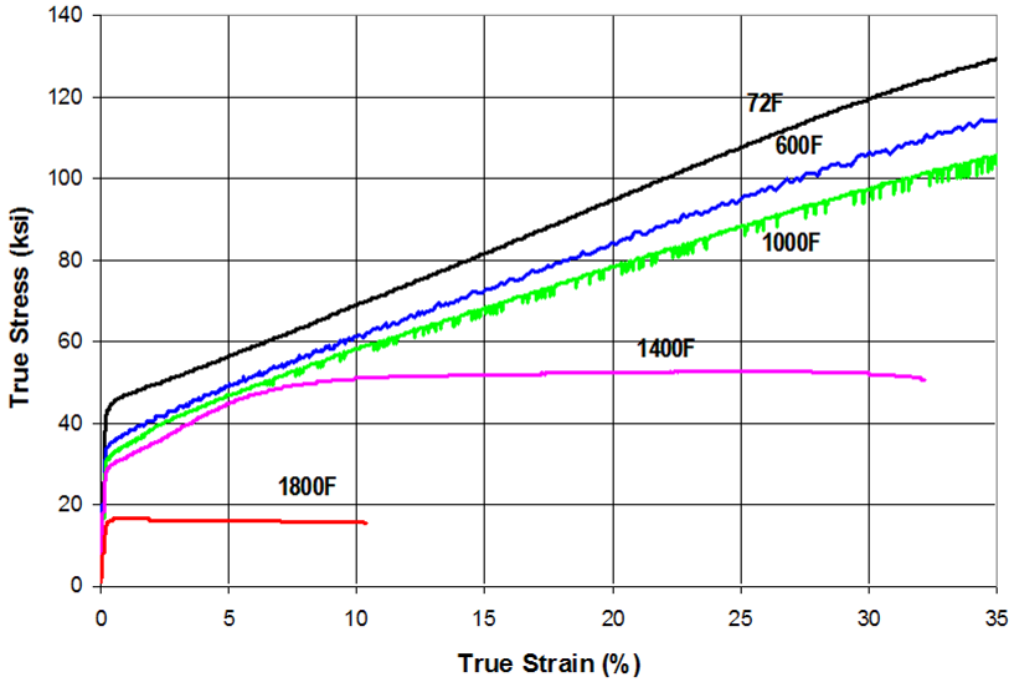

Figure 3 Temperature Dependent True Stress-Strain Curves of Inconel 182 Tested by Oak Ridge National Laboratories (ORNL)

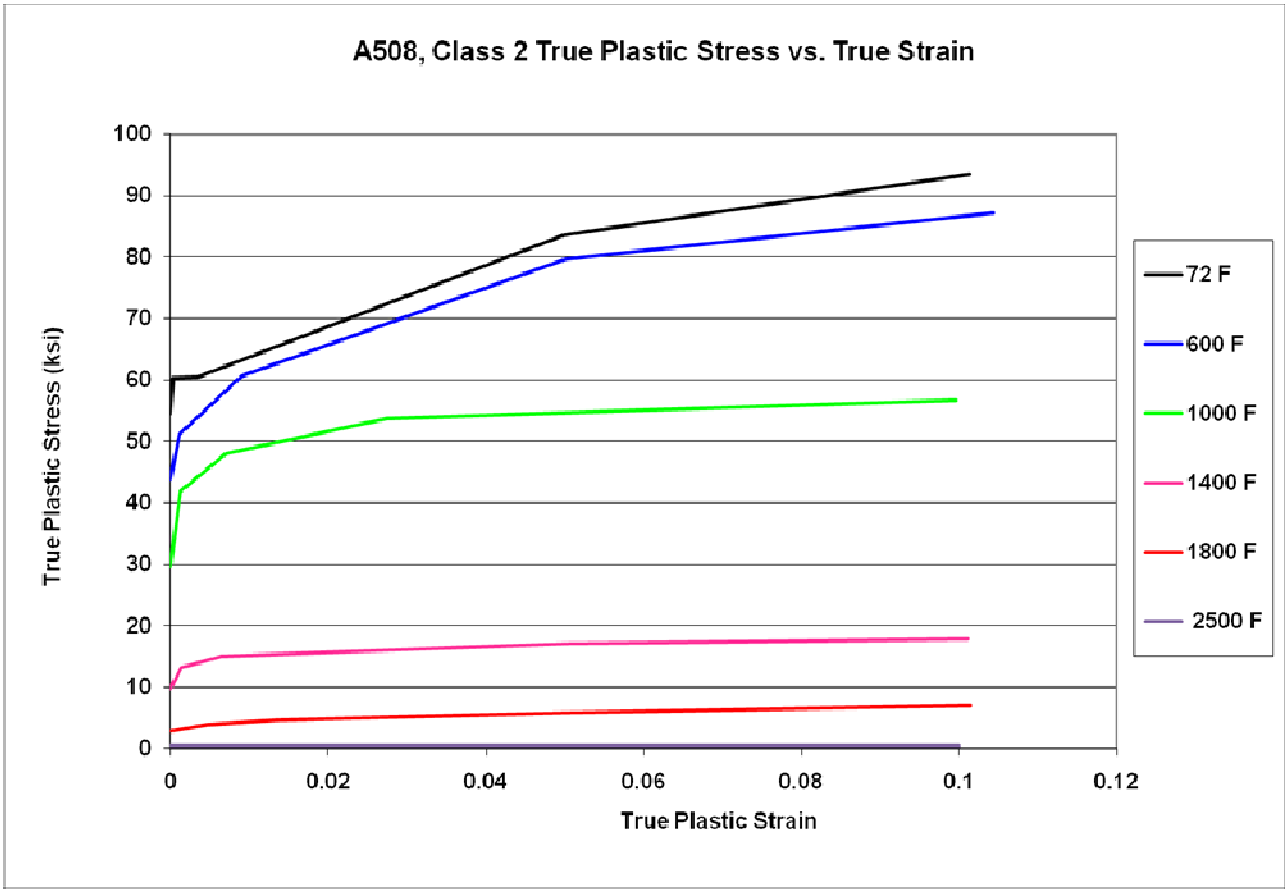

Figure 4 Temperature Dependent True Stress-Strain Curves of A508 Class 2

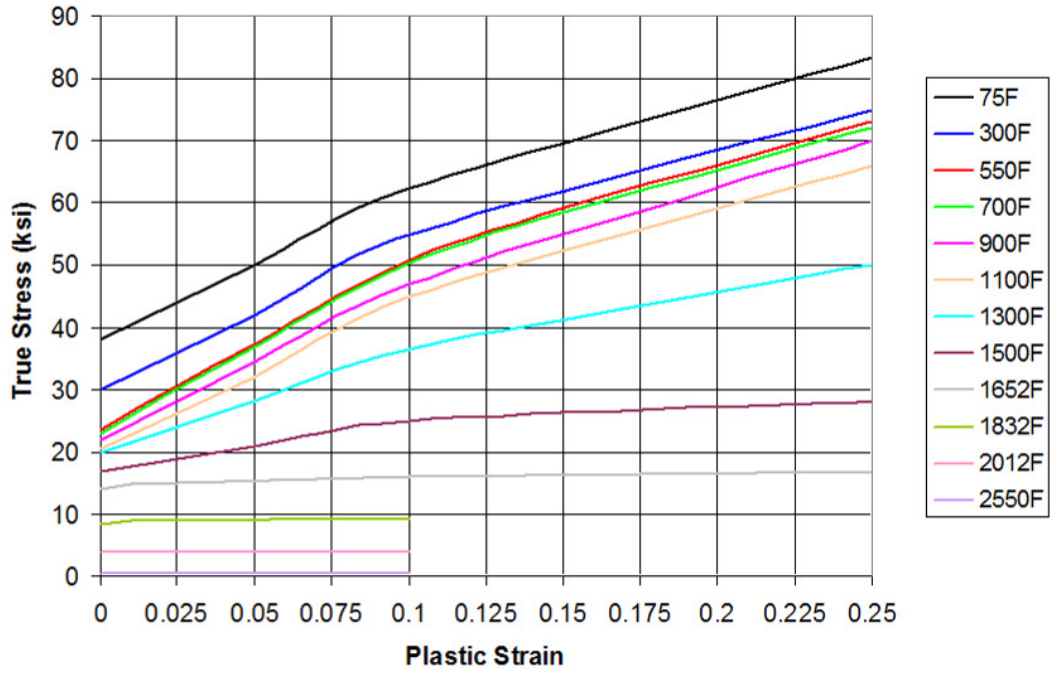

Figure 5 Temperature Dependent True Stress-Strain Curves of Type 316 Stainless Steel and Type 309 Stainless Steel Weld Materials

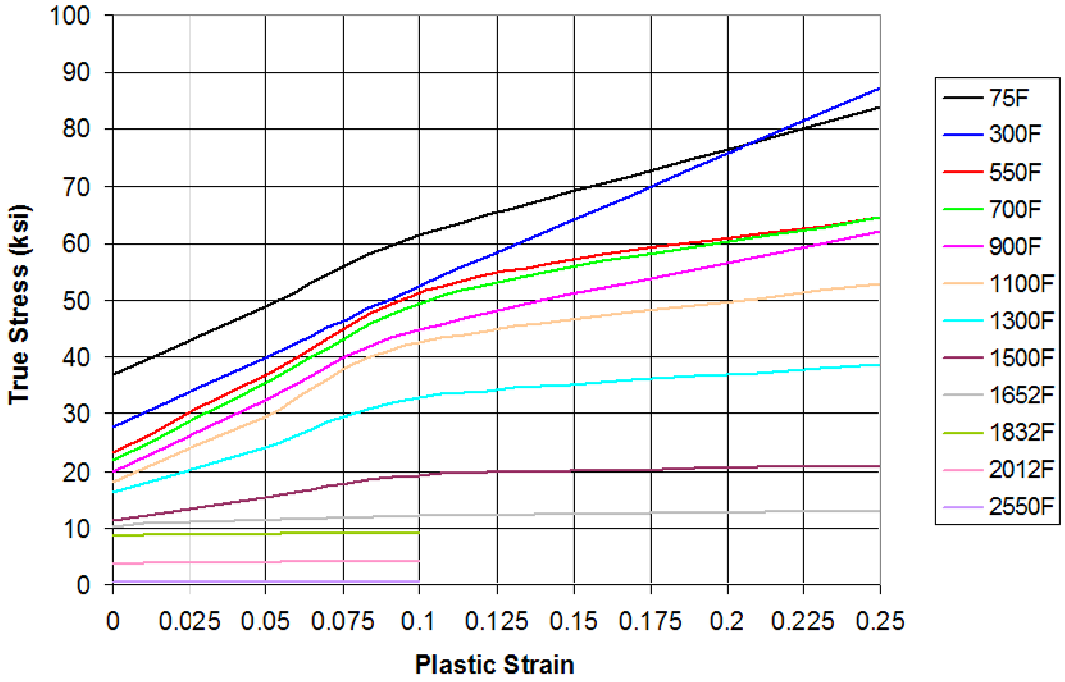

Figure 6 Temperature Dependent True Stress-Strain Curves of Type 304 Stainless Steel

Table 5 Temperature Dependent Creep Constants for all the Materials

$$\dot{\varepsilon} = \mathrm{A}\sigma^{n}t$$

A	n	T (^{o}F)
MATERIAL: A508 Class 2		
1.0000E-26	4.0000	70
2.2910E-12	6.0451	1000
3.2670E-07	4.8865	1200
3.2670E-07	4.8865	2500
MATERIAL: S309, S304, S316		
1.0000E-26	4.0000	70
9.2650E-25	9.7800	887
4.6900E-24	9.9700	932
1.6410E-21	9.0600	977
3.9710E-19	8.2000	1022
2.7540E-18	8.2000	1067
1.7060E-17	8.2000	1112
1.1700E-16	8.1800	1157
7.2180E-16	8.1600	1202
3.4110E-14	7.4200	1247
1.3300E-12	6.7200	1292
2.0930E-11	6.2500	1337
3.2310E-10	5.7700	1382
MATERIAL: INCO182		
1.0000E-26	4.0000	70
1.0000E-26	4.0000	990
2.1478E-16	6.1709	1000
4.6025E-15	6.6426	1100
4.6025E-15	6.6426	2500

$\dot{\varepsilon} = \text{Creep Rate}\ \frac{\text{in}}{\text{in} \cdot \text{hr}}$

$\mathrm{A} = \text{Material Constant}$

$\sigma = \text{Von Mises Stress}\ (\text{ksi})$

$\mathrm{n} = \text{Material Constant}$

$\mathrm{t} = \text{Time}\ (\text{hr})$

3.2 Weld Residual Stress Modeling Details

As indicated previously, the welding produced residual stresses were calculated using axi-symmetric models. The finite element model was subjected to a thermal analysis, which simulated the weld process functions of laying down the molten beads of weld filler metal, introducing heat energy into the weld bead and cooling the weld to an appropriate inter-pass temperature. The thermal analysis calculated the temperatures throughout the finite element model through the welding process. A subsequent stress analysis was performed which used the previously defined temperatures to calculate the elastic-plastic residual stresses and strains in the welded geometry due to the thermal effects of welding. ABAQUS finite element software was used for the 2D axi-symmetric analyses discussed in this report. Material properties used in the analyses varied with temperature and made use of the annealing simulation capabilities of the ABAQUS software to model weld bead melting [7].

Figure 7 shows the pressurizer surge nozzle axi-symmetric geometry used as an example of one of the three geometries studied. This configuration contained an A508-Class 2 low alloy steel nozzle with Type 304 stainless steel cladding on the inside and Inconel 82/182 buttering on the end. The stainless steel safe end component was welded to the buttered nozzle with Inconel 82/182 weld filler. After the primary Inconel weld was completed, an additional Inconel 82/182 thermal sleeve weld was added on the inner diameter of the pipe. (This thermal sleeve weld was only modeled for the surge line geometry. It was not included in the smaller diameter safety nozzle geometry or the larger diameter hot leg geometry since these geometries do not typically include a thermal sleeve.) The incorporation of the thermal sleeve weld for the surge line geometry tends to increase the inner diameter axial tension stresses. In close proximity to the Inconel weld is another weld fabricated with stainless steel weld filler material which connects the stainless steel safe end to the stainless steel piping.

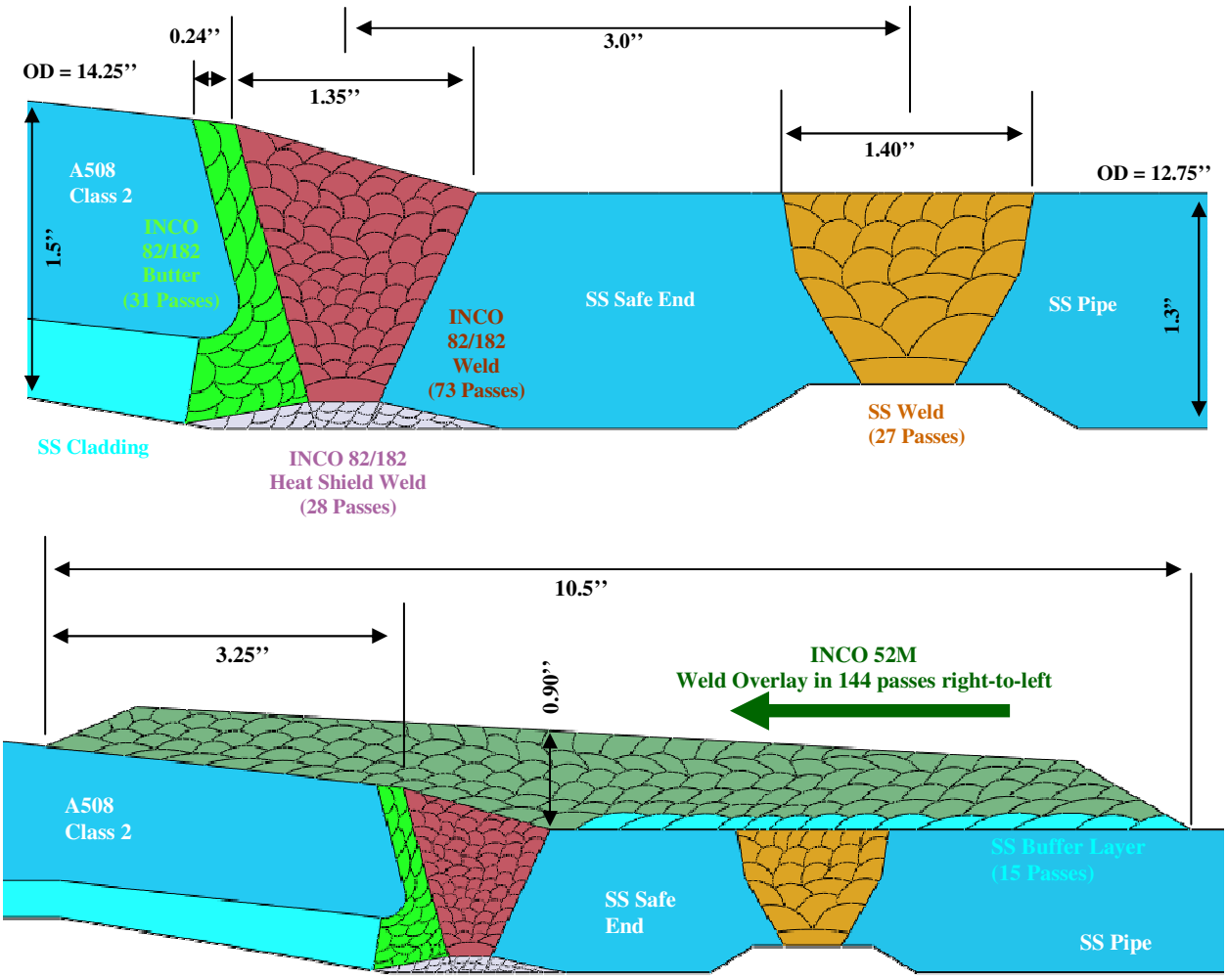

Figure 7 Surge Nozzle Geometry, Materials, and Weld Layout

The weld passes were individually added to the model as shown in Figure 8. A relationship between weld heat energy and pipe thickness was developed from test data. Actual weld parameters of voltage and current were measured for multiple weld passes on several pipe thicknesses and were documented in Table C-3 of Barber [8]. A linear curve fit of this data was constructed to create an equation describing heat energy input per linear inch of weld pass as a function of pipe thickness. Equation 1 shows the linear equation describing heat input per weld bead length in (J/in) versus pipe thickness in inches. This equation, and an additional efficiency multiplication factor of 75 percent, was used to create the heat energy input values used for the specific pipe thicknesses examined in this analysis.

$$\frac{Energy}{Length}\left(\frac{J}{in.}\right) = 15{,}393\left(\frac{J}{in^2}\right)\cdot t(in.) + 13{,}265\left(\frac{J}{in.}\right) \qquad (1)$$

A more detailed description of the weld analysis energy input follows. The analysis steps, per pass, for the axi-symmetric model included a thermal analysis and then a stress analysis using the results from the previous thermal analysis. The steps were as follows:

- Deposition of weld pass for t = 0.01 seconds at molten temperature.
- Heating of weld pass calculated as:

$$\frac{(I \cdot V \cdot \eta)}{\nu} := A \cdot \Delta z \cdot q' \cdot \Delta t \qquad (2)$$

$$q' := \left[\frac{(I \cdot V \cdot \eta)}{(A \cdot \Delta z \cdot \Delta t \cdot \nu)} \right] \cdot (\text{conversion factor})$$

$$\Delta t := \frac{\Delta z}{\nu}$$

I = Weld Current (Amps)

V = Weld Voltage (Volts)

η = Efficiency (0.75)

ν = Speed (in/sec)

A = Weld pass cross section area (in^2)

Δz = Unit Depth (1 inch)

Δt = $\Delta z / \nu$ (sec)

q' = Power Input per volume [(BTU/sec)/in^3]

Conversion Factor = 0.0009472 [(BTU/sec)] = 1 Watt

- Cooling of the weld pass for t ≈ 300 sec. allowing the weld pass to cool to below 66 C (150 F) before applying the next pass.

Figure 8 shows the transient thermal analysis steps used to model the thermal portion of the weld residual stress analysis for the example surge nozzle geometry. The heat input was adjusted as necessary from the curve fit data to assure that the weld beads remained at the weld filler material melting temperature during the deposition of each weld bead. Heat was distributed through the model by conduction, and away from the pipe by convection (8.5×10^{-5} Btu/sec in^2 F, 44 BTU/hr ft^{2o}F), simulating the presence of room temperature air inside and outside the welded pipe. Between weld passes, the weld was allowed to cool to an inter-pass temperature of 66 C (150 F). The root pass of the Inconel weld was ground out and re-welded as a final step in the weld process. This step is not always performed during plant fabrication, but was included here because it increases the interior tension stresses in the weld and is thus conservative. The weld was allowed to cool to room temperature when the final weld pass was completed in each weld.

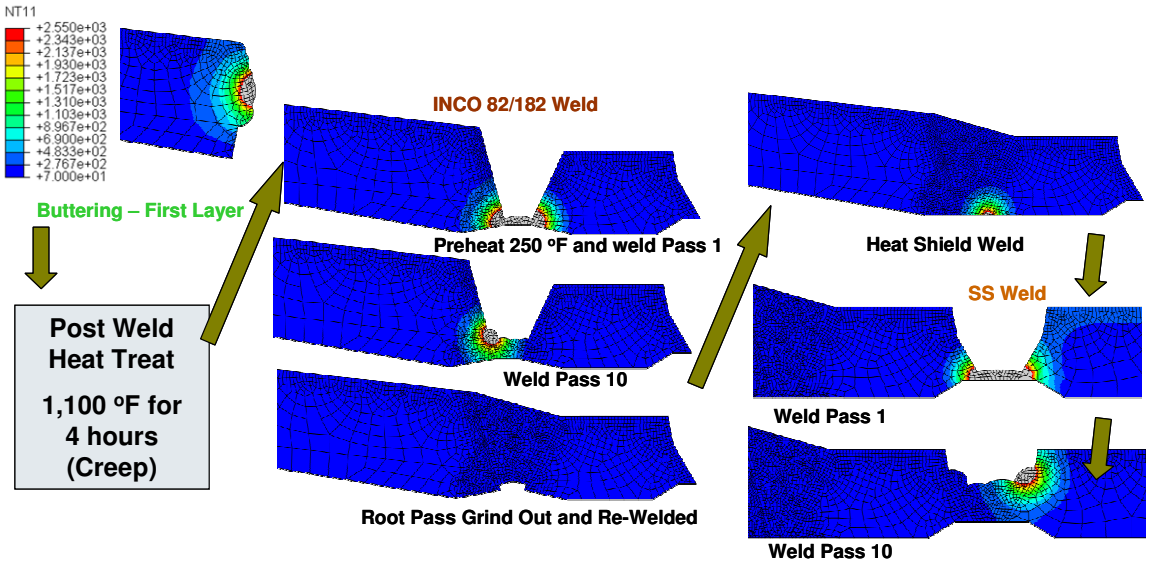

Figure 8 Details of the Welding Residual Stress Thermal Modeling

The stress portion of the two dimensional axi-symmetric analysis used the results from the temperature analysis and ABAQUS software to develop the residual stresses over the same time steps as were used in the thermal analysis and to assign the proper welding strains, including the effects of melting and annealing of the weld and parent material.

The finite element mesh consisted of ABAQUS axi-symmetric thermal elements DCAX3 and DCAX4 for the thermal analysis and their corresponding axi-symmetric structural elements CAX3 and CAX4R for the structural analysis. For subsequent three dimensional analyses, the two dimensional weld residual stresses were mapped to three dimensional elements of type C3D6 and C3D8R, respectively. Figure 2 shows the mesh density used to develop the weld residual stresses for the two dimensional axi-symmetric surge nozzle model. The finely meshed two-dimensional model used to develop the weld residual stresses for this surge nozzle geometry had approximately 8,000 elements.

The boundary conditions used in these studies held the nozzle end of the model fixed except in the load cases in which temperature was increased. In this case, the nozzle side boundary conditions fixed the models' displacements in the axial direction and allowed free expansion in the radial direction to simulate the unrestricted uniform thermal growth of the structure. This conditions best simulates the overall expansion of the structure due to thermal growth. The piping side end of the model was allowed to remain free in the axial and radial directions. This boundary is conservative because the compression stresses in the dissimilar metal weld would be made more compressive due to the FSWOL and operating pressures and temperatures if any axial restrictions in displacement were placed on the pipe segment. It is for this reason that the pipe end of the model was left free, so that the localized effect of the weld residual stresses and the weld overlay could be isolated.

Figure 7 shows the pressurizer surge nozzle geometry used here as an example of the dissimilar metal weld layout. The materials are designated in the figure as well as the areas to be welded and the number of simulated weld passes in each welded area. Figure 8 shows a graphic representation of the thermal portion of the weld residual stress development analysis.

The analysis used to develop the weld residual stresses in the model requires six steps per weld pass, and follows the same step-by-step process as is used in the welding process that it is simulating. The thermal modeling of each weld pass deposition requires three of the six analysis steps, and the stress modeling requires a duplicate three steps.

In the first step, the elements representing the weld pass being deposited are added individually to the model at a temperature slightly above the melting temperature of the weld material. This step is done in a steady state thermal analysis and the "instantaneous" appearance of the molten weld pass is made to take place in 0.01 seconds. In the second step, the weld pass is heated in a transient thermal analysis step as power is added to the weld bead for the duration representing the time it takes the weld head to traverse one inch of the weld pass (8.55 seconds in this case). In this step, edges of surrounding weld beads re-melt in the area around the perimeter of the heated weld pass. The third step is another transient analysis in which the weld power is shut off, and the weld pass is allowed to cool to an inter-pass temperature of approximately 66 C (150 F) in 300 seconds. When one weld is complete, the cooling time is increased to 3,000 seconds to allow the structure to cool to room temperature.

The temperature data produced in the thermal analyses is used as input for an equal number of stress analysis steps for each weld pass. The non-linear material properties for each material are used to calculate the stress, strain, and plastic deformation caused by the welding process.

Using the pressurizer surge nozzle geometry shown in Figure 7 as an example, the welding simulation steps include the pass-by-pass welding of the butter layer as it is built up in 31 passes and several layers. After the butter layers are finished and allowed to cool to room temperature, the nozzle, with butter layers applied, is subjected to a post weld heat treatment at 593 C (1,100 F) for 4 hours in a visco-elastic analysis step which uses the creep properties of the materials to allow for the stress reduction produced by the heat treatment process. The assembly is allowed to cool to room temperature in a separate analysis step over a duration of two hours.

Before welding the safe end in place, the butter area is pre-heated to 121 C (250 F). The dissimilar metal weld is then built up pass-by-pass, as was the butter layer, but using 73 passes in this case. When the Inconel 82/182 weld is completed, it is allowed to cool to room temperature. The root-pass of this weld is then ground out and re-welded in several analysis steps. The grinding and re-welding process is not always performed by the industry, but this internal weld repair contributes to the high tensile axial stresses at the inside surface that are the cause of PWSCC. After the root pass is re-welded and cooled to room temperature, the heat shield fill-in weld is subsequently welded in place.

The heat shield fill-in weld step is not included in all surge nozzles, but is used in some cases where an additional thermal sleeve is added after the safe end is welded in place. This fill-in weld also contributes to inner diameter axial tensile stresses in the dissimilar metal weld area and is therefore included in this analysis. In this case, the fill-in weld is completed in 28 passes. The thermal sleeve and its fill-in weld are unique to the surge nozzle design, and are not included in either the hot leg or the safety nozzle that were also studied.

There is a secondary stainless steel weld in close proximity to the dissimilar metal weld in geometries such as the pressurizer surge nozzle and the pressurizer safety nozzle which have a safe-end component which acts as a transition between the dissimilar metal weld and the stainless steel piping system. In the surge nozzle geometry used as an example here, the centerline distance between the dissimilar metal weld and the secondary stainless steel weld is 75 mm (3.0 inches) as shown in Figure 7. The secondary stainless steel weld was completed in 27 weld passes in this case and was then allowed to cool to room temperature. The weld residual stresses are built into the model with each weld pass that is added.

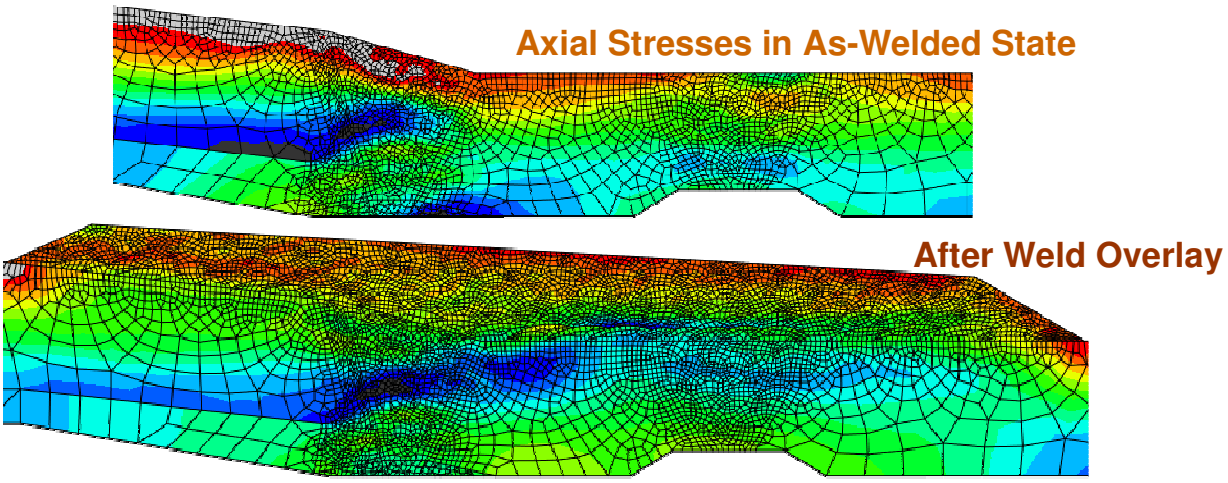

Figure 9 Axial Stresses before and after the Surge Nozzle FSWOL Application

Figure 9 shows the axial stress pattern in the pressurizer surge nozzle before and after the application of the FSWOL.

Operating temperatures in the range of 300 C (572 F) to 322 C (611 F) were used for the analyses. Internal operating pressure of 15.5 MPa (2,250 psi) is applied to the interior surfaces of the model. An end cap load is applied to the free end of the pipe. The end cap load was calculated using the following equation for the surge nozzle geometry.

$$P_{\text{end cap}} = \frac{P \cdot r^2}{\left(R^2 - r^2\right)} = \frac{2235\frac{\text{lbs}}{\text{in}^2} \cdot \left(5.0625\text{in}\right)^2}{\left(\left(6.375\text{in}\right)^2 - \left(5.0625\text{in}\right)^2\right)} = 3815.7\frac{\text{lbs}}{\text{in}^2} \qquad (3)$$

$P = \text{Pressure}$

$R = \text{Outer Radius}$

$r = \text{Inner Radius}$

3.3 Modeling Cracks

One concern with the FSWOL is the effect it would have on undetected cracks. In order to evaluate this concern, three sets of analyses were performed:

1. In the first case, a crack was introduced in the inconel weld and allowed to grow at operating pressure and temperature, but without the FSWOL.
(Crack Growth Operating Pressure and Temperature)

2. In the second case, a crack was introduced in the Inconel weld, the FSWOL was then applied, and then the operating temperatures and pressures were subsequently applied.
(Crack Growth FSWOL Operating Pressure and Temperature)

3. In the final analysis, the crack was forced to grow at operating temperature and pressure but after the FSWOL was applied. In this case a FSWOL was applied pre-emptively to an uncracked pipe and then a crack was subsequently introduced and forced to grow through the FSWOL-mitigated stress field (post FSWOL)
(FSWOL Operating Pressure and Temperature Crack Growth)

In the cases where the cracks were introduced before the application of the FSWOL, cracks 75 percent of the thickness and 100 percent of the circumference were modeled to simulate the situation in which a very large crack went undetected. In the cases in which the crack is present along with the FSWOL a crack depth of 100 percent of the original pipe thickness and a full 360 degrees around the circumference was modeled. Assuming that the weld is inspected with an Appendix VIII qualified technique, the likelihood of a full 360 degree internal surface crack, 75 to 100 percent of the original pipe wall thickness in depth going undetected is quite low, such that the assumption of the existence of an undetected crack of this size is most likely conservative. Circumferential indications have been found to occur in the Inconel weld and at the interface between the Inconel butter layer and the A508 nozzle material (see Figure 10), but with the exception of the recent experience at Crystal River[9], few have progressed to greater than 30 percent of the wall thickness. Both potential crack locations (at the butter/ferritic steel interface and at the butter/weld interface) were analyzed, with similar results and will be described in more detail in the results section of this report.

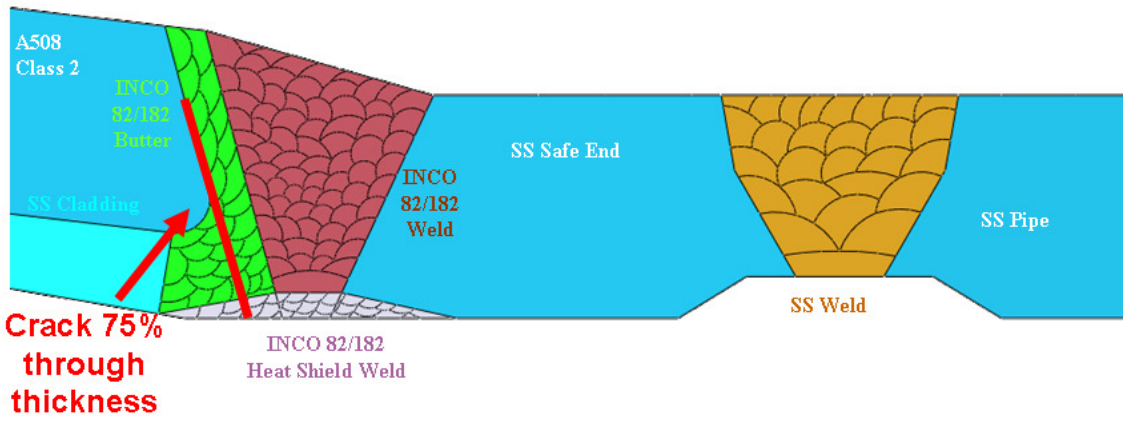

Figure 10 Crack between Butter and A508 Class 2 Steel

The cracks were introduced using the ABAQUS crack propagation analysis procedure using an artificial crack growth versus time equation. The crack surfaces were defined allowing for self contact and surface interaction properties including friction in areas of crack closure. An arbitrary coefficient of friction of 0.15 was used in these analyses so that that crack surfaces were not frictionless. The cracks were made to grow in 1.25 mm (0.05 inch) steps so that the crack tip stress intensity factor could be calculated as the crack grew. Figure 11 shows the axial stress after the crack was introduced and operating pressure and temperature were applied to the pressurizer surge nozzle geometry with no FSWOL applied. The figure shows, in an exaggerated displacement plot, that the crack opens to a depth of 30 percent of the thickness of the nozzle at which time it reaches the compressive stress region which is formed by the weld residual stress field. (Note, as will be discussed later, his compressive stress state approximately 30 percent

through the wall thickness typically only occurs when there is a secondary stainless steel weld in close proximity to the DMW. When there is no secondary weld the stresses remain tensile through more of the wall thickness. In these cases the crack will remain open further through the wall.) Though the crack surface is de-bonded along 75 percent of the thickness, it only opens for the inner 30 percent of the thickness because of the residual stresses which produce an axially compressive region in the middle of the wall thickness.

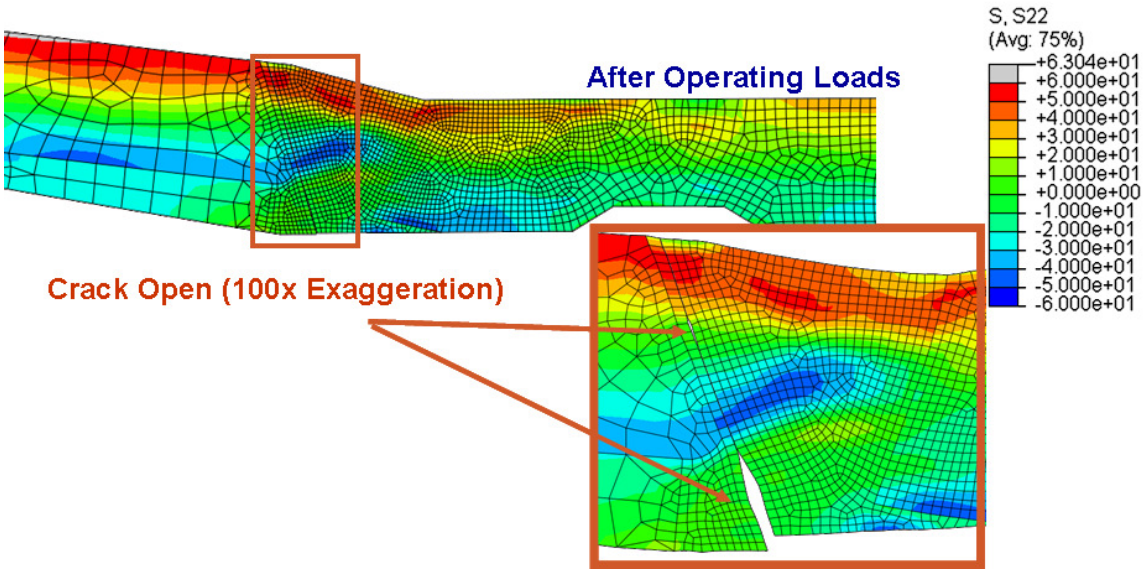

Figure 11 Axial Stress with Crack and no FSWOL (ksi units) Applied

It is highly unlikely that a circumferential crack would be able to progress into the tensile region near the outer surface unless a severe overload occurred because it would have to grow through the compressive region of the weld residual stresses near the middle of the wall thickness. In the hypothetical occurrence of this unlikely event, it is worth examining the stress intensity factors at the crack tip, and the theoretical crack growth rate due to PWSCC effects. Stress intensity factor versus crack depth was plotted for all cases

There are three types of loading that a crack can experience as described by Anderson [10]. In Mode I loading the principal load is applied normal to the crack plane and tends to open the crack. This is the primary mode affecting circumferential cracks in the geometry studied here. Mode II describes in-plane shear loading that tends to slide one crack face with respect to the other, and Mode III loading refers to out-of-plane shear loading. Neither of these latter two loading modes are major contributors to crack growth in this case. Mode II effects are small in these models, and Mode III effects are nonexistent in an axi-symmetric model.

The stress intensity factor at the crack tip, K_I, can be described by Equation 4 for this case. The stress intensity factor is derived from the energy release rate, G_I, and described by Krueger in [11]. Of interest are the values for the stress intensity factor before and after the application of the FSWOL.

$$K_I = \sqrt{\frac{G_I E}{(1-\mu^2)}} \quad (4)$$

K_I = Crack tip stress intensity factor, $(\text{ksi}\sqrt{\text{in}})$

G_I = Energy release rate = $\frac{F\delta}{2\Delta a}$, (ksi - in)

E = Young's modulus, (ksi)

μ = Poisson's ratio

F = Crack tip force opening crack, (kips)

δ = Crack opening displacement one node from crack tip, (in)

Δa = Area of element preceding crack tip, unit depth for 2 - D problems, (in^2)

The use of Equation 4 is based on the well known crack closure integral (CCI) equations first introduced by Rybicki and Kanninen [12] and summarized by Krueger [11]. This is an approximation since it must be assumed that the crack grows mainly in an elastic field and no additional plasticity or minimal plasticity occurs during growth. This is typically the assumption made in modeling stress corrosion crack (SCC) growth in residual stress fields where the SCC growth law is governed by the stress intensity factor (K). There is some emerging controversy in the field as to the validity of this assumption, however, in the present analyses, minimal plasticity did occur during forced crack growth. Reference [13] compares K_I values calculated via CCI and those calculated using the finite element alternating method for cracks in residual stress fields. The agreement between the two methods was quite good.

The values of the stress intensity factor before and after the FSWOL have been calculated at the crack tip as the crack was forced to grow to its final depth through the thickness of the pipe using Equation 4.

A deterministic crack growth model for Inconel Alloy 82/182 weld metal material based on a statistical evaluation of the worldwide set of available laboratory test data for these materials using controlled fracture mechanics specimens is shown in Equation 5. The equation development is discussed in more detail in the Reference [14].

This equation was used to determine crack growth rates for PWSCC for the different K values calculated pre-FSWOL and post-FSWOL in this study.

$$\dot{a} = \alpha f_{alloy} f_{orient} K^{\beta} e^{\left[-\frac{Q_g}{R}\left(\frac{1}{T} - \frac{1}{T_{ref}} \right) \right]} \quad (5)$$

$\dot{a}$ = Crack growth rate at temperature T in m/sec (or in/h)

Q_g = Thermal activation energy for crack growth
130 kJ/mole (31.0 kcal/mole)

R = Universal gas constant 8.314×10^{-3} kJ/mole °K
(1.103×10^{-3} kcal/mole °R)

T = Absolute operating temperature at location of crack, °K (or °R)

T_{ref} = Absolute reference temperature used to normalize data,
598.15 °K (or 1076.67 °R)

α = Power - law constant, 1.5×10^{-12} at 325 °C for $\dot{a}$ in units of m/s
and K in units of MPa$\sqrt{m}$
(2.47×10^{-7} at 617 °F for $\dot{a}$ in units of in/hr and K in units of ksi$\sqrt{in}$)

f_{alloy} = 1.0 for alloy 182 and 0.385 for alloy 82

f_{orient} = 1.0 except 0.5 for crack propagation that is clearly
perpendicular to the dendrite solidification direction

K = Crack tip stress intensity factor, MPa$\sqrt{m}$ (or ksi$\sqrt{in}$)

β = Exponent, 1.6

3.4 Pipe/Nozzle Geometries

As part of this effort four pipe/nozzle geometries were considered:

- Medium diameter pressurizer surge nozzle geometry
- Small diameter pressurizer safety nozzle geometry
- Large diameter cold leg reactor pressure vessel nozzle and reactor coolant pump outlet nozzle geometries

3.4.1 Pressurizer Surge Nozzle Geometry

Figure 12 shows a revolved version of the axi-symmetric pressurizer surge nozzle geometry with the weld area highlighted. The surge nozzle is located at the bottom of the pressurizer pressure vessel, and the piping faces downward. Figure 13 shows the details of the surge nozzle geometry including the materials used for the model. The nozzle is modeled as A508 Class 2 carbon steel, the cladding as Type 304 stainless steel, the butter, dissimilar metal weld and heat shield fill-in weld are modeled as Inconel 82/182 weld metal, and the safe end, secondary stainless steel weld, and pipe are modeled as Type 316 stainless steel material. Actually, the stainless steel weld is Type 309 but the stress-strain properties for Type 309 and Type 316 are assumed to be the same, see Table 3 and Figure 5.

Figure 13 also shows the dimensions of the surge nozzle model. The surge nozzle is an intermediate sized nozzle which typically connects to a stainless steel pipe with an outside diameter in the range of 10 to 14 inches. For these analyses a pipe outer diameter of 324 mm (12.75 inches) and a pipe thickness of 33 mm (1.3 inches) were used. The figure also shows the individual weld passes that were modeled for each welded area. The butter was modeled in 31 passes while the dissimilar metal weld was modeled with 73 passes, the heat shield weld with 28 individual passes, and the stainless steel weld with 27 passes.

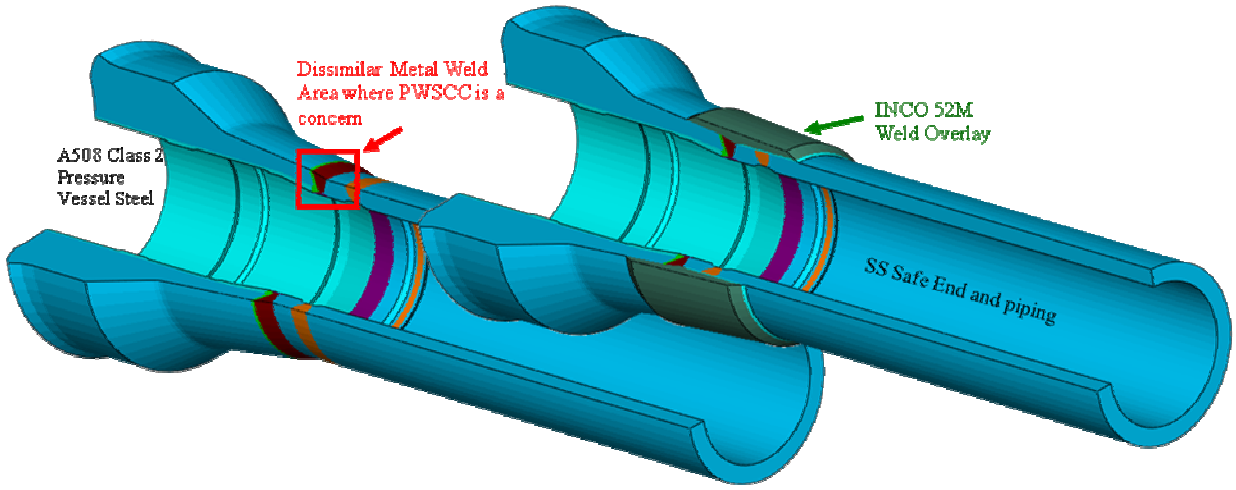

Figure 12 Pressurizer Surge Nozzle Geometry used in Surge Nozzle Analyses

There are two major differences between the surge nozzle geometry and the single butt weld geometry used in boiling water reactor piping which have great effects on the weld residual stresses. The first difference is the use of a safe end component which requires a secondary stainless steel weld to join the nozzle to the pipe system. In this case the secondary stainless steel weld is 75 mm (3 inches) away from the dissimilar metal weld, and has a profound effect on the stress state in the dissimilar metal weld. The

effect of this weld will be explored in the results and sensitivity study sections of this report. The second major difference is the use of a heat shield fill-in weld on the inside of the surge nozzle dissimilar metal weld. This weld is only used in the surge nozzles, and is not used in all surge nozzles, but depends on the type of thermal shield used in a particular plant. This weld has a similar effect as an inner diameter full circumference weld repair, in increasing the axial tension stresses on the inner diameter of the dissimilar metal weld. The effect of this weld will be explored in the results and sensitivity study sections of this report.

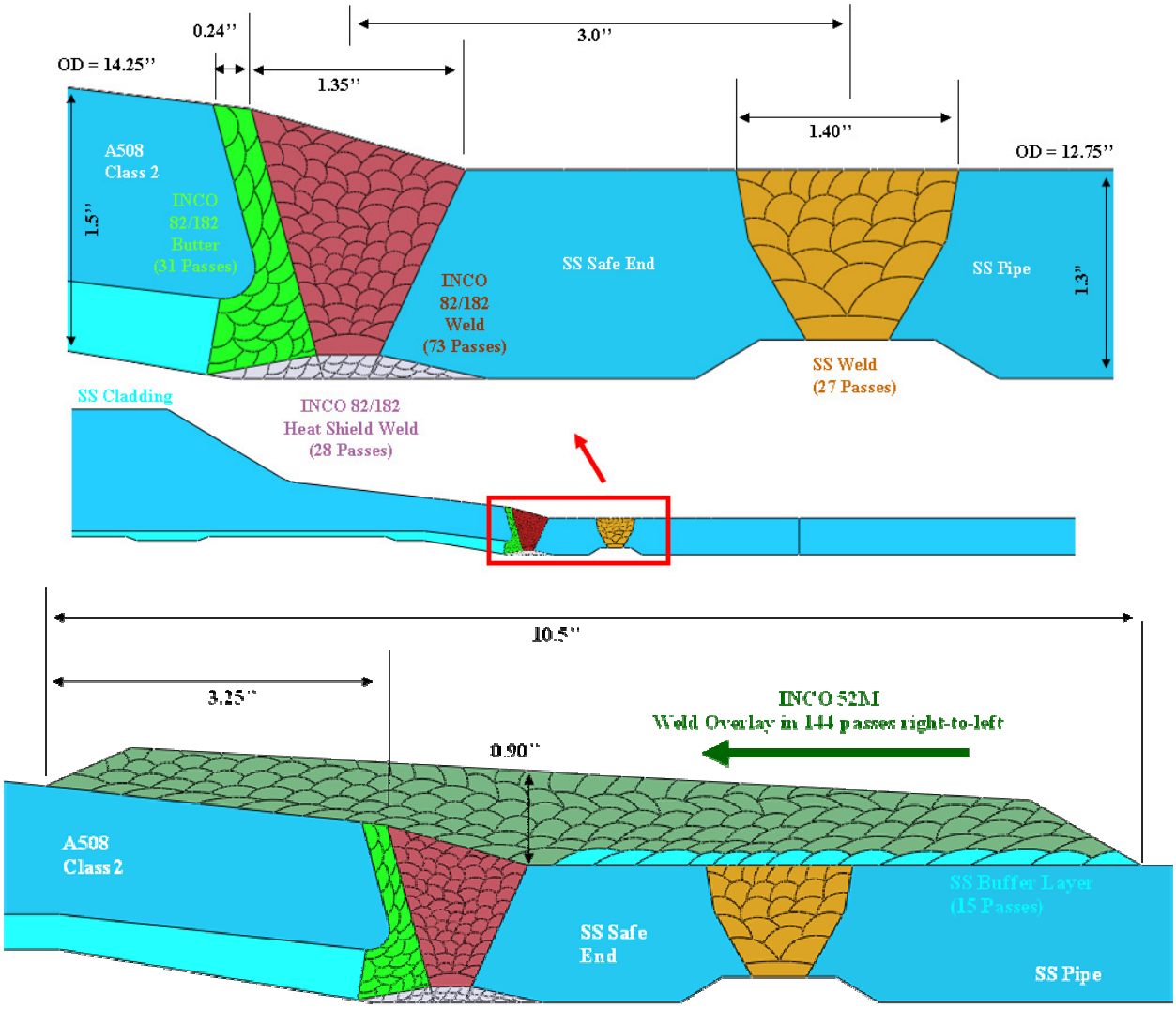

Figure 13 Surge Nozzle Dimensions used in Surge Nozzle Analyses

3.4.2 Pressurizer Safety Nozzle Geometry

Figure 14 shows a revolved version of the axi-symmetric pressurizer safety nozzle geometry with the weld area highlighted. The safety nozzle is located at the top of the pressurizer pressure vessel on the opposite side from the surge nozzle, and thus the piping for the safety nozzle faces upward. Figure 15 shows the details of the safety nozzle geometry including the materials used for the model. The nozzle is A508 class 2 carbon steel. The cladding, pipe and safe end are stainless steel, the butter and dissimilar metal weld are made from Inconel 82/182, and the secondary stainless steel weld is made from Type 309 stainless steel weld material.

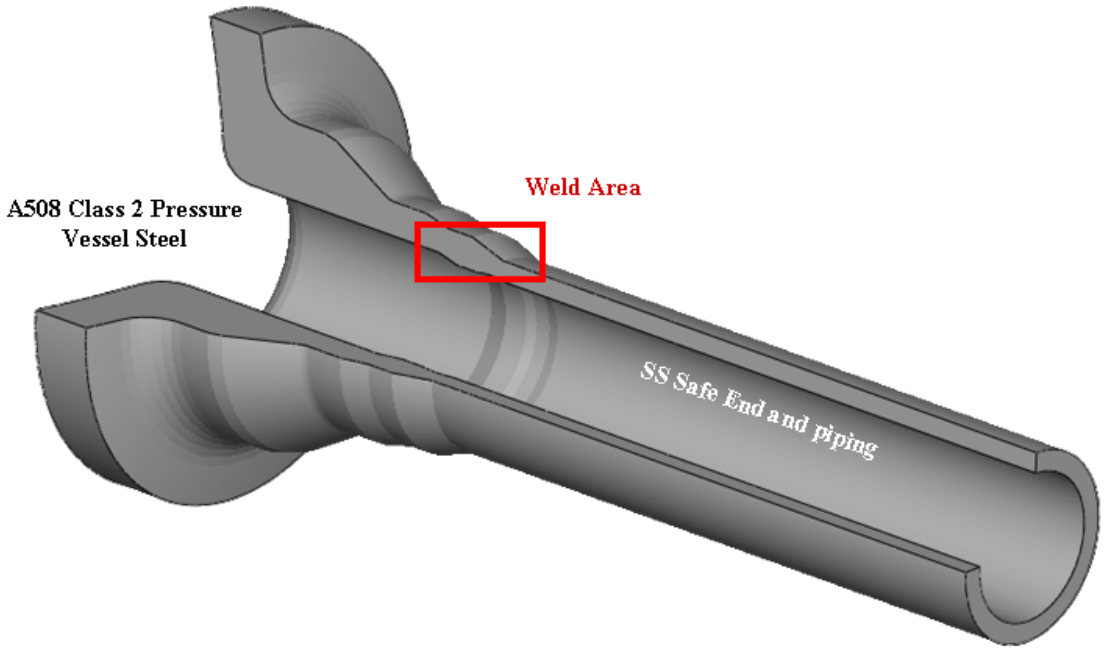

Figure 14 Safety Nozzle Geometry used in Safety Nozzle Analyses

Figure 15 also shows the dimensions of the safety nozzle model. The safety nozzle is a smaller sized nozzle. For these analyses a pipe outer diameter of 168 mm (6.62 inches) and a pipe thickness of 18.2 mm (0.715 inches) was used. The figure also shows the individual weld passes that were modeled for each weld. The butter was modeled in 26 passes while the dissimilar metal weld was modeled with 21 passes, and the stainless steel weld with 17 passes.

The safety nozzle is very similar to the surge nozzle in materials and geometry. Both have a secondary stainless steel weld in close proximity to the dissimilar metal weld (66 mm [2.6 inches]) away from the DMW for the safety nozzle). The safety nozzle has a larger butter layer in proportion to the dissimilar metal weld than does the surge nozzle. It never has a heat shield fill-in weld and of course is of smaller size, but otherwise they are very similar.

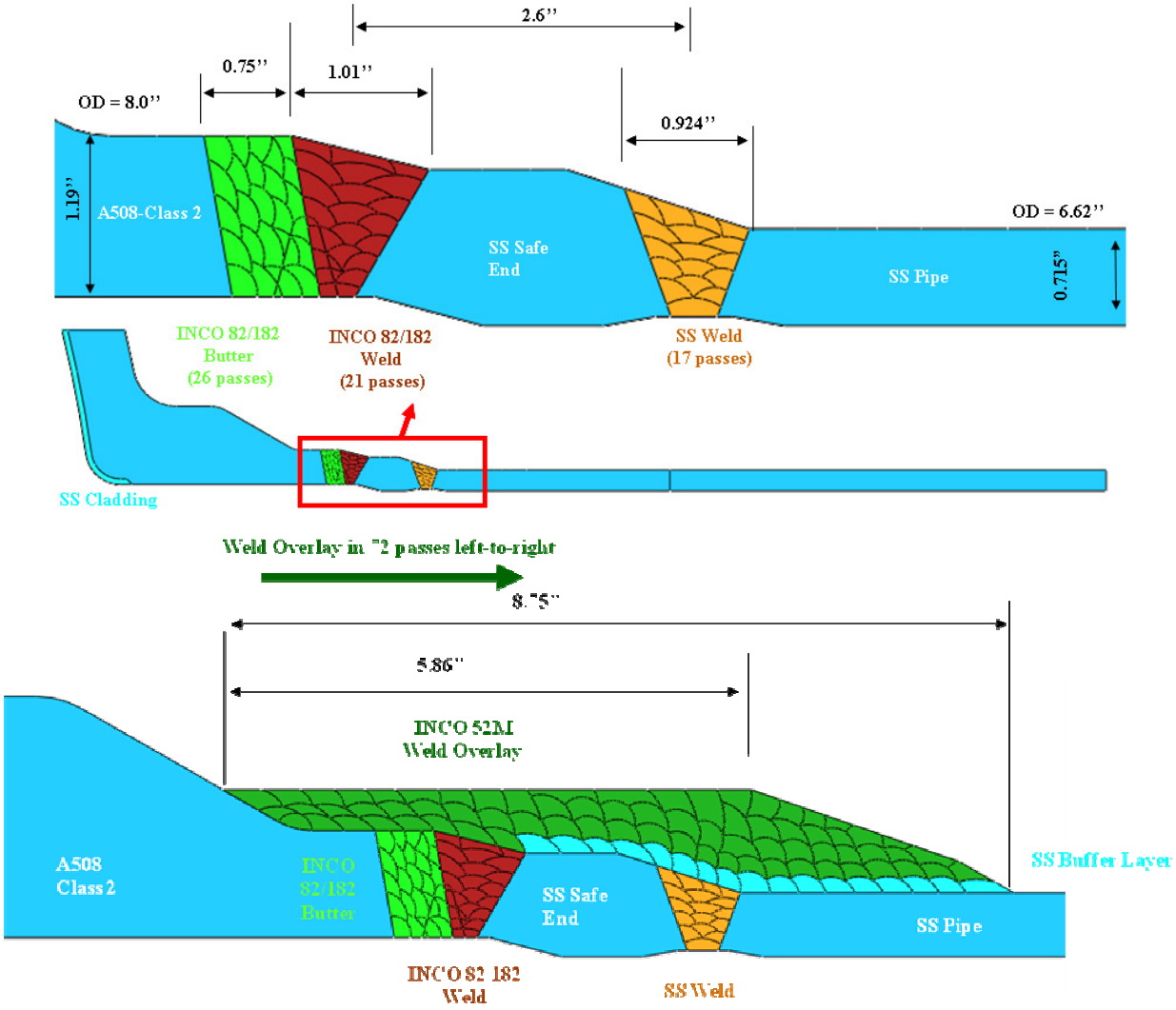

Figure 15 Safety Nozzle Dimensions used in Safety Nozzle Analyses

3.4.3 Reactor Pressure Vessel Cold Leg Nozzle and Reactor Coolant Pump Outlet Nozzle

Figure 16 shows a revolved version of the axi-symmetric cold leg nozzle geometry with the weld area highlighted. Figure 17 shows the details of the cold leg nozzle geometry including the materials used for the model. The nozzle is A508 class 2 carbon steel. The cladding, pipe and safe end are stainless steel, the butter and dissimilar metal weld are made from Inconel 82/182, and the secondary stainless steel weld is made from Type 309 stainless steel weld material. This model included a 25% inner diameter weld repair in the dissimilar metal weld as indicated in the figure. The results without the inner diameter repair are included with the sensitivity study results.

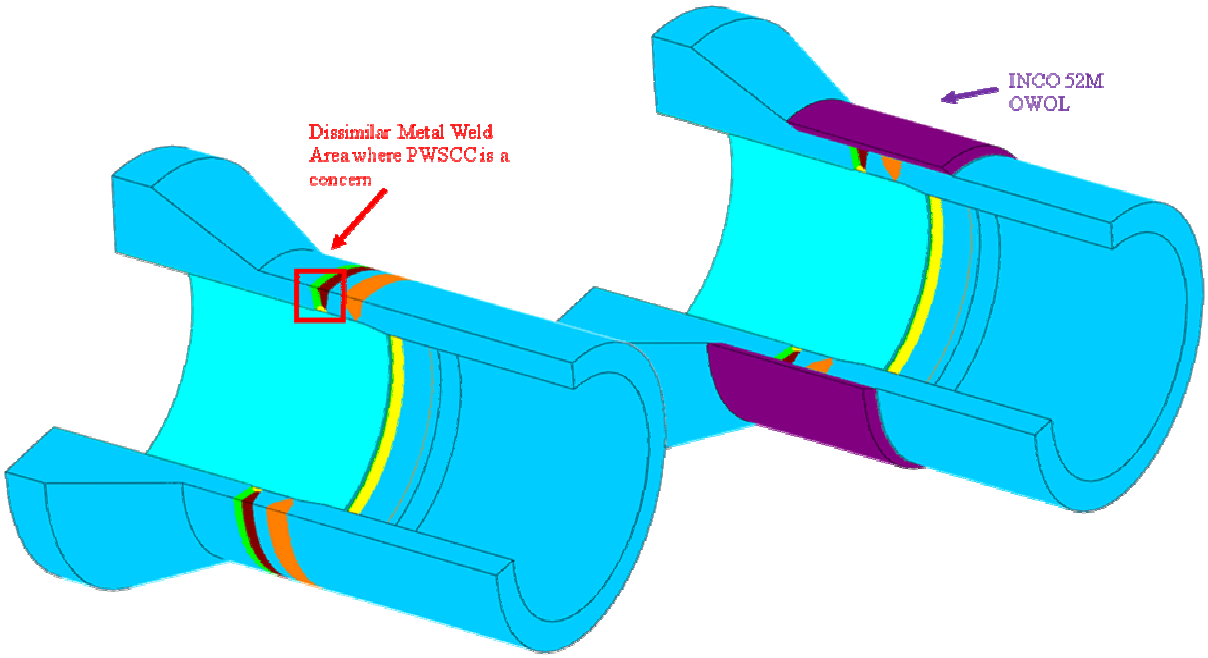

Figure 16 Cold Leg Nozzle Geometry used in Safety Nozzle Analyses

Figure 17 also shows the dimensions of the cold leg nozzle model. The cold leg nozzle is a larger sized nozzle. For these analyses a pipe outer diameter of 889 mm (35 inches) and a pipe thickness of 87 mm (3.43 inches) was used. The figure also shows the individual weld passes that were modeled for each weld. More rectangular weld passes were used in this analysis, rather than the more natural shaped passes that were used in the other analyses, to make meshing the model easier. The butter, Inconel weld and weld repair passes were roughly 2.5 mm by 5.0 mm (0.1 inches by 0.2 inches). The stainless steel weld passes were roughly 2.5 mm by 6.3 mm (0.1 inches by 0.25 inches), and the buffer layer, and OWOL weld passes were 2.5 mm by 16 mm (0.1 inches by 0.625 inches). For this sized nozzle, only the OWOL was modeled. This figure shows the width and thickness of the OWOL geometry for this sized nozzle.

The cold leg nozzle is similar to the surge and safety nozzles in materials and geometry. Both have a secondary stainless steel weld in close proximity to the dissimilar metal weld (95 mm (3.73 inches)) between centerlines of the Inconel weld and the stainless steel safe end weld).

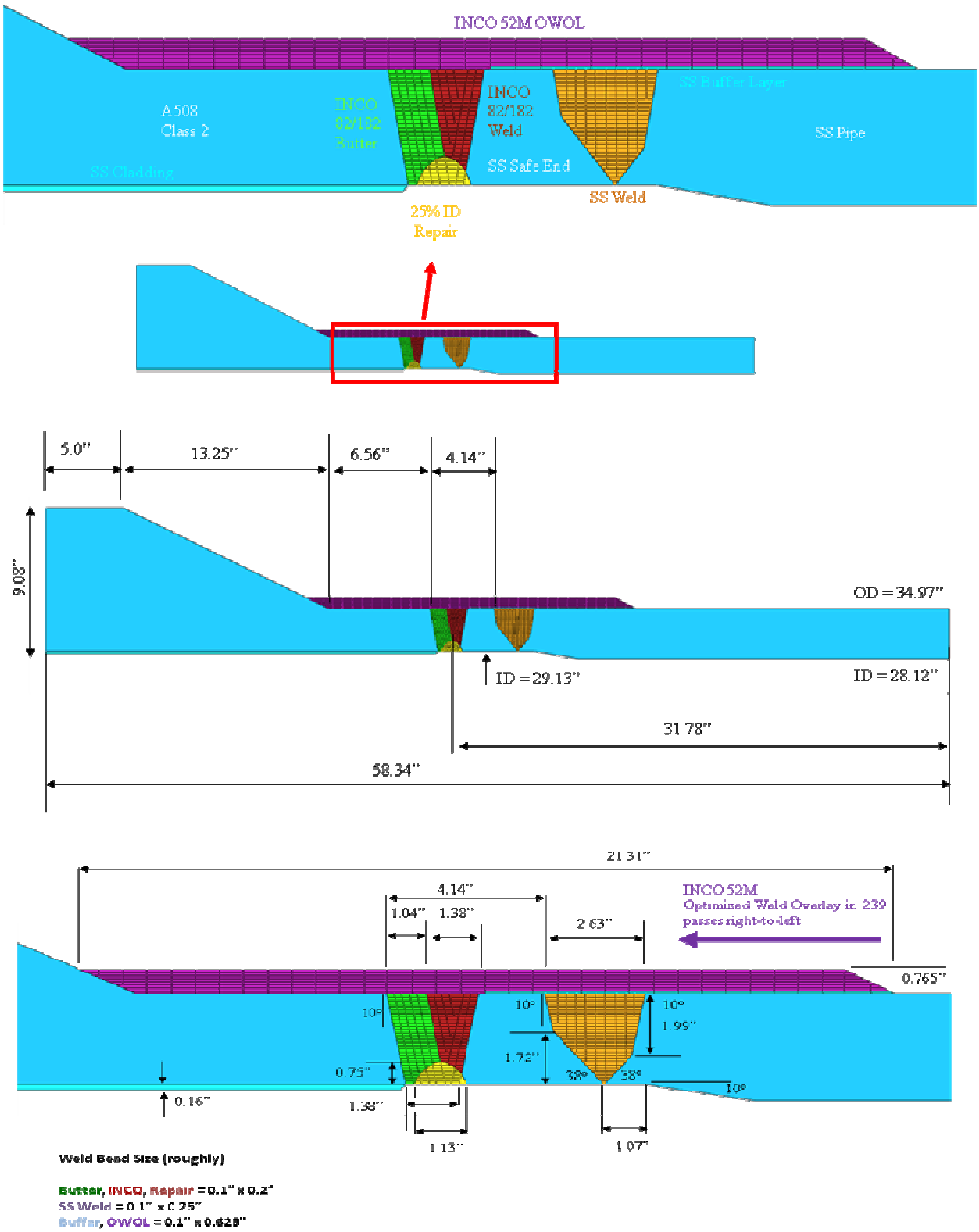

Figure 17 Cold Leg RPR Nozzle Geometry used in Cold Leg Analyses

Figure 18 shows a revolved version of the axi-symmetric reactor coolant pump outlet nozzle with the dissimilar metal weld area highlighted. The RCP nozzle is downstream of the cold leg nozzle, and is part of the same run of piping that returns cooled water from the steam generator and reactor coolant pump to the reactor pressure vessel. Figure 19 also shows the details of the RCP nozzle geometry including the materials used for the model. In this orientation, the carbon steel pipe material is shown on the left with the cast stainless steel pump outlet material shown on the right with the dissimilar metal weld and safe end weld in the middle. (Note, for the RCP outlet nozzle geometry considered the primary loop piping is a ferritic steel while for the cold leg/RPV nozzle geometry considered the primary loop piping is stainless steel.) Figure 19 shows that both an OWOL and FSWOL were modeled for this geometry to evaluate the differences in results produced for this case with a rather short weld overlay.

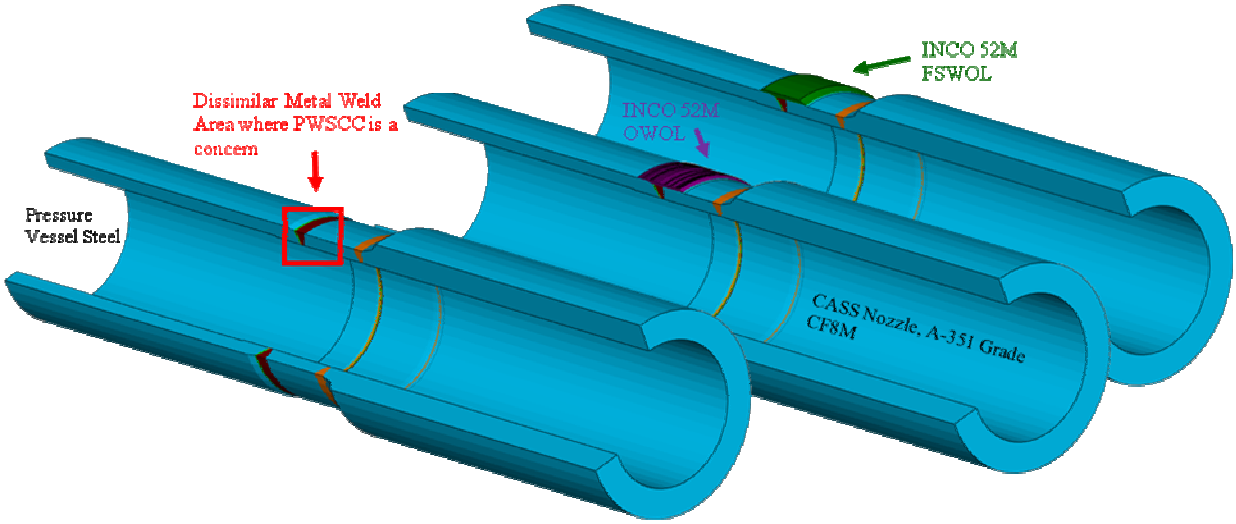

Figure 18 Reactor Coolant Pump Geometry

Figure 19 also shows the dimensions of the RCP nozzle model. The RCP nozzle is similar in size to the cold leg nozzle. For these analyses a pipe outer diameter of 858.5 mm (33.8 inches) and a pipe thickness of 84 mm (3.3 inches) was used on the left end. The figure also shows the individual weld passes that were modeled for each weld. The butter was modeled in 77 passes while the dissimilar metal weld was modeled with 117 passes, and the stainless steel weld with 57 passes.

The RCP nozzle is similar to the other nozzles in material use, but is different in geometry. For the RCP nozzle, the stiffer, thicker section is on the stainless steel side, and the stainless steel safe end weld is far away from the dissimilar metal weld. In this case it is 406 mm (16 inches) away from the DMW centerline. For this model a 25% inner diameter repair was modeled in the Inconel weld in the standard analysis. A case with no ID repair, and one with a 50% ID repair were examined as part of a sensitivity study to evaluate the effect of these repairs on the final stress state and the effectiveness of the weld overlays.

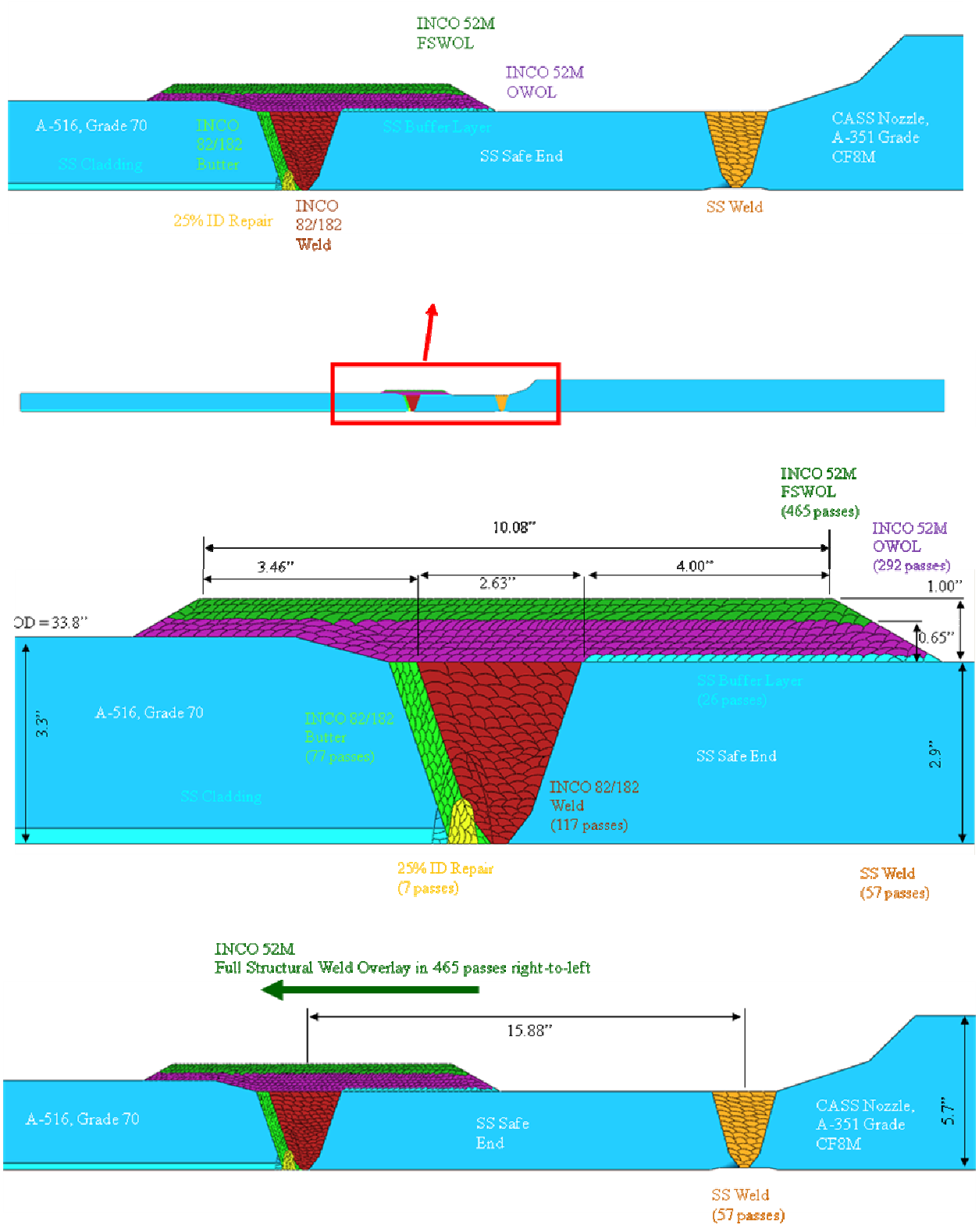

Figure 19 Reactor Coolant Pump Dimensions used in Reactor Coolant Pump Analysis

3.5 Sensitivity Analyses

Several sensitivities studies were conducted to evaluate the effect of different variables on the efficacy of the weld overlay. The majority of the sensitivity studies were confined to the surge nozzle model because it had the most complex geometry and number of welded areas. The various sensitivity analyses considered as part of this effort included:

- The effect of the weld overlay weld sequence was examined. The weld overlay was created in a right to left direction, in a left to right direction, and in a pattern simulating two weld heads operating at the same time in the same direction, but axially offset.
- The effect of the secondary stainless steel weld was examined for the surge nozzle geometry. The weld residual stresses developed by the secondary stainless steel weld were eliminated from the finished weldment and the final stress state for this case was compared to the normal case where the weld residual stresses from the secondary stainless steel weld were included in the analyses. The efficacy of the FSWOL was examined for this case.
- Sensitivity studies were done on each model to examine the effect of weld overlay thickness on the residual stresses for typical dissimilar metal weld configurations. For the surge and safety and RCP nozzle geometries the study included thicknesses up to FSWOL. For the cold leg nozzle, the study also looked at the effect of layer thickness, but only up the final OWOL thickness.
- A study was done examining the effect of inner diameter repair depth on stresses before and after weld overlay repair. For the RCP nozzle, 0%, 25% and 50% inner diameter repair depths were examined. For the cold leg nozzle only 0% and 25% inner diameter repair depths were examined.
- Artificial 360 degree circumferential cracks were forced to grow through the dissimilar metal weld. Crack opening behavior was recorded and crack tip stress intensity factors were calculated for the situations in which a crack was forced to grow in the weld before the FSWOL was applied, and after the FSWOL was applied. These evaluations were for both the surge and safety nozzle geometries for two different crack locations. The calculations were done with the crack forced to grow at the interface of the butter and the dissimilar metal weld, and also at a location between the carbon steel nozzle material and the butter layer.

4. RESULTS

In this section the results are presented. First the results from the axi-symmetric finite element weld residual stress analyses are presented. Next, the results from a series of crack growth analyses through the weld residual stress fields are presented. Finally the results from the three-dimensional analyses are presented.

4.1 Axi-symmetric Weld Residual Stress Analyses Results

The results of the axi-symmetric analyses will be presented below for the surge nozzle, safety nozzle, cold leg/RPV nozzle, and reactor coolant pump outlet nozzle geometries before and after the weld overlay application. Axial and hoop stresses will be shown in stress contour plots and in graphical format. Two types of graphs will be used to show the stress profiles. One plots the stresses on a path through the thickness of the dissimilar metal weld from the inner diameter to the outer diameter. The other type of graph will show the stress values along the inside surface of the model along the length of the area of interest. The location of the dissimilar metal weld, and the secondary stainless steel weld in all four geometries considered, will be indicated on the graphs which show the inner diameter stress along the length of the nozzle.

4.1.1 Pressurizer Surge Nozzle Results

The pressurizer surge nozzle weld residual stresses were developed as shown in Figure 8. Though described previously in some detail, the process deserves another explanation here. The figure shows the initial welding of the butter layer plus the post weld heat treatment of the buttered nozzle at 593 C (1,100 F) for four hours in which creep properties are allowed to relax the welding residual stresses in the butter layer. The butter layer is then pre-heated to 121 C (250 F), and the dissimilar metal weld is then built up pass-by-pass until the weld is complete as shown in Figure 13. This process joins the stainless steel safe end to the carbon steel nozzle. The DMW is allowed to cool to approximately 66 C (150 F) between passes and to room temperature after the weld is complete. The root pass is then ground out and re-welded. In the next step the heat shield fill-in weld is built up on the inner diameter of the dissimilar metal weld. In this case, the heat shield fill-in weld spans the butter layer as well. When the heat shield fill-in weld is completed and cooled to room temperature, the secondary stainless steel weld is built up and then allowed to cool to room temperature once completed.

Figure 20 shows the axial stress contour plot after the Inconel weld and thermal sleeve fill-in weld have been finished (top figure), after the stainless steel weld has been finished (middle figure), and after the FSWOL has been completed (bottom figure). The arrows through the weld indicate the path followed for the graphed data shown in Figure 21.

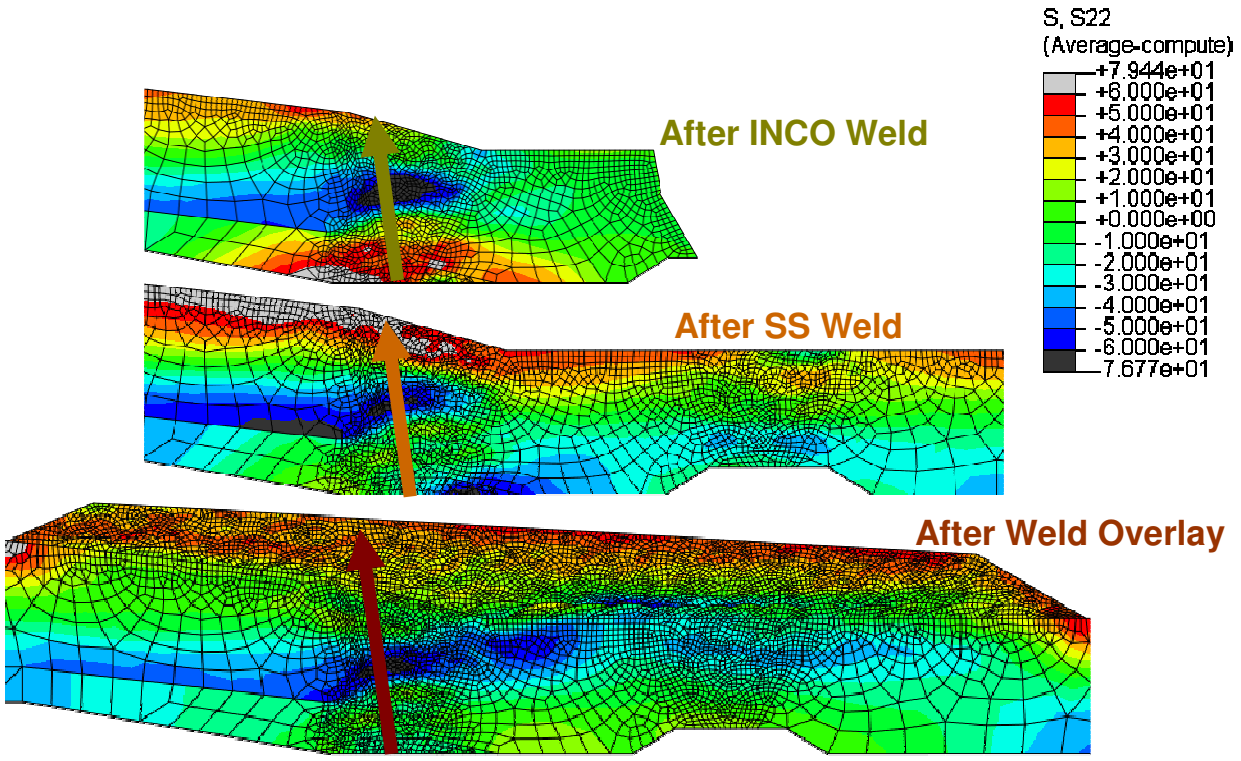

Figure 20 Surge Nozzle Axial Stresses Through Thickness

The axial stress contour plot and graph show that the Inconel weld is in tension at the inner diameter, compression in the center, and tension at the outer diameter after the dissimilar metal weld is completed. The application of the stainless steel weld has the effect of lessening the tension stress on the inner diameter of the Inconel weld, and in fact, making it compressive in this cross section on the inner diameter surface. In this cross section, the axial stress remains approximately the same after applying the FSWOL, with the compression stresses at the inner diameter being slightly reduced.

The PWSCC occurrences are typically found in the dissimilar metal weld at the interface between the A508 material and the butter layer, or between the butter and the Inconel weld. The weld residual stresses in the stainless steel weld are of less importance.

PWSCC is caused by high tensile weld residual stresses on the inner diameter of the pipe. Between 1993 and 2007 there have been at least eight PWR plants around the world that have found indications in dissimilar metal welds, of which, at least three axial cracks grew through the wall to the point of leaking. No circumferential cracks have been found which have grown through the thickness of the pipe and leaked [13,14].

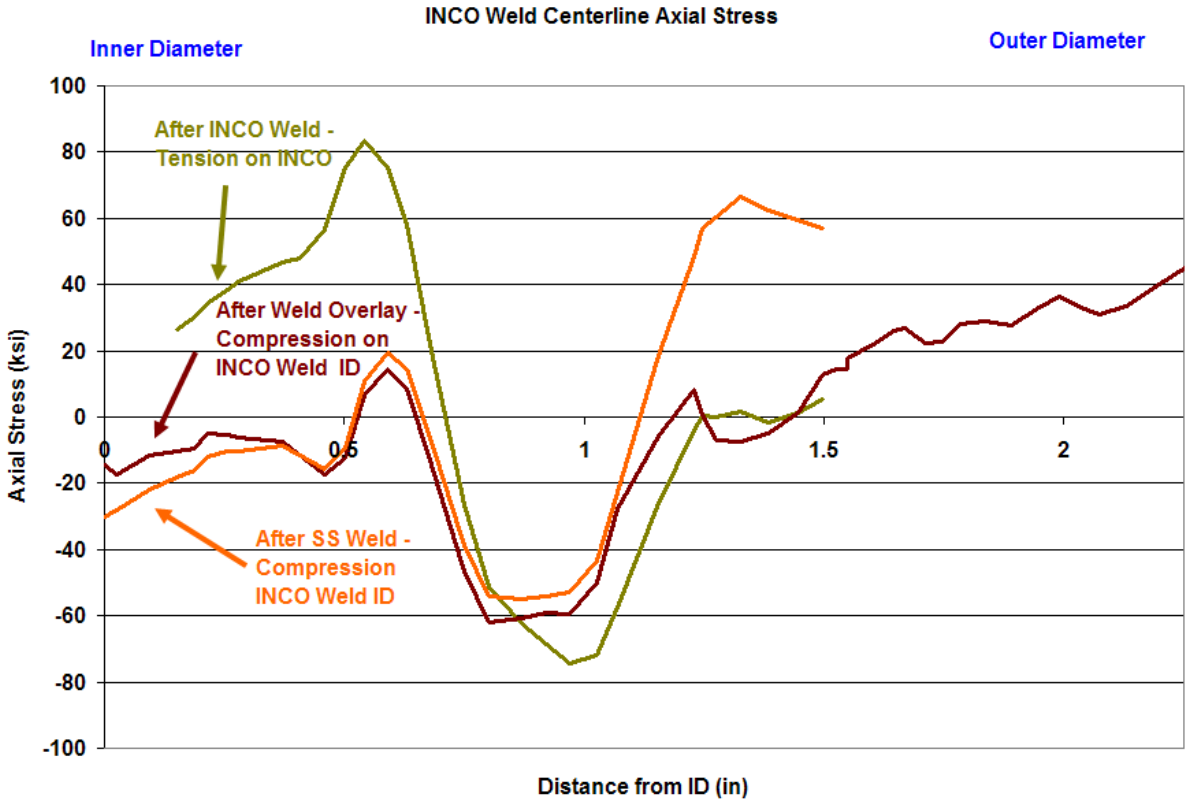

Figure 21 Surge Nozzle Through Thickness Axial Stresses

Figure 21 shows that the Inconel weld is for the most part in compression over the inner half of its thickness after the FSWOL is applied despite the compression reduction at the inner diameter.

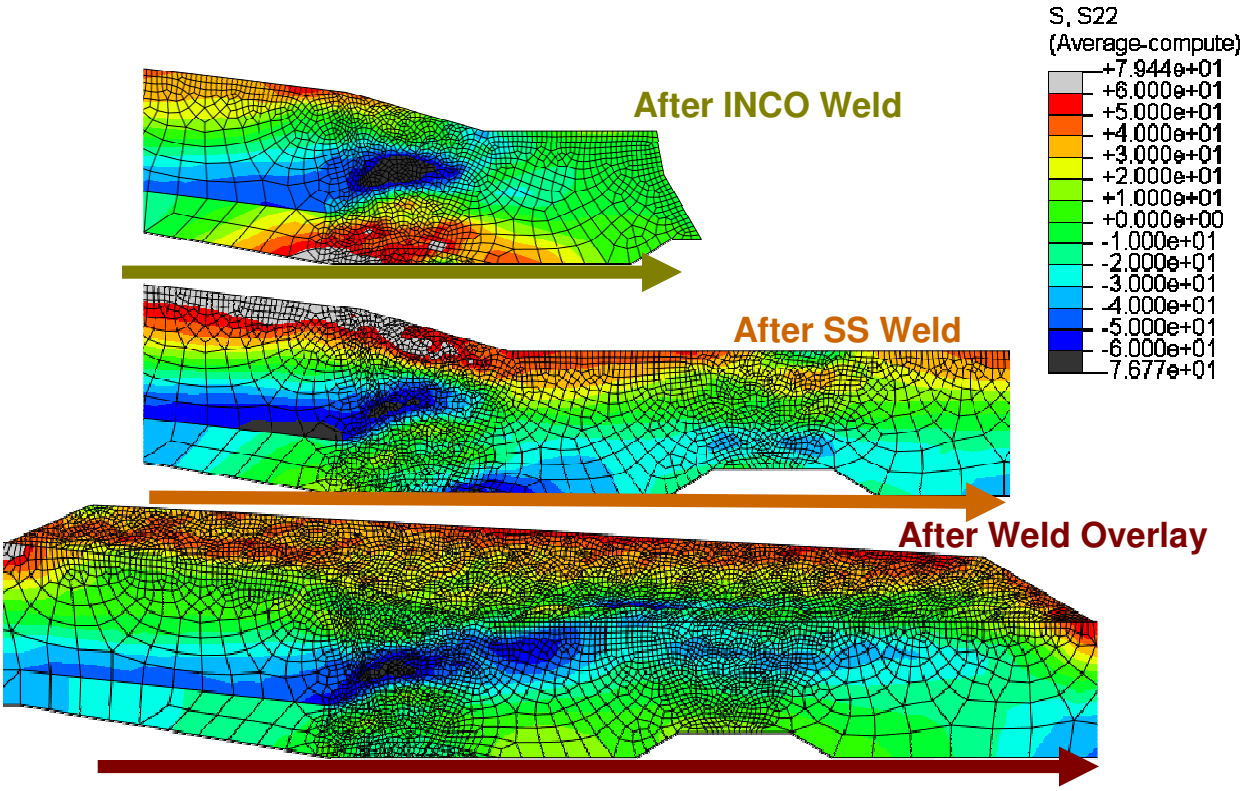

Figure 22 Surge Nozzle Inner Diameter Axial Stresses

Figure 22 and Figure 23 show the inner diameter path and axial stress along that path. Figure 23 indicates the position of both the dissimilar metal weld and the secondary stainless steel weld with color coded vertical bars on the graph, and an appropriately scaled section of the model shown above the graph.

One can see that the stress was very high in the butter and dissimilar metal weld before the secondary stainless steel weld was made. Once the secondary stainless steel weld was completed, the stresses along the inner diameter were primarily compressive except in the area of the transition between the carbon steel nozzle and the butter. In this area the stresses remain tensile in the range of 138 MPa (20 ksi). After the FSWOL is completed, the stresses along the inner diameter of the DMW have been made compressive or reduced to near zero. Note also that the stresses are also compressive along the entire inside surface of the safe end after the secondary stainless steel weld is fabricated. However, after the FSWOL is applied, the safe end stresses along the safe end become tensile (less than 138 MPa (20 ksi). This may be important for those cases in which the safe end is fabricated from Alloy 600 material which is susceptible to PWSCC.

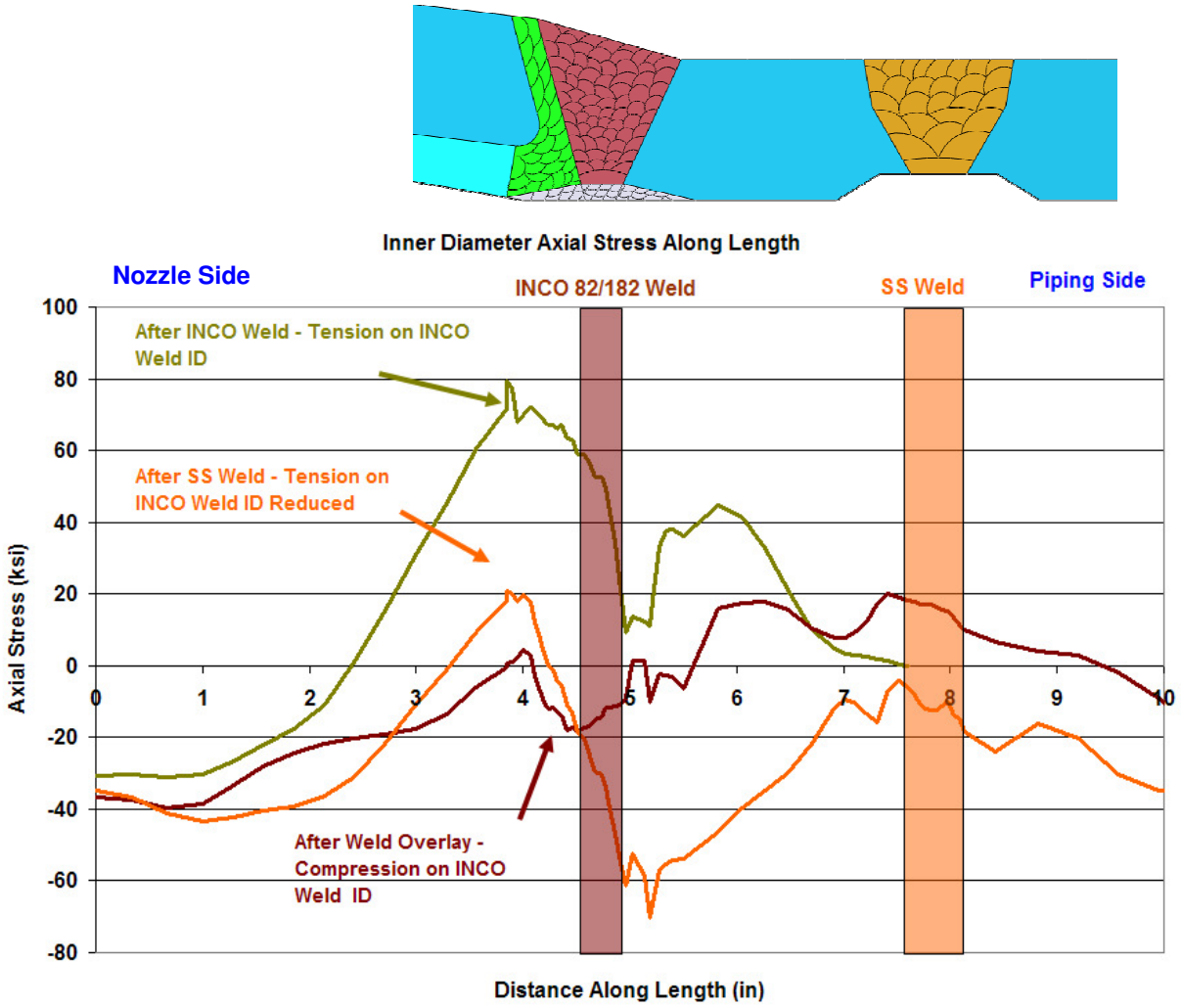

Figure 23 Surge Nozzle Inner Diameter Axial Stresses Along Length of the Pipe at the Inside Surface

Figure 24 and Figure 25 show the through thickness hoop stresses before and after the application of the FSWOL. The stress contour plot and the graph show that the secondary stainless steel weld has the effect of reducing the hoop stress in the dissimilar metal weld, but not to the extent that it does for the axial stresses. The FSWOL decisively reduces the through thickness hoop stresses into compression for approximately the inner 80 percent of the original wall thickness.

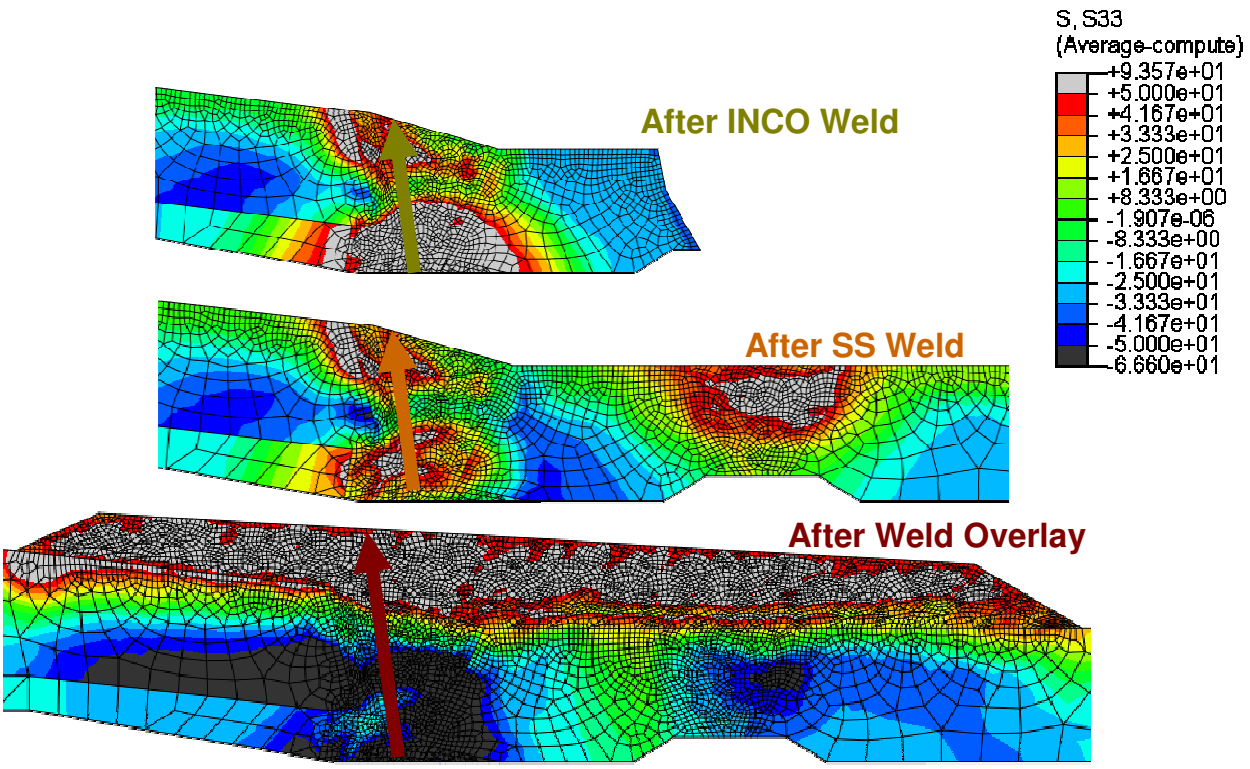

Figure 24 Surge Nozzle Through Thickness Hoop Stresses

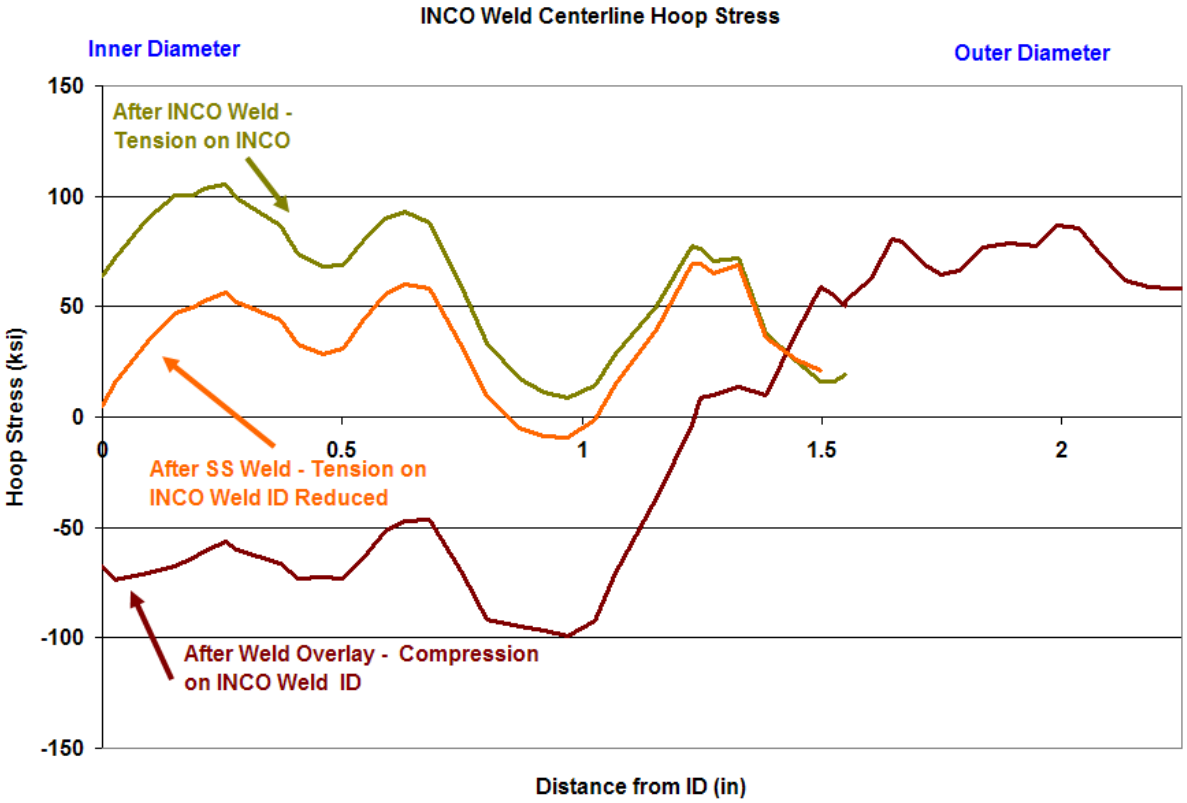

Figure 25 Surge Nozzle Through Thickness Hoop Stresses

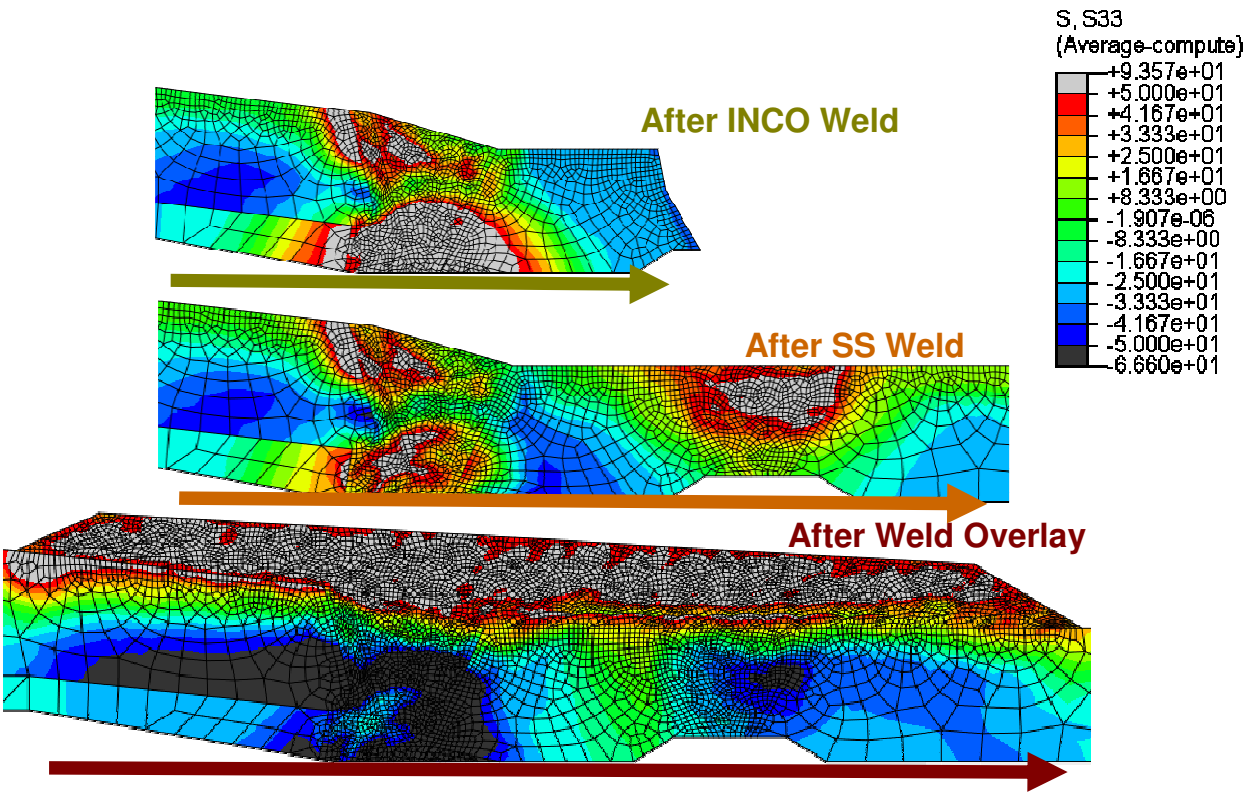

Figure 26 Surge Nozzle Inner Diameter Hoop Stresses

Figure 26 and Figure 27 show the inner diameter hoop stresses along the length of the dissimilar metal weld area of the surge nozzle. The graph shows that hoop stresses are very high on the inner diameter of the DMW before the secondary stainless steel weld is made, and are reduced, but remain tensile after the stainless steel weld is completed. The stresses remain especially high in the area of the butter transition to the carbon steel nozzle. The FSWOL reduces the hoop stresses in the area of concern to be compressive over the entire length of the dissimilar metal weld area.

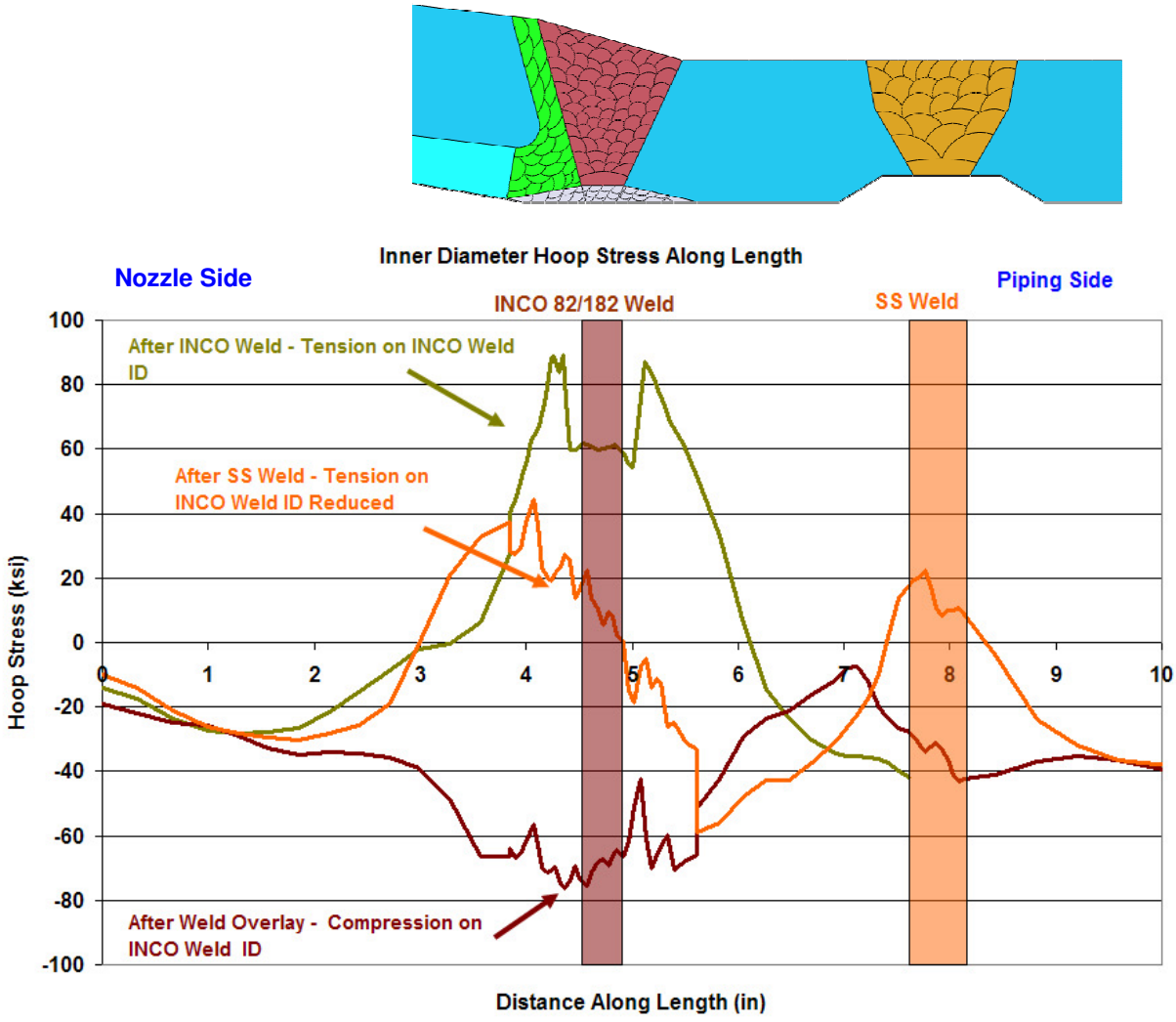

Figure 27 Surge Nozzle Inner Diameter Hoop Stresses

The previous surge nozzle stress plots and graphs were all made at room temperature and pressure. The following graphs show the effect of operating pressure and temperature on the surge nozzle axial and hoop stresses. An operating pressure of 15.5 MPa (2,250 psi) was used throughout this study for all of the geometries. An operating temperature of 300 C (572 F) was used for the surge nozzle analyses. While this value is lower than the actual pressurizer surge nozzle service temperature, as shown in subsequent analyses, the effect of this relatively small difference in temperature is not expected to be significant.

Figure 28 shows the axial stress in the surge nozzle dissimilar metal weld after the FSWOL (top figure), after the application of the operating pressure including the end load on the pipe (middle figure), and finally it shows the stresses after operating temperature has been added (bottom figure). The path and color code for the through thickness stress graphs to follow are also indicated on this figure. Figure 29 shows the through thickness axial stress and Figure 30 shows the through thickness hoop stress. The magnitude of the inner diameter axial compressive stress is increased (more compressive) by the application of operating pressure and temperature. The axial compression is increased from 103 MPa (-

15 ksi) to 206 MPa (-30 ksi). The hoop stress at the inner diameter remains relatively unchanged at a value of -448 MPa (-65 ksi) by the application of operating loads.

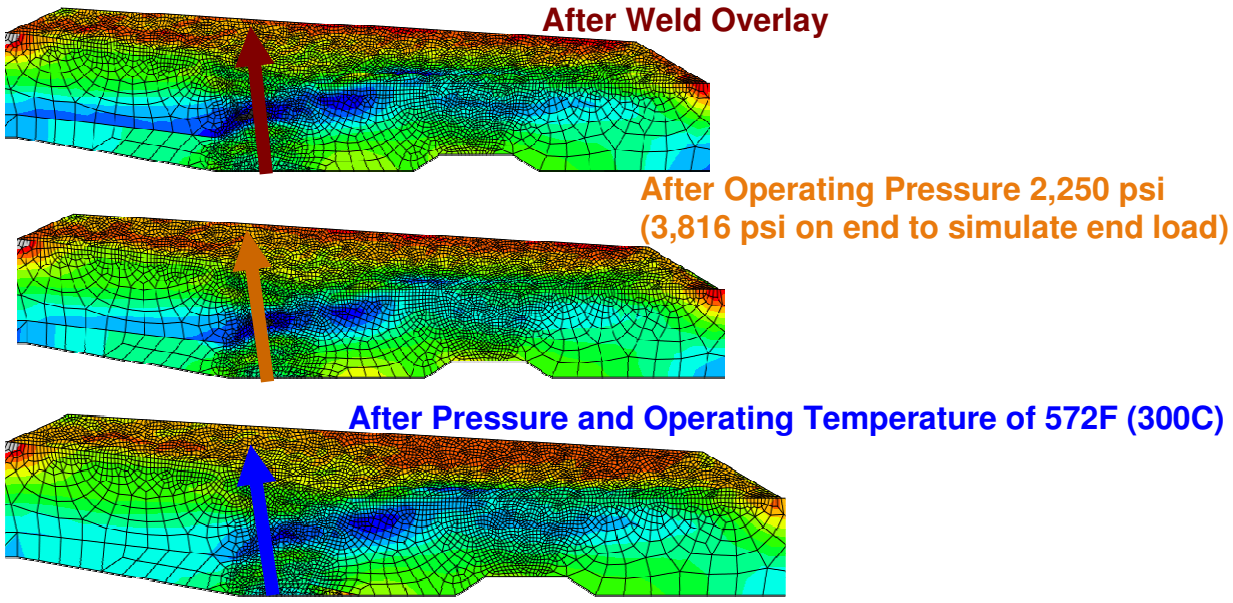

Figure 28 Surge Nozzle Post-FSWOL Axial Stresses with Operating Pressure and Temperature

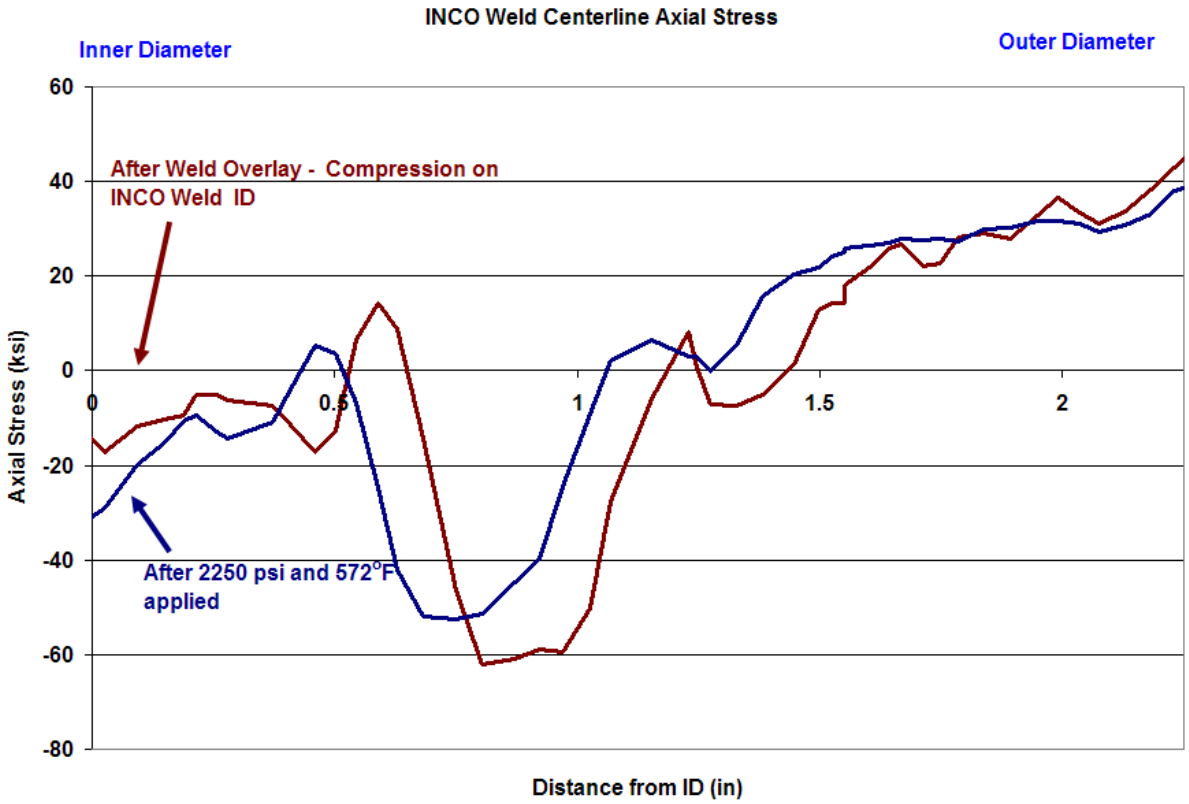

Figure 29 Surge Nozzle Through Thickness Axial Stresses after the FSWOL is Applied and After the Operating Pressure and Temperature are Applied

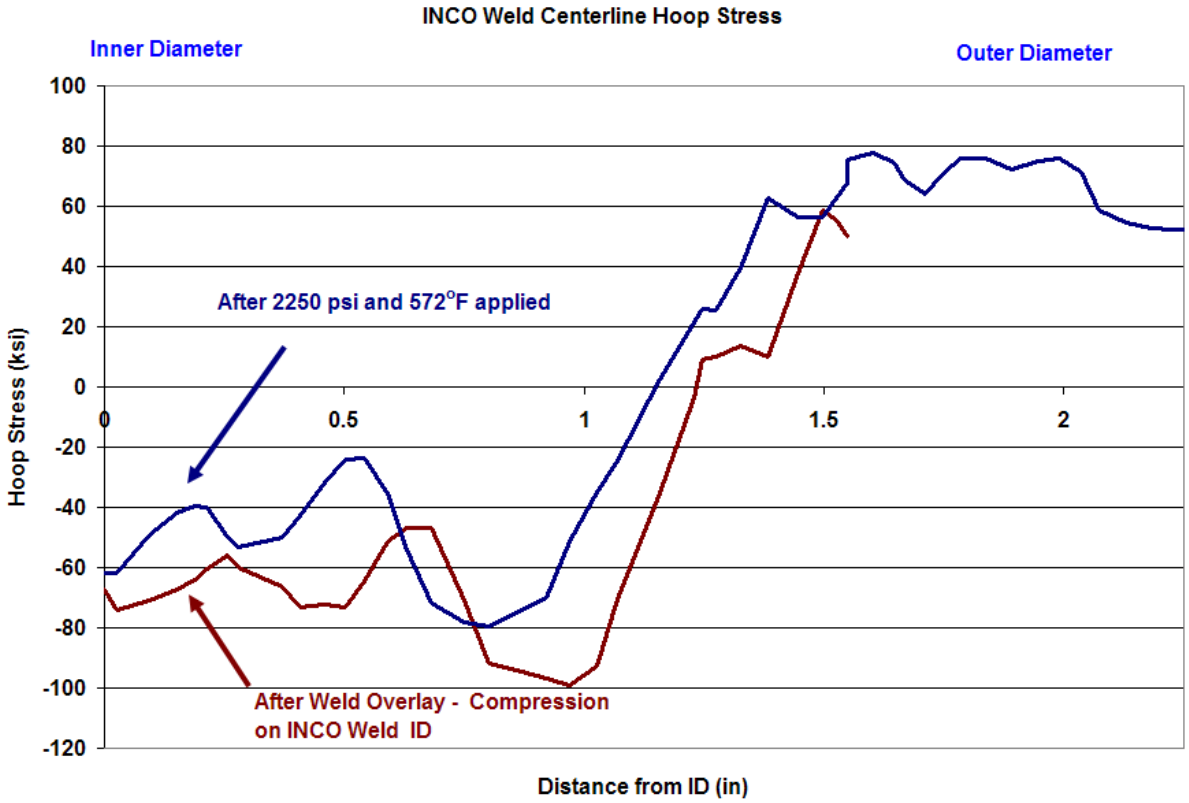

Figure 30 Surge Nozzle Through Thickness Hoop Stresses after the FSWOL is Applied and After the Operating Pressure and Temperature are Applied

4.1.2 Pressurizer Safety Nozzle

The pressurizer safety nozzle is similar in geometry to the surge nozzle, but is smaller in size. The geometry and weld locations are shown in Figure 15. The weld residual stresses were developed as shown in Figure 31 in a similar fashion as to what was done for the surge nozzle. The figure shows the initial welding of the butter layer and the post weld heat treatment of the butter layer at 593 C (1,100 F) for four hours in which creep properties are allowed to relax the welding residual stresses in the butter layer. The butter layer is then pre-heated to 121 C (250 F), and the dissimilar metal weld is then built up pass by pass until the weld is complete. This process joins the stainless steel safe end to the carbon steel nozzle. The welded joint is allowed to cool to approximately 66 C (150 F) between passes and to room temperature after the weld is complete. The root pass is ground out and re-welded as a final step in the dissimilar metal weld. Next, the secondary stainless steel weld is built up and allowed to cool to room temperature.

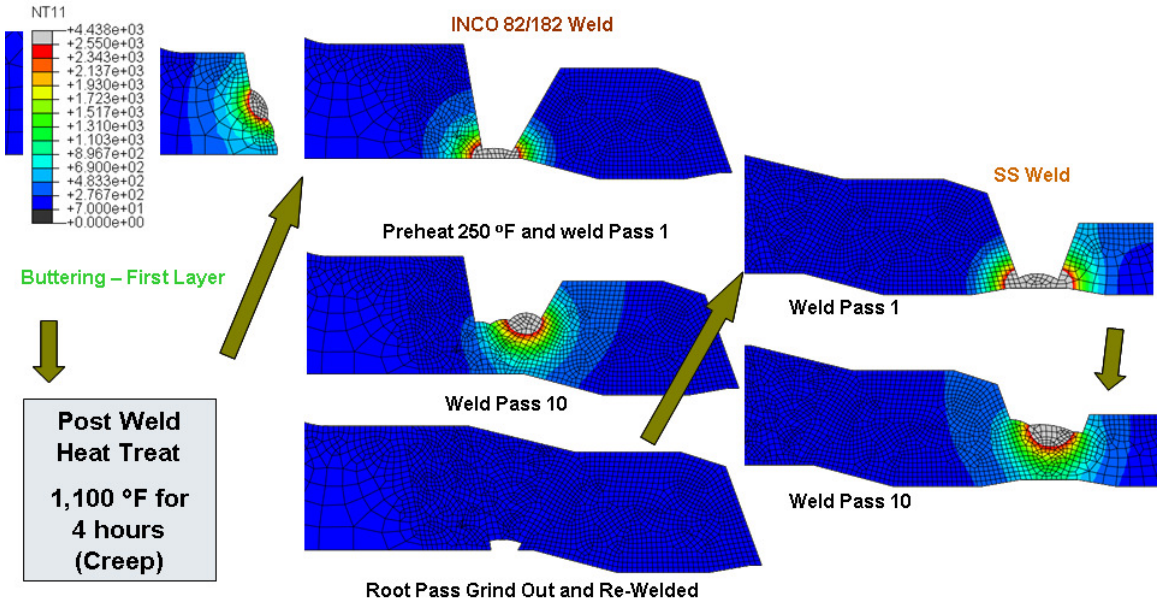

Figure 31 Safety Nozzle Weld Deposition

Figure 32 shows the schematic of the axi-symmetric application of the safety nozzle FSWOL. Figure 15 shows more detailed dimensions of the safety nozzle geometry including the FSWOL.

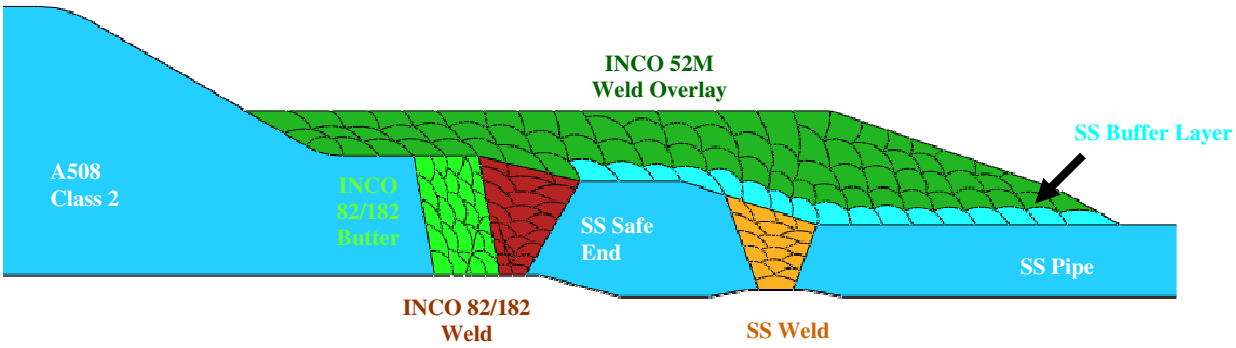

Figure 32 Safety Nozzle FSWOL Application

Figure 33 shows the axial stress contour plot after the Inconel weld has been completed (top figure), after the stainless steel weld has been completed (middle figure), and after the FSWOL has been fabricated (bottom figure). The arrows through the weld indicate the path followed for the graphed data shown in Figure 34. The graph shows results similar to those produced in the surge nozzle. The axial stress at the inner diameter is high after the dissimilar metal weld is completed. The secondary stainless steel weld connecting the safe end to the stainless steel piping greatly reduces the inner diameter stress at the dissimilar metal weld. In this geometry, the secondary stainless steel weld places the inner diameter firmly in a compressive stress region at this cross section. The FSWOL further reduces the axial stresses to be in compression through about half the thickness of the original weld, but the stress at the inner

diameter of this cross section is actually increased slightly in this cross section by the FSWOL, though still strongly compressive.

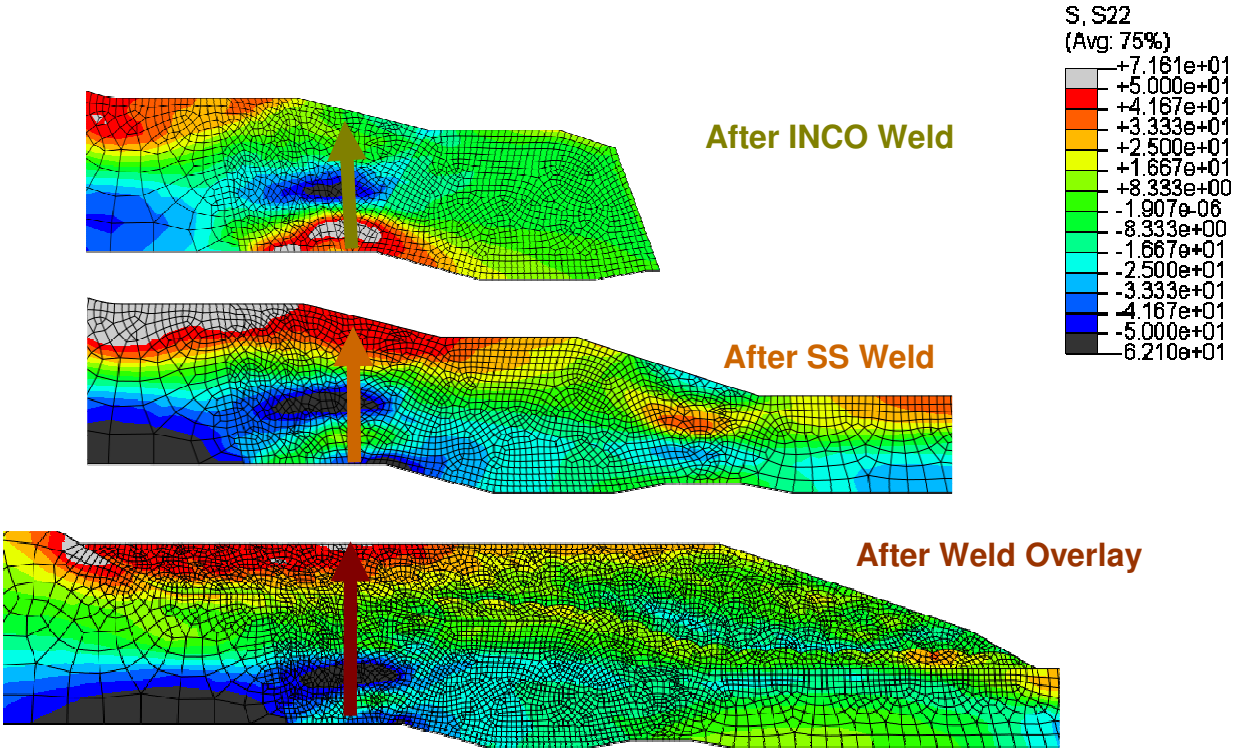

Figure 33 Safety Nozzle Through Thickness Axial Stresses

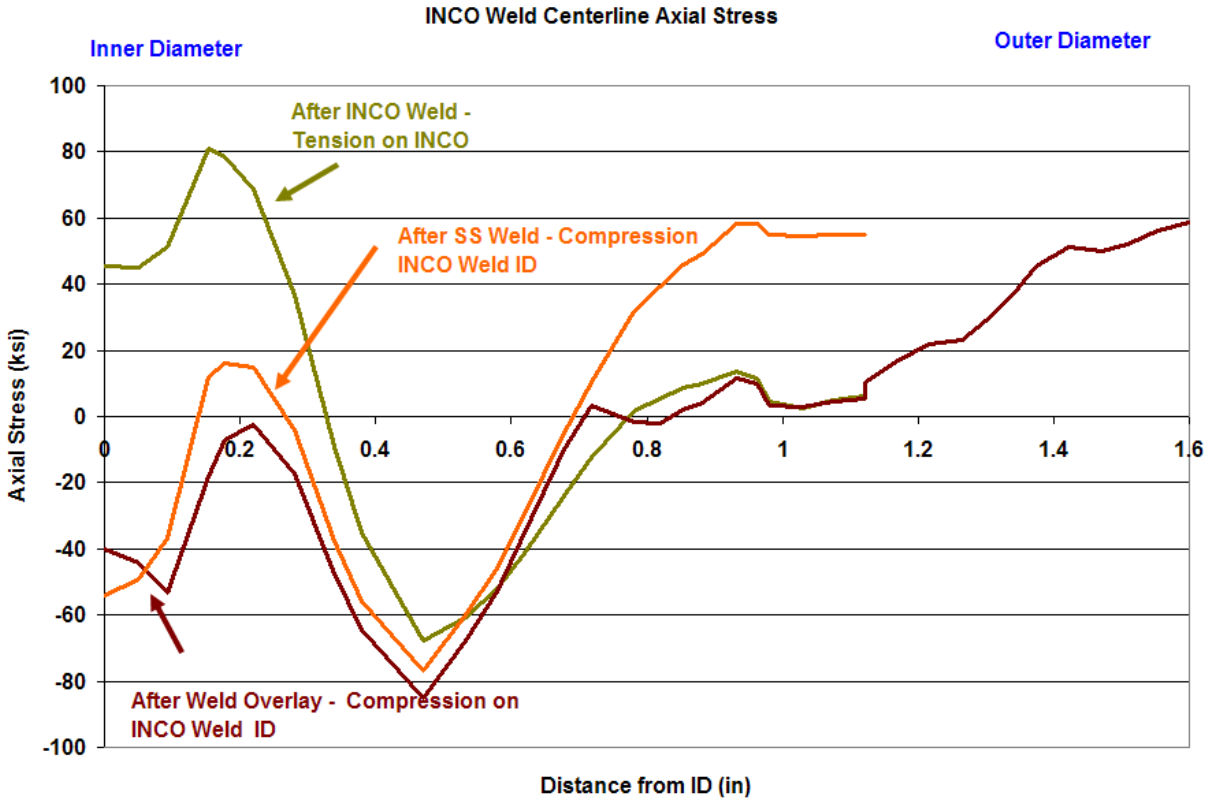

Figure 34 Safety Nozzle Through Thickness Axial Stresses

Figure 35 and Figure 36 indicate the path and inner diameter axial stresses. The cross section of the safety nozzle and vertical color coded bars are used in the graph for reference to indicate the location of the dissimilar metal weld and the secondary stainless steel weld. The graph is similar to that of the surge nozzle, in which the stresses on the inner diameter of the dissimilar metal weld are highly tensile before the secondary stainless steel weld is completed. They are greatly reduced by the stainless steel weld and are further reduced in the butter area by the FSWOL. Though the FSWOL actually increases the stresses slightly in the area of the dissimilar metal weld, the overall effect is the increase in compression in the area of the butter.

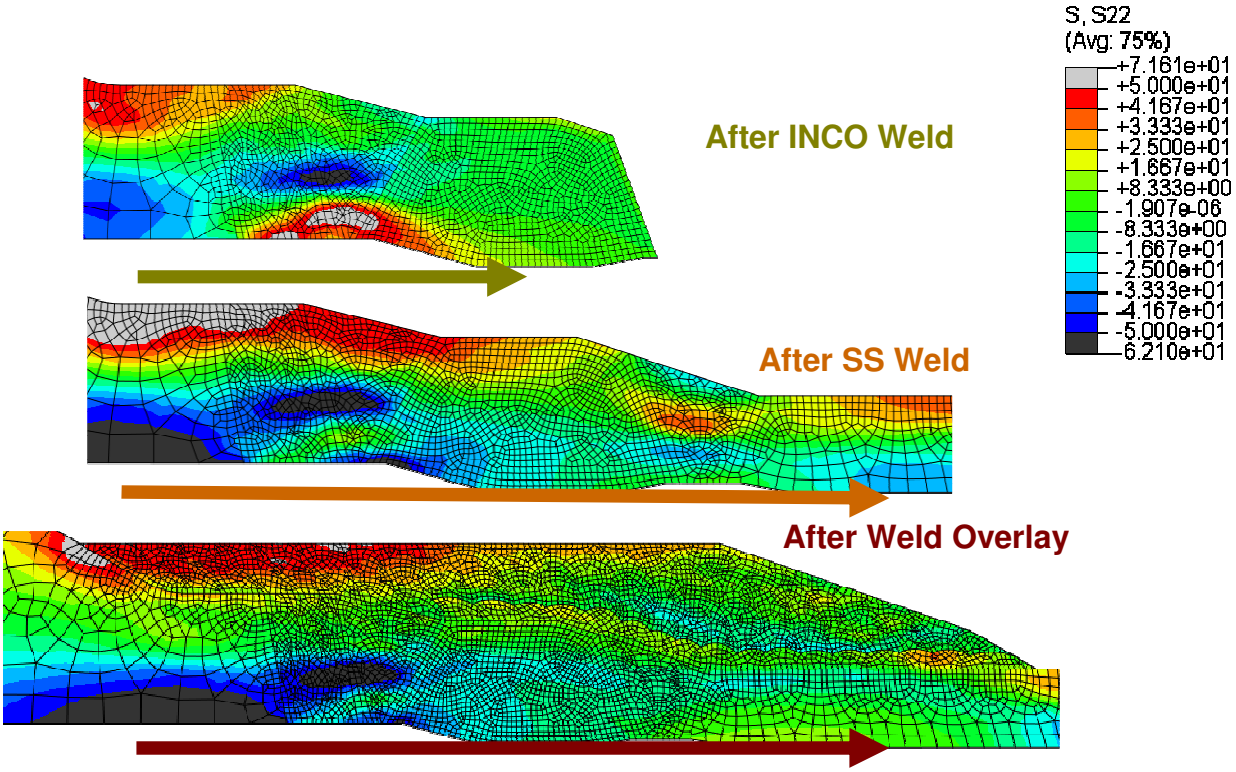

Figure 35 Safety Nozzle Inner Diameter Axial Stresses

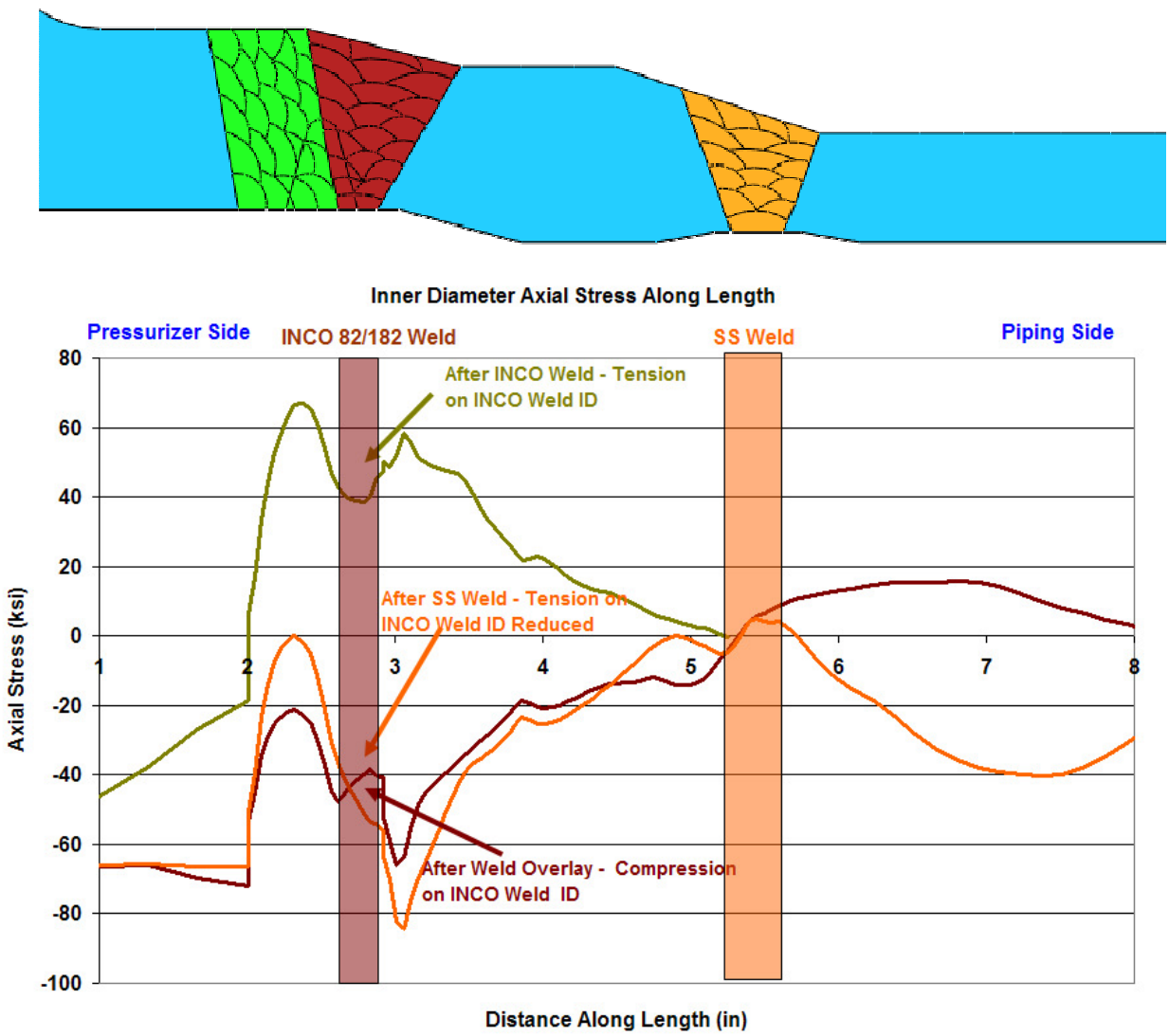

Figure 36 Safety Nozzle Inner Diameter Axial Stresses Along Length of the Pipe at the Inside Surface

Figure 37 and Figure 38 show the through thickness hoop stress along the path indicated. The graph shows that the dissimilar metal weld hoop stress is greatly reduced by the secondary stainless steel weld. The FSWOL further reduces the hoop stress through the thickness and places it in compression through the entire thickness of the original weld.

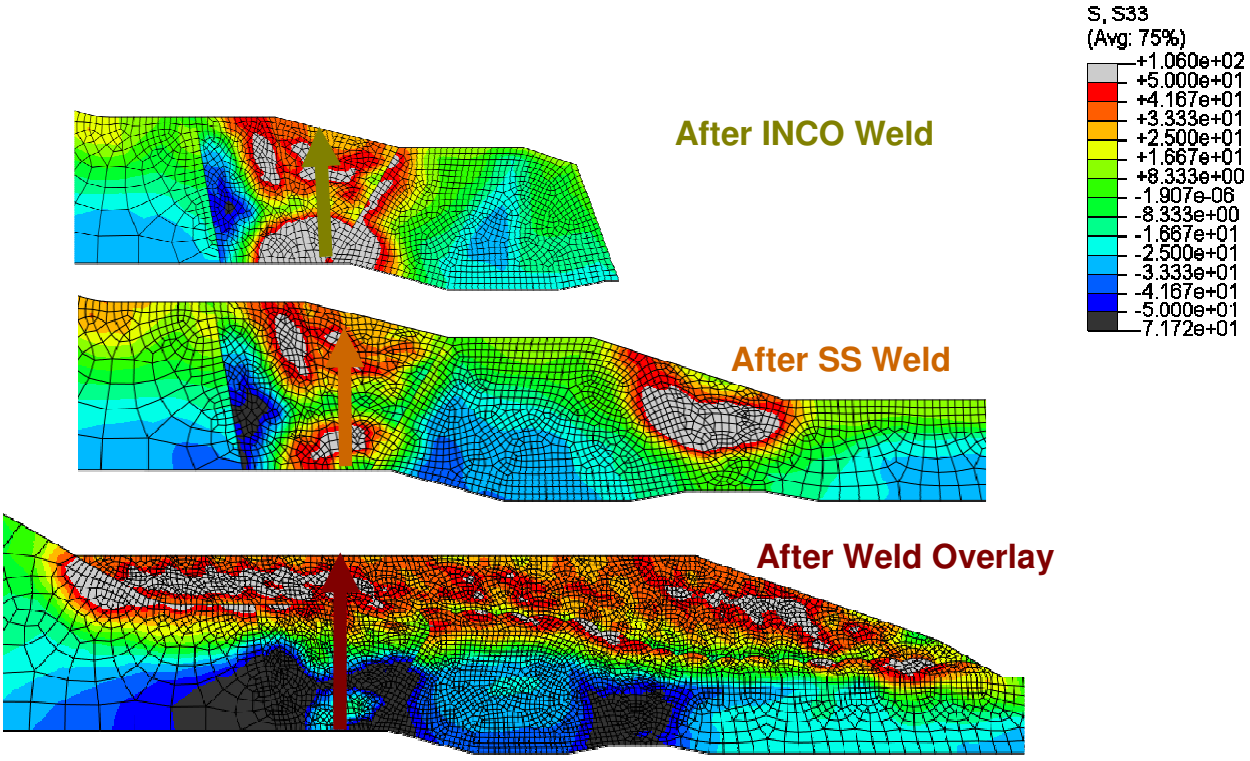

Figure 37 Safety Nozzle Through Thickness Hoop Stresses

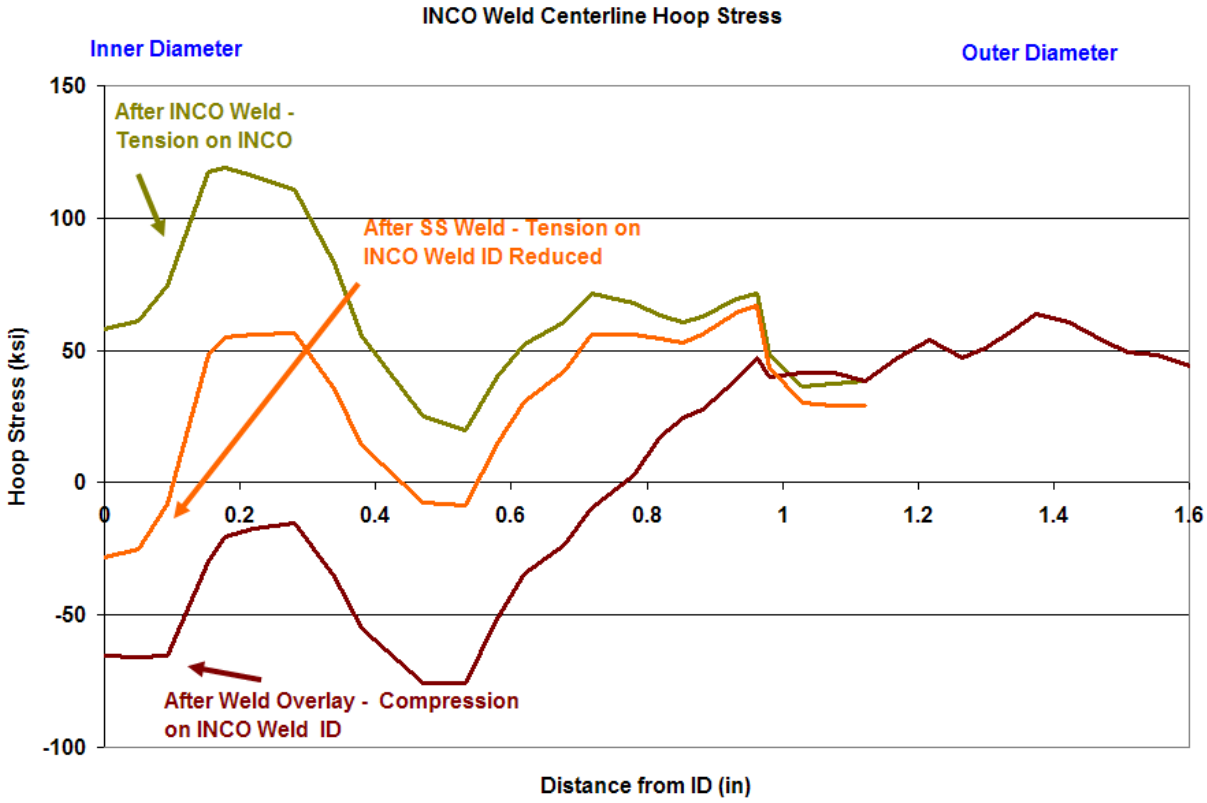

Figure 38 Safety Nozzle Through Thickness Hoop Stresses

Figure 39 and Figure 40 show the inner diameter hoop stress along the path indicated. The hoop stress is compressive along the inside surface after the application of the FSWOL for the entire area of the dissimilar metal weld.

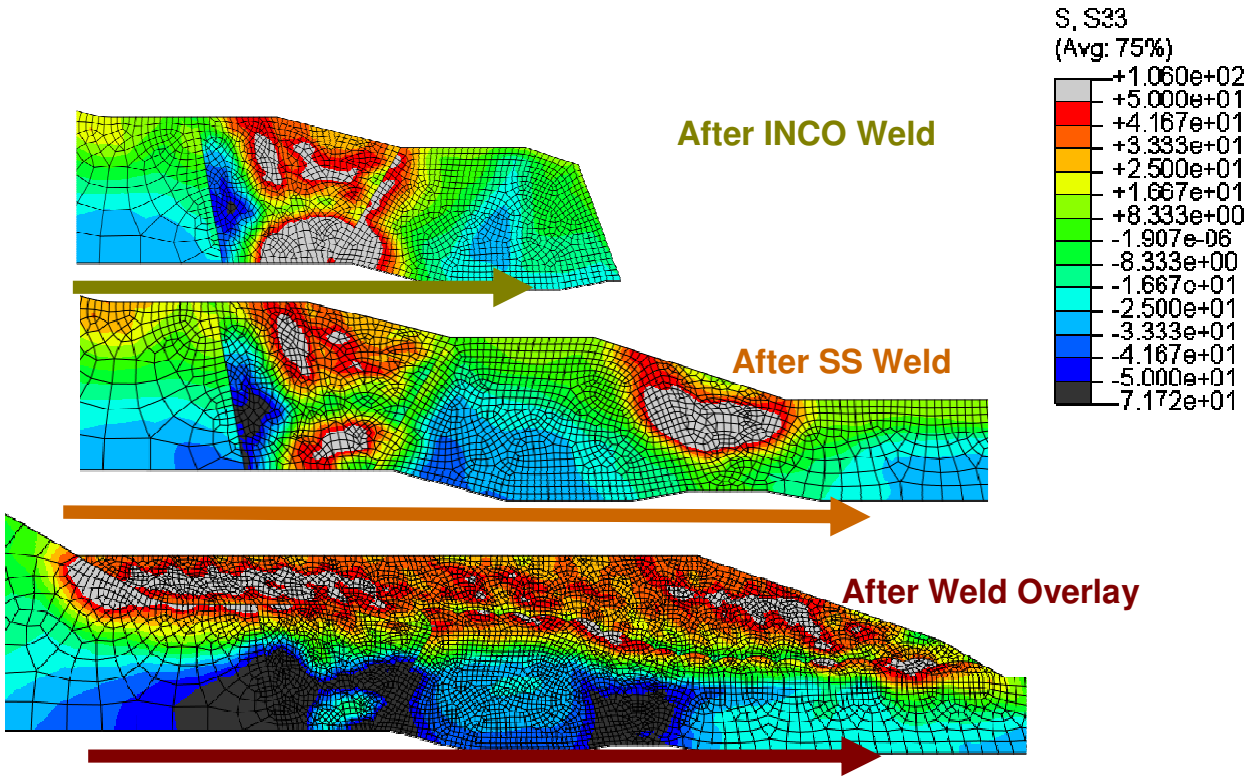

Figure 39 Safety Nozzle Inner Diameter Hoop Stresses

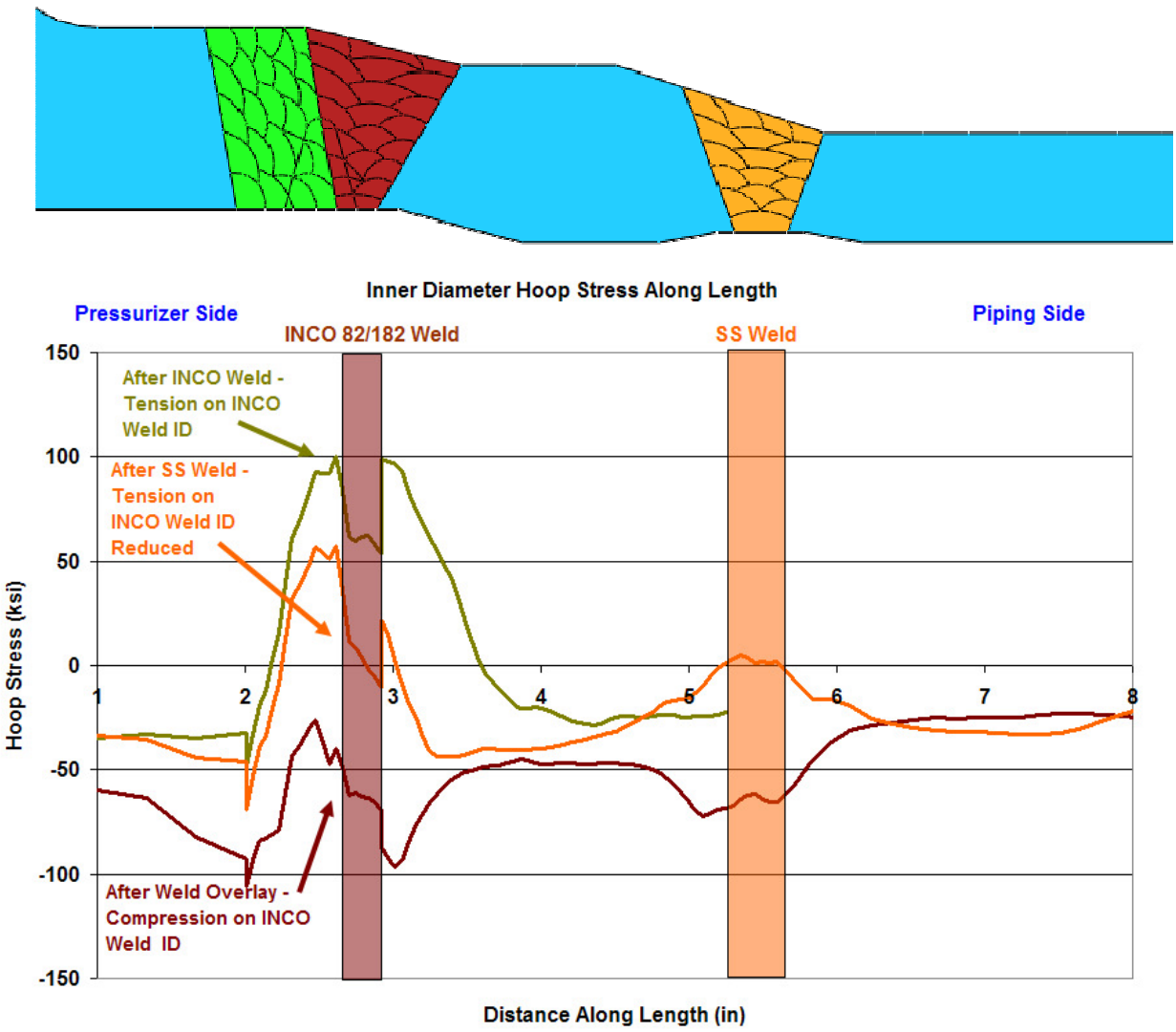

Figure 40 Safety Nozzle Inner Diameter Hoop Stresses Along Length of Pipe at Inside Surface

Figure 41 through Figure 43 show the effect of operating pressure and temperature on the axial and hoop stresses through the thickness of the safety nozzle. The stress contour plot shows the path used to describe the through thickness stresses. For this geometry, the standard operating pressure of 15.5 MPa (2,250 psi) was applied and then an operating temperature of 322 C (611F) was added. The axial stresses are only slightly affected by the application of operating pressure and temperature. As seen before, the hoop stresses are increased with the application of temperature and pressure, with the inner diameter remaining in compression at this cross section.

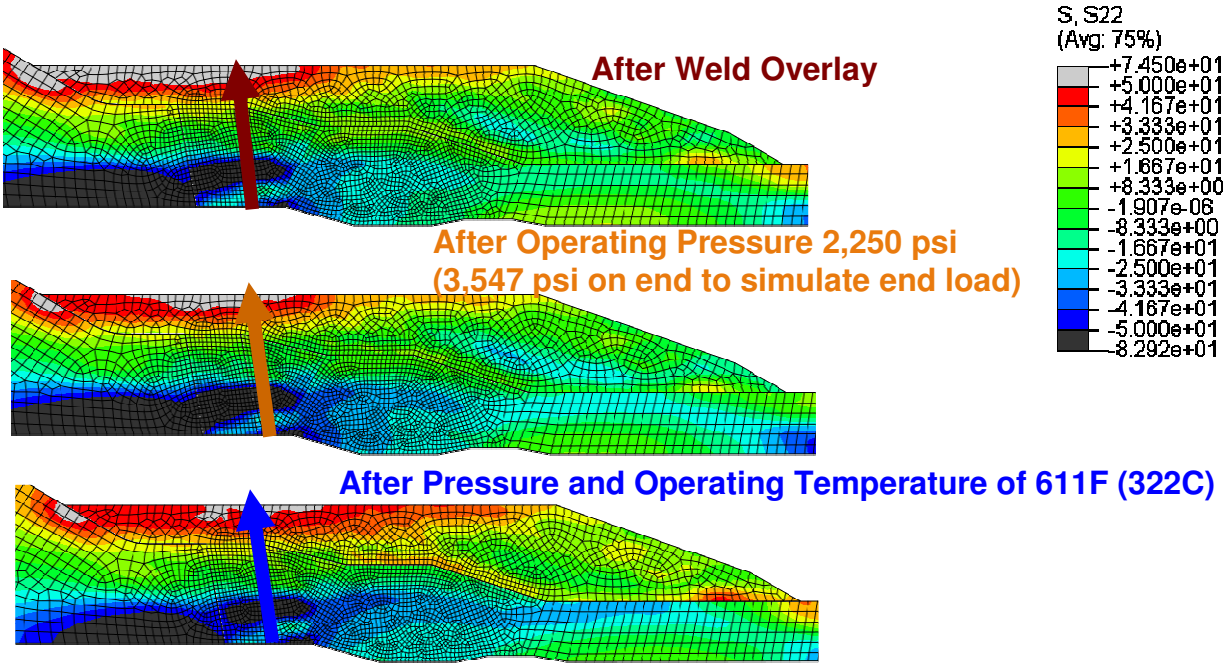

Figure 41 Safety Nozzle Axial Stresses with Operating Pressure and Temperature

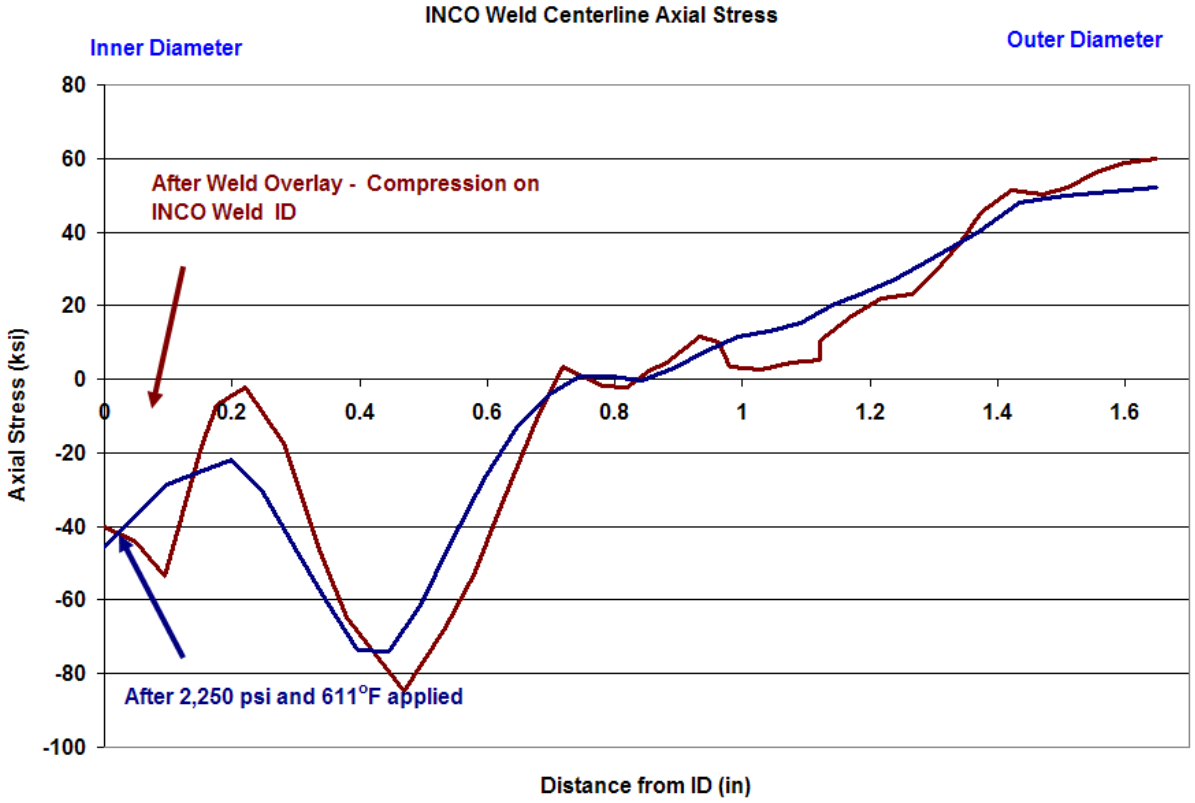

Figure 42 Safety Nozzle Post-FSWOL Axial Stresses with Operating Pressure and Temperature

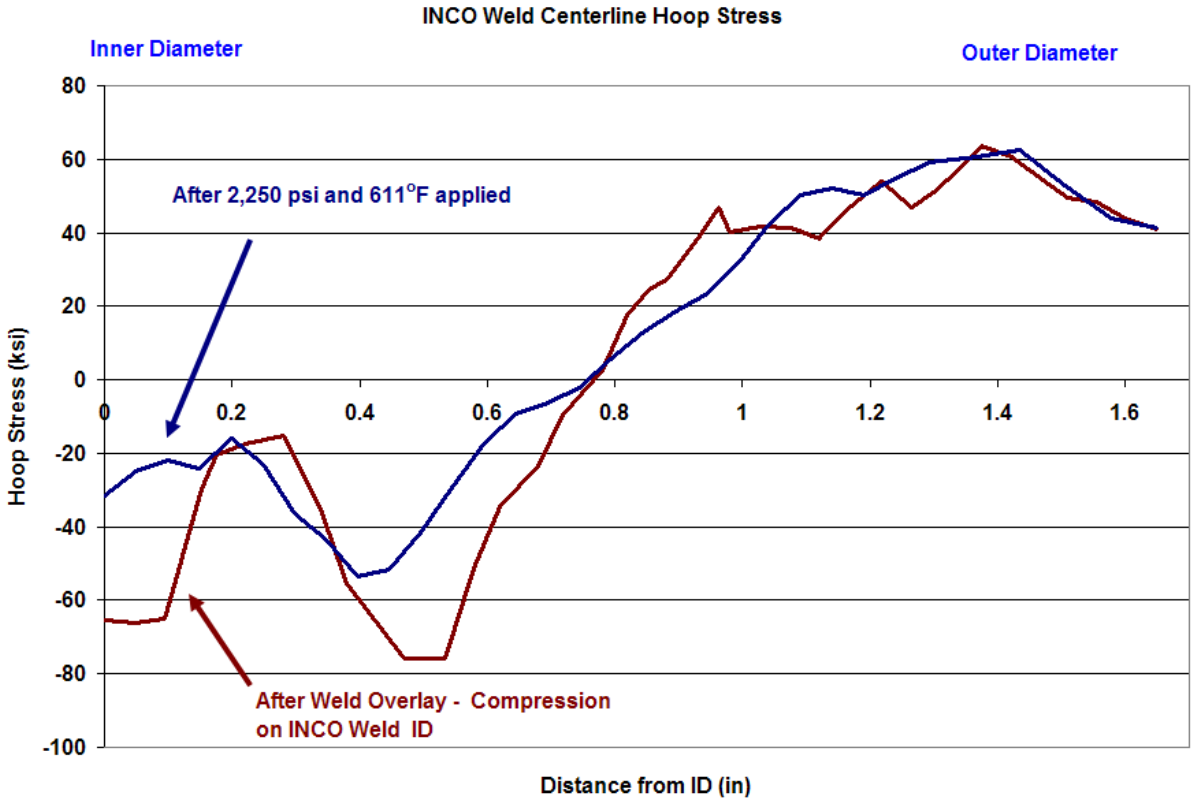

Figure 43 Safety Nozzle Post-FSWOL Hoop Stresses with Operating Pressure and Temperature

4.1.3 Cold Leg Reactor Pressure Vessel Nozzle

The cold leg/RPV nozzle weld residual stresses were developed in a similar way as those shown in Figure 8 for the surge nozzle. The notable exceptions are that this model includes a 25% inner diameter weld repair, which is simulated in addition to the root pass grind out and re-weld. The 25% ID weld repair is handled in a similar fashion with the repair being removed in one step, and then weld material is replaced, simulating the welding process, from the root of the weld toward the inner diameter of the pipe in seven passes.

Figure 44 shows the axial stress contour plot before the stainless steel safe end weld but after all Inconel welding is complete including the 25% ID repair (top figure), after the stainless steel safe end weld is finished (middle figure), and after the OWOL has been completed (bottom figure). The arrows through the weld indicate the path followed for the graphed data shown in Figure 45.

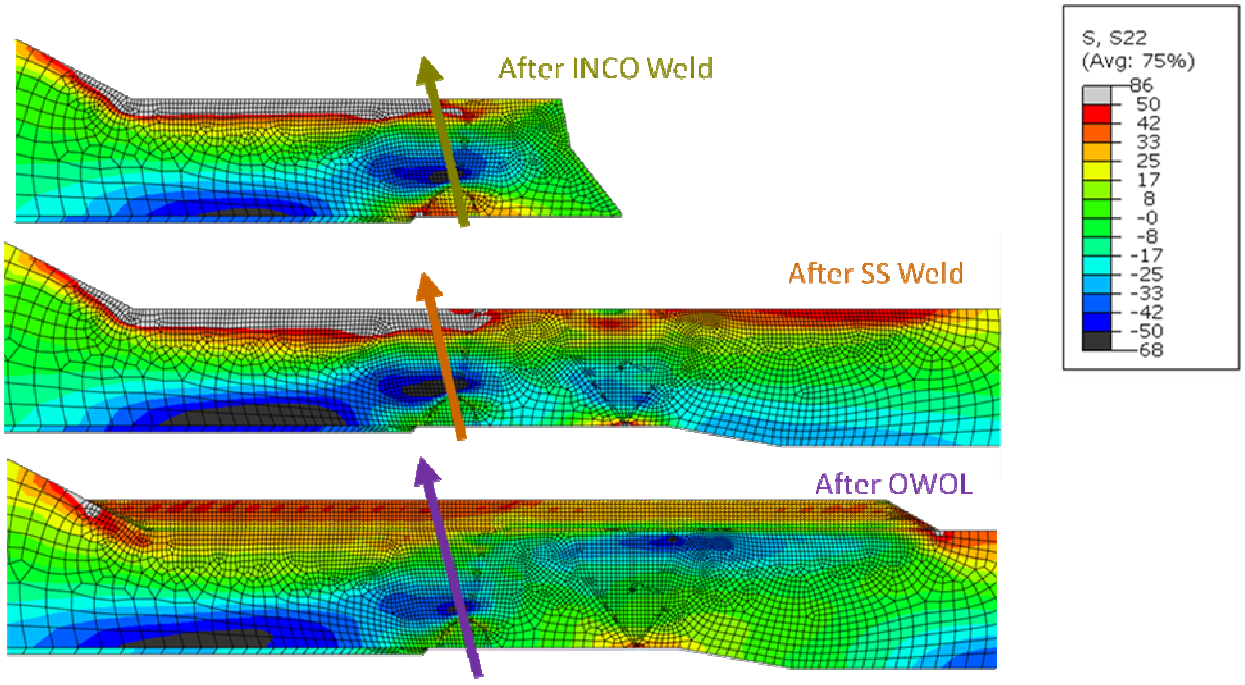

Figure 44 Cold Leg Nozzle Axial Stresses Through Thickness (ksi)

The axial stress contour plot and graph show that the Inconel weld is in tension at the inner diameter, compression in the center, and tension at the outer diameter after the dissimilar metal weld is completed. The application of the stainless steel weld has the effect of lessening the tension stress on the inner diameter of the Inconel weld, and in fact, making it compressive in this cross section on the inner diameter surface. In this cross section, the axial stress is slightly increased after applying the OWOL, with the compression stresses near zero.

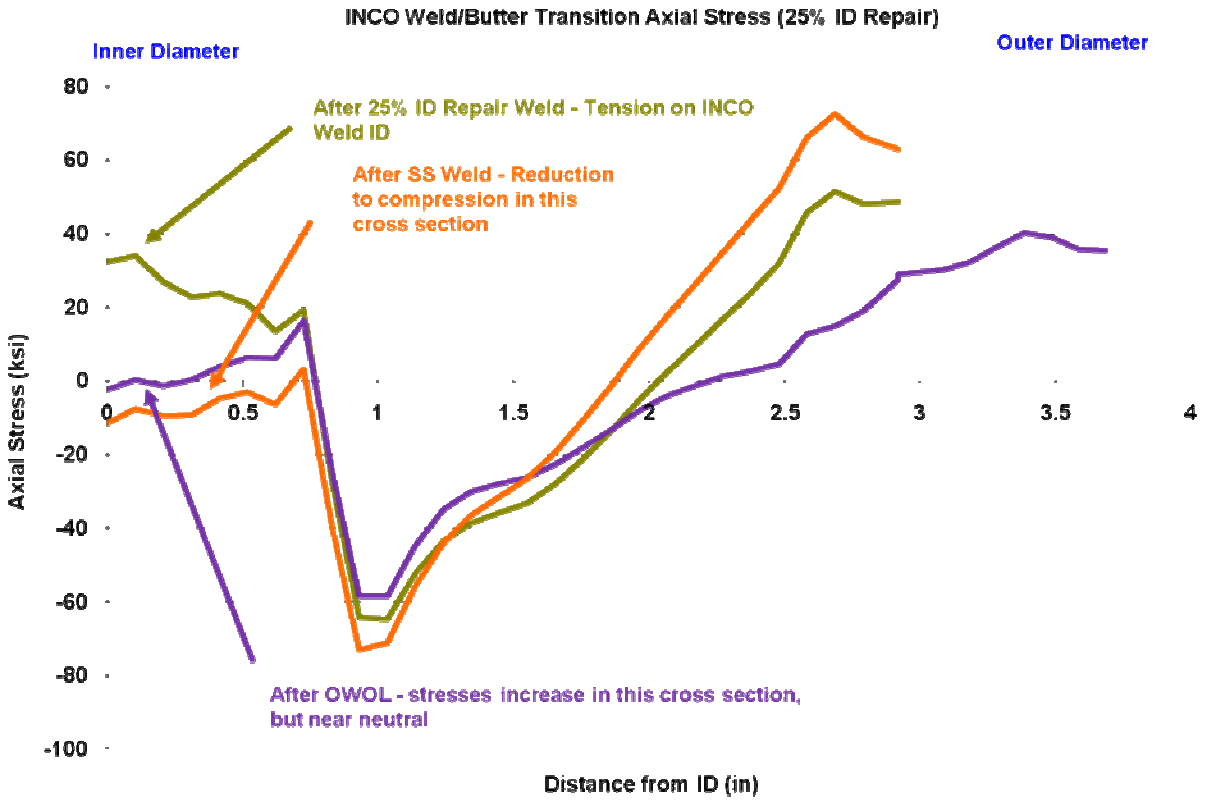

Figure 45 Cold Leg Nozzle Through Thickness Axial Stresses

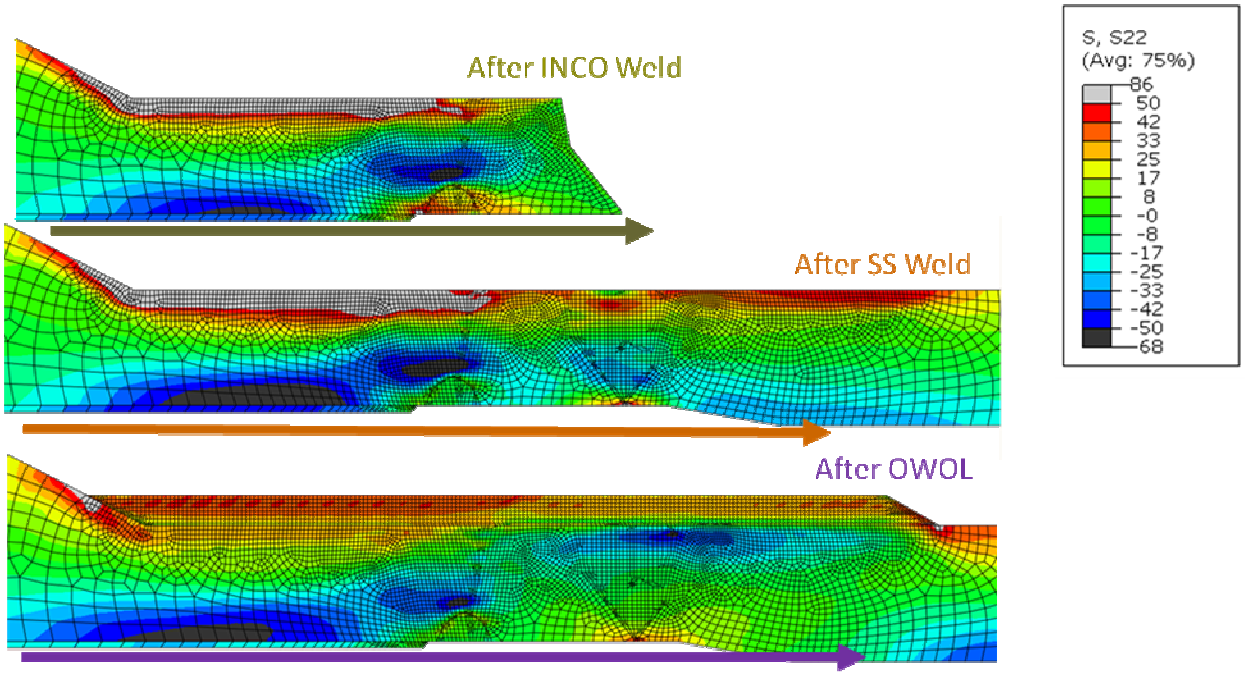

Figure 46 Cold Leg Nozzle Inner Diameter Axial Stresses (ksi)

Figure 46 and Figure 47 show the inner diameter path and axial stress along that path. Figure 47 indicates the position of both the dissimilar metal weld and the secondary stainless steel weld with color coded vertical bars on the graph.

One can see that the stress was very high in the butter and dissimilar metal weld before the secondary stainless steel weld was made. Once the secondary stainless steel weld was completed, the stresses along the inner diameter were primarily compressive except in the area of the transition between the carbon steel nozzle and the butter. In this area the stresses remain tensile in the range of 69 MPa (10 ksi). After the OWOL is completed the maximum tension stress is slightly reduced to 35 MPa (5 ksi), but the area that was already compressive after the secondary stainless steel weld was complete has had its compressive stresses reduced by the application of the OWOL. These results indicate little improvement for the application of the OWOL at room temperature, but the graphs that follow indicate that a beneficial effect is achieved when operating pressure and temperature are applied to the nozzle.

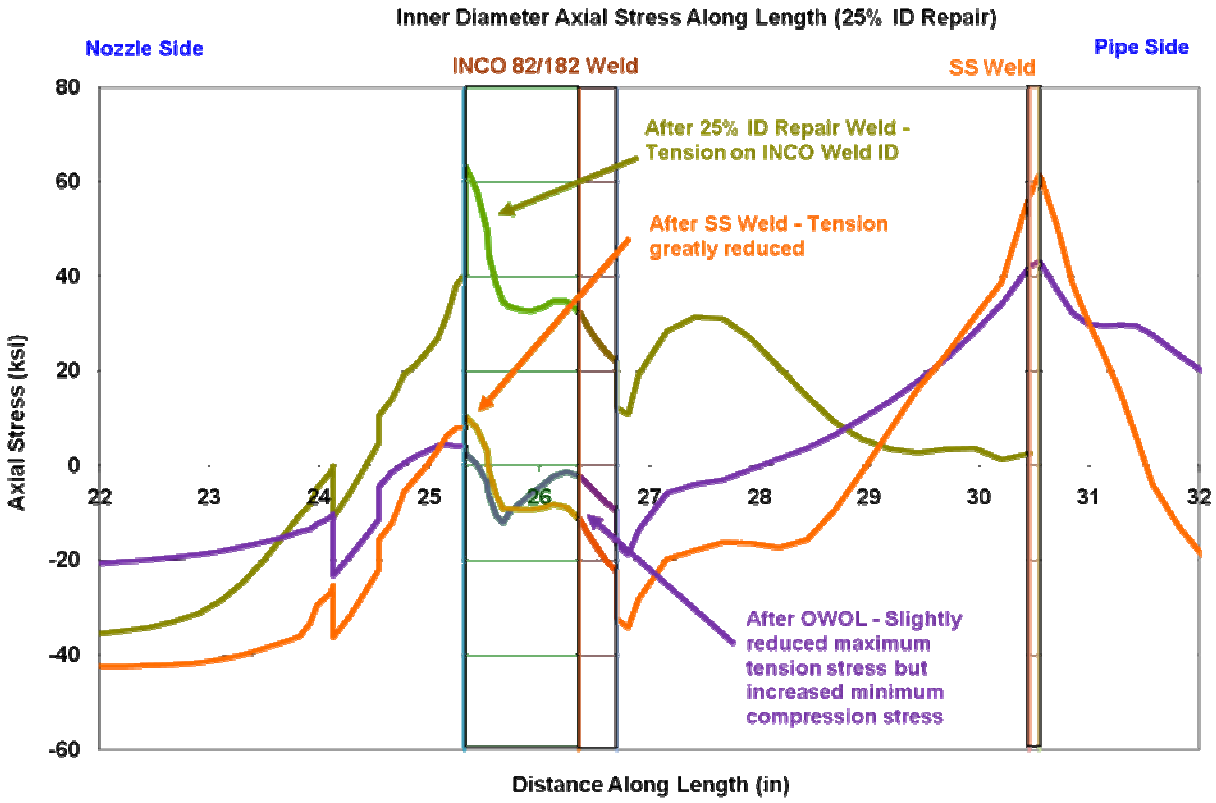

Figure 47 Cold Leg Nozzle Inner Diameter Axial Stresses Along Length of the Pipe at the Inside Surface

Figure 48 and Figure 49 show the through thickness hoop stresses before and after the application of the OWOL. The stress contour plot and the graph show that the secondary stainless steel weld has the effect of reducing the hoop stress in the dissimilar metal weld, but not to the extent that it does for the axial stresses. The ID stress remains in tension in this cross section. The OWOL reduces the through thickness hoop stresses into compression for approximately the inner 50 percent of the original wall thickness with the exception of one small spike into the tensile region at a quarter of the way through the original thickness at the peak of the 24% through thickness ID weld repair.

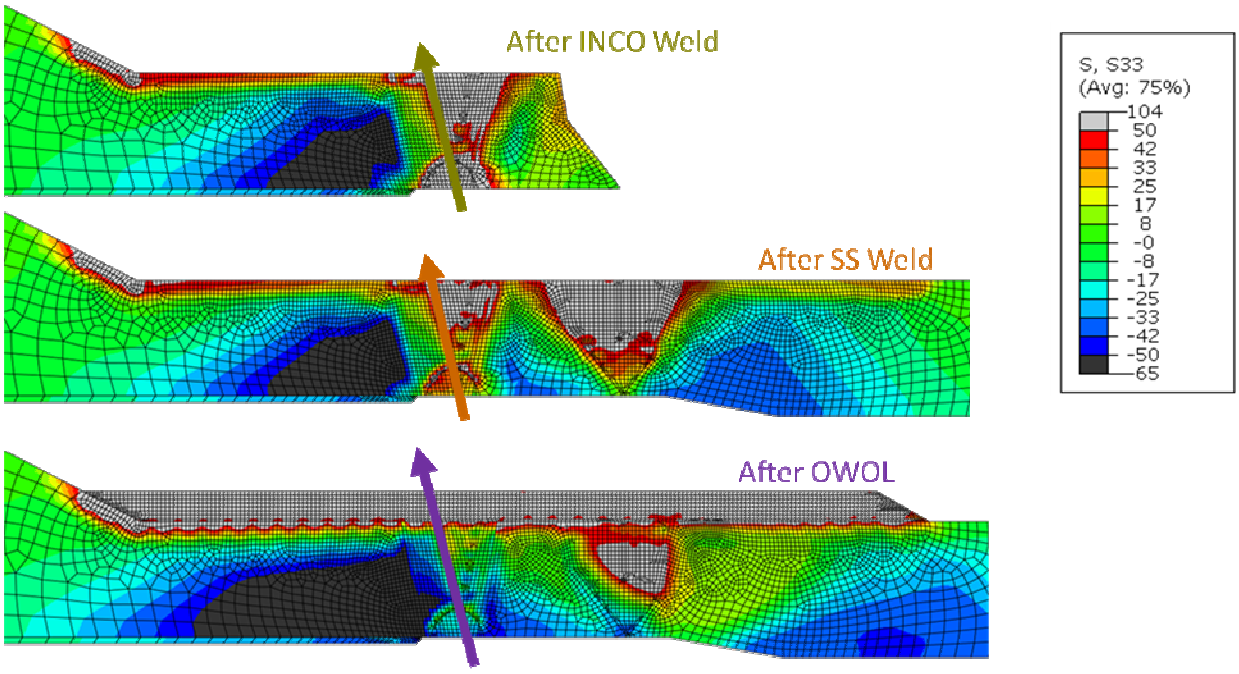

Figure 48 Cold Leg Nozzle Through Thickness Hoop Stresses (ksi)

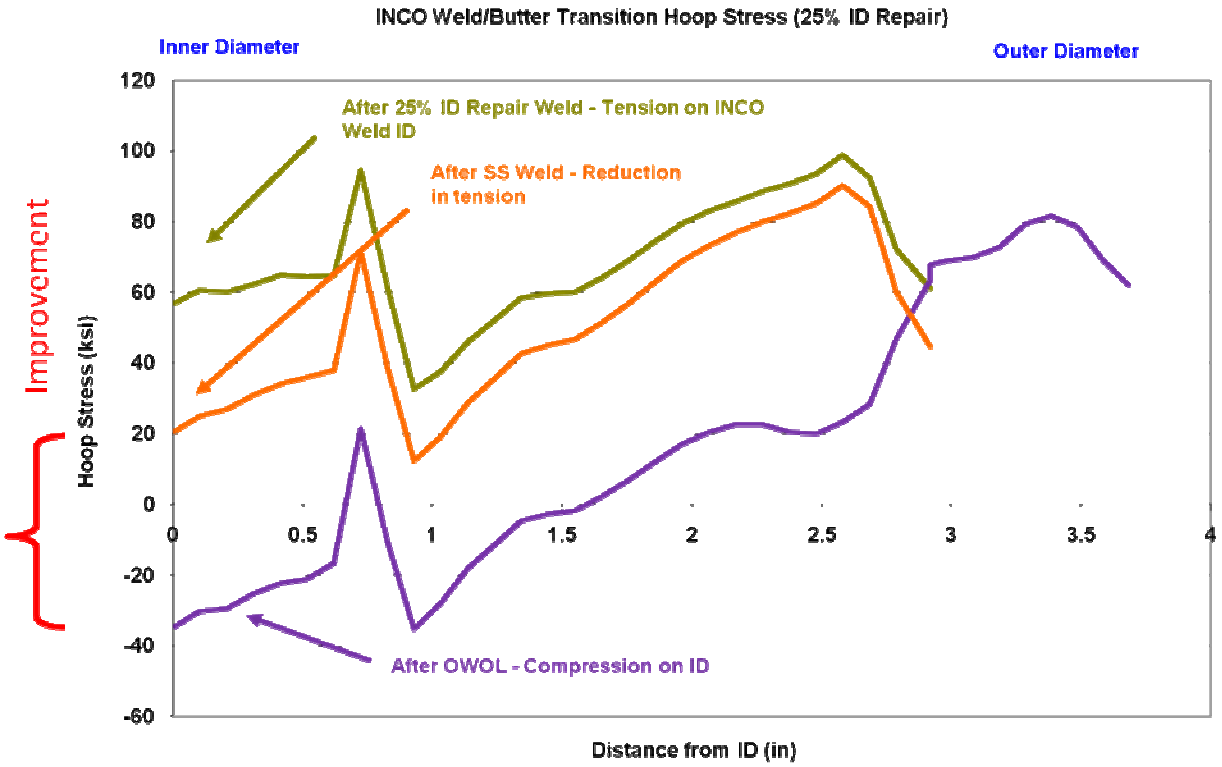

Figure 49 Cold Leg Nozzle Through Thickness Hoop Stresses

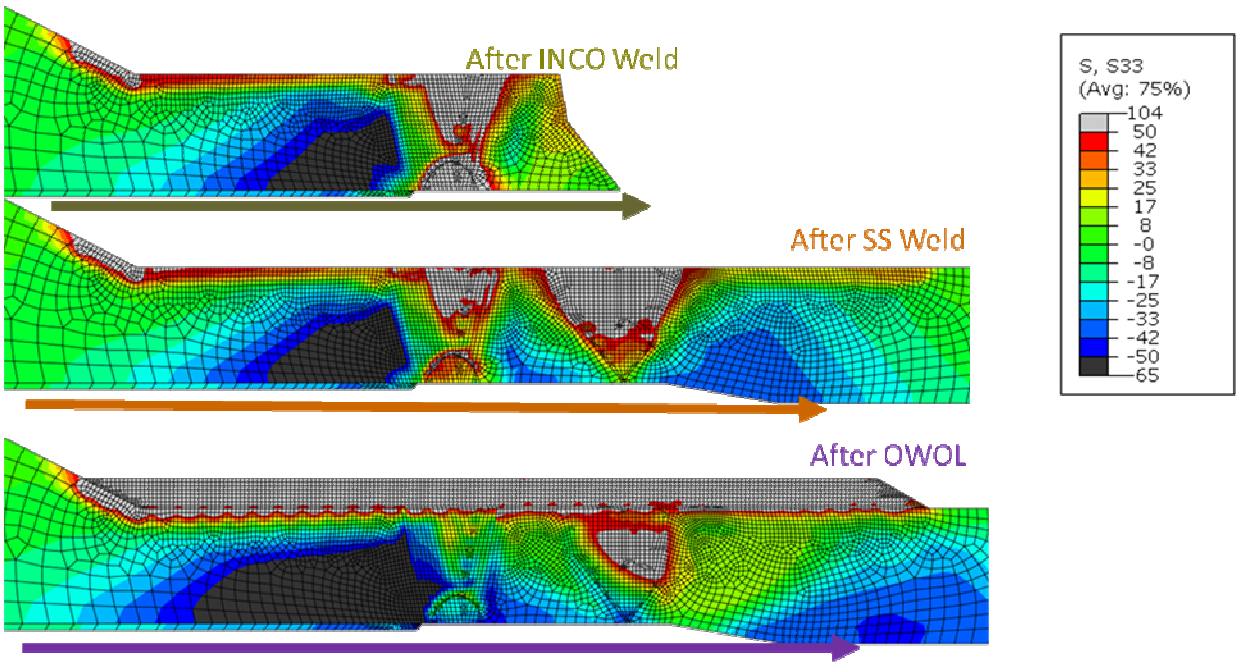

Figure 50 Cold Leg Nozzle Inner Diameter Hoop Stresses (ksi)

Figure 50 and Figure 51 show the inner diameter hoop stress along the length of the dissimilar metal weld area of the surge nozzle. The graph shows that hoop stresses are very high on the inner diameter of the DMW before the secondary stainless steel weld is made, and are reduced, but remain tensile after the stainless steel weld is completed. The stresses are uniformly high at 414 MPa (60 ksi) in the DMW area before the secondary stainless steel weld, and reduced to a uniform 138 MPa (20 ksi) after it is made. The OWOL reduces the hoop stresses in the area of concern to be compressive over the entire length of the dissimilar metal weld area.

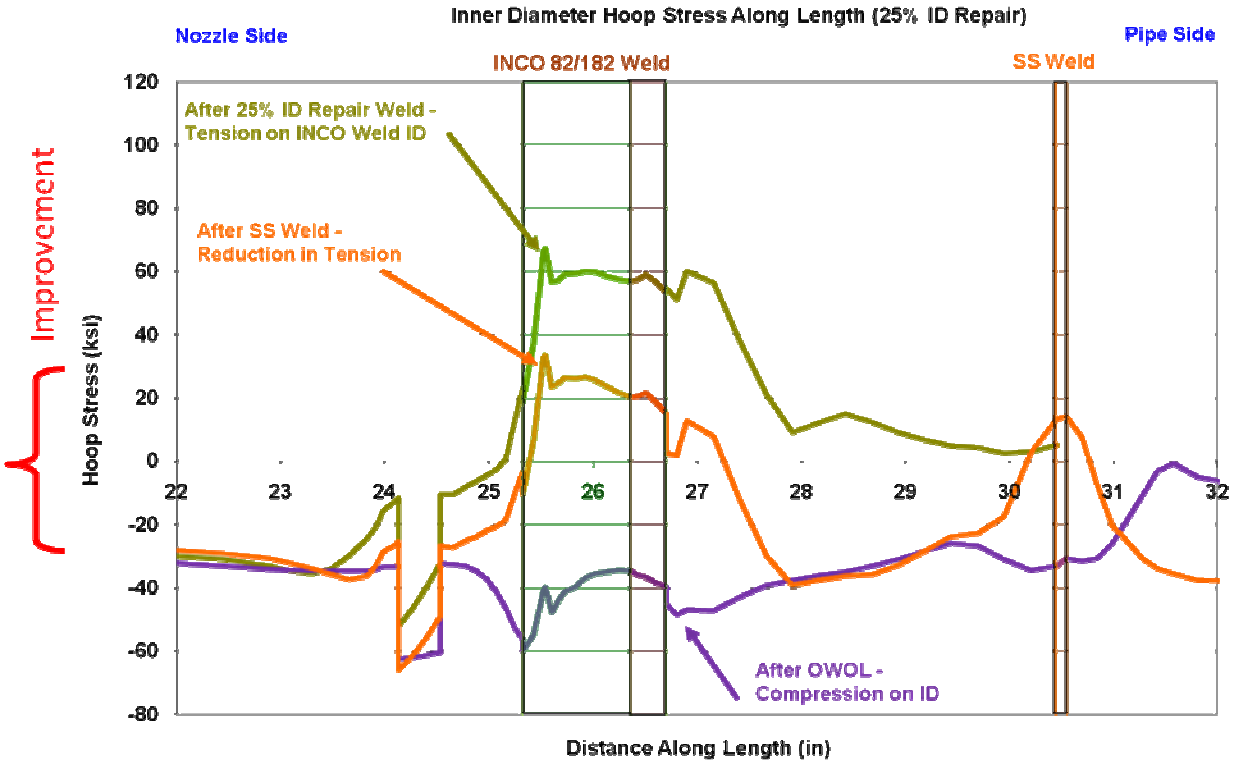

Figure 51 Cold Leg Nozzle Inner Diameter Hoop Stresses

The previous cold leg nozzle stress plots and graphs were all made at room temperature and pressure. The following graphs show the effect of operating pressure and temperature on the cold leg nozzle axial and hoop stresses. An operating pressure of 15.5 MPa (2,250 psi) was used throughout this study for all of the geometries. An operating temperature of 300 C (572 F) was used for the cold leg nozzle analyses. The same temperature was used for all of the geometries studied to have a standard basis of comparison. The effect of small variations in temperature is not expected to be significant.

No stress contour plot are shown for this case, but Figure 52 shows the inner diameter axial stress in the cold leg nozzle dissimilar metal weld area before weld overlay, and then after OWOL at room temperature and then at operating temperature and pressure for each case. The cases are color coded, and the dashed curves indicate the cases at operating pressure and temperature. One can see the application of operating pressure and temperature does little to change the pre-OWOL stresses in the DMW area. The OWOL reduces the peak tension stress but also reduces the maximum compressive stresses in the DMW area at room temperature. The application of operating conditions has a marked beneficial effect after the

OWOL and reduces the maximum stress to -69 MPa (-10 ksi) and maintains the remainder of the stresses in the DMW region compressive below the values achieved in the at room temperature analyses.

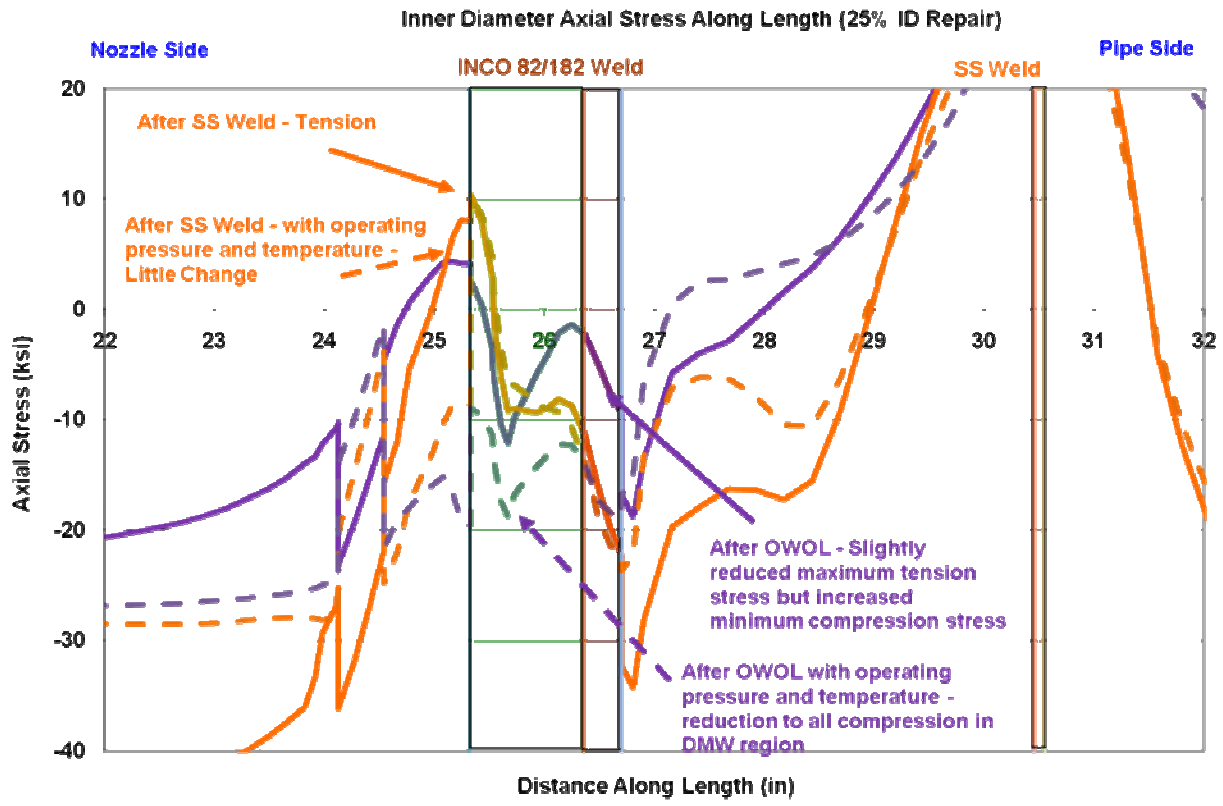

Figure 52 Cold Leg Inner Diameter Axial Stresses after the OWOL is Applied and After the Operating Pressure and Temperature are Applied

Similarly, Figure 53 shows the inner diameter hoop stress in the cold leg nozzle dissimilar metal weld area before weld overlay, and then after OWOL at room temperature and then at operating temperature and pressure for each case. The cases are color coded, and the dashed curves indicate the cases at operating pressure and temperature. One can see the application of operating pressure and temperature increases the stress in each case.. The case before weld overlay (shown in orange) has high tension stresses at room temperature in the Inconel weld area which are only increased by operating temperature and pressure. The OWOL reduces the stresses greatly with the whole dissimilar metal weld area in compression at room temperature. Operating conditions raise the stresses in the DMW area, but they remain in compression for the whole area of concern.

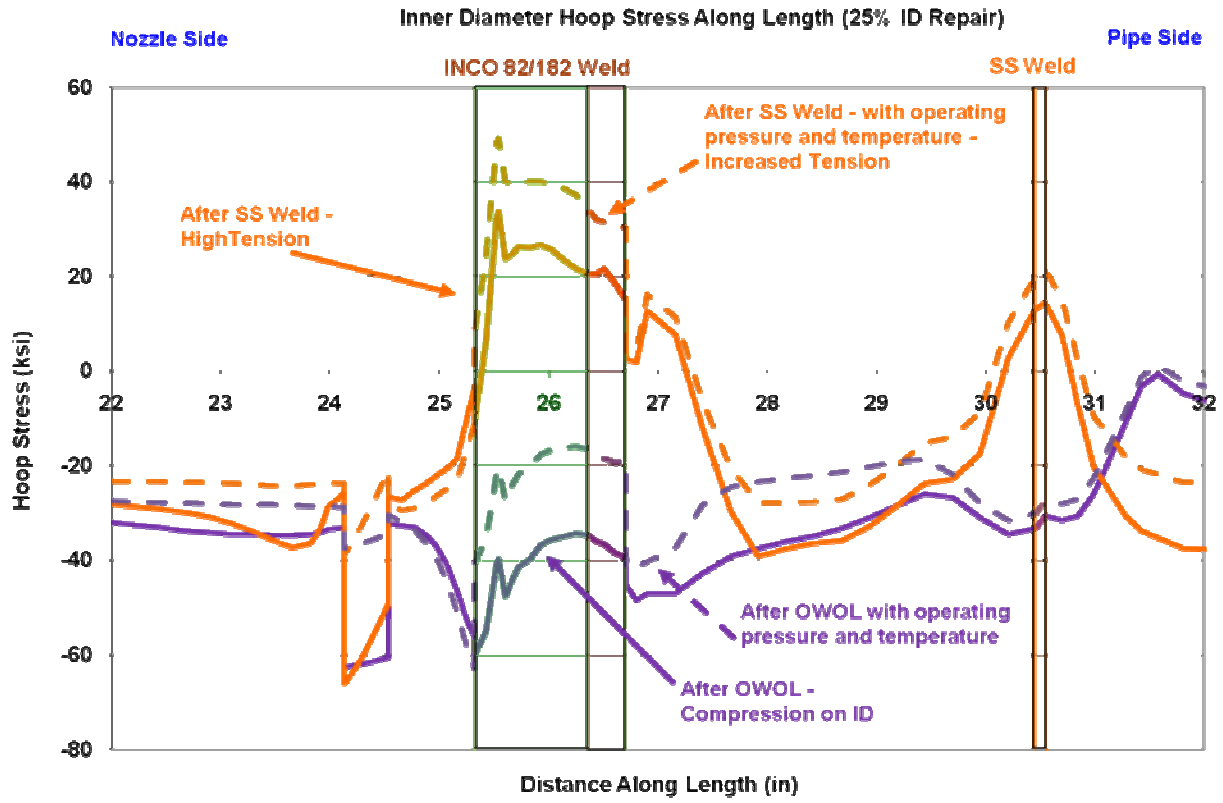

Figure 53 Cold Leg Inner Diameter Hoop Stresses after the OWOL is Applied and After the Operating Pressure and Temperature are Applied

4.1.4 Reactor Coolant Pump Outlet Nozzle

The reactor coolant pump outlet nozzle weld residual stresses were developed in a similar way as those shown in Figure 8 for the surge nozzle. The notable exceptions are that this model includes a 25% inner diameter weld repair, which is simulated in addition to the root pass grind out and re-weld. The 25% ID weld repair is handled in a similar fashion with the repair being removed in one step, and then weld material is replaced, simulating the welding process, from the root of the weld toward the inner diameter of the pipe in seven passes.

Figure 54 shows the axial stress contour plot before any weld overlay but after all normal welding is complete including the 25% ID repair (top figure), after the OWOL is finished (middle figure), and after the FSWOL has been completed (bottom figure). The arrows through the weld indicate the path followed for the graphed data shown in Figure 55.

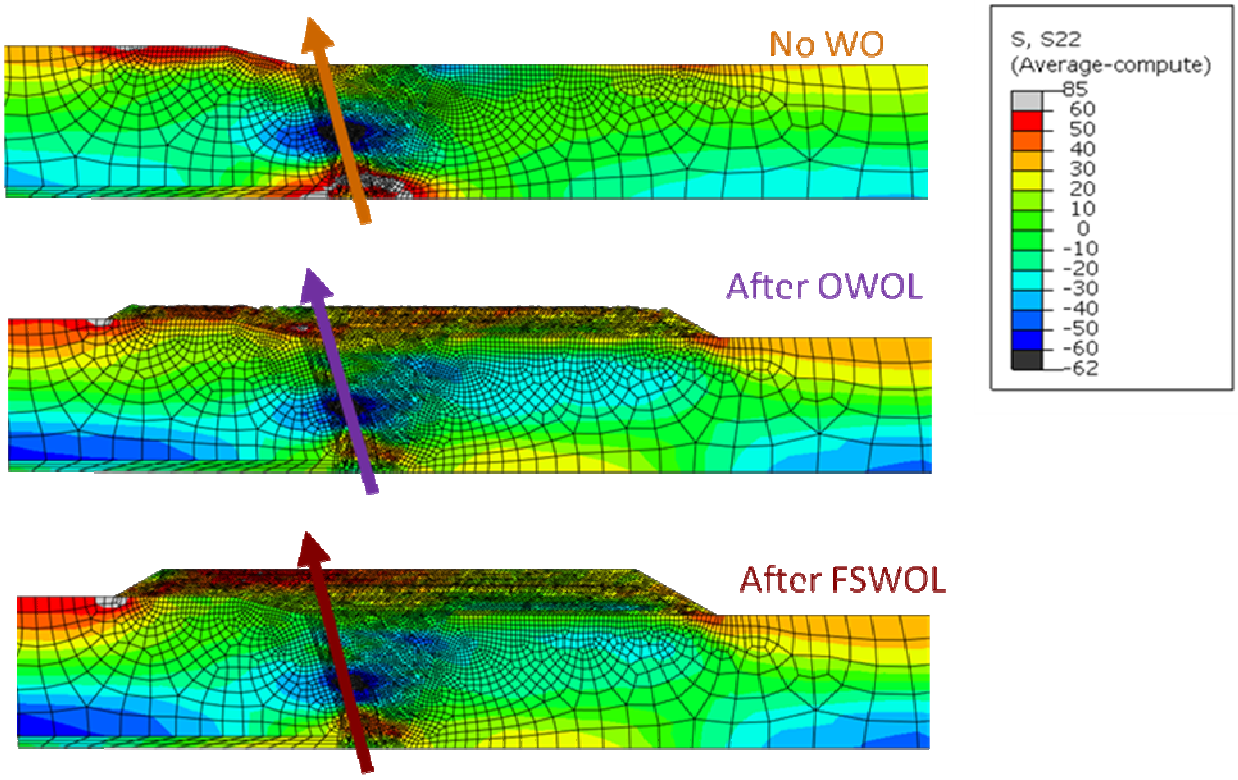

Figure 54 Reactor Coolant Pump Axial Stresses Through Thickness (ksi)

The axial stress contour plot and graph show that the Inconel weld is in tension at the inner diameter, compression in the center, and tension at the outer diameter after the dissimilar metal weld is completed and after the stainless steel safe end weld is complete. The application of the stainless steel weld has almost no effect in lessening the tension stress on the inner diameter of the Inconel weld in this case because it is located so far away (403 mm]16 inches]) from the Inconel weld unlike in the other geometries studied. In this cross section, the axial is reduced to near zero with the OWOL, and is reduced to 68 MPa (10 ksi) for the FSWOL.

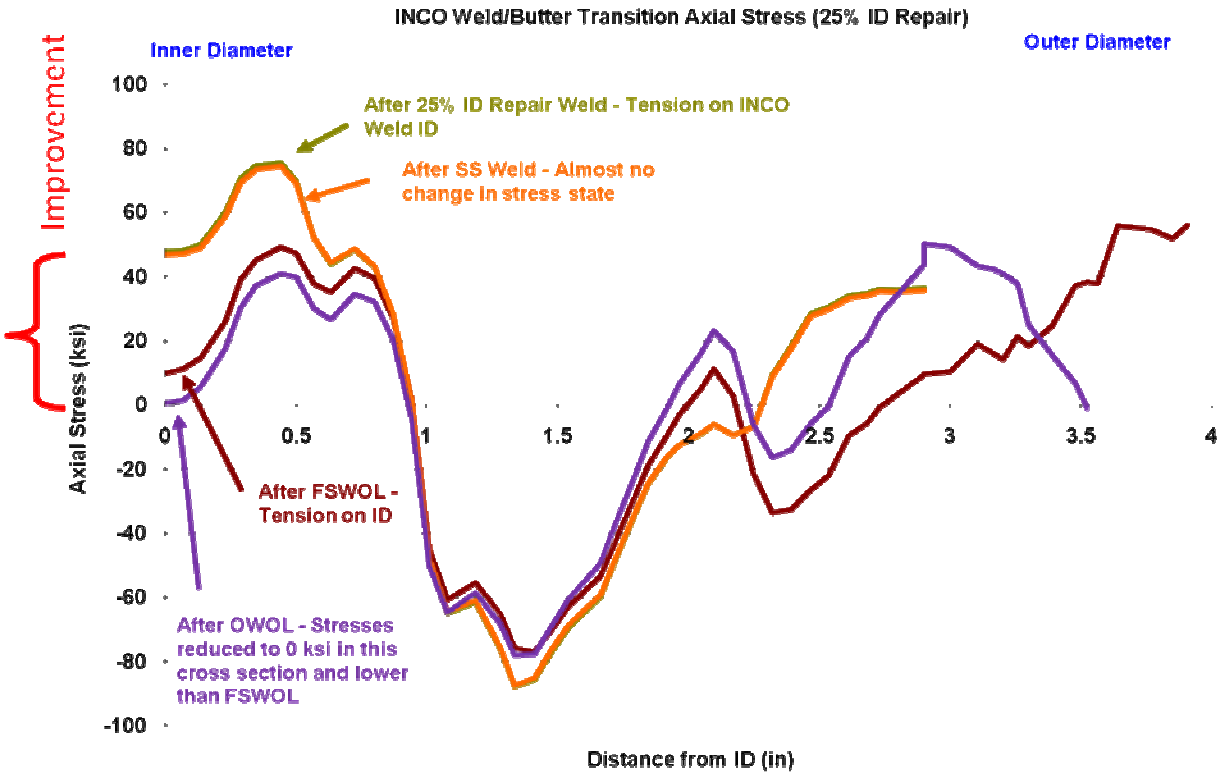

Figure 55 Reactor Coolant Pump Through Thickness Axial Stresses

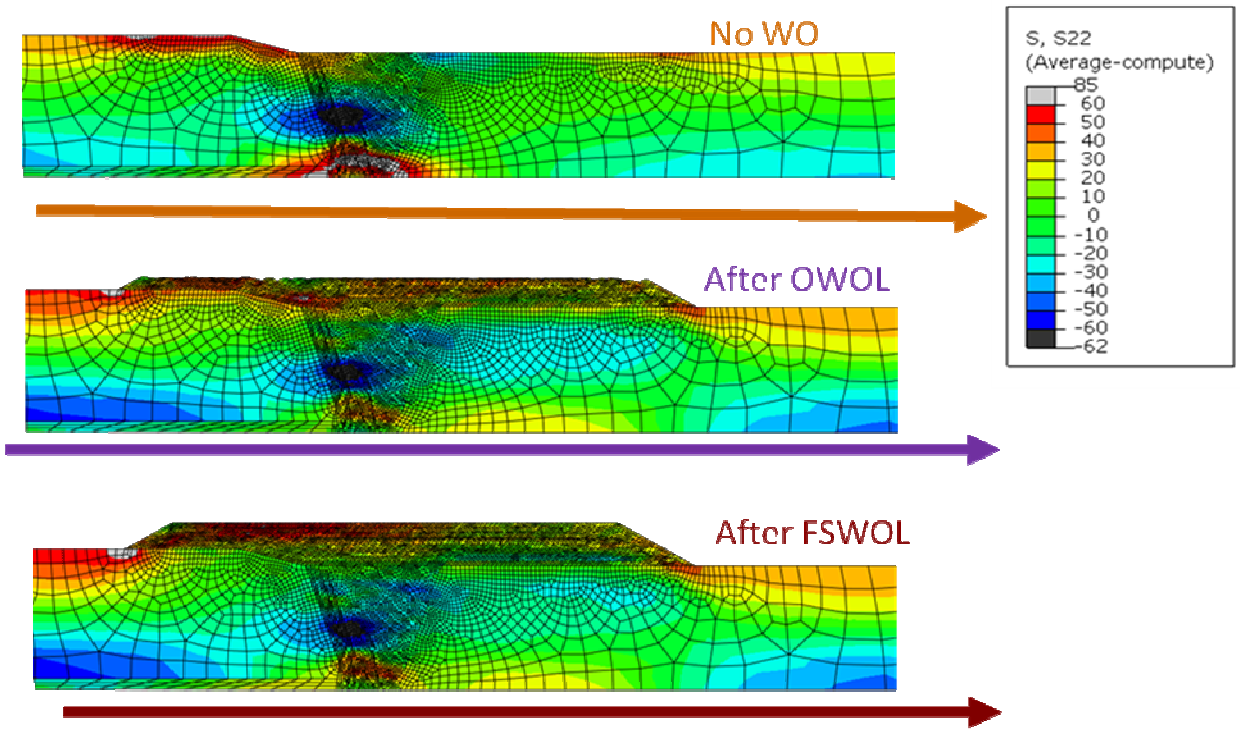

Figure 56 Reactor Coolant Pump Inner Diameter Axial Stresses (ksi)

Figure 56 and Figure 57 show the inner diameter path and axial stress along that path. Figure 57 indicates the position of the butter, the dissimilar metal weld and the secondary stainless steel weld with color coded vertical bars on the graph for reference.

One can see that the stress is very high on both sides of the dissimilar metal weld region including the butter and the Inconel weld. Again the graph shows that the effect of completing the stainless steel safe end weld is minimal on changing the stress pattern in the dissimilar metal weld area. The stresses remain above 138 MPa (20 ksi) and up to 414 MPa (60 ksi) in the dissimilar metal weld area before weld overlay. After the OWOL is completed, the stresses along the inner diameter of the DMW have been made compressive or reduced to less than 90 MPa (13 ksi). However, after the FSWOL is completed, for this case, the stresses increase but remain under 138 MPa (20 ksi) in the dissimilar metal weld area.

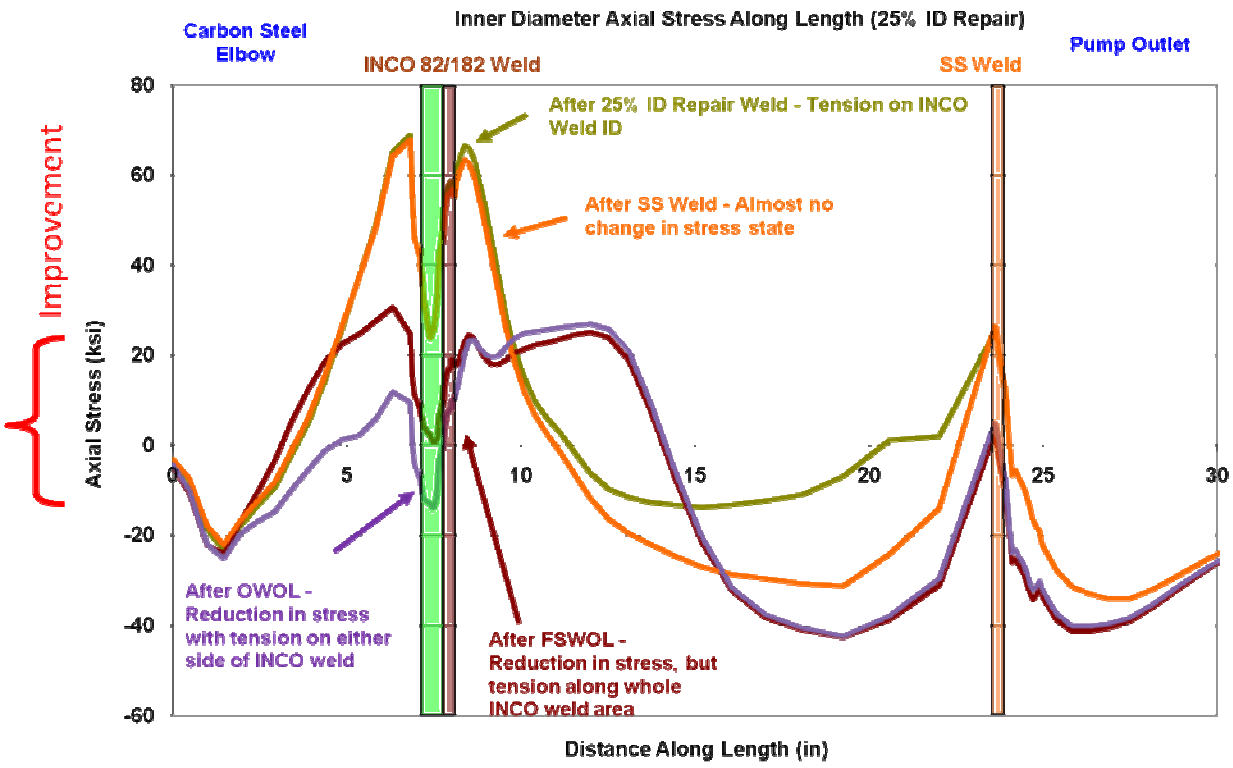

Figure 57 Reactor Coolant Pump Inner Diameter Axial Stresses Along Length of the Pipe at the Inside Surface

Figure 58 and Figure 59 show the through thickness hoop stresses before and after the application of the weld overlays. The graph shows that the secondary stainless steel weld has no effect of reducing the hoop stress in the dissimilar metal weld because of its distance from the dissimilar metal weld. Both the OWOL and the FSWOL reduce the through thickness hoop stresses into compression for approximately the inner 2/3 of the original wall thickness. For hoop stress the FSWOL reduces the stresses more than the OWOL for this cross section.

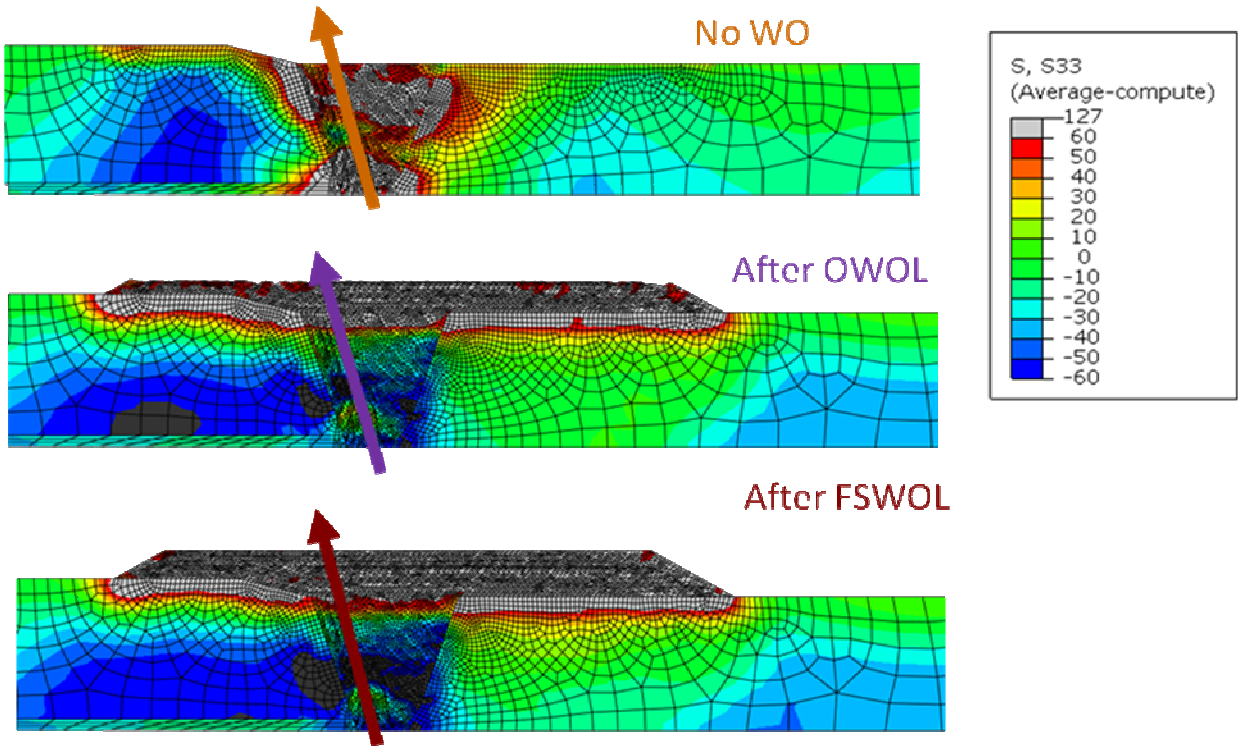

Figure 58 Reactor Coolant Pump Through Thickness Hoop Stresses (ksi)

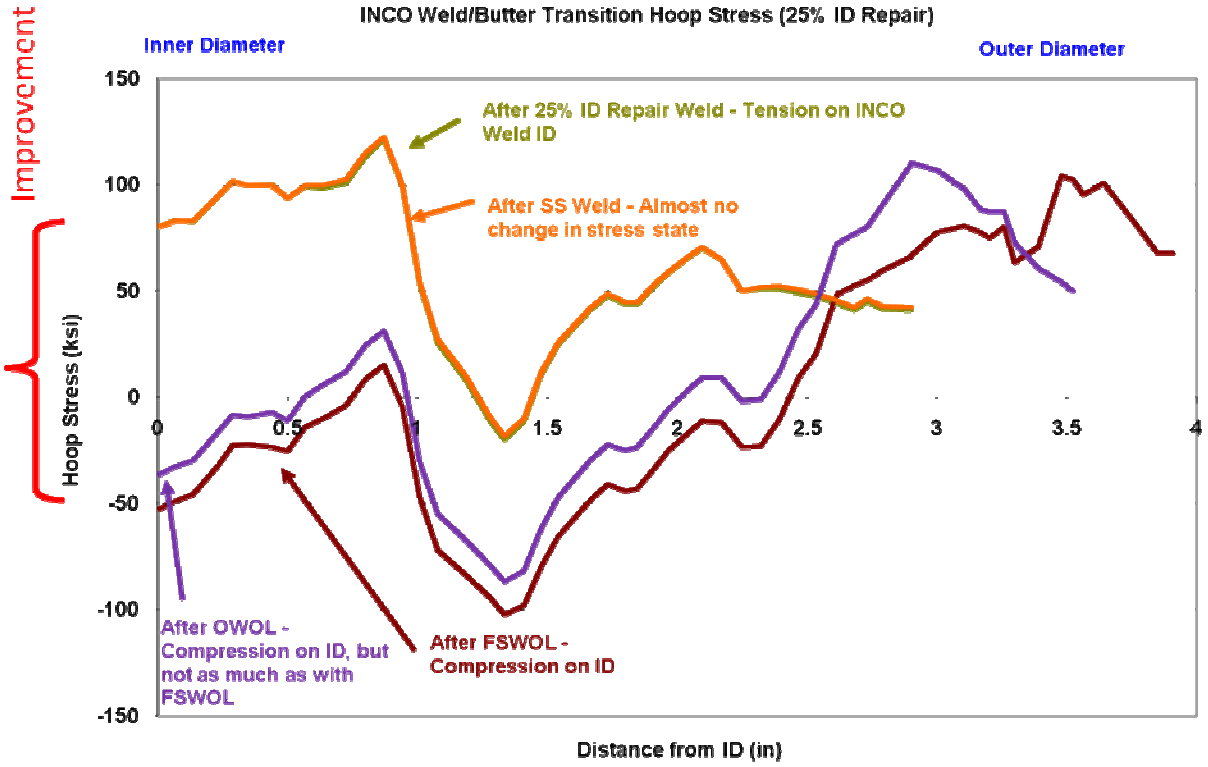

Figure 59 Reactor Coolant Pump Through Thickness Hoop Stresses

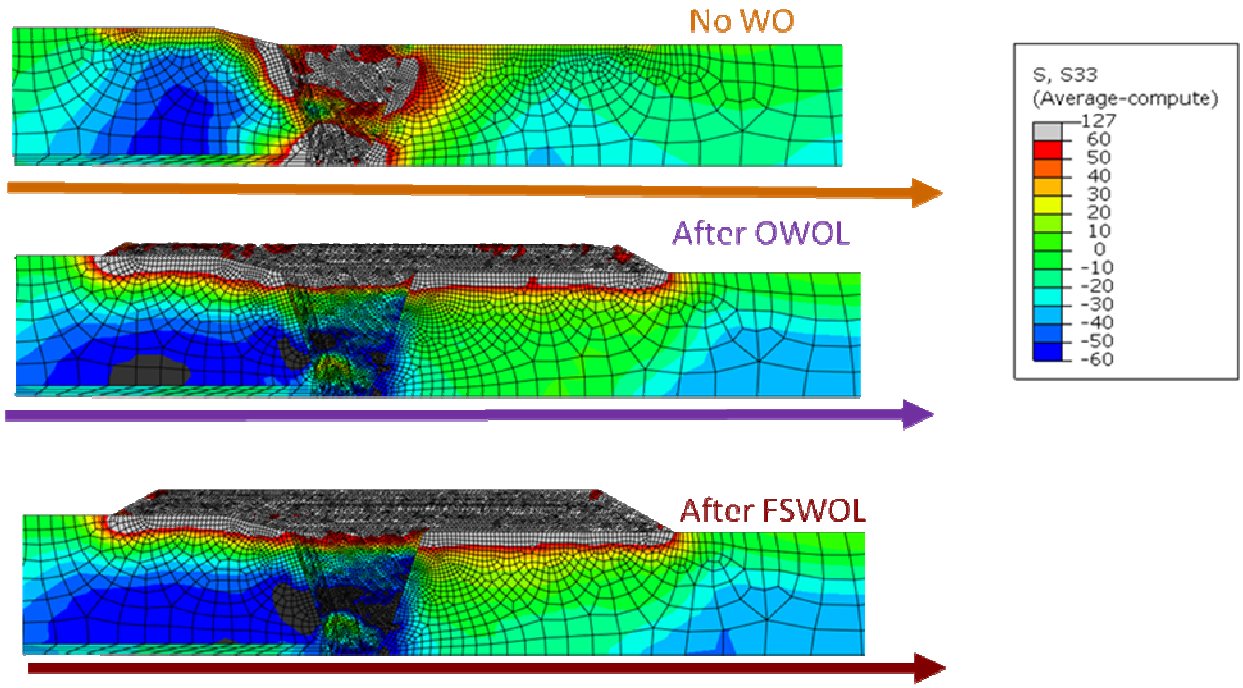

Figure 60 Reactor Coolant Pump Inner Diameter Hoop Stresses (ksi)

Figure 60 and Figure 61 show the inner diameter hoop stresses along the length of the dissimilar metal weld area of the reactor coolant pump outlet nozzle. The graph shows that hoop stresses are very high on the inner diameter of the DMW before the secondary stainless steel weld is made, and are not reduced at all when it is completed. The OWOL and FSWOL reduce the hoop stresses in the area of concern to be compressive over the entire length of the dissimilar metal weld area with very little difference in the results between the effect of the OWOL and the FSWOL for this geometry.

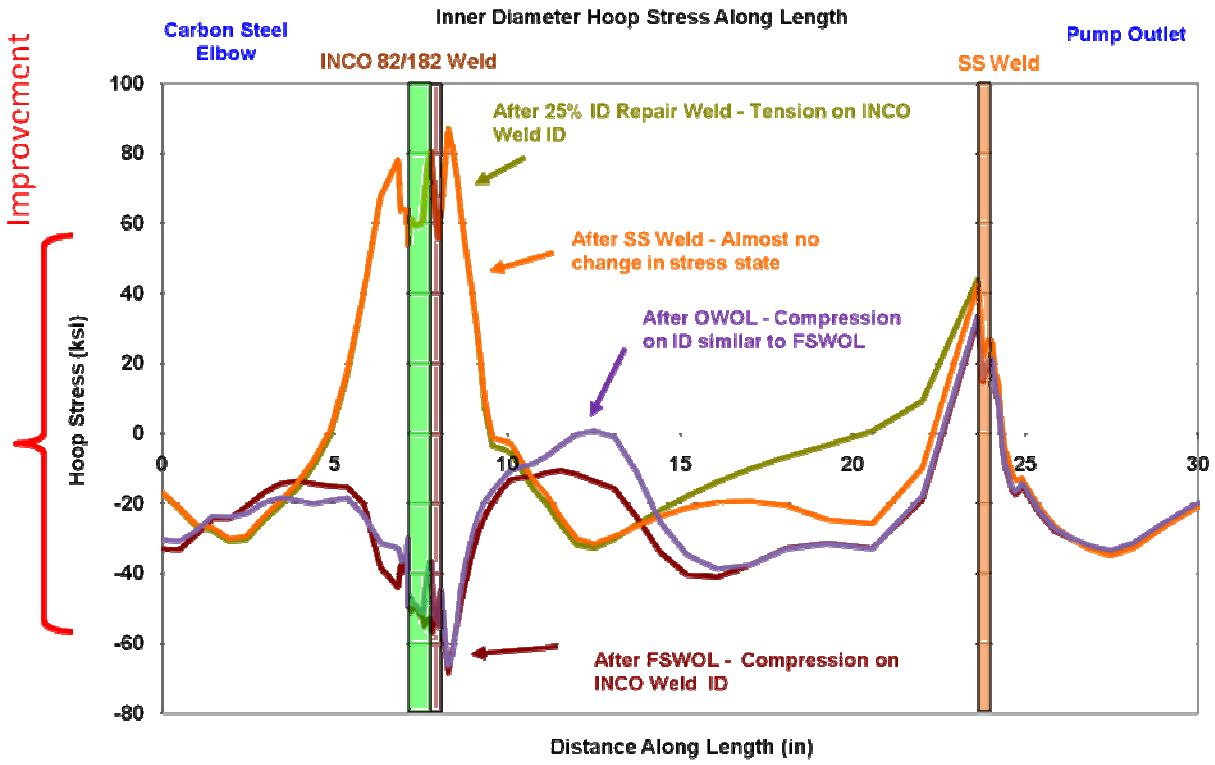

Figure 61 Reactor Coolant Pump Inner Diameter Hoop Stresses

The previous reactor coolant pump outlet nozzle stress plots and graphs were all made at room temperature and pressure. The following graphs show the effect of operating pressure and temperature on the reactor coolant pump axial and hoop stresses. An operating pressure of 15.5 MPa (2,250 psi) was used throughout this study for all of the geometries. An operating temperature of 300 C (572 F) was used for the reactor coolant pump analyses. The same temperature was used for all of the geometries studied to have a standard basis of comparison. The effect of small variations in temperature is not expected to be significant.

No stress contour plot are shown for this case, but Figure 62 shows the inner diameter axial stress in the reactor coolant pump dissimilar metal weld area before weld overlay, after OWOL and then after FSWOL at room temperature and then at operating temperature and pressure for each case. The cases are color coded, and the dashed curves indicate the cases at operating pressure and temperature. One can see the application of operating pressure and temperature reduces the stresses in each case. The case before weld overlay (shown in orange) has high tension stresses at room temperature in the Inconel weld area which are reduced by operating temperature and pressure, but remain tensile. The OWOL and FSWOL reduce the stresses further at room temperature, but continue to remain in tension in the Inconel weld area. After the application of operating pressure and temperature, both the OWOL and FSWOL reduce the stresses in the Inconel weld area to be completely in compression. The OWOL and FSWOL results are very similar in the Inconel weld area with the OWOL giving better results by about 69 MPa (10 ksi) in the butter area.

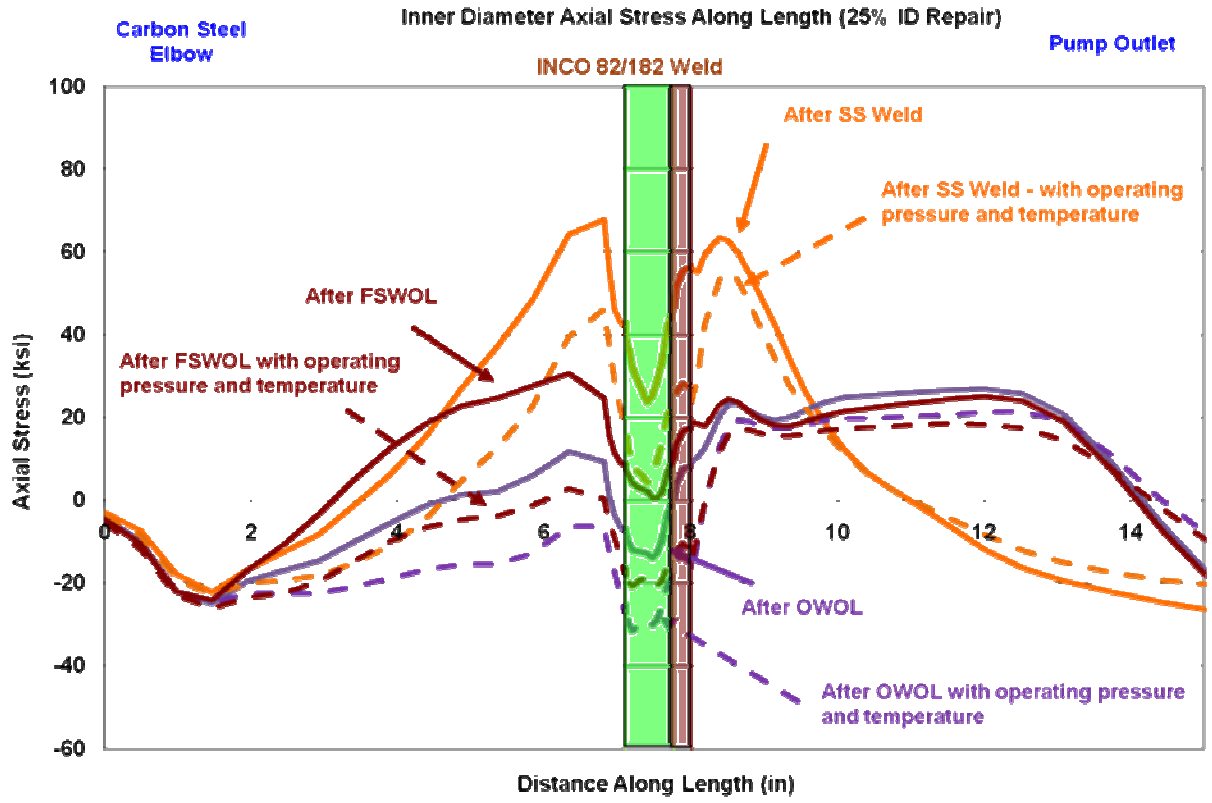

Figure 62 Reactor Coolant Pump Inner Diameter Axial Stresses After the OWOL and FSWOL are Applied and After the Operating Pressure and Temperature are Applied

Similarly, Figure 63 shows the inner diameter hoop stress in the reactor coolant pump dissimilar metal weld area before weld overlay, after OWOL and then after FSWOL at room temperature and then at operating temperature and pressure for each case. The cases are color coded, and the dashed curves indicate the cases at operating pressure and temperature. One can see the application of operating pressure and temperature reduces the stresses in each case. The case before weld overlay (shown in orange) has high tension stresses at room temperature in the Inconel weld area which are reduced by operating temperature and pressure, but remain highly tensile. The OWOL and FSWOL reduce the stresses greatly with the whole dissimilar metal weld area in compression. Both OWOL and FSWOL give similar results in this case. The application of operating pressure and temperature further reduces the hoop stress on the butter side of the DMW, but increases it only slightly on the Inconel weld side. For all practical purposes, the OWOL and FSWOL behave similarly for this geometry.

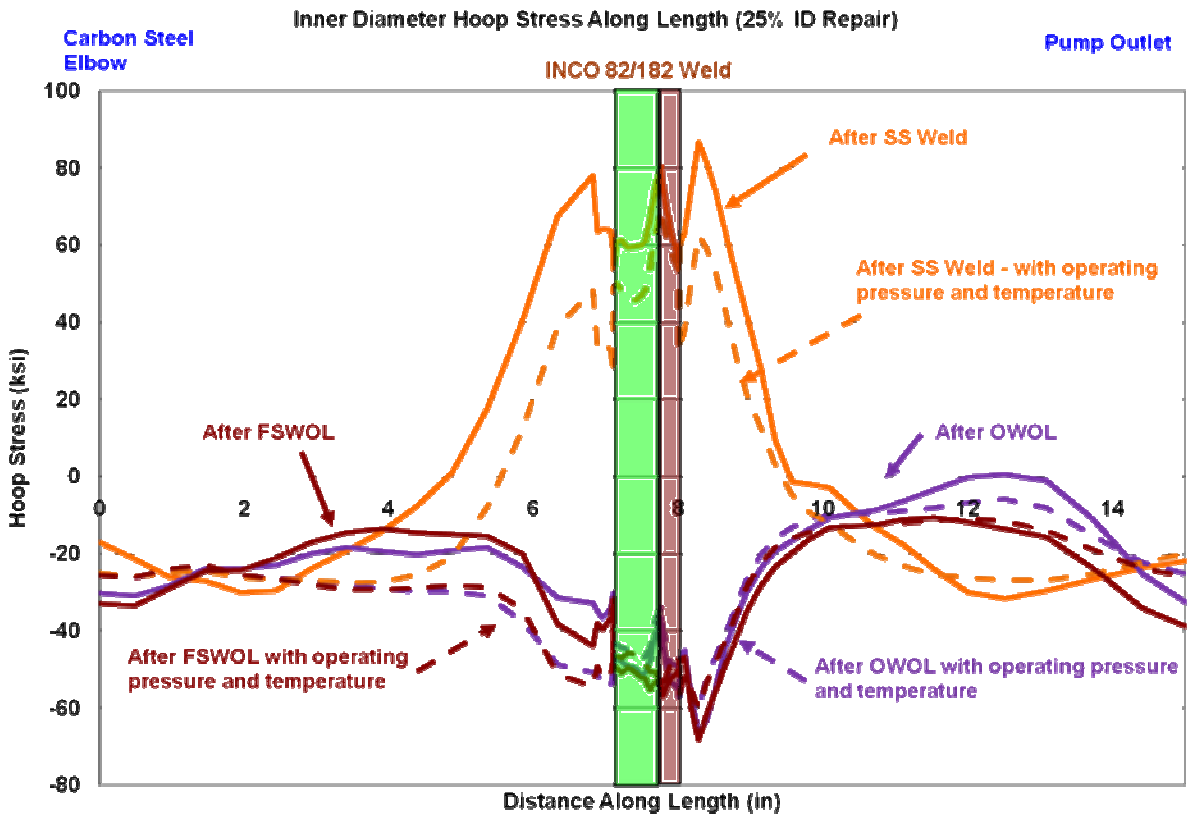

Figure 63 Reactor Coolant Pump Inner Diameter Hoop Stresses after the OWOL and FSWOL are Applied and after the Operating Pressure and Temperature are Applied

4.1.5 Sensitivity Analyses

Several sensitivities studies were conducted to evaluate the effect of different variables on the efficacy of weld overlays. The majority of the sensitivity studies were confined to the surge nozzle model because it had the most complex geometry and number of welded areas. The sensitivity analyses conducted as part of this effort included:

- The effect of the secondary stainless steel weld was examined for the surge nozzle geometry. The weld residual stresses developed by the secondary stainless steel weld were eliminated from the finished weldment and the final stress state for this case was compared to the normal case where the weld residual stresses from the secondary stainless steel weld were included in the analyses. The efficacy of the FSWOL was examined for this case as well.
- The effect of FSWOL on surge nozzle geometry without the weld residual stresses of the heat shield fill-in weld was evaluated.
- The effect of the FSWOL weld sequencing was examined. The resulting post-FSWOL residual stress patterns were compared for cases in which the FSWOL was applied from right-to-left for the surge nozzle geometry as shown in the previous examples, for the FSWOL being applied left-to-right, and finally with the weld being applied right-to-left, but with the use of two simultaneously operating axially-offset weld heads.

- Sensitivity studies were conducted on each model to examine the effect of weld overlay thickness on the residual stresses for typical dissimilar metal weld configurations. For the surge and safety and RCP nozzle geometries the study included thicknesses up to FSWOL. For the cold leg nozzle, the study also looked at the effect of layer thickness, but only up the final OWOL thickness.
- A study was conducted examining the effect of inner diameter repair depth on stresses before and after weld overlay repair. For the RCP nozzle, 0%, 25% and 50% inner diameter repair depths were examined. For the cold leg nozzle only 0% and 25% inner diameter repair depths were examined.
- Artificial 360 degree circumferential cracks were forced to grow through the dissimilar metal weld. Crack opening behavior was recorded and crack tip stress intensity factors were calculated for the situations in which a crack was forced to grow in the weld before the FSWOL was applied and after the FSWOL was applied. These evaluations were done for both the surge and safety nozzle geometries with two different crack locations. The calculations were done with the crack forced to grow at the interface of the butter and the dissimilar metal weld, and also calculated for the location between the carbon steel nozzle material and the butter layer.

4.1.5.1 Effect of Second Stainless Steel Weld on the FSWOL Results

The surge nozzle, safety nozzle and cold leg geometries considered as part of this effort all have a secondary stainless steel weld in close proximity to the dissimilar metal weld. For these geometries, the secondary stainless steel weld connects the stainless steel safe end to the stainless steel piping system.

The welding of the dissimilar metal weld itself produces high inner diameter axial tensile stresses in the area of the dissimilar metal weld. These high axial tensile stresses are greatly reduced by the application of a nearby secondary stainless steel weld as shown in Figure 23Figure 36Figure 47 and not affected by one that is placed far away from the dissimilar metal weld by a long safe end as shown in Figure 57 In this sensitivity study, the safe end and stainless steel pipe were added to the nozzle as a single piece with only the dissimilar metal weld. The safe end and pipe were added as one component without the effect of the residual stresses due to the secondary stainless steel weld.

Figure 64 shows a comparison of the axial stresses in the range of -414 MPa (-60 ksi) to 414 MPa (60 ksi) for the surge nozzle geometry with and without the weld residual stresses of the secondary stainless steel weld. The left column of stress contour plots shows the results after the secondary stainless steel weld and after the application of the FSWOL, both for the case where the effect of the secondary stainless steel weld is included in the analyses. The right column of stress contour plots shows the same results, but with the original stress state produced by only the butter layer and the dissimilar metal weld and without the effect of the secondary stainless steel weld. The top right figure shows that the inner diameter axial stresses are highly tensile under the dissimilar metal weld for the case without the secondary stainless steel weld. However, the axial stress results after the FSWOL has been applied are almost identical for the cases of with and without the secondary stainless steel weld residual stresses. The stresses in the case without the stainless steel weld are slightly less compressive, but the FSWOL has nonetheless produced a significant improvement in the inner diameter stress state.

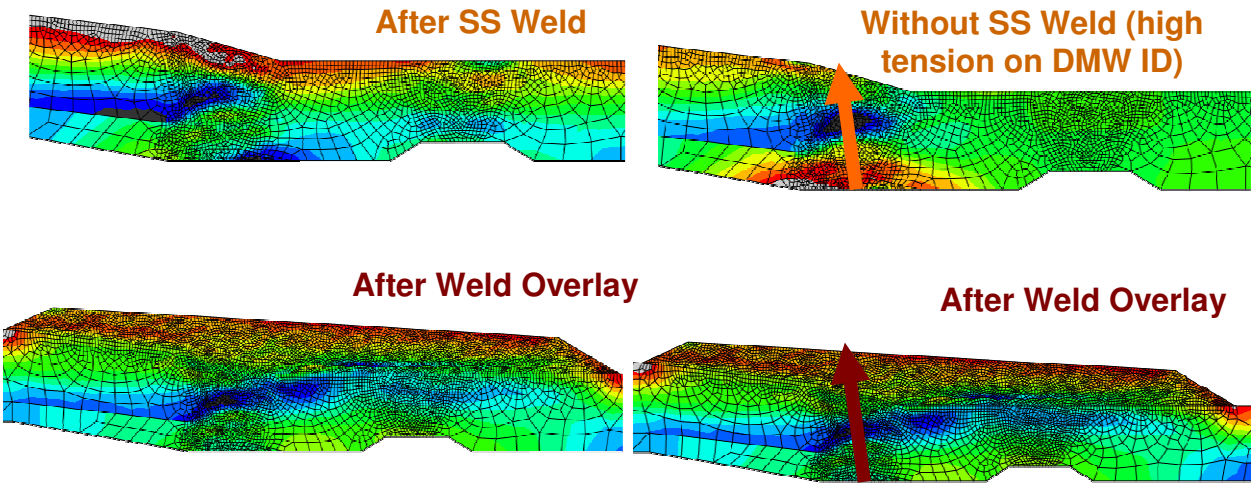

Figure 64 Surge Nozzle Axial Stresses for the FSWOL without the Secondary Stainless Steel Weld

Figure 65 shows the axial stress results from the study. The post-FSWOL results shown in the stress contour plot, and more dramatically in the graph, are similar to those found in Figure 21 and Figure 23for the surge nozzle geometry with the secondary stainless steel weld. The axial stress at the inner diameter of the dissimilar metal weld is 379 MPa (55 ksi) before the FSWOL is applied and is reduced to -138 MPa (-20 ksi) after the FSWOL is applied. While the secondary stainless steel weld produces a beneficial effect on the stress profile of the dissimilar metal weld, the post-overlay stresses without the benefit of the secondary stainless steel weld (bottom right figure in Figure 64) are very similar to the post-overlay stresses with the benefit of the secondary stainless steel weld (bottom left figure in Figure 64).

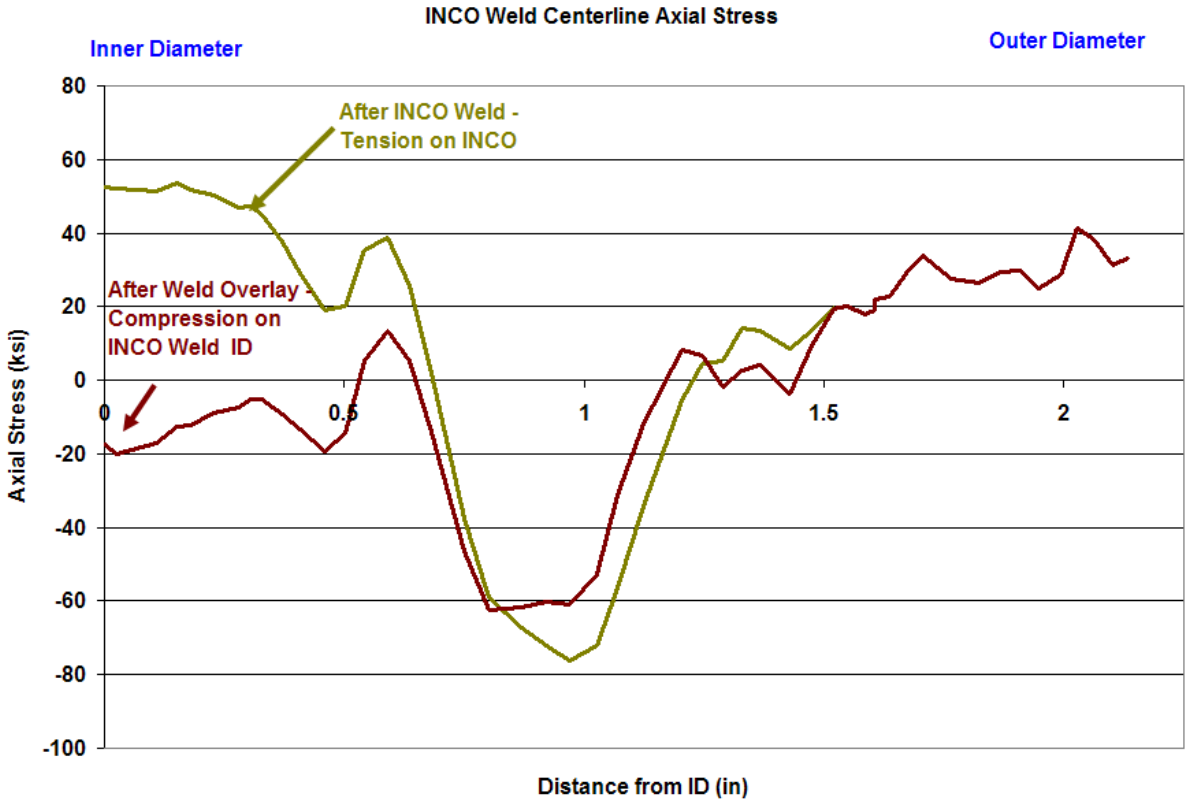

Figure 65 Comparison of the Surge Nozzle Through Thickness Axial Stresses after Applying the FSWOL, without the Beneficial Effect of the Secondary Stainless Steel Weld, to the Surge Nozzle Through Thickness Axial Stresses for the DMW prior to Fabricating the Secondary Stainless Steel Weld

4.1.5.2 Effect of Heat Shield Fill-In Weld on the FSWOL Results

The surge nozzle has a heat shield fill-in weld under the dissimilar metal weld in some applications. This weld was included as a worst case in this analysis, since it produces the similar effect as a full circumference inner diameter repair weld of increasing the inner diameter tension stresses.

The welding of the dissimilar metal weld itself produces high inner diameter axial tensile stresses, and the welding of the heat shield fill-in weld exacerbates the issue. In this study, the welding operation was the same, except for the fact that the heat shield fill-in weld was not performed before the secondary stainless steel weld was done to connect the safe end to the stainless steel piping system.

Figure 66 shows a comparison of the axial stresses in the range of -414 MPa (-60 ksi) to 414 MPa (60 ksi) for the surge nozzle geometry with and without the weld residual stresses of the heat shield fill-in weld. The left column of stress contour plots shows the results with the original weld sequence including the heat shield fill-in weld, and then after the application of the FSWOL (bottom left figure). The right column of stress contour plots shows the same results, but with the stress state produced by only the butter layer and the dissimilar metal weld and without the effect of the heat shield fill-in weld. The top right figure shows that there is an area of tension about a quarter of the way through the thickness from the inner diameter, but otherwise the plots look similar. The axial stress results after the FSWOL has

been applied are almost identical for the cases of with and without the heat shield fill-in weld residual stresses.

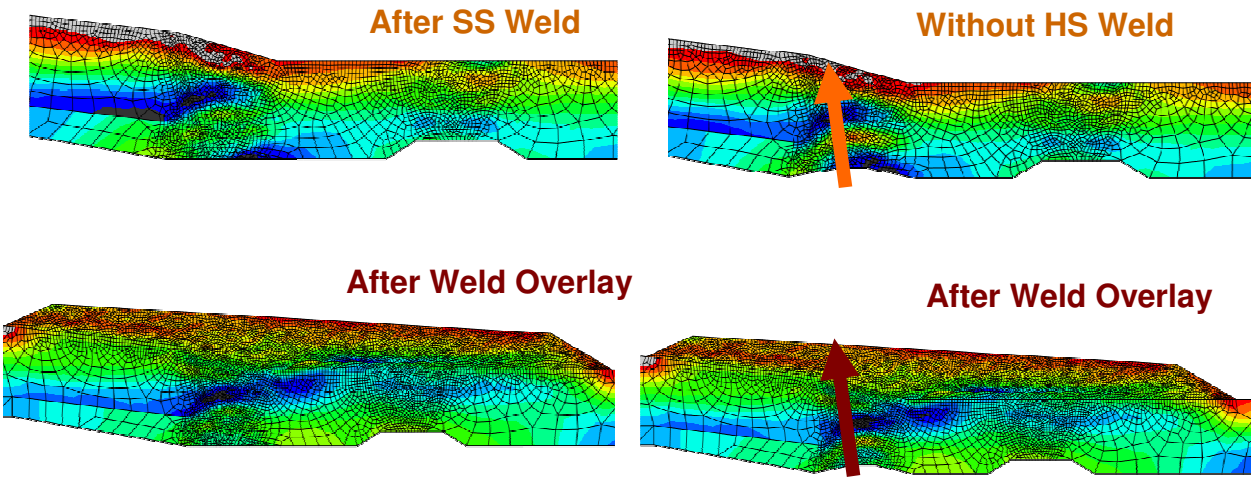

Figure 66 Surge Nozzle Axial Stresses for the FSWOL without Heat Shield Fill-In Weld

Figure 67 shows the axial stress results from the study. The post-FSWOL results shown in the graph are not changed much by the lack of the heat shield fill-in weld. The stresses at the inner diameter are about the same in the -138 MPa (-20 ksi) range, and the stresses are slightly more tensile about one quarter of the way through the thickness in the case without the heat shield fill-in weld.

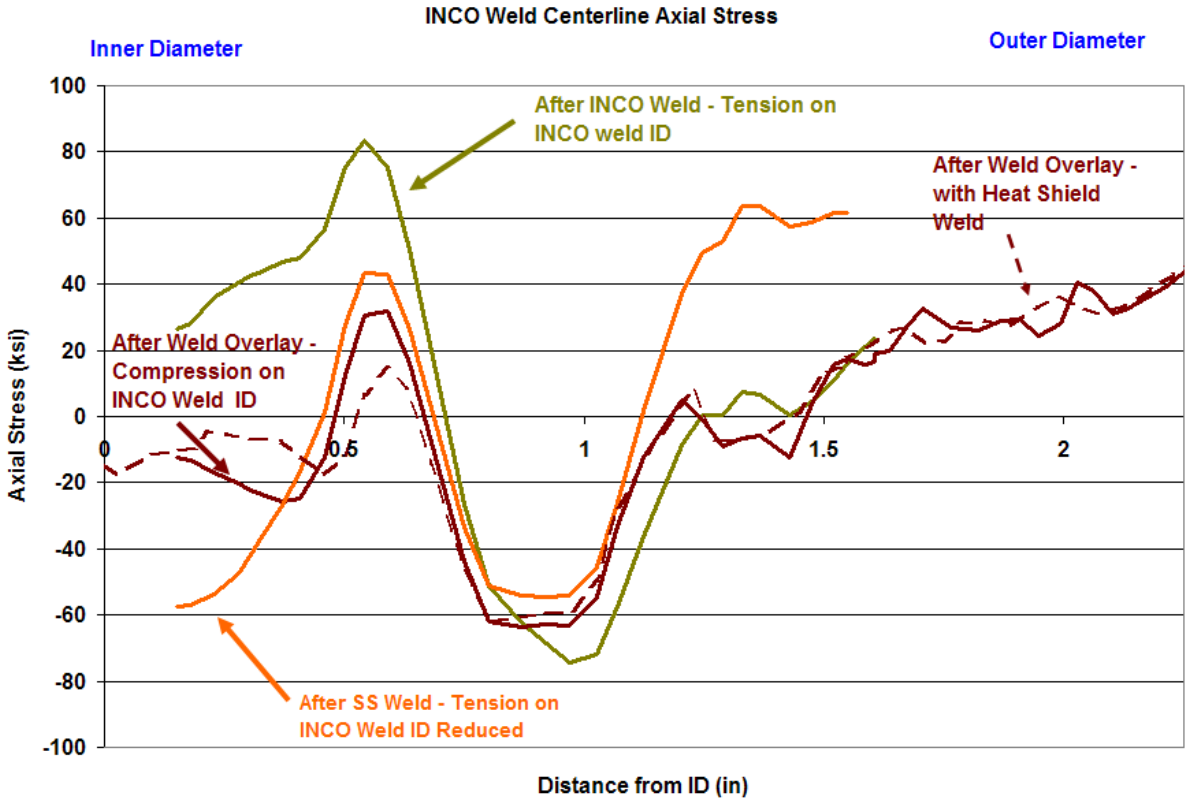

Figure 67 Surge Nozzle Through Thickness Axial Stresses after Applying the FSWOL without Heat Shield Fill-In Weld

4.1.5.3 Effect of FSWOL Weld Sequencing on Weld Residual Stress

A fourth sensitivity study was performed on the surge nozzle geometry on which the FSWOL weld sequence was altered. The original examples for the surge nozzle had all of the FSWOL weld passes placed from right-to-left in successive layers. The first sensitivity study shows the effect of reversing that order. The original right-to-left pattern for the surge nozzle is the traditional method for this geometry because the welding is performed in the direction against gravity. Therefore, for the safety nozzle which points in the opposite direction on the top side of the pressurizer vessel, the traditional FSWOL direction would be opposite and left-to-right.

Figure 68 shows the difference in axial stress patterns with the two weld directions. There is a noticeable difference in the stress patterns in the dissimilar metal weld which is more easily explained in the graphs shown in Figure 69 and Figure 70. The through thickness axial stress is about the same for each weld sequence. The inner diameter axial stresses (Figure 70) are almost identical for both weld sequence directions up to the dissimilar metal weld. The peak stresses, in the transition between the butter to the nozzle steel, are the same. In the dissimilar metal weld area, the non-traditional left-to-right sequence for the surge nozzle produces slightly more compressive stresses, and in the safe end area, the non-traditional left-to-right weld sequence produces stresses that are consistently compressive or near zero up to the secondary stainless steel weld, while the traditional right-to-left sequence produces tensile stresses up to 138 MPa (20 ksi) tensile in the safe end.

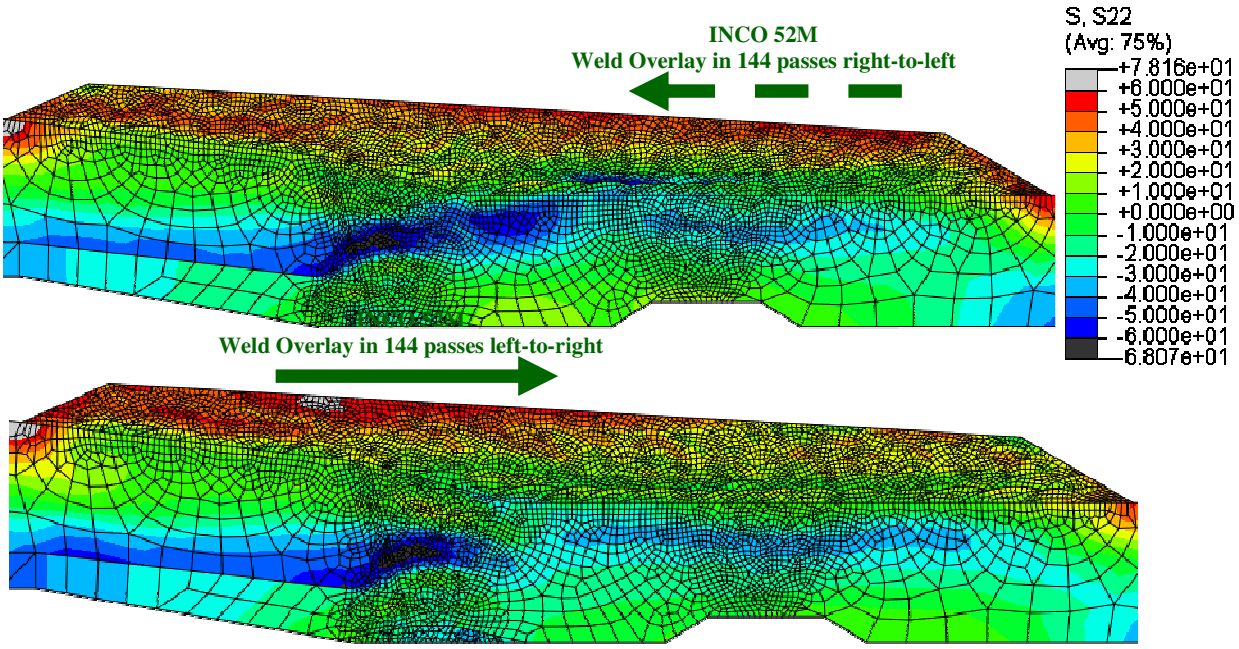

Figure 68 Surge Nozzle FSWOL Opposite Weld Direction Study Axial Stresses

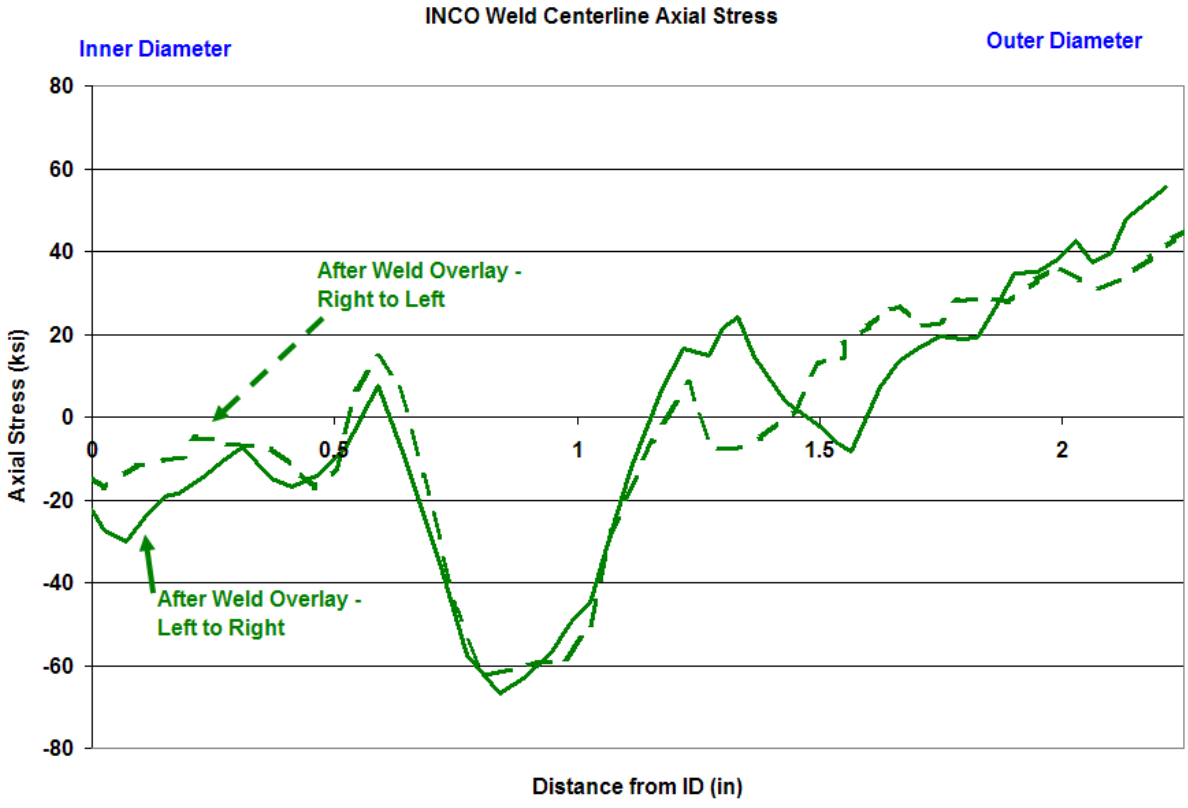

Figure 69 Surge Nozzle FSWOL Opposite Weld Direction Study Through Thickness Axial Stresses

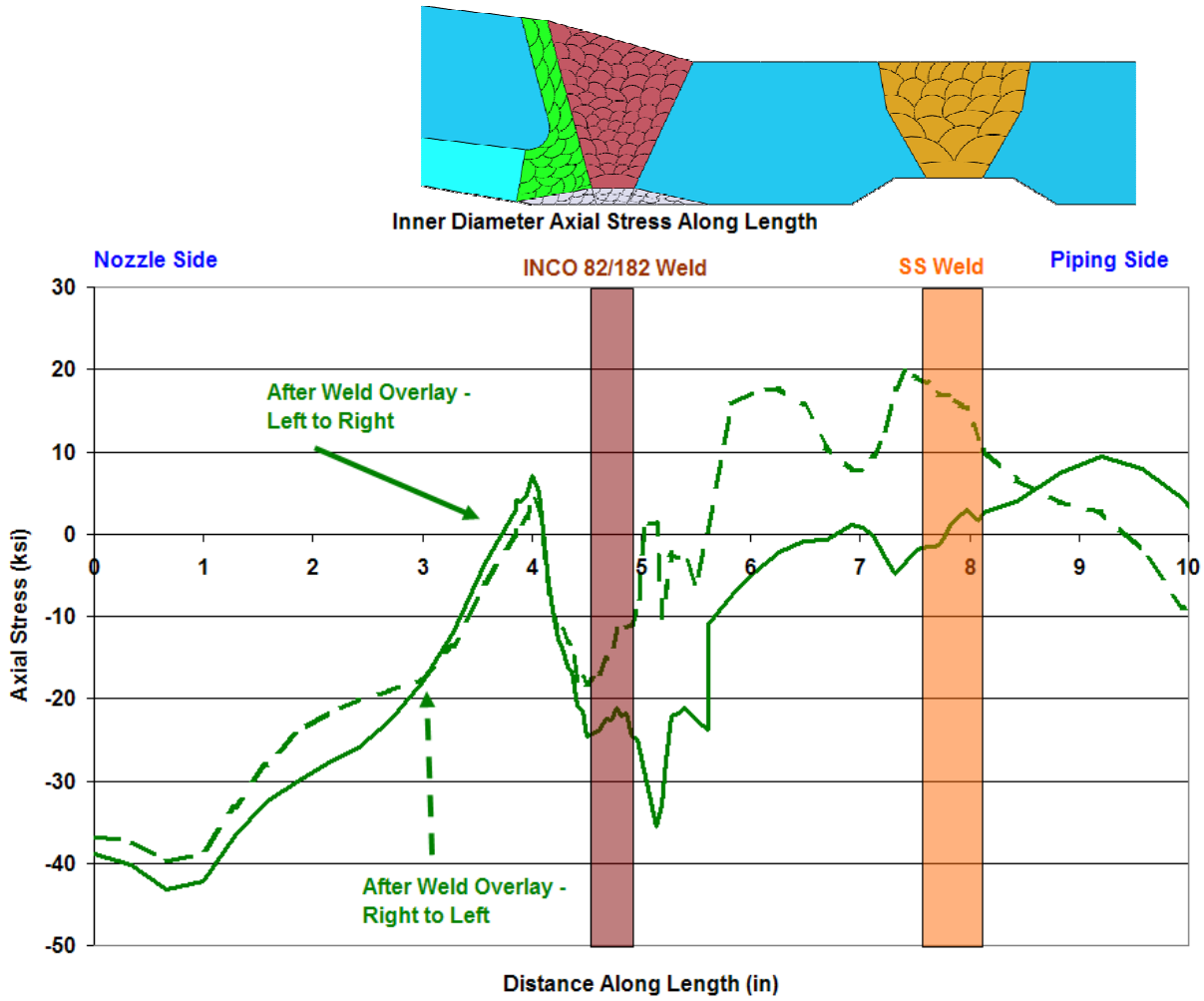

Figure 70 Surge Nozzle FSWOL Opposite Weld Direction Study Inner Diameter Axial Stresses

The second part of the FSWOL weld sequence sensitivity study examined the effect of performing the weld overlay in the traditional right-to-left direction, but with two simultaneous weld heads starting at two different locations along the length of the FSWOL. This method might be used to complete the FSWOL in reduced time by doubling the amount of welding done in a given time.

Figure 71 shows the concept. The first weld head starts at the far right extent of the FSWOL while the second weld head simultaneously starts half way along the length of the FSWOL. Each weld head proceeds right-to-left to build up successive layers of weld until the FSWOL is completed.

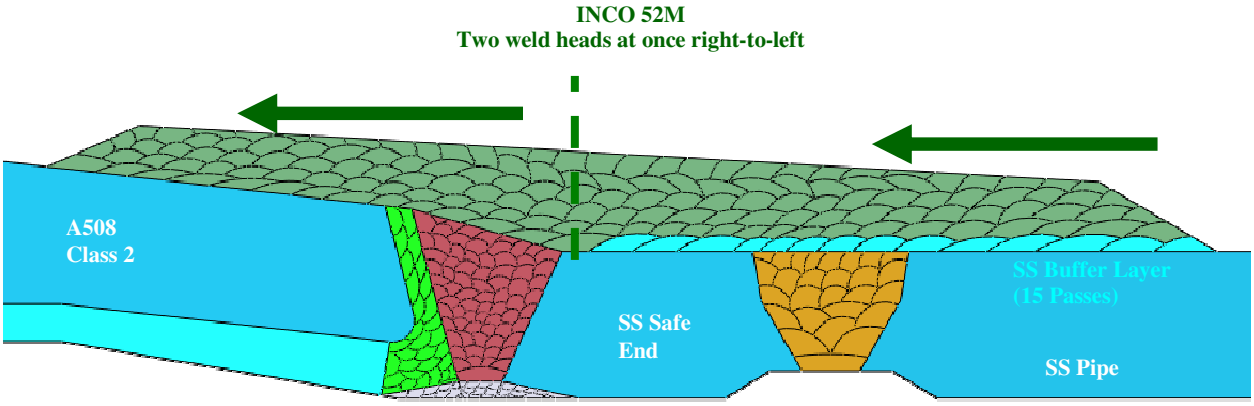

Figure 71 Surge Nozzle FSWOL Analysis using Simultaneous Weld Deposition

Figure 72 shows the axial stress profiles produced for both of these cases, i.e., single head right to left sequence and dual heads right to left sequence. There is a significant difference in the results produced by the FSWOL in the two cases. Figure 73 and Figure 74 show the dissimilar metal weld, through thickness axial stresses and the inner diameter axial stresses, respectively. In both cases the dual head process results in a less favorable resultant residual stress field.

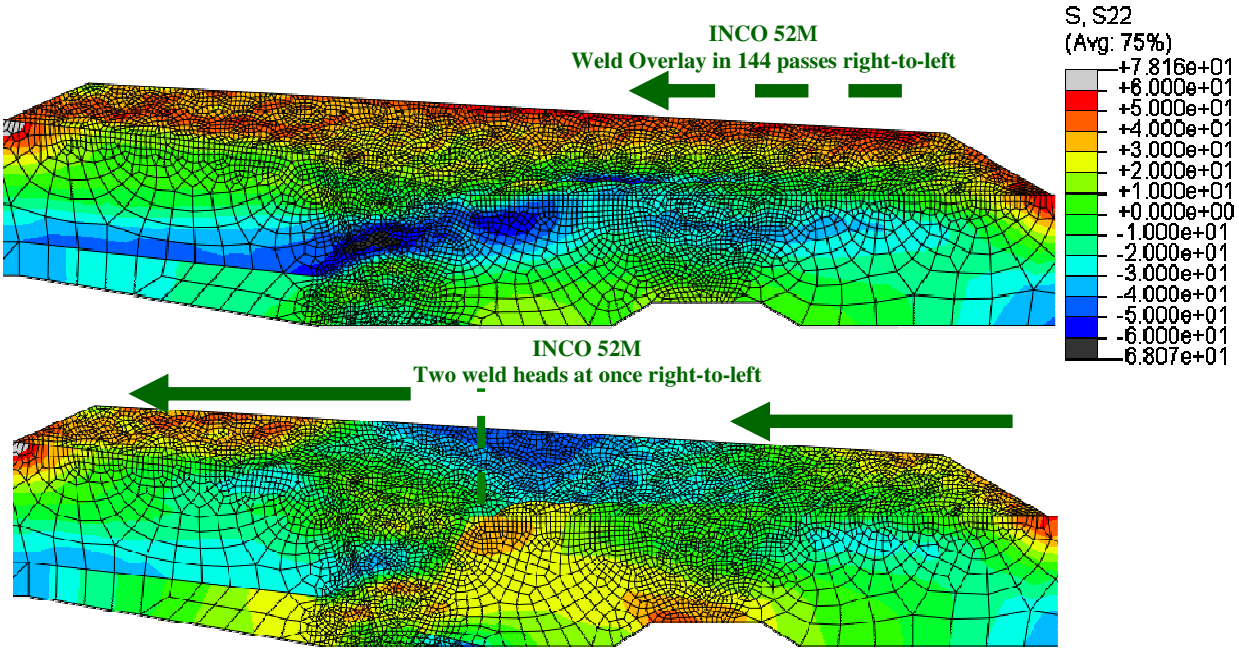

Figure 72 Surge Nozzle FSWOL Axial Stress Results from Simultaneous Weld Deposition Analysis

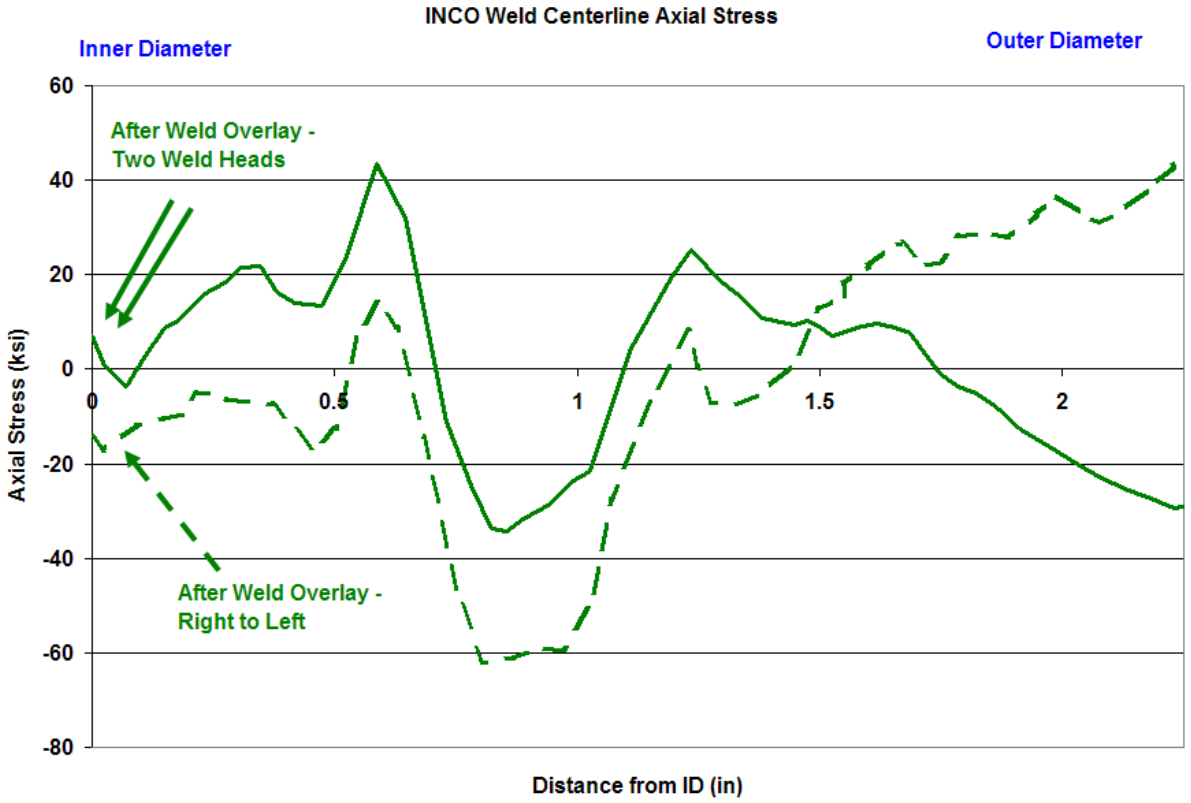

Figure 73 Surge Nozzle FSWOL Through Thickness Axial Stress Results from Simultaneous Weld Deposition Analysis

It is important to note that changes in weld sequencing in the field from that which was analyzed can negate any claimed weld residual stress benefit predicted for the weld overlay. Several sensitivity studies were conducted to evaluate the effect of weld overlay weld sequencing on the resulting weld residual stress field. Some sequence changes evaluated created large changes in the resulting weld residual stress field. In designing a full structural weld overlay or an optimized weld overlay for a certain geometry it is crucial that the design that is evaluated and approved is the design that is actually created in the field.

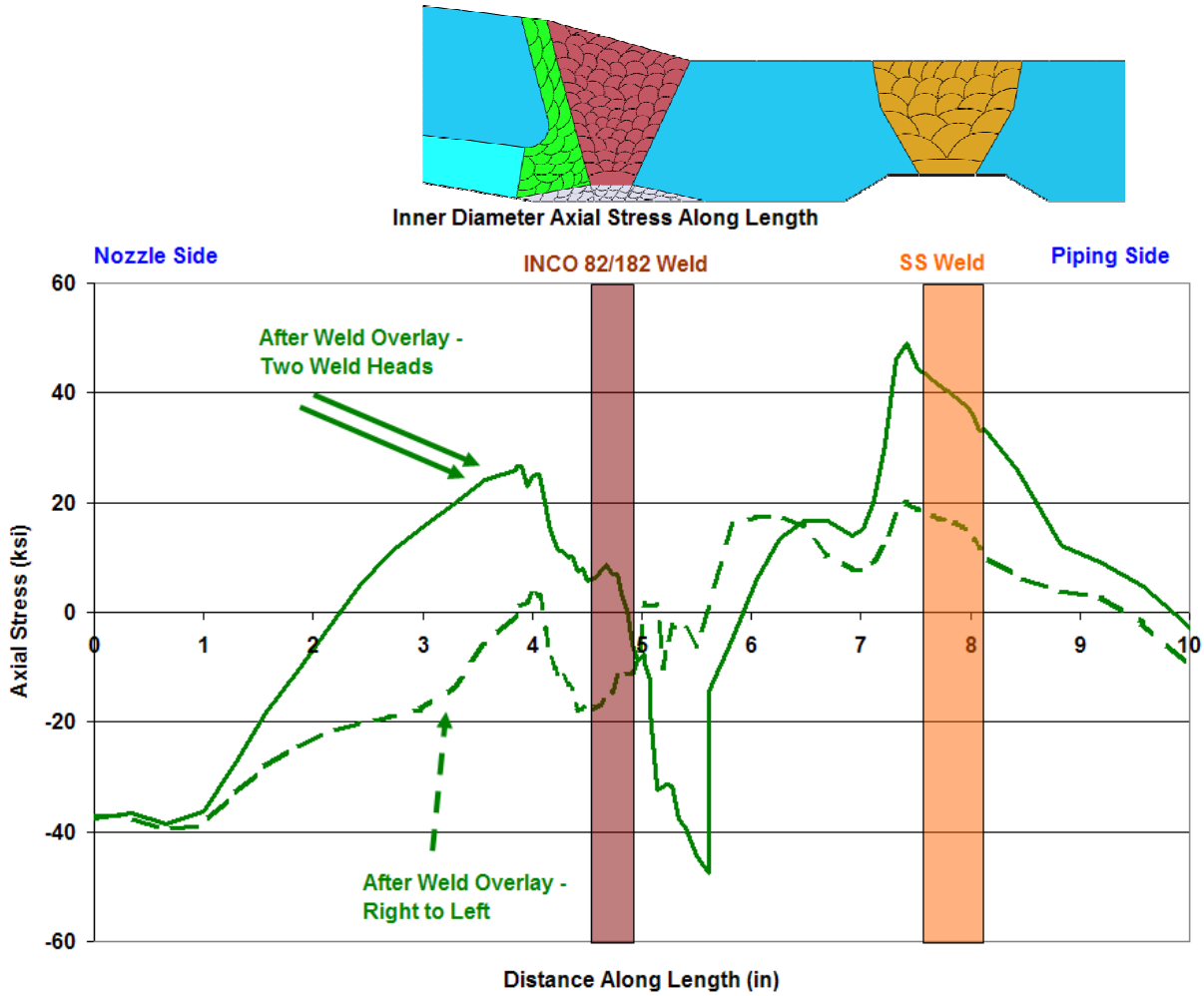

Figure 74 Surge Nozzle FSWOL Inner Diameter Axial Stress Results from Simultaneous Weld Deposition Analysis

4.1.5.4 Effect of Weld Overlay Thickness on Dissimilar Metal Weld Residual Stresses

Sensitivity studies were done on each model to examine the effect of weld overlay thickness on the residual stresses for typical dissimilar metal weld configurations. For the surge, safety, and RCP nozzle geometries the study included thicknesses up to FSWOL. For the cold leg nozzle geometry, the study also looked at the effect of layer thickness, but only up to the final OWOL thickness.

Figure 75 defines the layers of weld overlay examined in this study. All are a subset of the FSWOL. The stresses through the thickness and along the inner diameter were examined as was done previously, but in this case, they were plotted after each layer of the weld overlay was applied. The temperature of the nozzle was allowed to cool to below 38 C (100 F) after the last weld bead in each layer.

Pressurizer Safety Nozzle

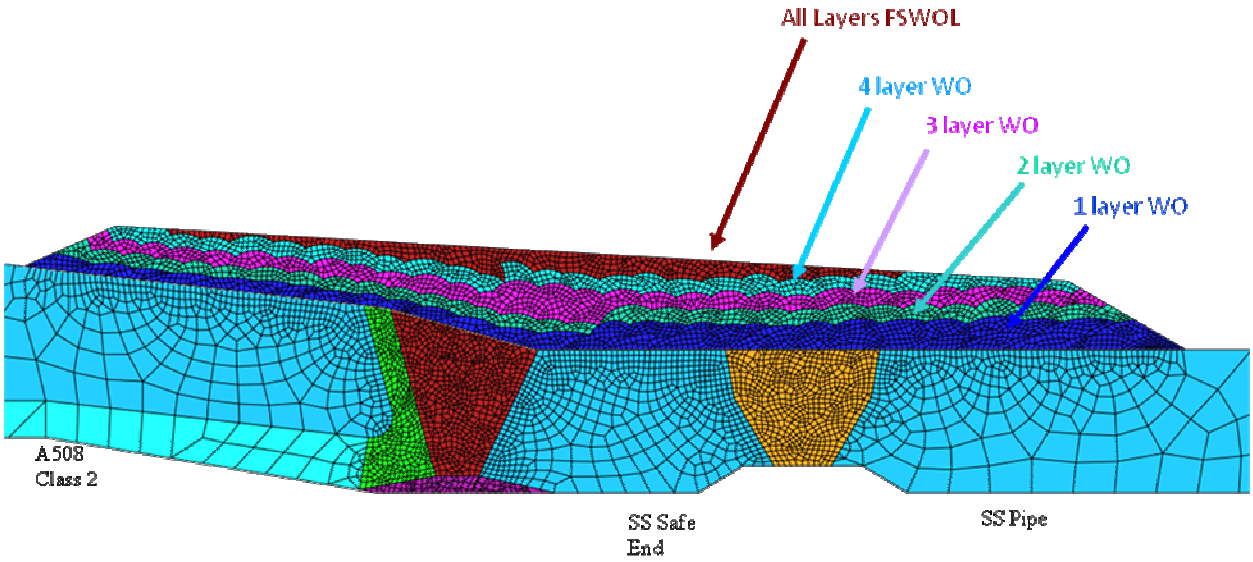

Figure 75 Pressurizer Surge Nozzle Weld Overlay Layers Studied

Figure 76 shows the axial stress contour plot before, during and after the FSWOL is completed. The arrows show the through thickness path plotted in Figure 77 which shows the axial stress results for the layers as defined in Figure 75. The graph shows that the results at the inner diameter are very similar after each of the weld overlay layers.

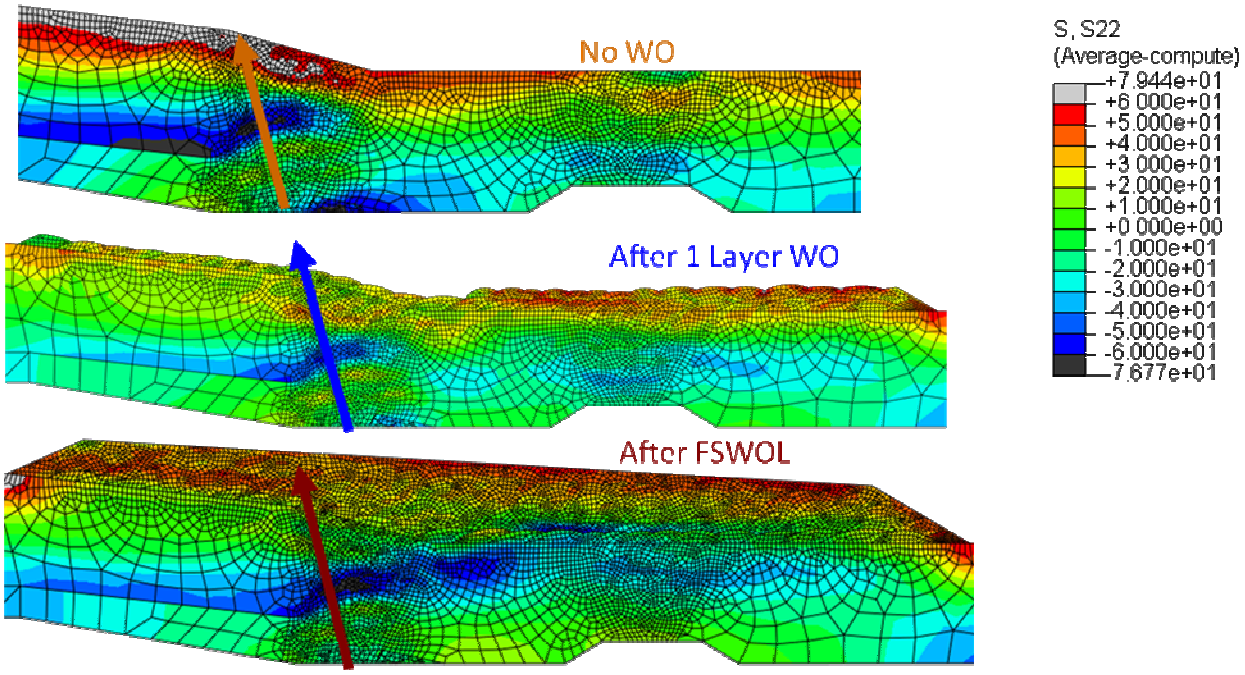

Figure 76 Surge Nozzle Axial Stresses showing Through Thickness Path Graphed (ksi)

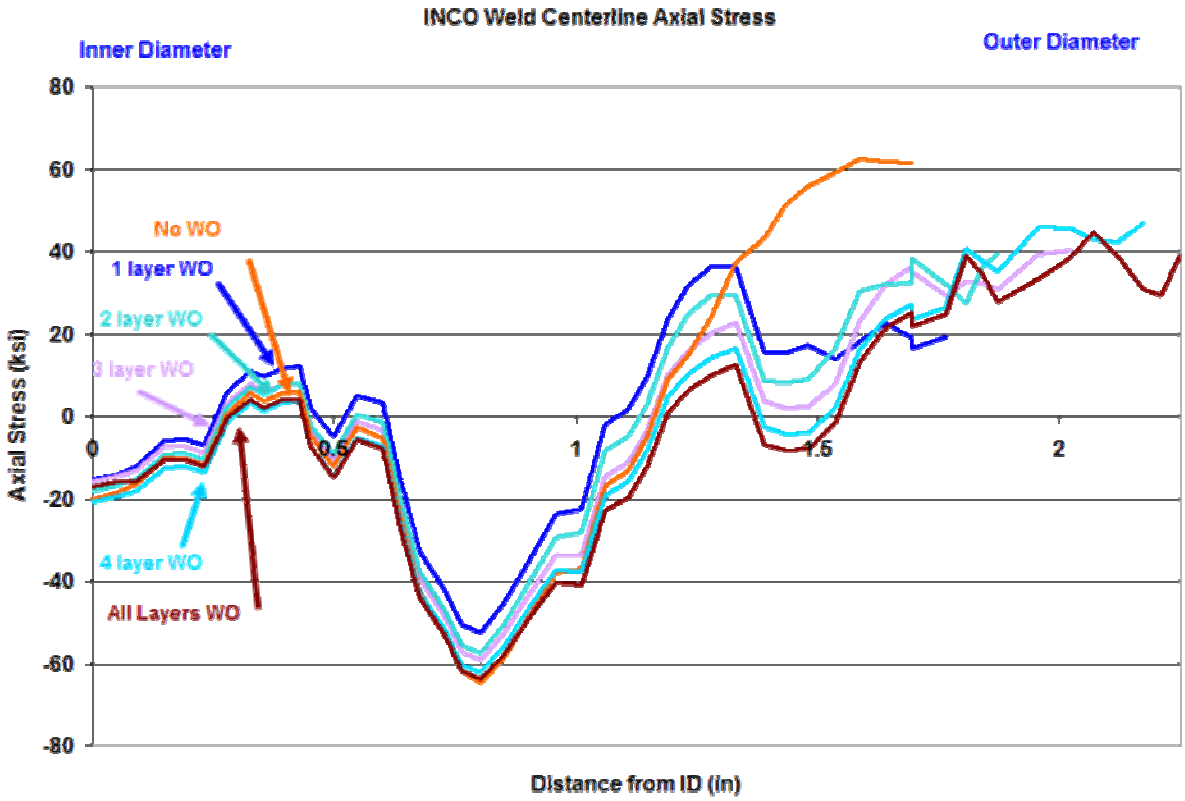

Figure 77 Surge Nozzle Through-Wall Axial Stresses through Weld Overlay Process

As was shown previously, it is important to look at the stresses on the inner diameter along the whole length of the PWSCC susceptible area to examine the effect on the most highly stressed region.

Figure 78 shows the axial stress along the inner diameter of the surge nozzle. The vertical bars in the graph indicate the location of the butter layer as well as the Inconel weld and the secondary stainless steel weld with the same color coding as used in the previous graphs. The maximum axial tension stress on the inner diameter is found at the transition between the Inconel butter layer and the pressure vessel steel as shown previously. The graph shows that each subsequent layer of weld overlay material reduces the axial tension stress at this maximum stress location. The effect is almost linear with thickness. It should be noted that the axial tension in the dissimilar metal weld area remains in tension in all cases, and is only reduced to near zero with the application of the FSWOL thickness.

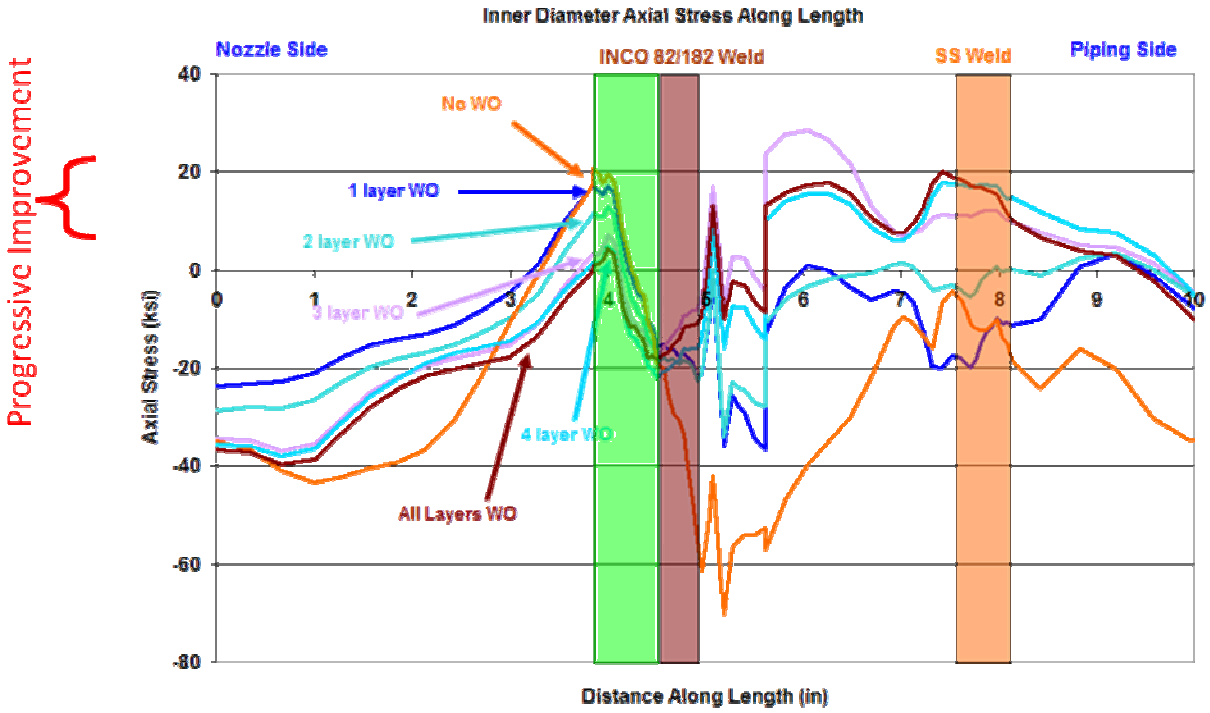

Figure 78 Surge Nozzle ID Axial Stresses Through Weld Overlay Process

Figure 79 shows the hoop stress contour plot before, during and after the FSWOL is completed. The top stress contour plot shows that there is high hoop tension through the dissimilar weld area. One would expect axial PWSCC cracks to grow entirely through the wall thickness in this stress field. The arrows show the through thickness path plotted in Figure 80 which shows the hoop stress results for the layers as defined in Figure 75. The graph shows that unlike the axial stress in this cross section, the hoop stress is greatly affected by the thickness of the weld overlay. It also shows that even though one and two layers of weld overlay can put the inner diameter in compression, there are tension stresses just below the surface. It takes three layers to keep the through wall hoop stress in compression.

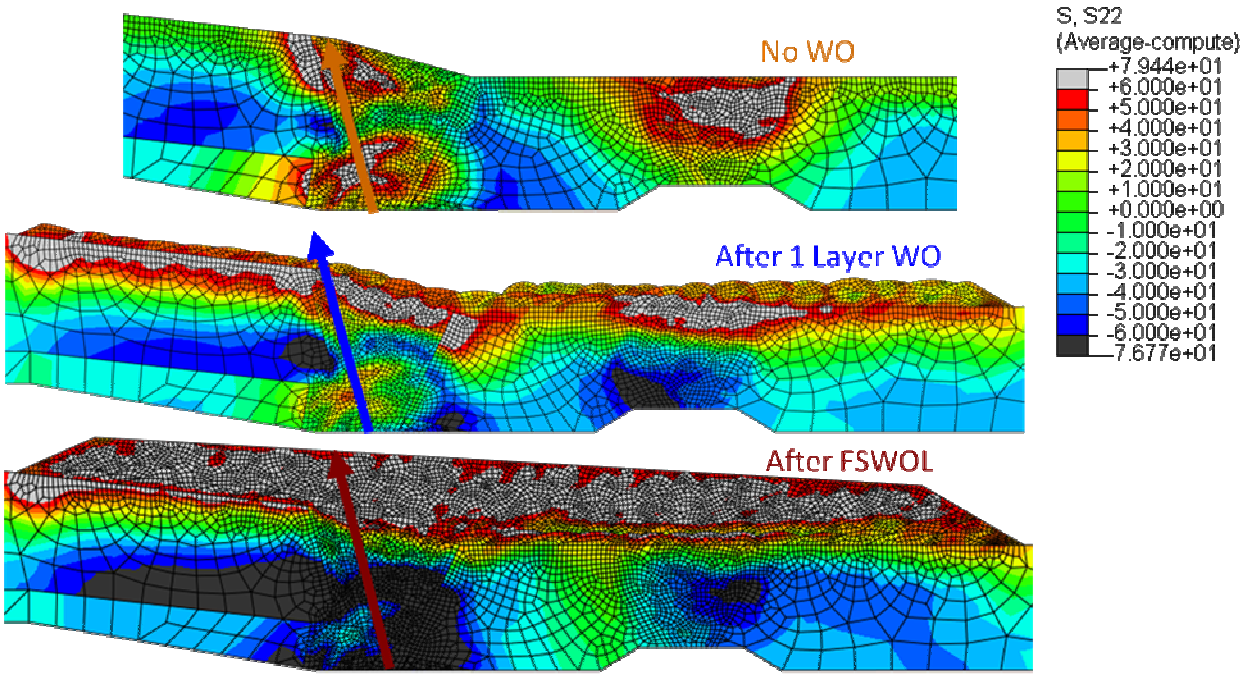

Figure 79 Surge Nozzle Hoop Stresses showing Through Thickness Path Graphed (ksi)

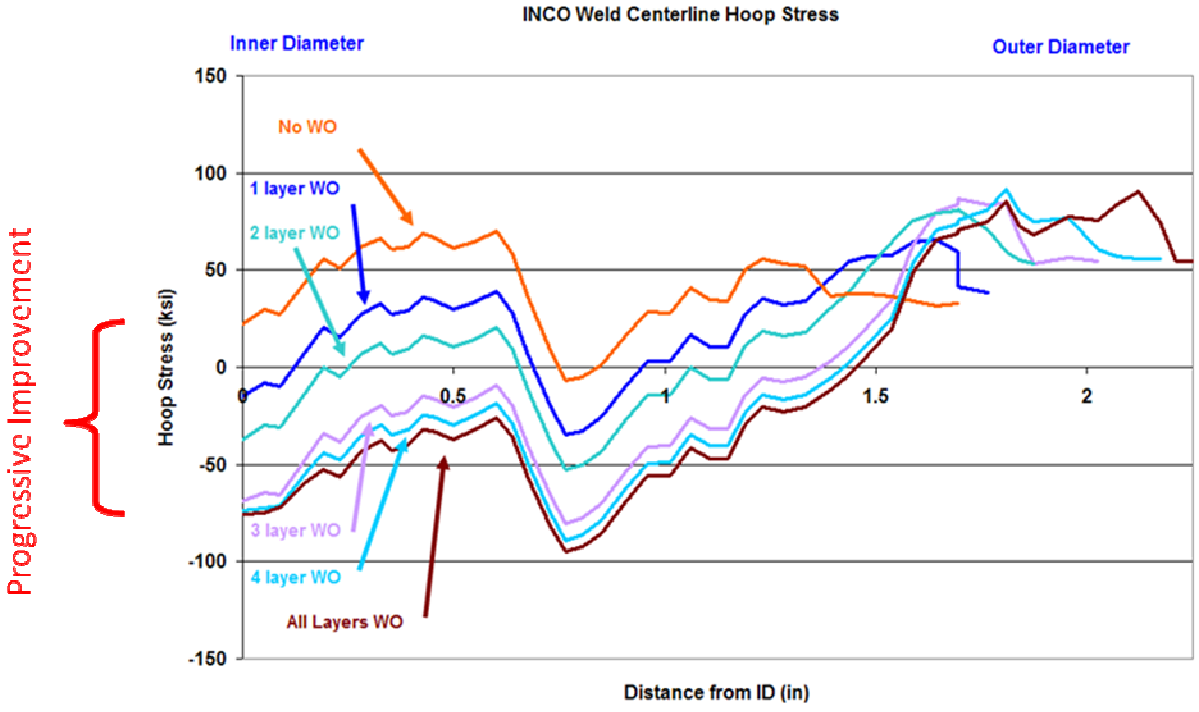

Figure 80 Surge Nozzle Through Thickness Hoop Stresses

The effect is even more dramatic when one looks at the maximum stress on the inner diameter of the surge nozzle. Figure 81 shows the inner diameter hoop stress. The figure shows that the beneficial compressive stress of the FSWOL drops off quickly with thinner layers of weld overlay material. Though the change with each layer of weld overlay material is dramatic, the chart also shows that a single layer is enough to reduce the hoop tension stress from 303 MPa to 83 MPa (44 ksi to 12 ksi), and two layers puts the entire PWSCC susceptible region in compression.

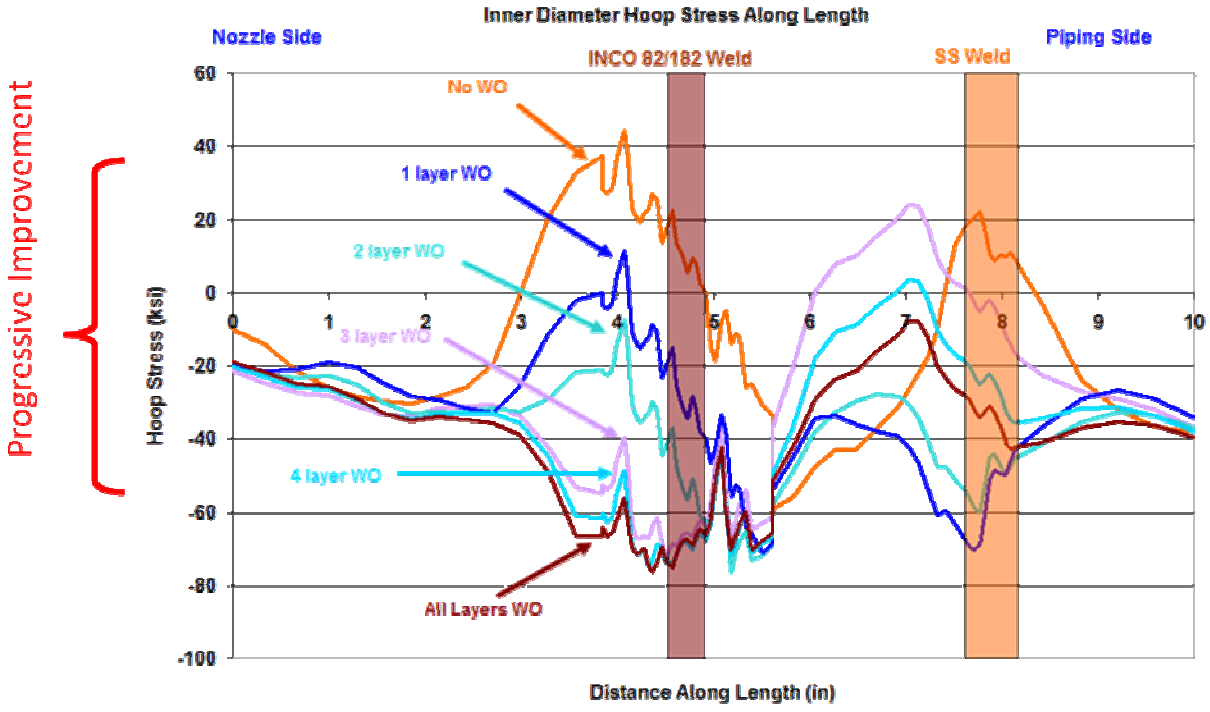

Figure 81 Surge Nozzle ID Hoop Stresses through Weld Overlay Process

Figure 82 shows a normalized comparison of stress reduction vs. weld overlay thickness for the surge nozzle geometry. Both axial and hoop stress are changed in a nearly linear fashion with weld overlay thickness for this geometry. That is not the case for the other geometries studied in this section. The effect of stress reduction vs. weld overlay thickness seems to be highly dependent on both geometry and weld sequencing.

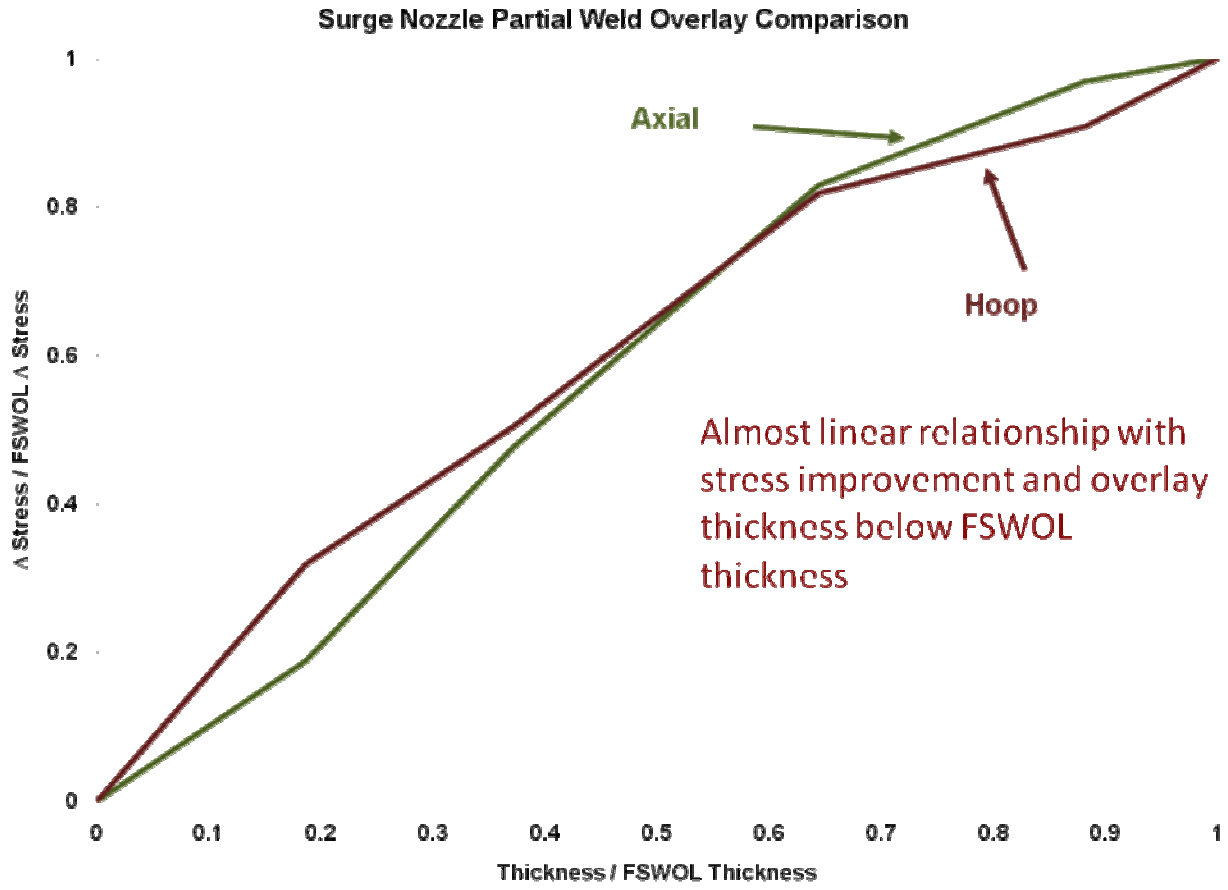

Figure 82 Surge Nozzle Comparison of OverlayThickness versus Stress Improvement Effect

Pressurizer Safety Nozzle

A similar analysis was done for looking at the pressurizer safety nozzle results. Figure 83 defines the layers of weld overlay examined in this study. All are a subset of the FSWOL. The layer divisions were made with no other criterion than they were the size of the weld beads that were modeled in the initial analysis. The temperature of the nozzle was allowed to cool to below 38 C (100 F) after the last weld bead in each layer.

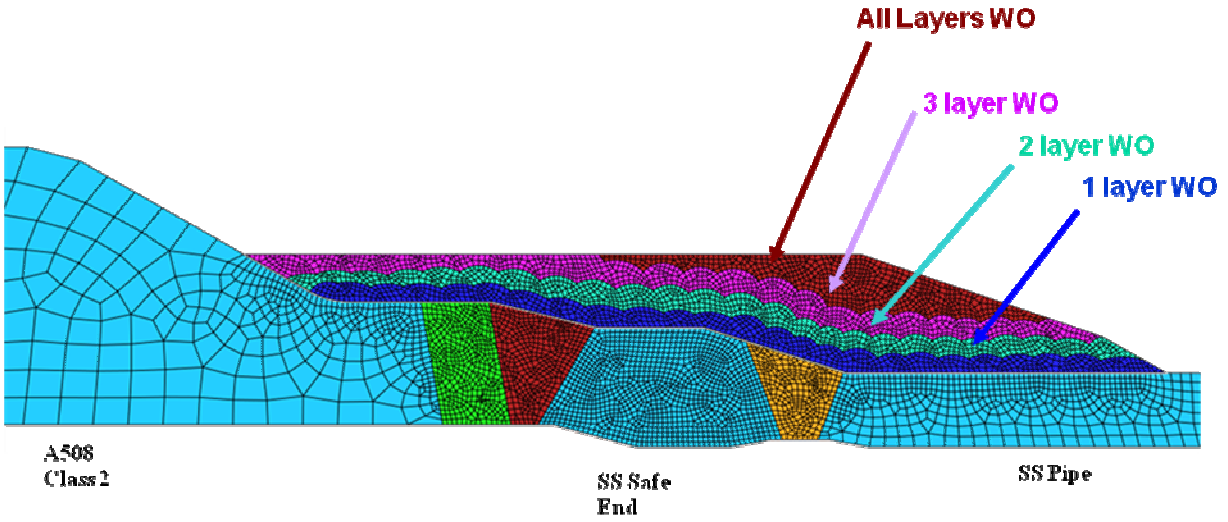

Figure 83 Pressurizer Safety Nozzle Weld Overlay Layers Studied

Figure 84 shows the axial stress contour plot before, during and after FSWOL is completed. The arrows show the through thickness path plotted in Figure 85 which shows the axial through thickness stress results for the layers as defined in Figure 83. The through thickness graph shows that for this cross section the stress behavior is unexpected. As layers are applied, the stresses oscillate. One layer is far worse than no layers, and then two layers are better, but three layers are worse again. Only completion of the FSWOL brings the stresses in this cross section below the original values with no overlay. For this geometry it is important to look at the stresses along the whole inner diameter of the area of interest.

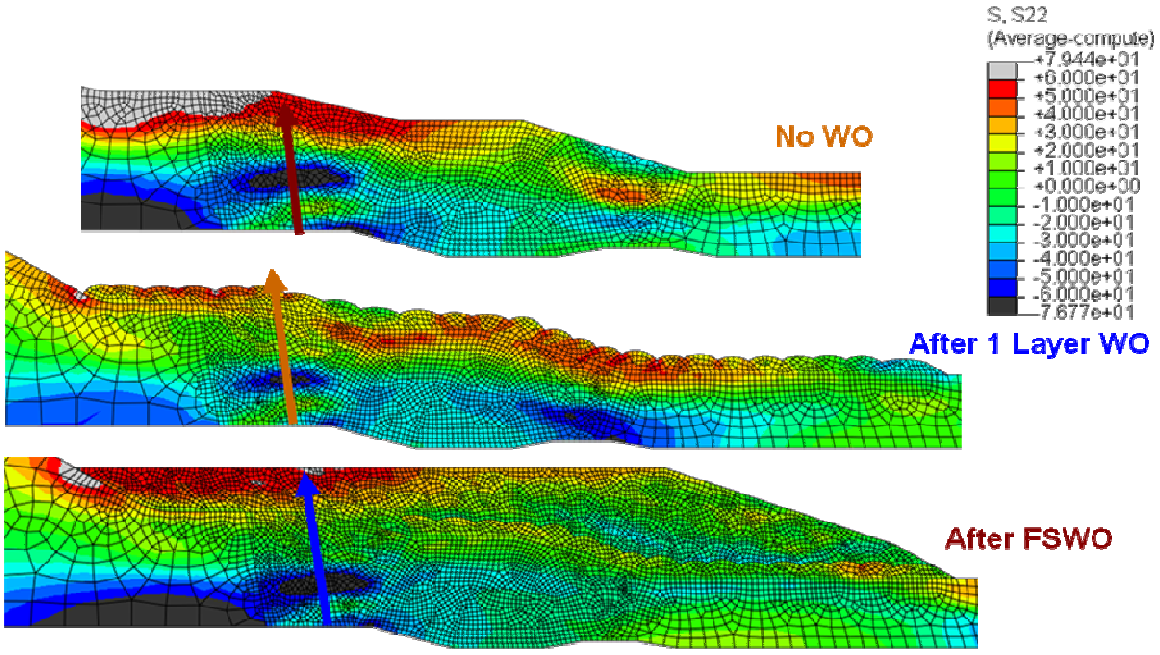

Figure 84 Safety Nozzle Axial Stresses showing Through Thickness Path Graphed (ksi)

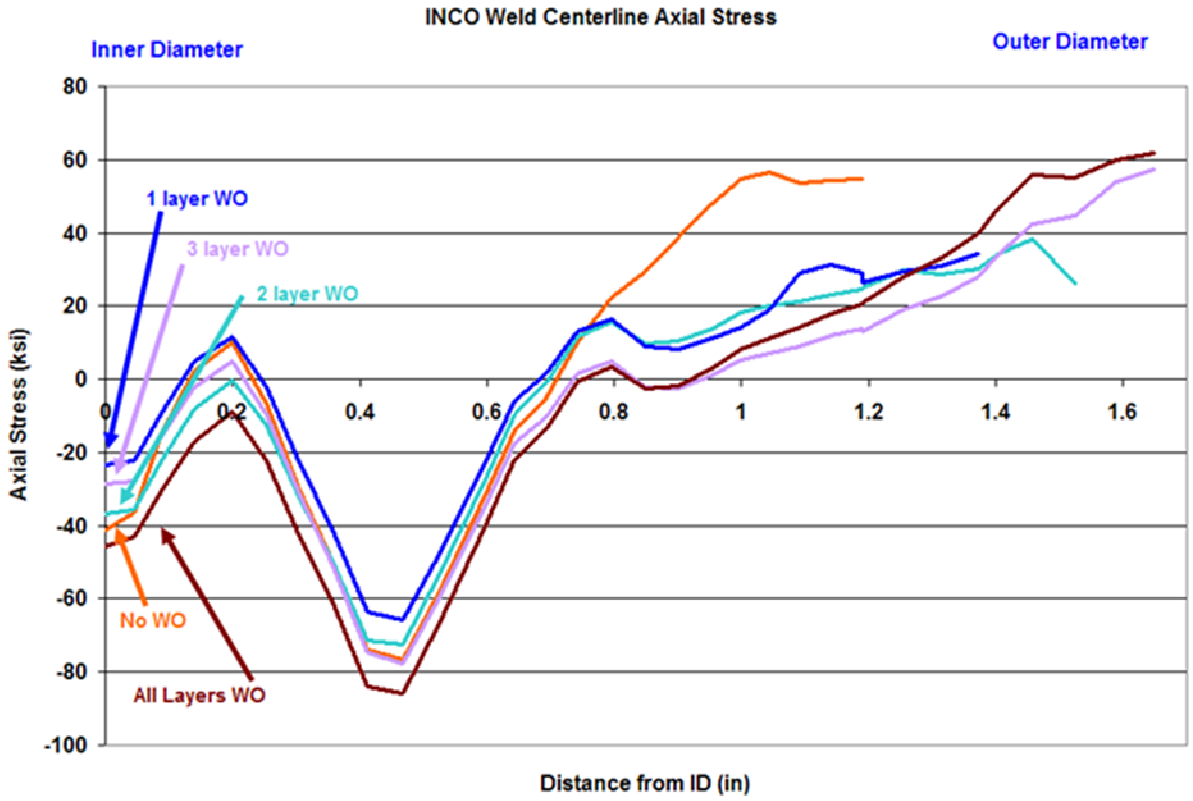

Figure 85 Safety Nozzle Axial Stresses through Weld Overlay Process

Figure 86 shows the axial stress along the inner diameter of the safety nozzle. The vertical bars in the graph indicate the location of the Inconel weld and the secondary stainless steel weld with the same color coding as used in the previous graphs. The maximum axial tension stress on the inner diameter is found at the transition between the butter layer and the ferritic pressurizer vessel steel as shown previously. The graph shows the same oscillating behavior that the previous through thickness graph did. If one looks at only the maximum axial stress in the Inconel weld area, one sees that the application of one layer makes the peak stress higher than it was with no weld overlay and even makes the stress tensile when it was originally already in compression. Layers two and three reduce the stress from the original value. Finally as the FSWOL is completed, the stresses are made well below the original peak values.

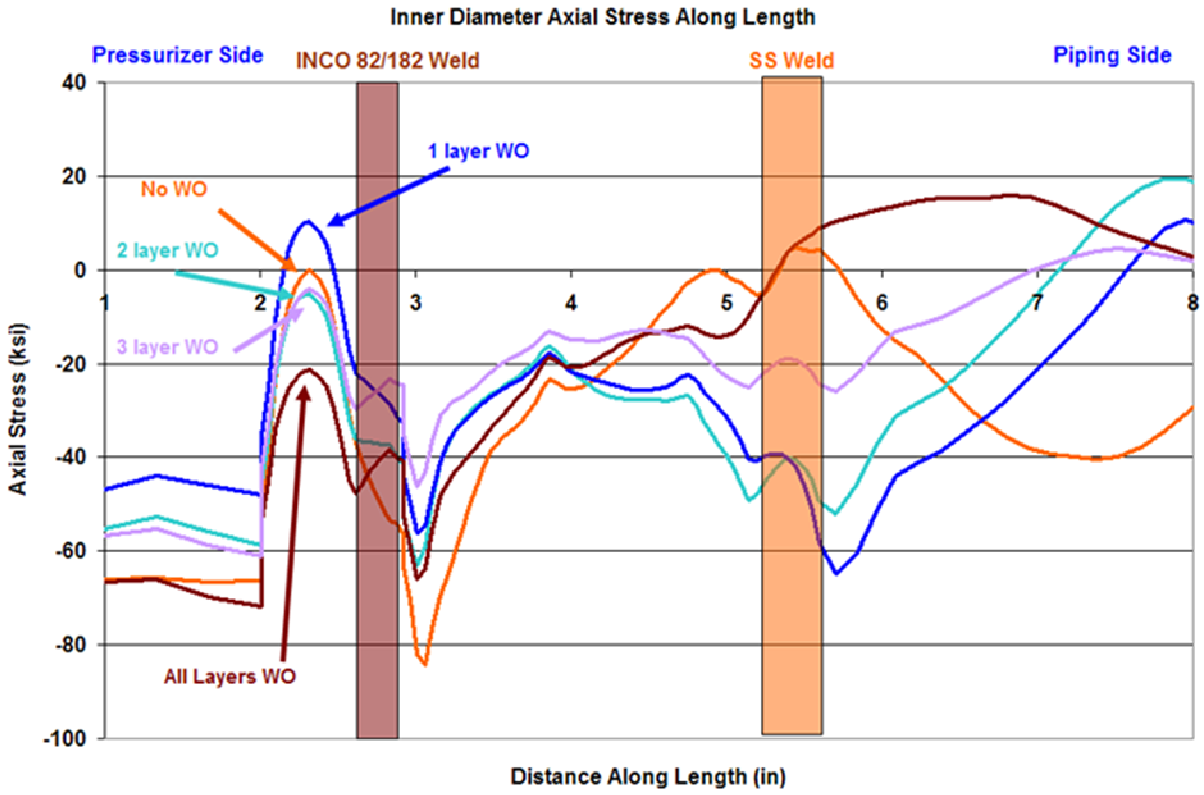

Figure 86 Safety Nozzle ID Axial Stresses Through Weld Overlay Process

Figure 87 shows the hoop stress contour plot before, during and after the FSWOL is completed. The top stress contour plot shows that there is high hoop tension through the dissimilar weld area. The arrows show the through thickness path plotted in Figure 88 which shows the hoop stress results for the layers as defined in Figure 83. The graph shows that unlike the axial stress in this cross section, the hoop stress is greatly affected by the thickness of the weld overlay and in a progressive fashion. Increased weld overlay thickness reduces the stress at the inner diameter. The stress becomes compressive after the application of just one layer, and becomes completely compressive for half the original thickness after three layers are applied.

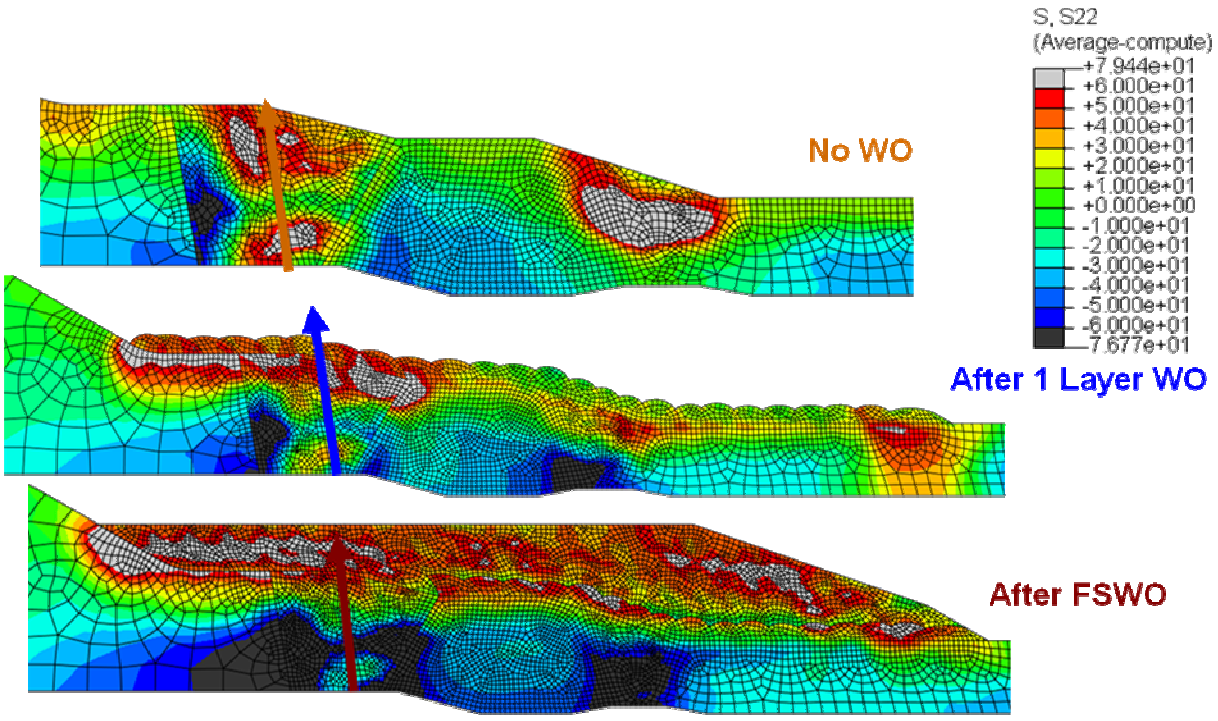

Figure 87 Safety Nozzle Hoop Stresses Showing Through Thickness Path Graphed (ksi)

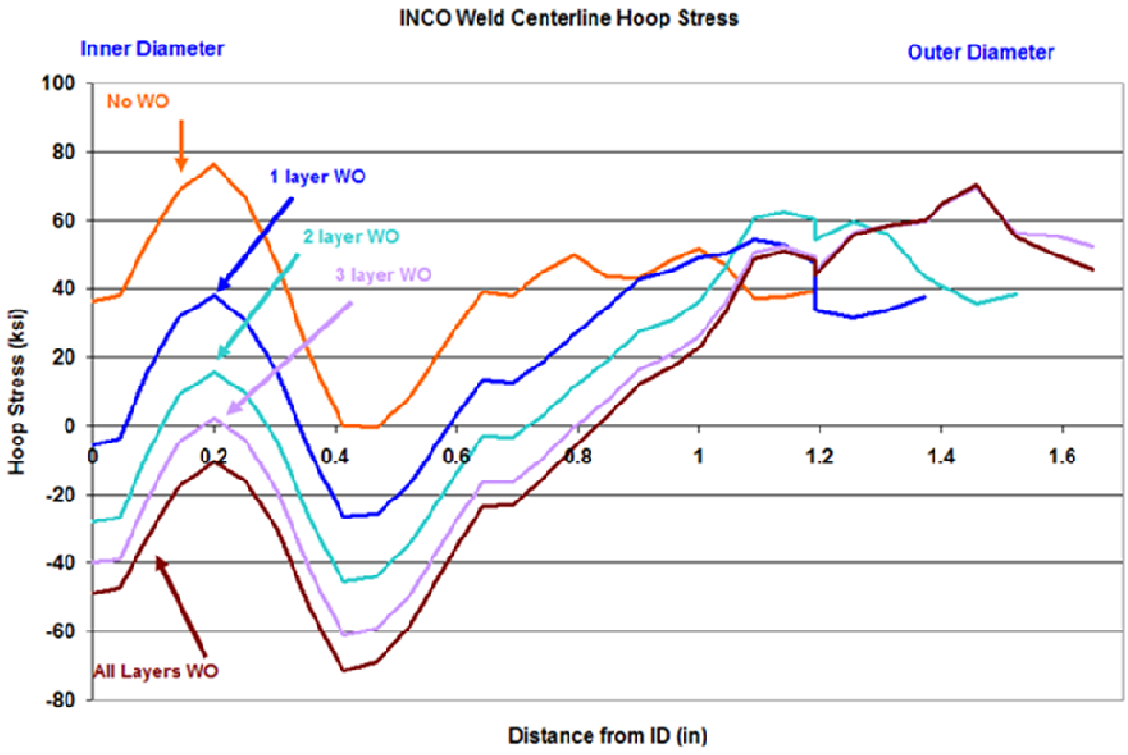

Figure 88 Safety Nozzle Through Thickness Hoop Stresses

The effect is even more dramatic when one looks at the maximum stress on the inner diameter of the surge nozzle. Figure 89 shows the inner diameter hoop stress. The graphs shows an almost uniform improvement in maximum stresses with the addition of more overlay thickness.

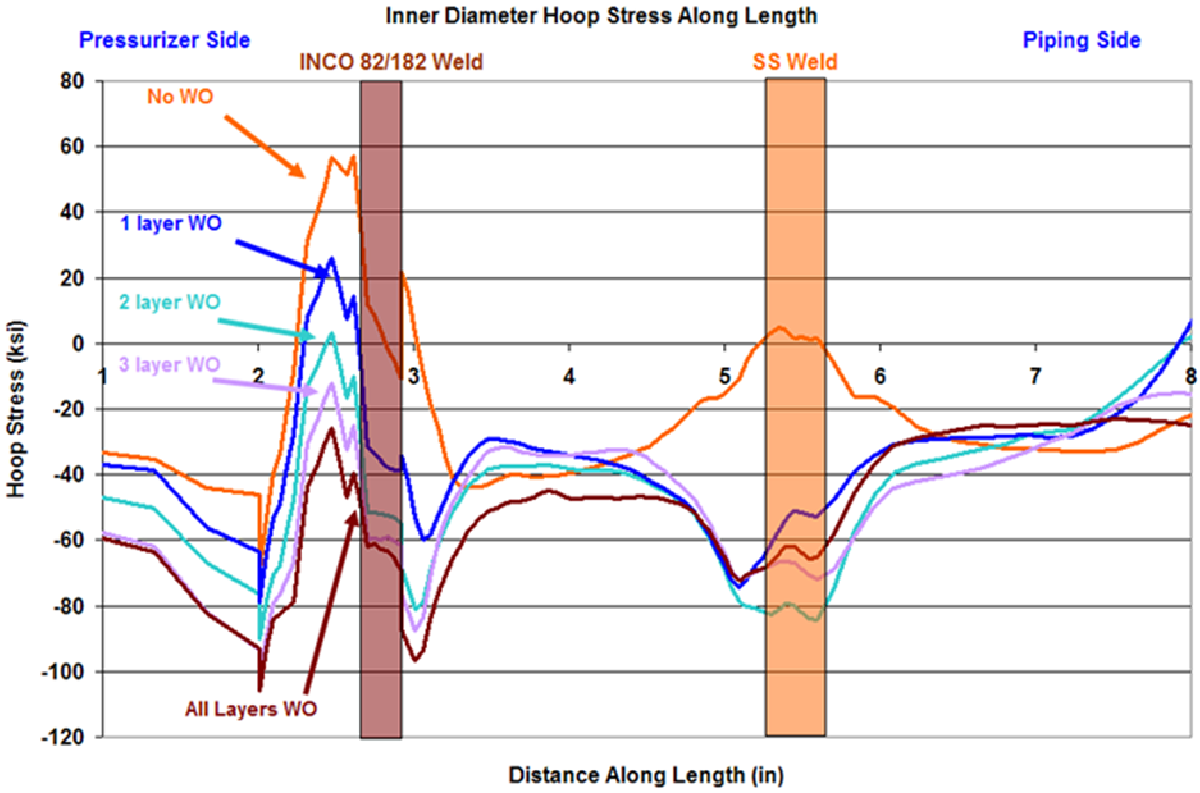

Figure 89 Safety Nozzle ID Hoop Stresses through Weld Overlay Process

Cold Leg Nozzle

For the cold leg nozzle, the finite element modeling only included the OWOL thickness and not a complete FSWOL. Figure 90 defines the layers of weld overlay examined in this study. All are a subset of the OWOL. The stresses through the thickness and along the inner diameter were examined as was done previously. The temperature of the nozzle was allowed to cool to 21 C (70 F) after the last weld bead in each layer for this case and for the reactor coolant pump outlet nozzle to follow.

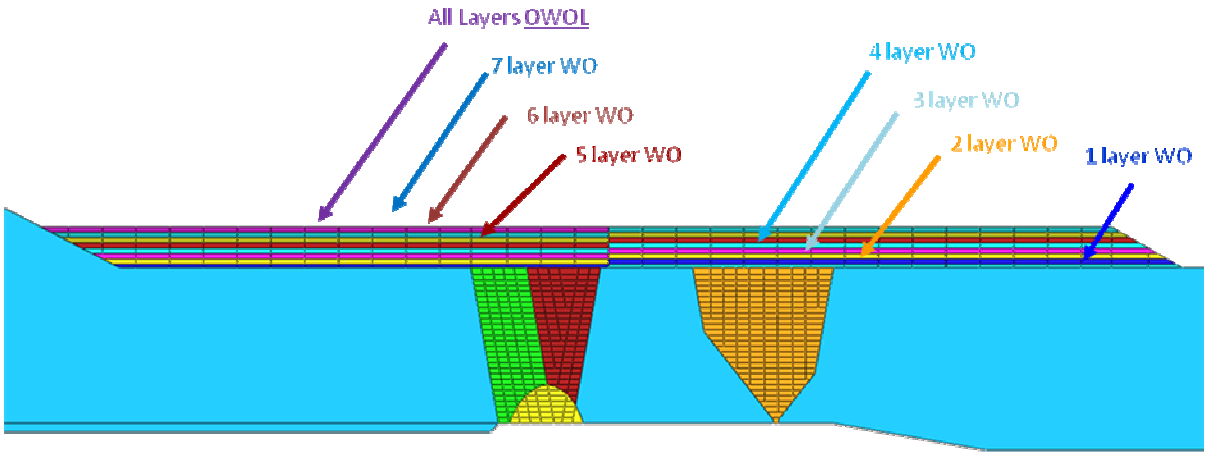

Figure 90 Cold Leg Nozzle Weld Overlay Layers Studied

Figure 91 which shows the axial stress results through the thickness at the interface between the butter and the Inconel weld for the layers as defined in Figure 90. The graph shows a similar oscillating behavior of the results as was shown previously for the safety nozzle. The application of one, two and three layers makes the inner diameter stress progressively higher than the original stress with no weld overlay. The fourth layer brings the stress back down, but not down to the level that they were with no weld overlay at all. The remaining layers do not change the stress much in this cross section.

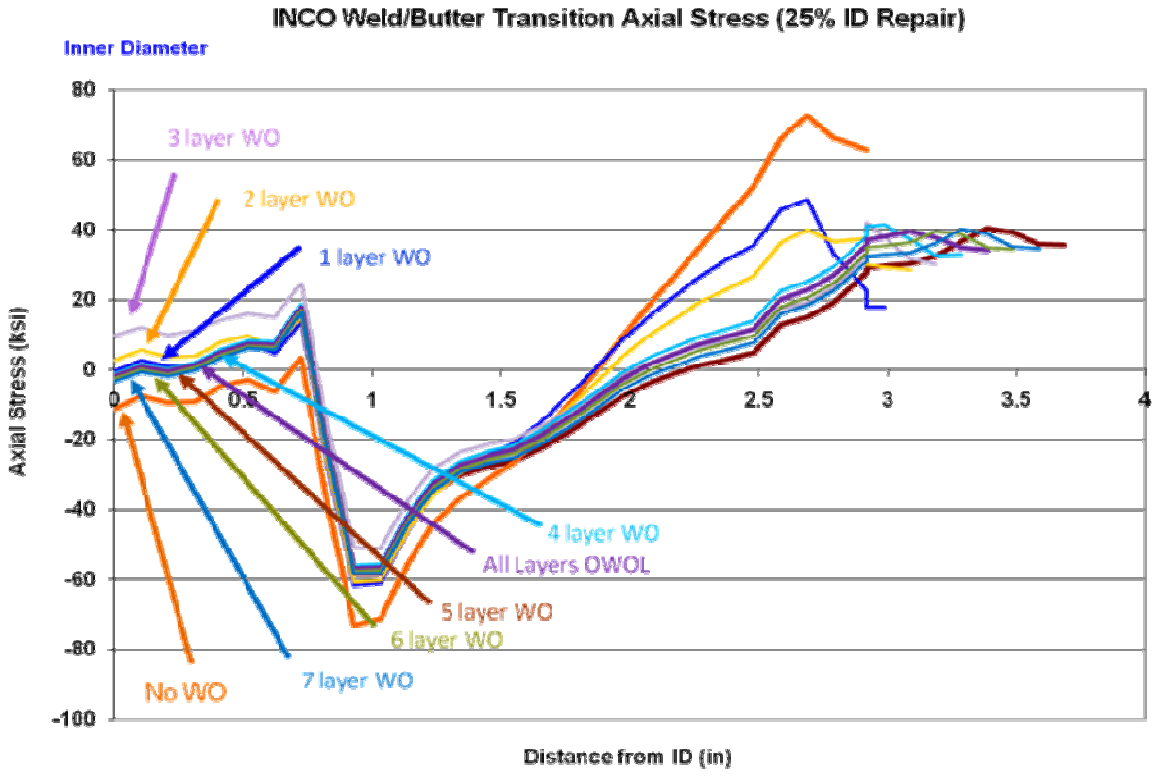

Figure 91 Cold Leg Nozzle Axial Stresses through Weld Overlay Process

As was shown previously, it is important to look at the stresses on the inner diameter along the whole length of the PWSCC susceptible area to examine the effect on the most highly stressed region. Figure 92 shows the axial stress along the inner diameter of the cold leg nozzle. For this case a smaller length of the nozzle is shown which includes only the butter and Inconel weld areas. The vertical bars in the graph indicate the location of the butter layer as well as the Inconel weld with the same color coding as used in the previous graphs. The maximum axial tension stress on the inner diameter is found at the transition between the Inconel butter layer and the ferritic pressure vessel steel as shown previously. The graph shows the same oscillation behavior as was displayed in the previous graph. The maximum stress with no weld overlay is 69 MPa (10 ksi). The stress in this area is increased to 186 MPa (27 ksi) after two layers are applied, and stresses remain higher than the original value until four layers are applied. The maximum stresses then remain lower than the original value with no weld overlay with subsequent layers changing the stress little. It is interesting to note that the stress improvement for layers four through OWOL at the maximum stress area becomes a determent about half way through the butter thickness. At this point the weld overlay increases the stress from the value with no weld overlay at all. Or course, it was shown earlier that the application of operating pressure and temperature reduce these stresses to values below what would be obtained with no weld overlay.

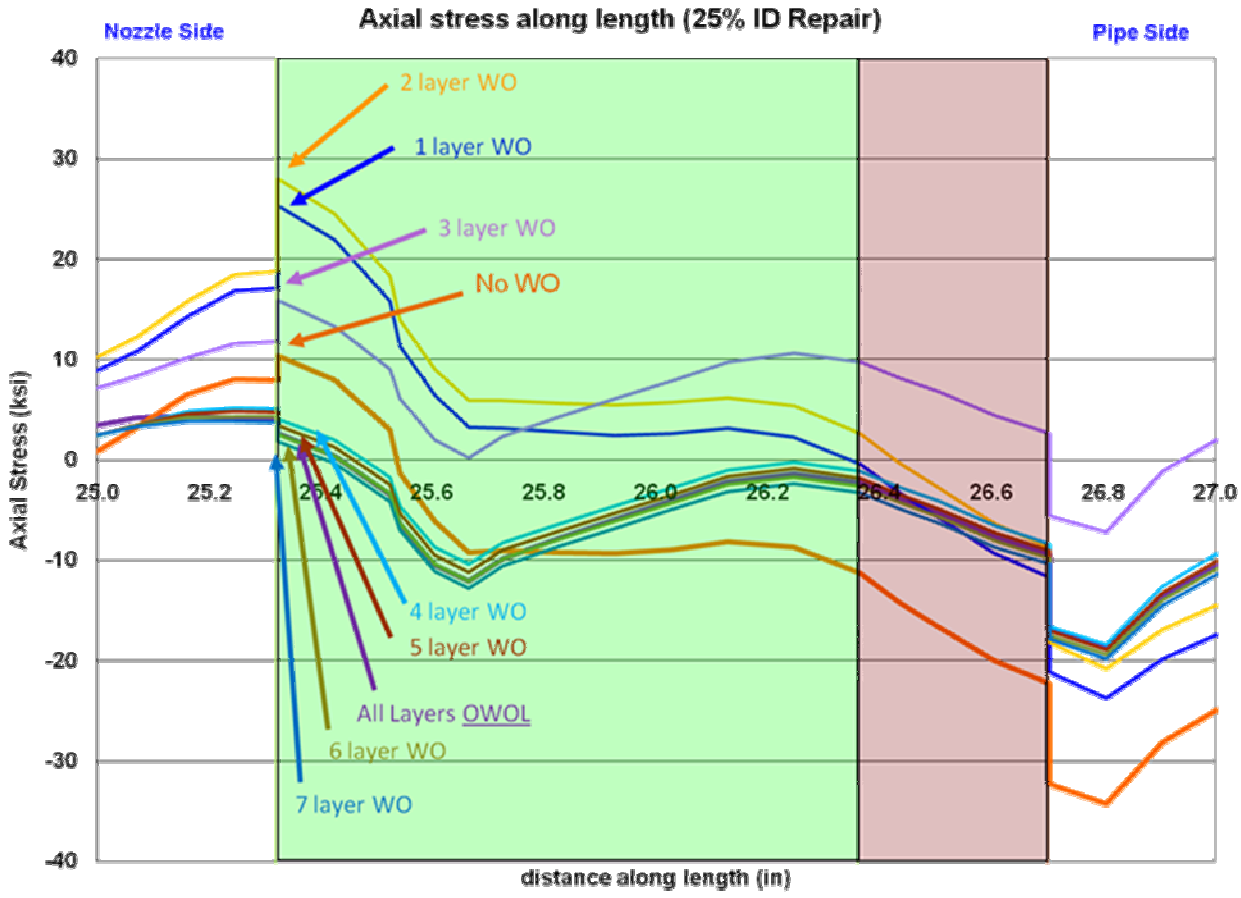

Figure 92 Cold Leg Nozzle ID Axial Stresses through the Weld Overlay Process

Figure 93 shows the inner diameter hoop stress. The graph shows that there is a progressive improvement in hoop stress with more layers of the weld overlay, but that this effect is not proportional to weld overlay thickness. The maximum value with no weld overlay is inboard of the transition between the butter and the pressure vessel steel. Application of layers one and two decrease the tension stress. The application of layer three makes a large change in the hoop stress and reduces the maximum value, and the whole area encompassing the dissimilar metal weld, into compression. Subsequent layers progressively improve on this by adding more compression.

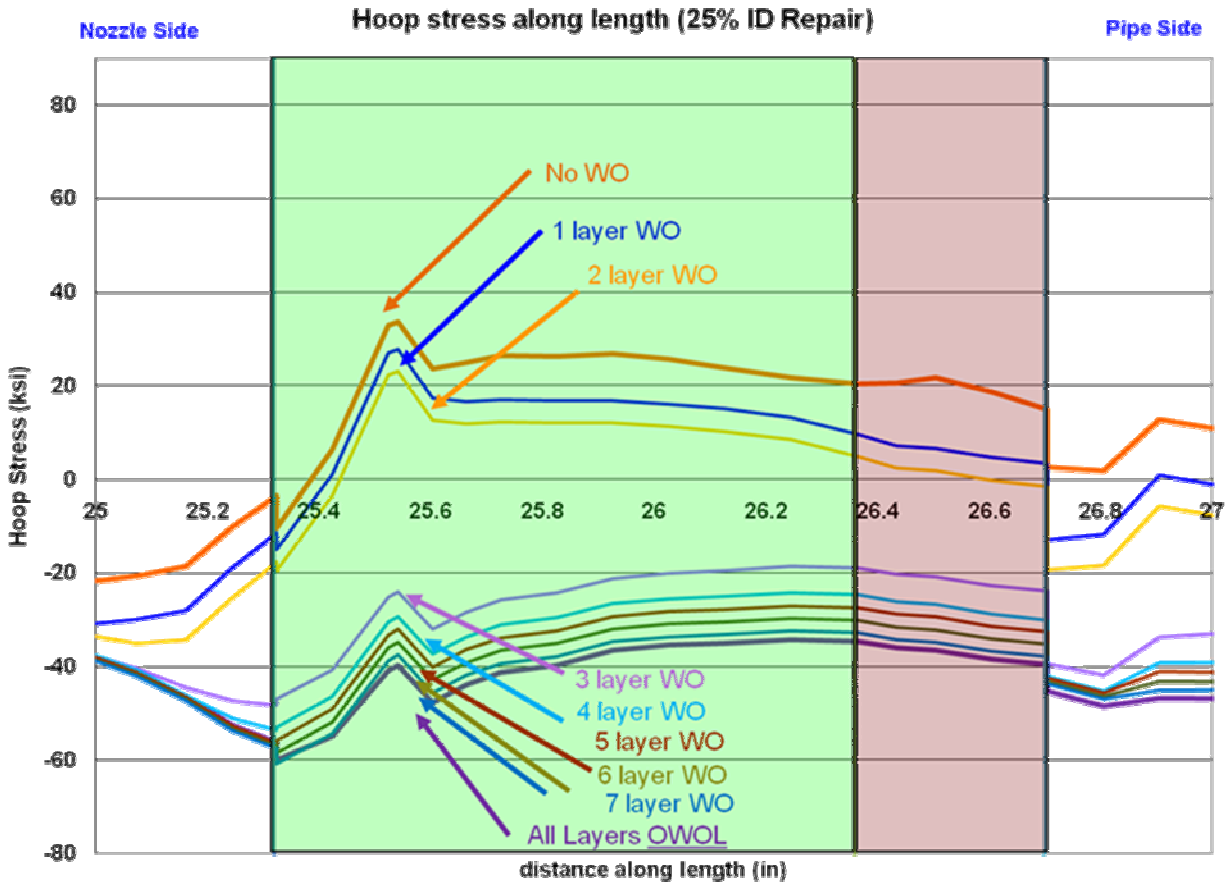

Figure 93 Cold Leg Nozzle ID Hoop Stresses through the Weld Overlay Process

Reactor Coolant Pump Outlet Nozzle

For the RCP outlet nozzle, the finite element modeling included both the OWOL and FSWOL thickness. Figure 94 defines the layers of weld overlay examined in this study. There are eight layers in all that make up the FSWOL, and the OWOL is complete after five of the eight layers. The stresses through the

thickness and along the inner diameter were examined as was done previously. The temperature of the nozzle was allowed to cool to 21 C (70 F) after the last weld bead in each layer for this case.

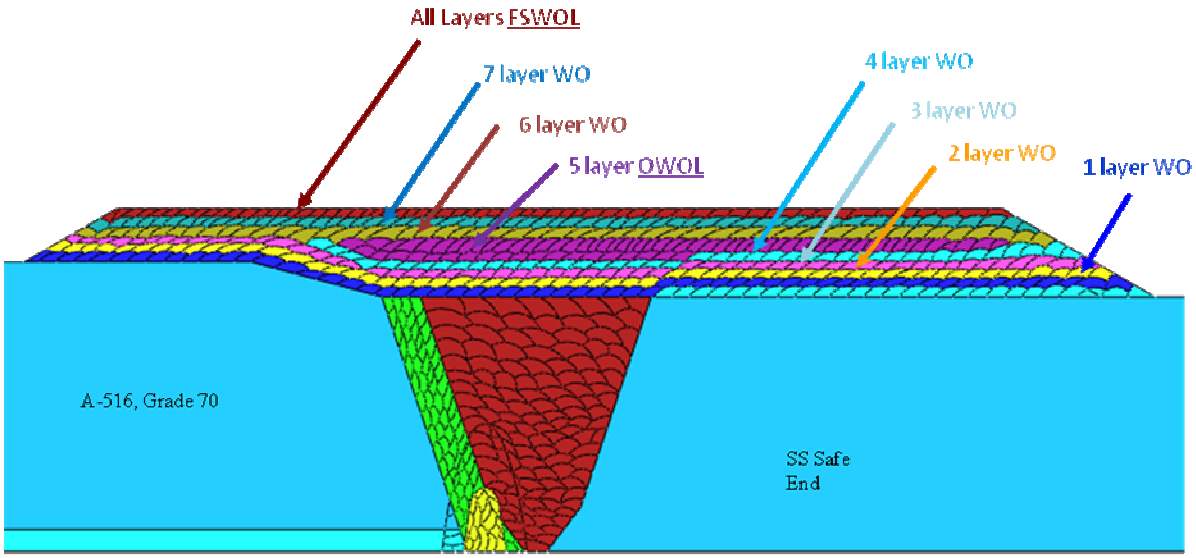

Figure 94 RCP Outlet Nozzle Weld Overlay Layers Studied

Figure 95 shows the axial stress along the inner diameter of the RCP outlet nozzle. The vertical bars in the graph indicate the location of the butter layer as well as the Inconel weld. The secondary stainless steel weld area was of less interest and is left out of these graphs. The maximum axial tension stress on the inner diameter is found at the interface of the butter the ferritic pipe material and slightly to the right of the Inconel weld in the safe end material and are in the range slightly higher than 414 MPa (60 ksi). The graph shows some of the same stress oscillation that was shown with the pressurizer safety nozzle and the cold leg nozzle. Application of layers one through three reduce the maximum stress, and layers five through eight raise the stress from the minimum achieved with layer three. Stresses with the OWOL are in the 69 MPa (10ksi) range on either side of the Inconel welds while stresses are in the 138 MPa (20 ksi) range in the same areas after the FSWOL. It was shown earlier, in Figure 62, that both the OWOL and FSWOL reduce the stresses in the Inconel weld area to compression with the application of operating pressures and temperatures, with the OWOL resulting in more compression.

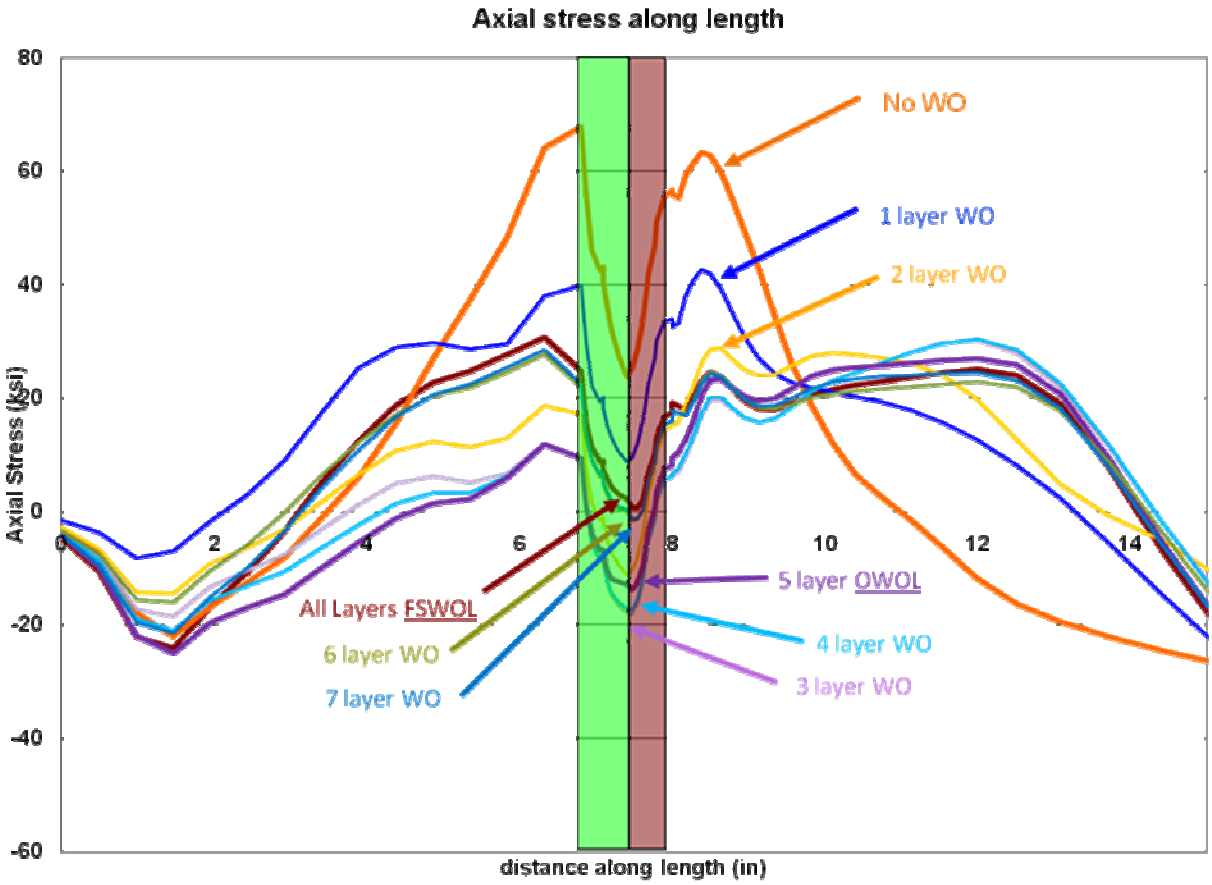

Figure 95 RCP Nozzle ID Axial Stresses through the Weld Overlay Process

Figure 96 shows the inner diameter hoop stress. The graph shows that the stress before the weld overlays is up to 550 MPa (80 ksi) in the butter\steel transition area, and is reduced to compression after two layers of overlay are applied. Subsequent layers do continue to reduce the hoop stress, but to a much lesser degree. The resulting compressive stress after the OWOL is very much the same as is produced after the FSWOL with little benefit gained from the added layers of weld material.

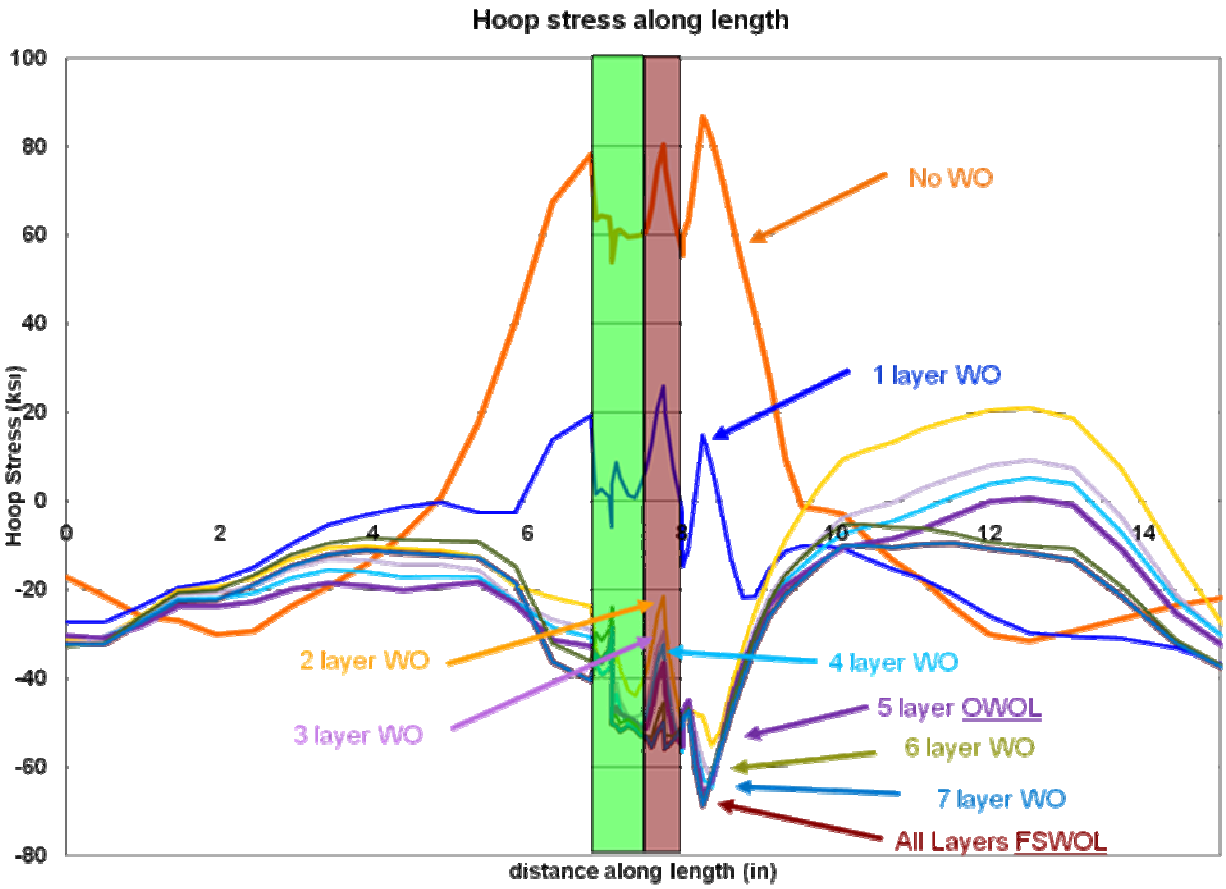

Figure 96 RCP Nozzle ID Hoop Stresses through the Weld Overlay Process

As a result of this study it was shown that the FSWOL is an effective method to reduce weld residual stresses at the pipe weld inside surface which can lead to PWSCC in DMWs in PWR piping systems if standard weld procedures are used. A study was conducted in which weld overlay thicknesses less that required for a full structural weld overlay were examined. The studies showed that the result produced by OWOL thickness weld overlays is highly dependent on the geometry. In the surge nozzle the axial stress reduction was progressive and almost linear with weld overlay thickness. The hoop stress also showed progressive reduction in stress with additional weld overlay material. The safety nozzle results showed oscillation in the axial stress with additional material initially increasing the tension stresses beyond those initially present. In this geometry no improvement in the maximum axial stress, at room temperature, was found until all four layers of the FSWOL were applied. The hoop stress reduction for the safety nozzle was progressive with thickness. The cold leg geometry showed that the improvement with layer thickness was similar after four layers were applied as was for eight layers in the axial stress direction and after three layers were applied in the hoop stress direction. For the RCP outlet nozzle, the OWOL actually produced better results than the FSWOL in the axial stresses, and the results were virtually the same for both OWOL and FSWOL in the hoop direction.

Analysis of weld procedures, sequencing and weld overlay thickness should be a standard part of designing full structural weld overlays for unique geometries. In addition to creating a more favorable weld residual stress state at the inside surface to mitigate PWSCC initiation and growth, the OWOL and

FSWOL are also beneficial from the standpoint of providing additional structural reinforcement and an additional leak barrier of a more resistant material to PWSCC (i.e., Alloy 52M) with the FSWOL of course providing more structural protection.

4.1.5.5 Effect of Inner Diameter Circumferential Repair Depth on Residual Stresses before and after Weld Overlay

A study was done examining the effect of inner diameter repair depth on stresses before and after weld overlay repair. For the RCP outlet nozzle, 0%, 25% and 50% inner diameter 360° circumferential repair depths were examined. For the cold leg nozzle 0% and 25% inner diameter repair depths were examined.

Cold Leg Nozzle

Figure 97 shows the weld area of the cold leg nozzle model with the various materials and welds highlighted. The weld repair is shown in the lower figure and is colored yellow. It has its peak at the interface between the butter layer and the Inconel weld. It is 25% through the original thickness of the weld area, and because the model is 2-D axisymmetric, the weld repair must be considered to span the entire circumference of the ID. The comparison of the results with no weld repair and with the weld repair will show the differences in the stresses that would be found in a nozzle with only a partial arc weld repair. The stresses in the model with the repair represent the stresses in the partial arc repair, and the stresses in the model with no weld repair represent the stresses elsewhere else.

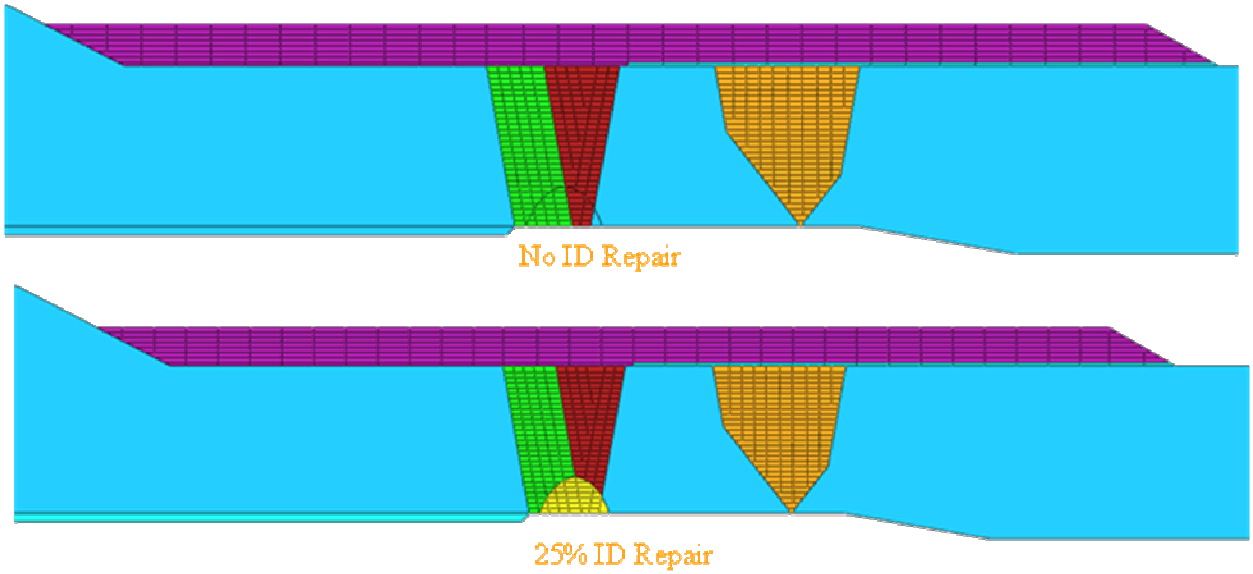

Figure 97 Cold Leg Nozzle with and without 25 percent ID Repair

Figure 98 shows the axial stresses after welding is complete, but before any weld overlay has begun. The case with no repair is shown on the top, and the case with the 25% ID repair is shown at the bottom. There is a noticeable difference in the stress results in the area of the repair. In the case without the repair, the compressive stresses begin closer to the ID, and there is a spike of tension stresses at the depth that the root pass grind out and re-weld took place. In the subsequent graphs the results for the case with

no ID repair will be shown in a solid orange curve, while the 25% ID repair results will be indicated by a dashed orange curve.

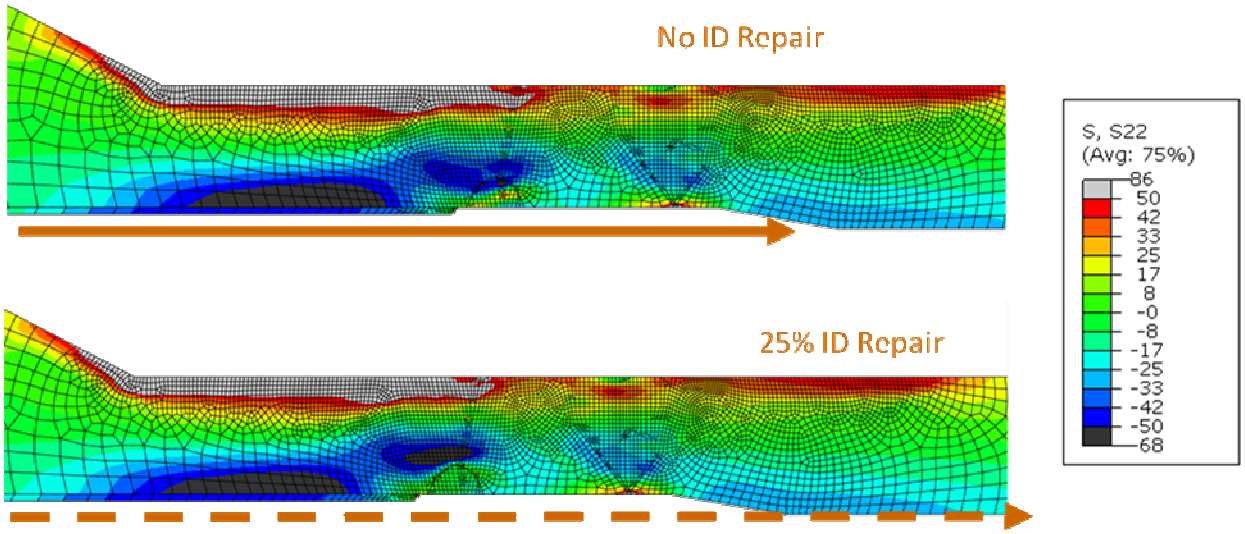

Figure 98 Cold Leg Axial Stresses before the Weld Overlay with and without 25 percent ID Repair (ksi)

Figure 99 shows the axial stresses along the inner diameter of the nozzle with the location of the butter, Inconel weld and stainless steel safe end weld indicated by vertical color coated bars. The graph shows that the highest tensile stress in the Inconel weld area is for the case without the 25% ID weld repair. The highest stress in the case with no ID repair is 138 MPa (20 ksi). The ID repair reduces this maximum to 69 MPa (10 ksi). The peak is also shifted toward the butter/steel interface that is at the left edge of the repair.

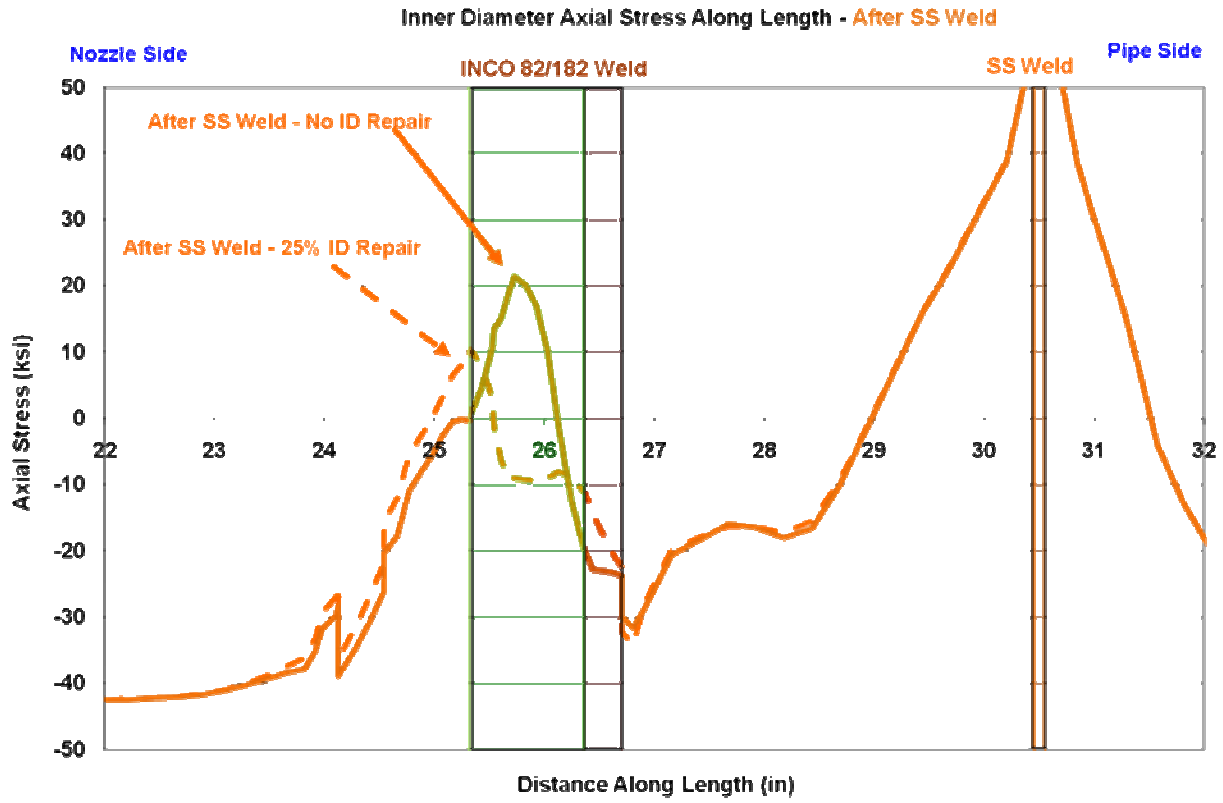

Figure 99 Cold Leg Nozzle Weld ID Axial Stresses before the Weld Overlay with and without 25% ID Repair

Figure 100 shows the through thickness axial stress at the butter/Inconel weld interface for this same case before any weld overlay has been applied. The graph shows that, for this cross section, the inner diameter stresses are negative for both the case with no weld repair and for the 25% weld repair. The stress patterns look very much alike. They both start out negative and proceed slightly upward toward the tensile region before plunging back into compression, and then finally ending tensile toward the outer diameter. The only marked difference between the two curves is that the plunge into compressive stresses takes place at 25 percent through the thickness for the weld repair that is 25 percent through the thickness.

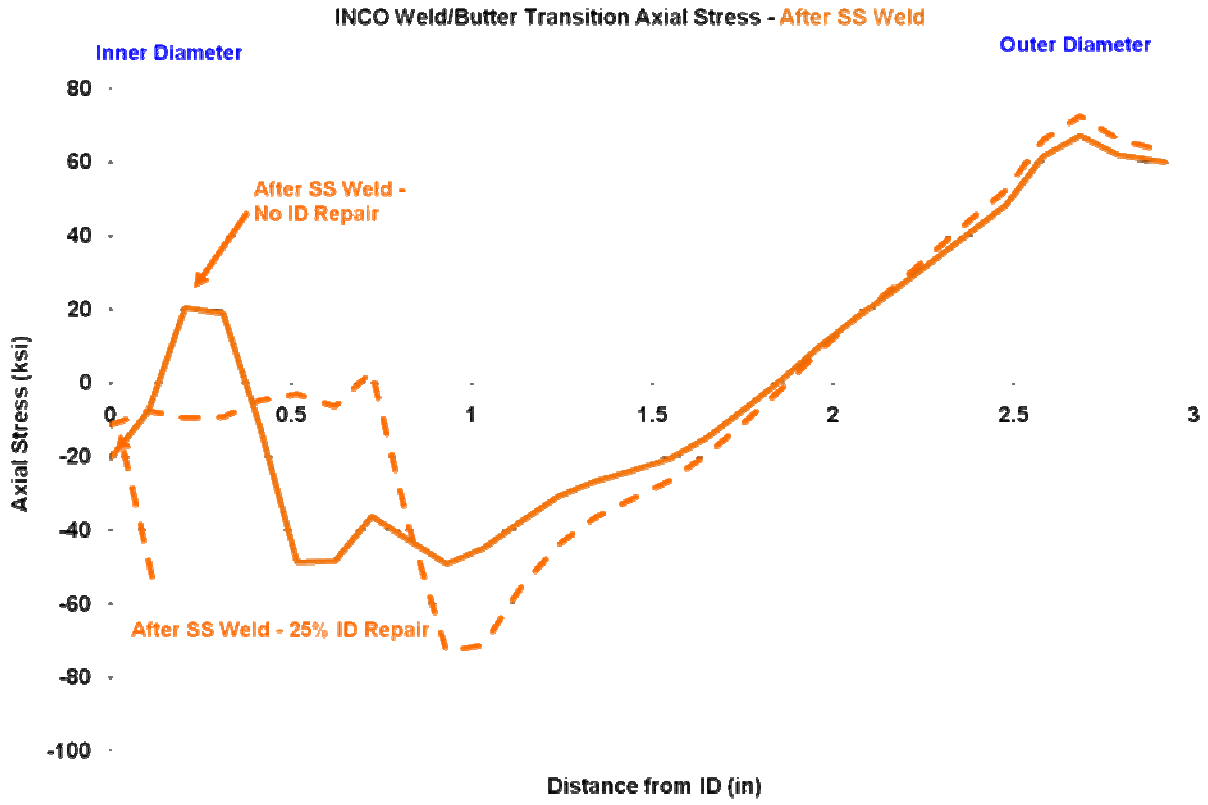

Figure 100 Cold Leg Nozzle Weld Through Thickness Axial Stresses before Weld Overlay with and without 25 percent ID Repair

Figure 101 shows the axial stress contour plot for the same two cases but after the OWOL has been applied. The stress contours look very much alike, but with the same exception that was pointed out in the previous stress contour plot. The 25 percent ID repair has pushed the area of compressive stress slightly beyond the depth of the repair.

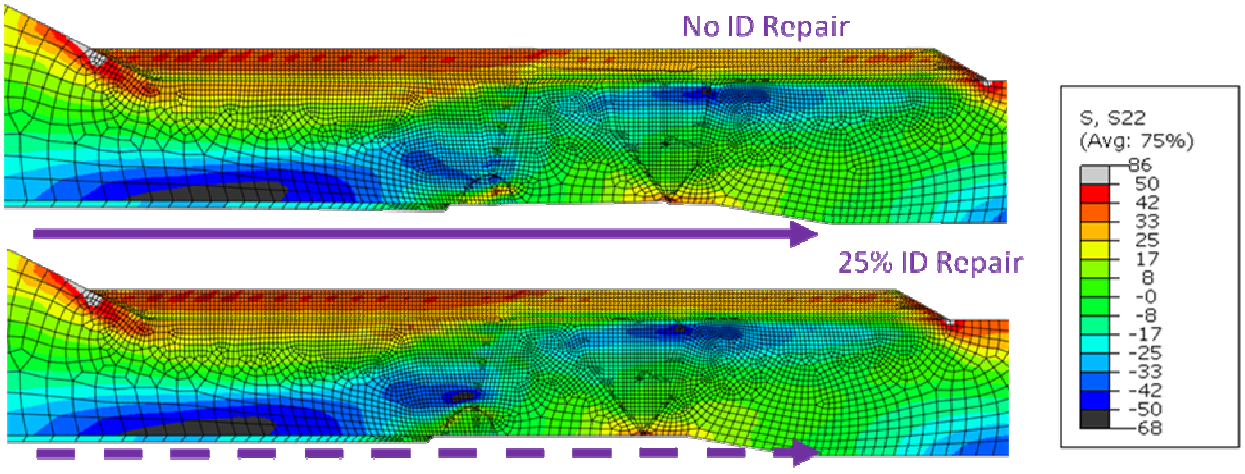

Figure 101 Cold Leg Axial Stresses after OWOL with and without 25 percent ID Repair (ksi)

Figure 102 shows the inner diameter axial stresses for the two cases. The graph looks similar to that which was shown for the case before the OWOL was applied except that the axial tensile stresses have been somewhat diminished. The compressive stresses have also been somewhat diminished. The peak tensile value in the Inconel weld area has been reduced from 138 MPa (20 ksi) to 117 MPa (17 ksi} for the case with no ID repair, and from 69 MPa (10 ksi) to 34 MPa (5 ksi) for the case with the ID weld repair. These results are at room temperature, and do not take into account the benefit in stress reduction caused by operating pressure and temperature.

Figure 103 shows the through thickness axial stress plot for the interface of the butter layer and Inconel weld. The graph has a similar profile as the one before the OWOL was applied, for this cross section. The curves both start out slightly compressive, and proceed into the tensile region before plunging into the compressive area, and then show equivalent tensile values toward the outer diameter. For this cross section, the stresses have been increased by the OWOL, but the location at which the curve representing the 25 percent ID repair still turns compressive at 25 percent of the way through the original wall thickness.

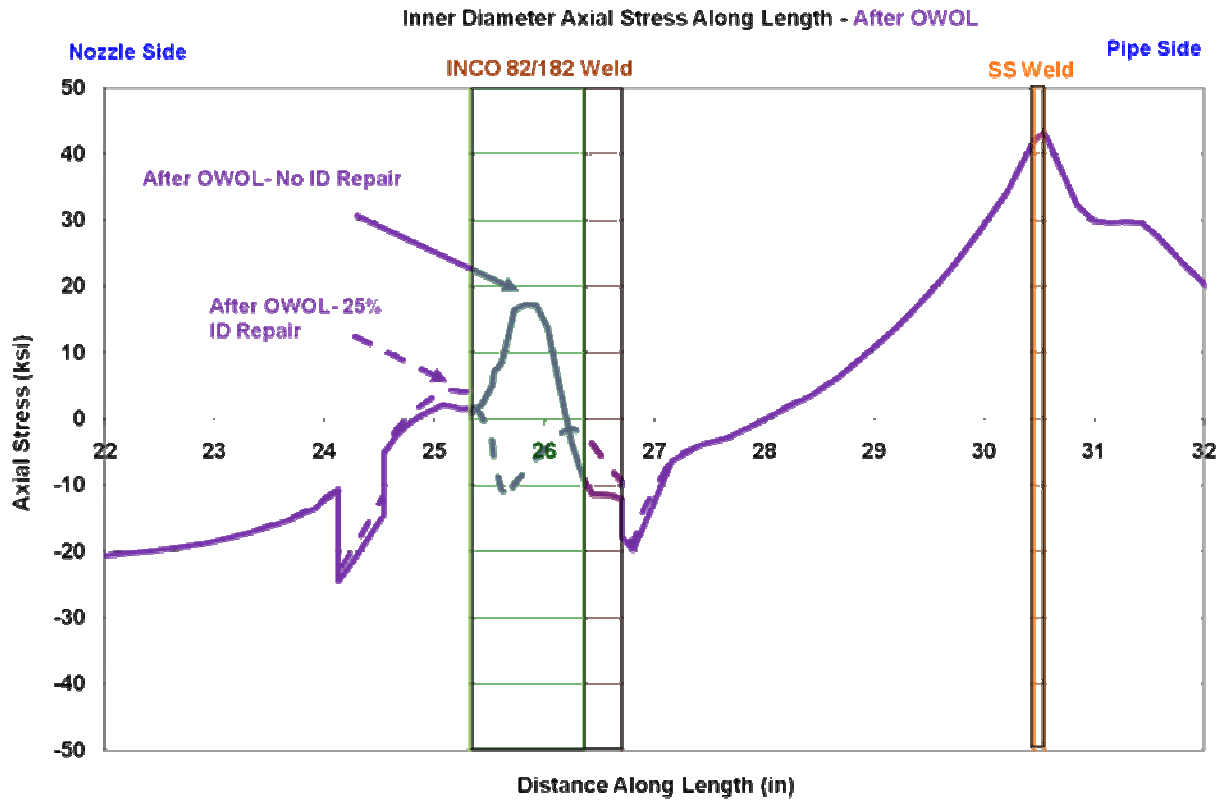

Figure 102 Cold Leg Nozzle Weld ID Axial Stresses after OWOL with and without 25 percent ID Repair

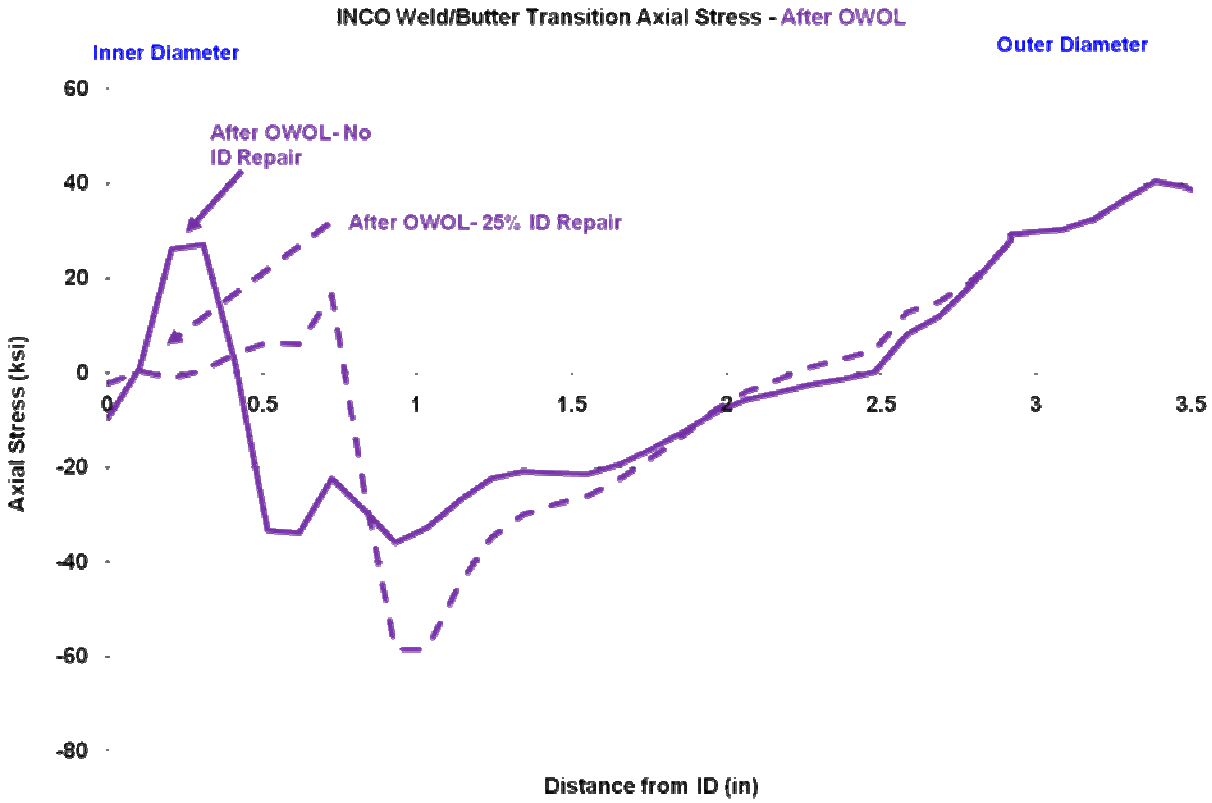

Figure 103 Through Thickness Axial Stresses after the OWOL with and without 25 percent ID Repair

Reactor Coolant Pump Nozzle

A similar sensitivity study was conducted for the reactor coolant pump outlet nozzle, but in this case 0%, 25% and 50% ID weld repairs were compared. Also this model had both the OWOL and FSWOL analyzed, so the comparative results from all of these cases are presented. Figure 104 shows the dissimilar metal weld areas of these models indicating the repairs in yellow. The peak of the 25% repair is at the interface between the butter and the Inconel weld. The peak of 50% weld goes deeper into the Inconel weld though it is made on the same centerline as the smaller repair. Each of the models had a root pass gring out and re-weld step as the final process in the Inconel weld but before the repair, if any.

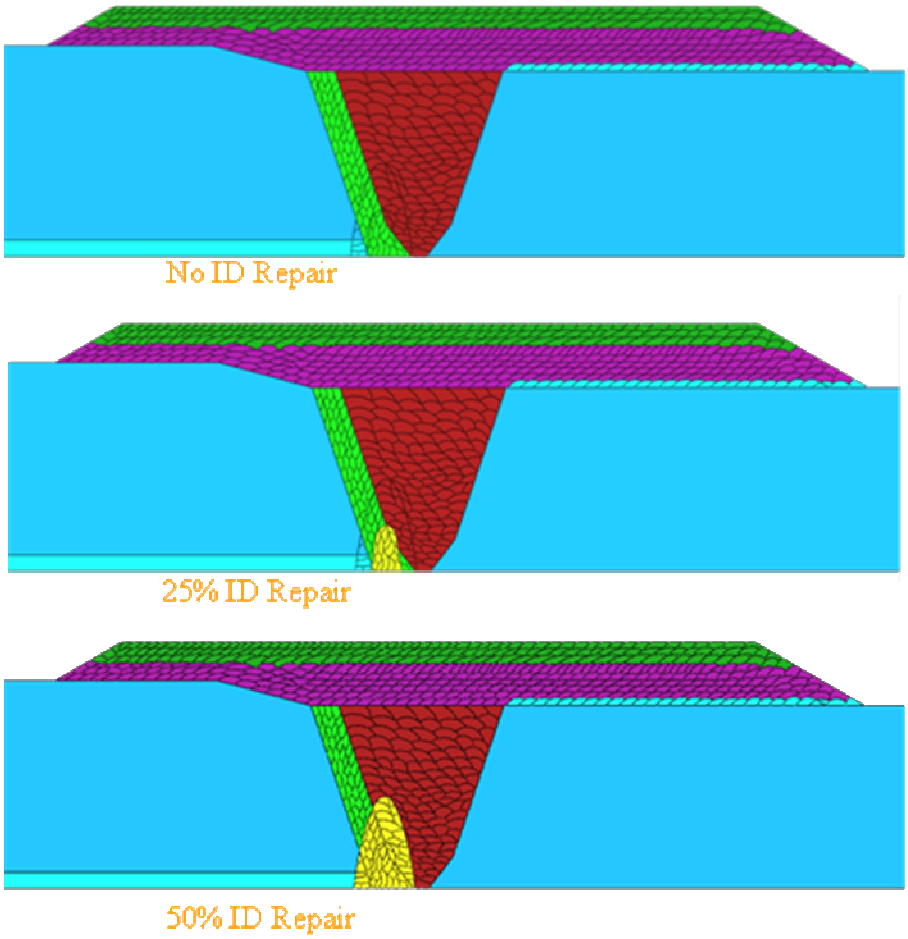

Figure 104 Reactor Coolant Pump with 0%, 25% and 50% ID Repair

Figure 105 shows the axial stress contour plot before any weld overlay has been performed for this model. The three plots show the distinct difference caused by the weld repair. The top model with no weld repair, but the root pass grind out and re-weld shows tension at the ID in the area of the re-weld, and a compressive region right above the tensile region. The 25% weld repair causes the ID tensile area to be more spread along the ID length on both sides of the repair, and causes the compressive region in the middle of the wall thickness to become more concentrated, and start just above the 25% weld repair. The 50% weld repair case, on the bottom, carries these changes a bit farther. The ID tension stresses are again

spread farther along the length of the ID on both sides of the repair, and the concentrated compressive region is pushed further through the thickness and starts just above the 50% repair depth.

The tensile stresses in this model are greater than in the cold leg because the RCP nozzle safe end is so much longer. The mitigating effect of the stainless steel safe end weld on the Inconel weld area is all but non-existent for this geometry.

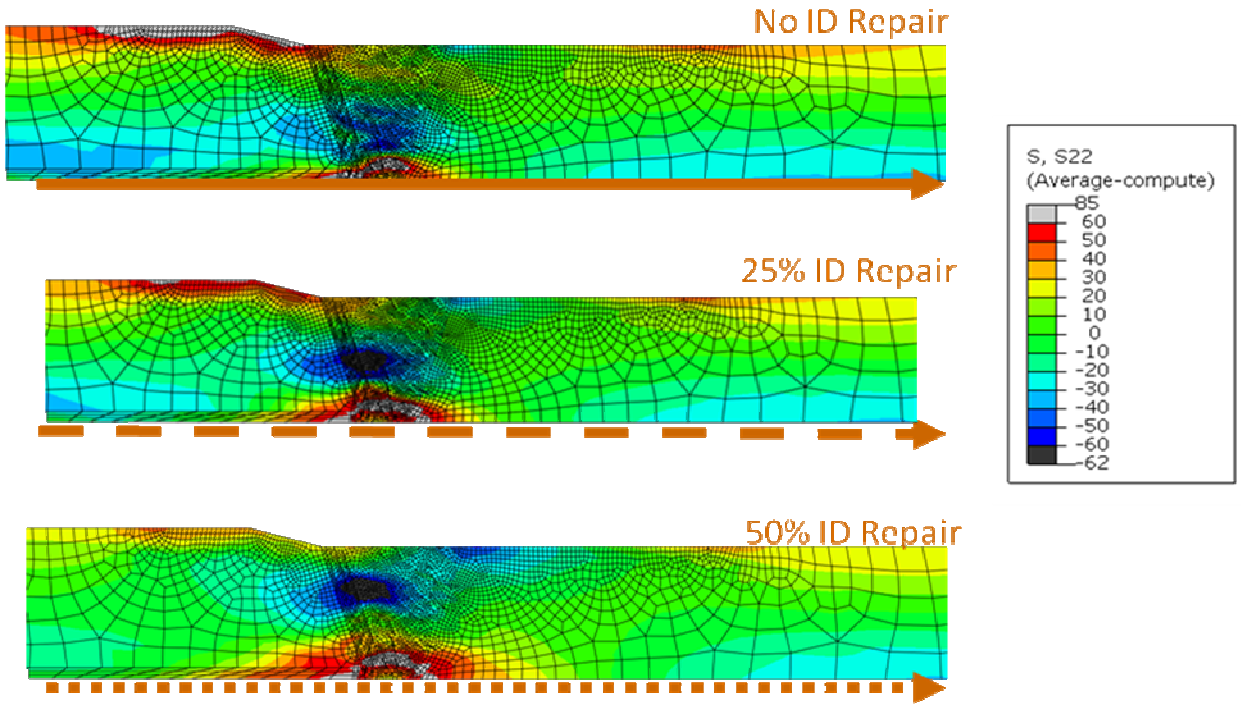

Figure 105 Axial Stresses before Weld Overlay with 0%, 25% and 50% ID Repair (ksi)

Figure 106 and Figure 107 show the axial stresses before applying the weld overlay in graphical form, first along the inner diameter and then through the thickness. The ID stress plot shows better the effect that is visible in the stress contour plots. The peak tensile stress is at the butter/ferritic steel interface in each case, and is slightly diminished by the 25% repair, and diminished slightly more by the 50% repair. Though the peak stress was reduced by the ID repair, the portion along the length of the ID of the nozzle that is exposed to tensile residual stresses is increased with each increase in repair depth and size.

The graph showing the through thickness stresses is somewhat similar to the one shown for the cold leg model except that the ID stresses are highly tensile because of the long safe end. The curves start out tensile, cross into compression at the depth of their respective repairs, and then become tensile again at the outer diameter.

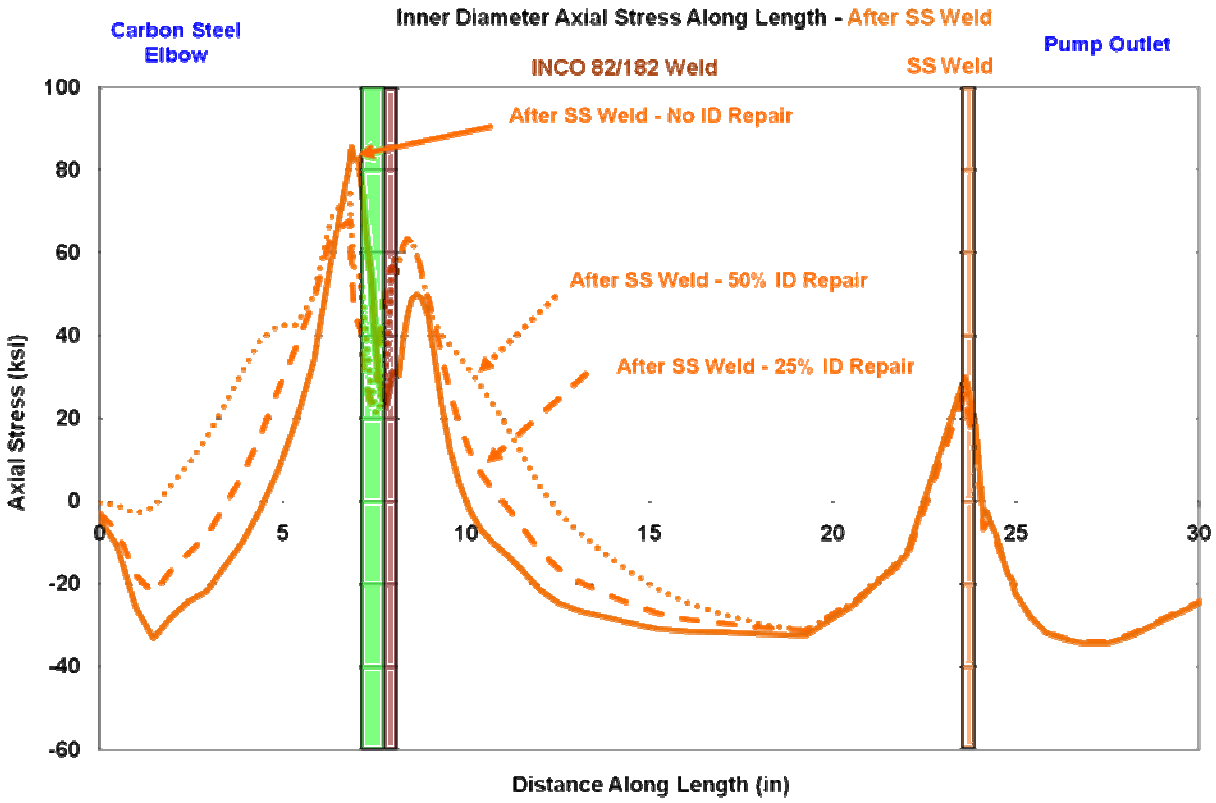

Figure 106 ID Axial Stresses before Weld Overlay with 0%, 25% and 50% ID Repair

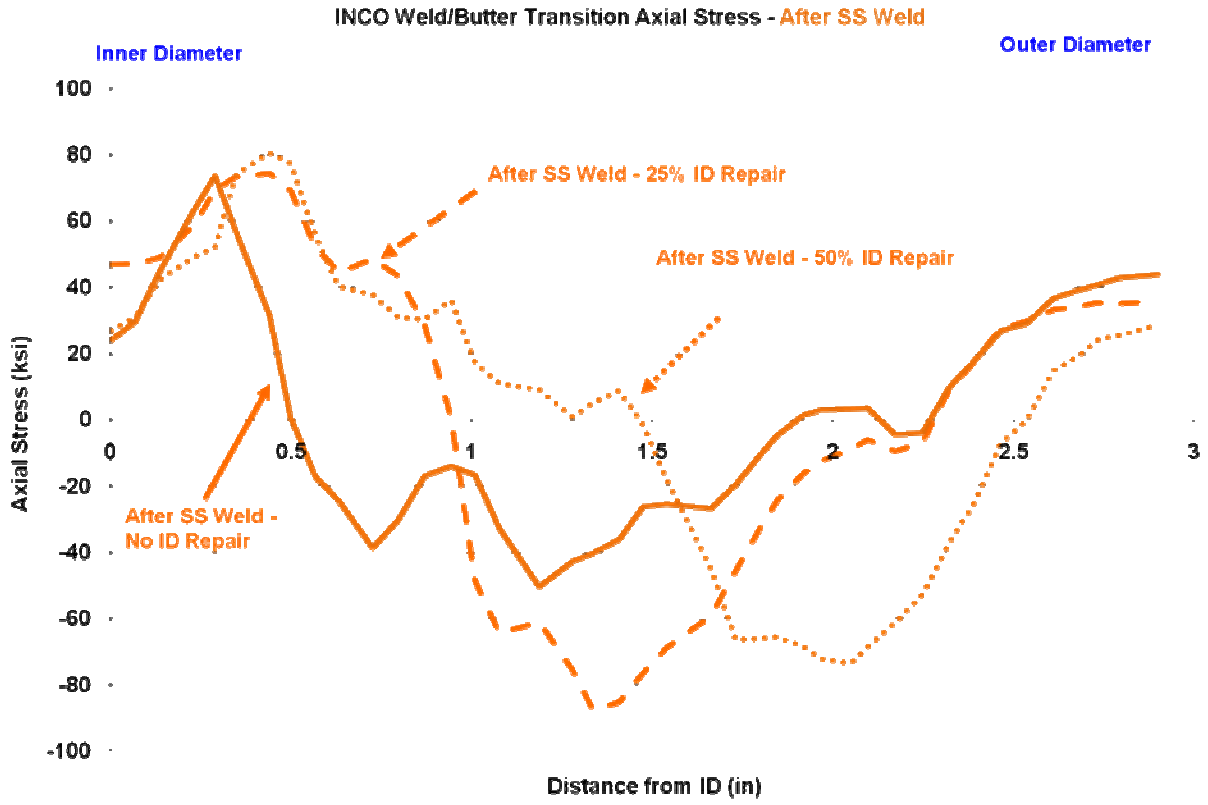

Figure 107 Through Thickness Axial Stresses before Weld Overlay with 0%, 25% and 50% ID Repair

Figure 108 shows the axial stress contour plot for the three repair cases after the OWOL has been applied. The diminishing of the inner diameter tensile stresses is evident in these plots. Figure 109 shows the ID axial stress graph. In comparing Figure 109 with Figure 106 it is evident that a large reduction in tensile stresses was achieved, and that more improvement was made to the cases with the weld repairs than to the one without. The maximum tensile stresses for this no repair case were reduced from 586 MPa (85 ksi) to 248 MPa (36 ksi) by the application of OWOL. These observations are at room temperature, and do not account for the improvement caused by the application operating pressure and temperature.

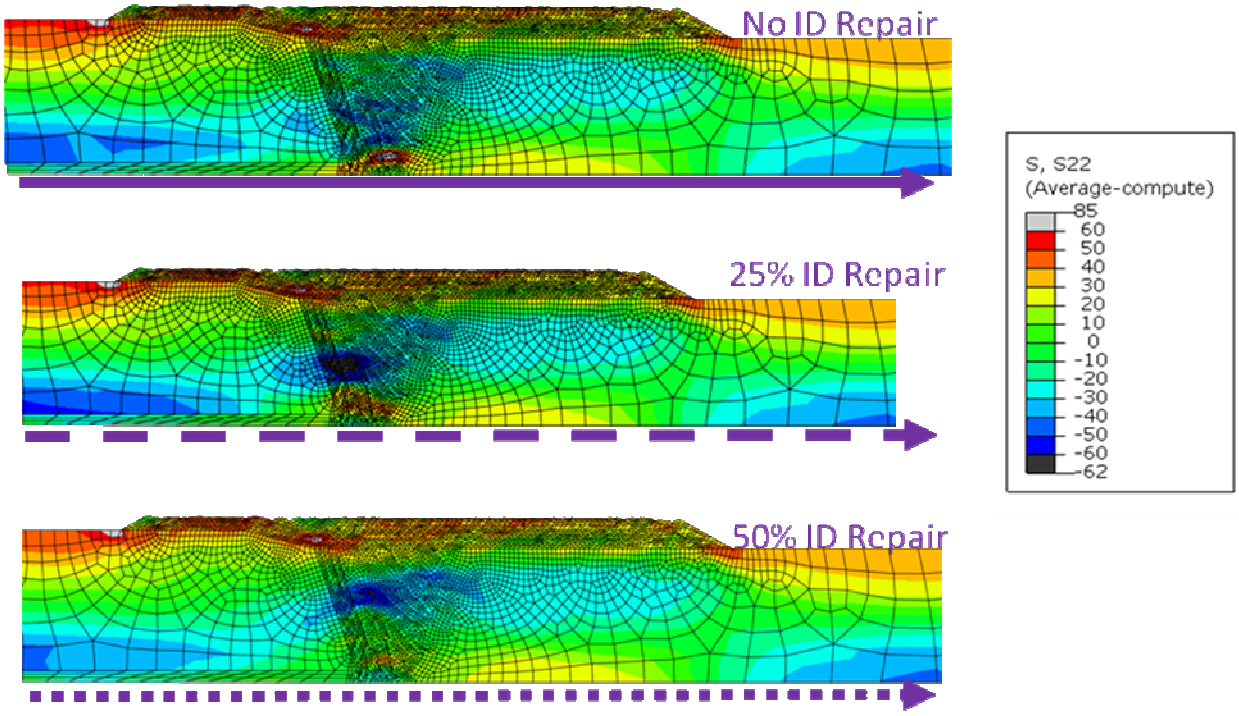

Figure 108 Axial Stresses after OWOL with 0%, 25% and 50% ID Repair (ksi)

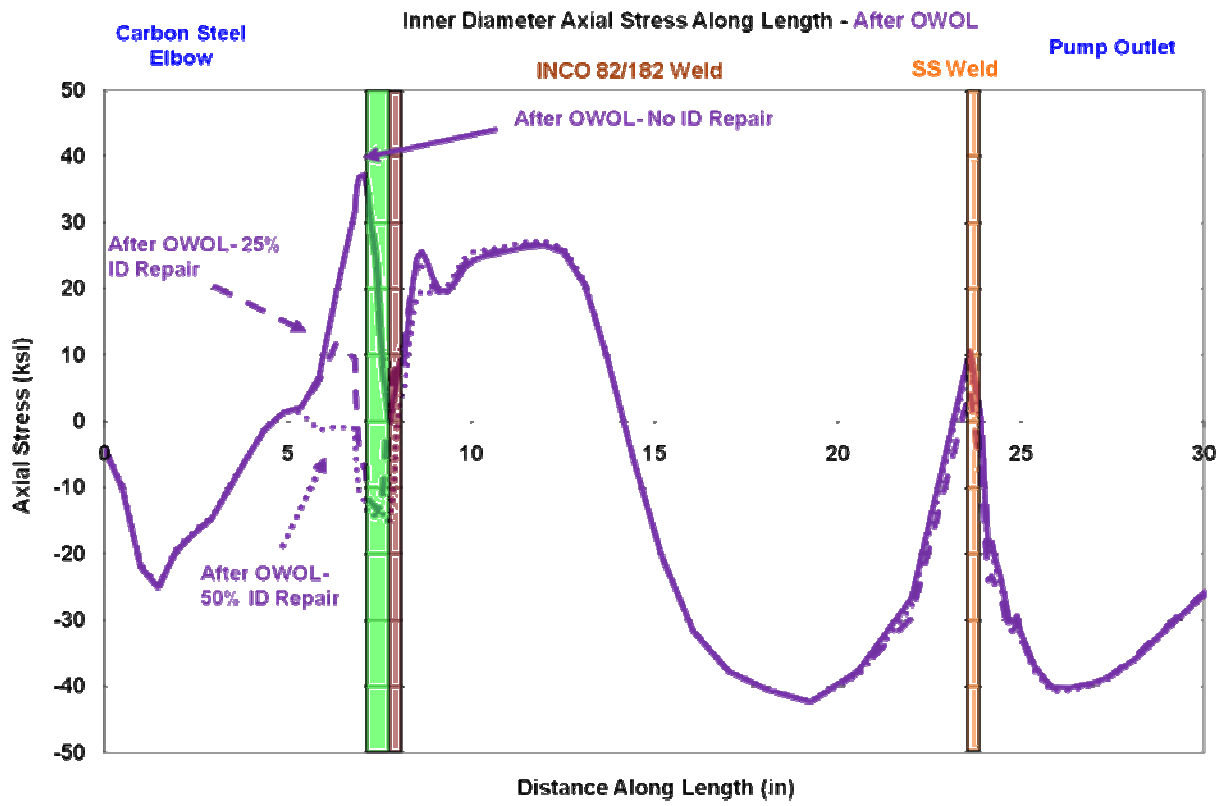

Figure 109 ID Axial Stresses after OWOL with 0%, 25% and 50% ID Repair

Figure 110 shows the through thickness axial stresses for the three cases. Again, these through thickness stresses are for the location at the interface of the butter and the Inconel weld. For this cross section, all of the ID stresses are zero, or negative. After an oscillation into tensile territory, each curve plunges into the compressive region at its respective repair depth and then back into tensile territory toward the original outer diameter and then back to neutral at the outer diameter of the OWOL.

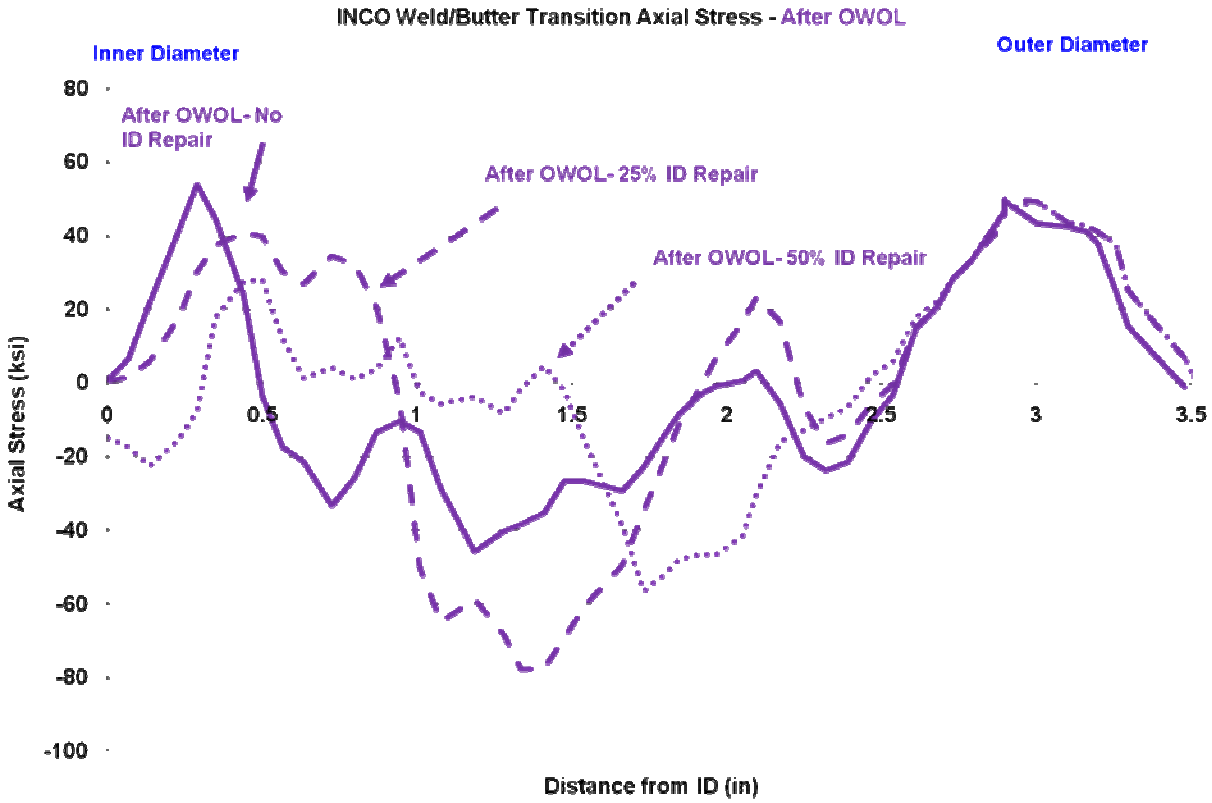

Figure 110 Through Thickness Axial Stresses after OWOL with 0%, 25% and 50% ID Repair

Figure 111 shows the axial stress contour plots after a weld overlay of full structural thickness has been completed. For this geometry, the ID axial stresses increase when compared with the case for an OWOL thickness.

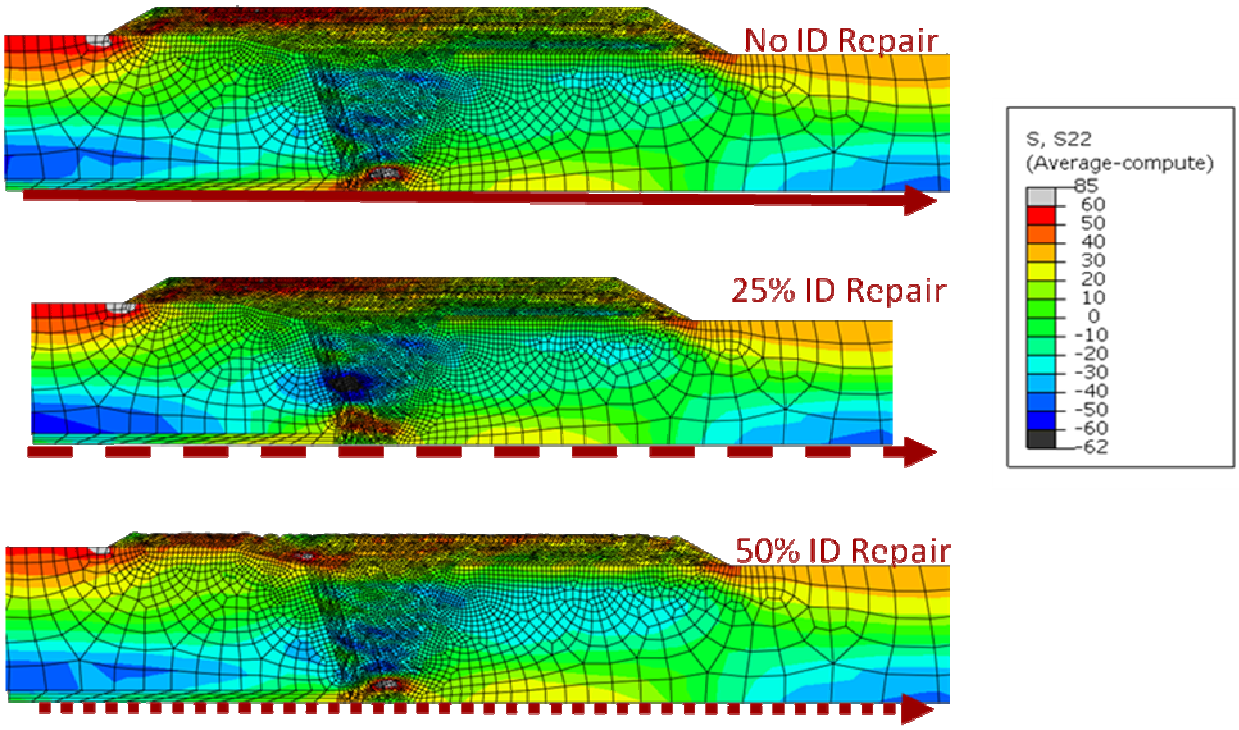

Figure 111 Axial Stresses after FSWOL with 0%, 25% and 50% ID Repair (ksi)

Figure 112 shows the ID axial stresses after applying the FSWOL which looks very much like the pattern after OWOL application with the values in the Inconel weld area slightly elevated. In comparing Figure 112 with Figure 105 the cases with 25% and 50% ID repairs still show more improvement than the case with no weld repair. Figure 113 shows the through thickness axial stresses at the butter/Inconel weld interface. They start out at the inner diameter a little higher than the OWOL case for the no-repair case and the 25% repair case (69 MPa [10ksi]) while the 50% repair case is at 0 ksi for this cross section. They go negative at their respective repair depths, and then turn positive near the original outer diameter and then continue to higher tensile values at the outer diameter of the FSWOL.

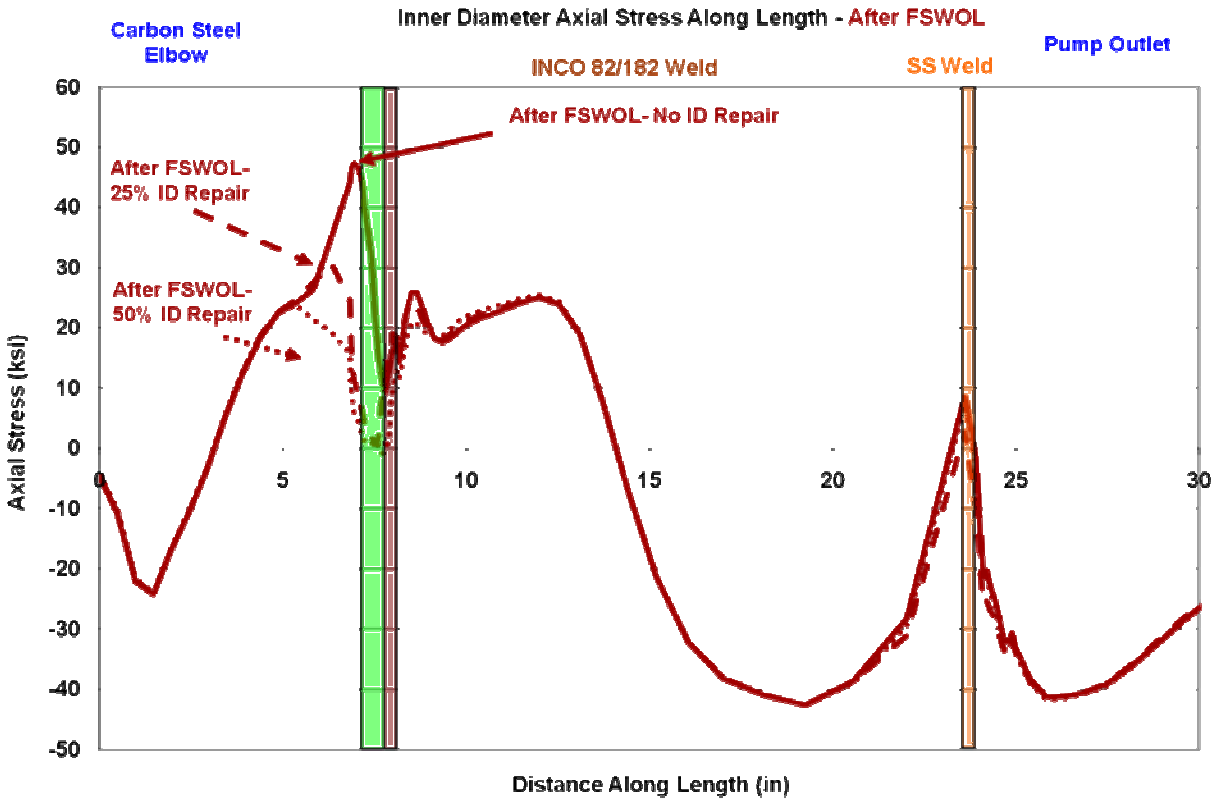

Figure 112 ID Axial Stresses after FSWOL with 0%, 25% and 50% ID Repair

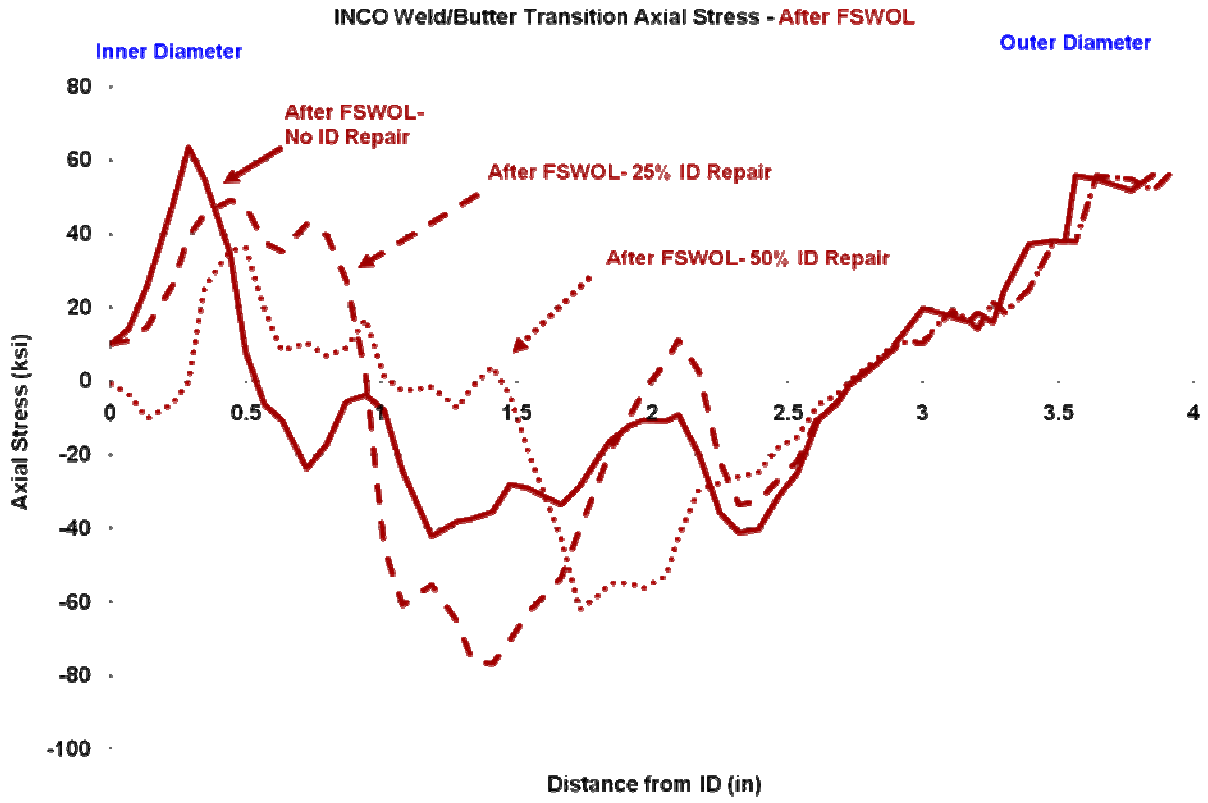

Figure 113 Through Thickness Axial Stresses after FSWOL with 0%, 25% and 50% ID Repair

Another sensitivity study was performed in which the weld residual stresses created by the standard root pass grind-out and replacement were compared to those caused by 25% and 50% through thickness 360° ID weld repairs in the dissimilar metal weld of a reactor pressure vessel cold leg nozzle and a reactor coolant pump outlet nozzle geometries.

The post welded state shows that the weld repairs expand the area of high tensile stresses around the dissimilar metal weld on the nozzle ID, but affect the maximum stress value much less.

The weld repairs do have a large effect on the depth at which the axial tension stress turns compressive through the thickness. The case with the 25% repair changes from axial tension to compression at 25% of the way through the thickness. This transition takes place at 50% through the thickness for the 50% repair.

4.2 Results of Crack Opening/Growth Analyses

One concern with the FSWOL is the effect it would have on existing cracks. The process is designed to provide enough structural material replacement to accommodate an existing through wall crack. The effects of the change in residual stresses caused by a FSWOL on an existing crack are explored here.

Three sets of analyses were performed for two crack locations for both the surge and safety nozzle geometries studied. The three crack growth scenarios are summarized below:

1. Crack Growth Operating Pressure and Temperature
2. Crack Growth FSWOL Operating Pressure and Temperature
3. FSWOL Operating Pressure and Temperature Crack Growth

In the first two cases, cracks 75 percent of the thickness and 100 percent of the circumference were modeled to simulate the situation in which a very large crack was repaired with a FSWOL. In the third case the crack was allowed to grow 100 percent of the way through the original pipe thickness. Circumferential cracks have been found to occur in the Inconel weld and at the interface between the Inconel butter layer and the A508 nozzle material, but with the exception of the recent experience at Crystal River none have been found to have progressed in depth to greater than 30 percent of the wall thickness. Both crack locations were analyzed in the surge nozzle and safety nozzle geometries. Cracks between the butter layer and the dissimilar metal weld will be designated as crack location 1 (Crack1), and those between the carbon steel nozzle material and the butter will be designated as crack location 2 (Crack2) in the figure captions.

The cracks were introduced into the analyses using the ABAQUS crack propagation analysis procedure. The crack surfaces were defined allowing for self contact and surface interaction properties including friction in areas of crack closure. A coefficient of friction of 0.15 was used for the analysis so that the crack surfaces would not have frictionless contact. It is assumed that the true coefficient of friction between surfaces in a PWSCC would be much higher than this value. The crack was forced to grow in 1.25 mm (0.05 inches) steps so that the crack tip stress intensity factor (K) could be calculated as the crack grew. For each geometry, the axial and hoop stress will be shown before the crack was introduced, after the crack was introduced, and after the FSWOL was applied. The figures will show an exaggerated displacement plot so as to help visualize the crack opening behavior in each case. In all cases, it will be shown that an axial crack should arrest when it reaches the area of compressively stressed material near the middle of the wall thickness if subjected solely to welding residual stresses.

There are three types of loading that a crack can experience as described by Anderson [10]. In Mode I loading the principal load is applied normal to the crack plane and tends to open the crack. This is the primary mode affecting circumferential cracks in the geometries studied here. Mode II describes in-plane shear loading that tends to slide one crack face with respect to the other, and Mode III loading refers to out-of-plane shear loading. Neither of these latter two loading modes are major contributors to crack growth in this case. Mode II effects are small in these models, and Mode III effects are nonexistent in an axi-symmetric model.

The stress intensity factor at the crack tip, K_I can be described by Equation 4 for this case. The stress intensity factor is derived from the energy release rate as calculated by G_I and described by Krueger [11]. Of interest are the values for the stress intensity factor (K) before and after the FSWOL was applied, and as the crack is forced to grow.

The use of Equation 4 is based on the well known crack closure integral (CCI) equations first introduced by Rybicki and Kanninen [12] and summarized by Krueger [11]. This is an approximation since it must be assumed that the crack grows mainly in an elastic field (no additional plasticity (or minimal plasticity) occurs during crack growth). This is typically the assumption made in modeling stress corrosion crack (SCC) growth in residual stress fields where the SCC growth law is governed by the stress intensity factor (K). There is some emerging controversy in the field as to the validity of this assumption, however, in the present analyses, minimal plasticity did occur during crack growth. Reference [13] compares K_I values calculated via the CCI method and the finite element alternating method for cracks in residual stress fields. The comparisons were quite good.

The EPRI has published a Materials Reliability Program (MRP) report addressing, among other things, crack growth due to PWSCC in Inconel Alloy 82/182 welds [14]. Equation 5 is a deterministic crack growth model for Inconel 82/182 weld metal material and was based on a statistical evaluation of the worldwide set of available laboratory test data for these materials using controlled fracture mechanics specimens. The equation development is discussed in more detail in Reference 14. The equation is used to convert the stress intensity factor into a crack growth rate. For convenience, in this report, the instantaneous crack growth rate is reported in terms of years required to break through the remaining thickness of material, assuming that the crack growth rate remains constant through the remaining thickness.

Subsequent analyses in which the crack was allowed to grow after operating pressure and temperature were applied show that the circumferential crack will only grow to about 35 percent of the original wall thickness because the axial compressive weld residual stresses developed toward the middle of the pipe thickness prevent further growth. Figures showing the calculation of the stress intensity factor, K, versus crack depth will be shown for each geometry and crack location. The stress intensity factor K goes to zero as the crack depth approaches 30 percent of the pipe thicknesses in all cases. The crack should self-arrest at this location.

Furthermore, the analysis in which the crack was forced to grow at operating pressure and temperature, but after the FSWOL was applied, shows that the compressive stresses created by the process should prevent the crack from initiating at all.

4.2.1 Surge Nozzle – Crack1

The first three cases examined have the simulated crack located at the interface between the butter layer and the dissimilar metal weld in the surge nozzle geometry as shown in Figure 114.

In the first scenario, the crack is forced to grow to 75 percent of the original wall thickness and then operating temperature and pressure are applied with no FSWOL. Figure 115 shows the axial stress in the surge nozzle after the crack was forced to grow and the operating loads were applied. The exaggerated displacement plot shows that the crack would open at the inner diameter and then close by itself somewhere in the middle of the thickness, and then open again once it reached the tensile stress field toward the outer diameter of the pipe. It is unlikely that the crack would grow beyond the zone where it is forced closed by the welding residual stresses without external forces well beyond normal operating loads. Some useful information that can be gathered from this model is the stress intensity factor as calculated by Equation 4 and the predicted crack growth rate as calculated by Equation 5. The crack growth rate equation gives a very small number so this rate was converted into a more easily graspable number of years required to grow through the remaining thickness of the pipe wall assuming that the crack growth remains constant through the remaining thickness.

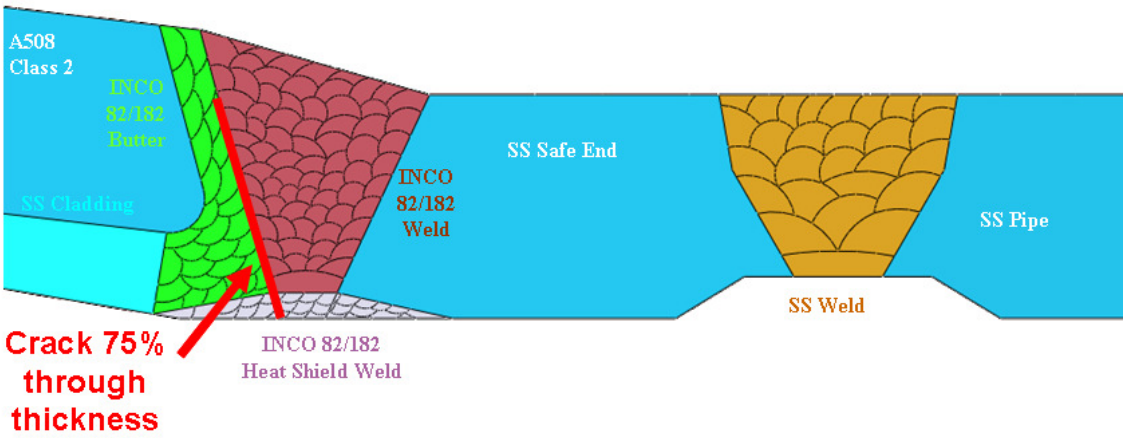

Figure 114 Surge Nozzle Crack through Butter/Weld Interface (Crack1)

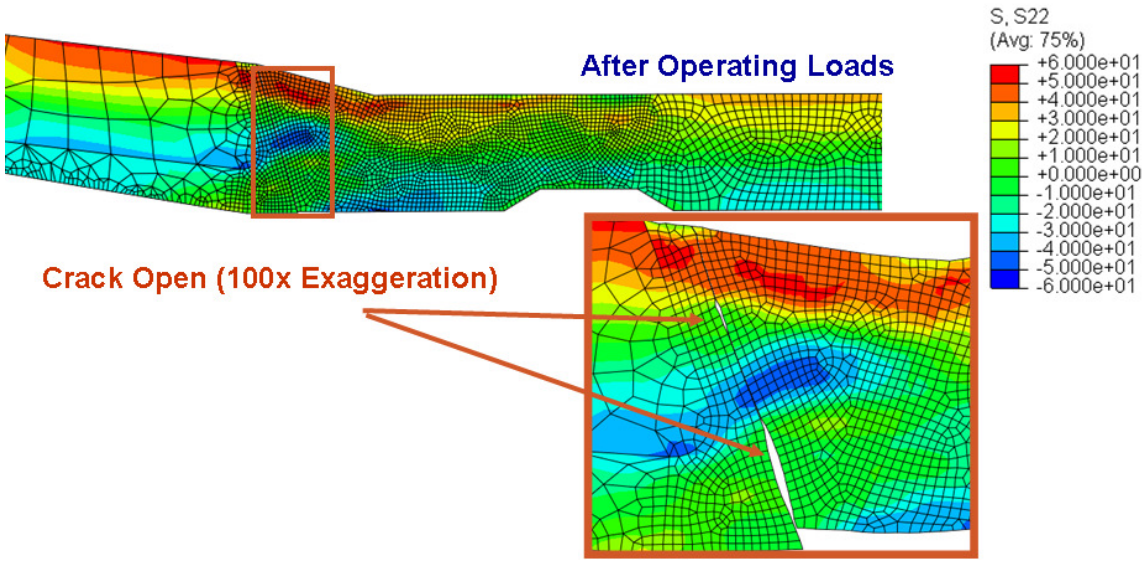

Figure 115 Surge Nozzle Axial Stresses with Crack before Applying the FSWOL

Figure 116 shows the stress intensity factor in (ksi-in $^{1/2}$) units for the Crack1 location in the surge nozzle geometry. The stress intensity factor is used to calculate the crack growth rate due to PWSCC. Two stress intensity factor curves are shown in this graph to illustrate a comparison made between the crack closure integral (CCI) method and the finite element alternating method (FEAM) of calculating the stress intensity factor. In all other cases in this report the stress intensity factor is calculated for the full 360 degree circumferential crack using the crack closure integral method described in Equation 4. A smaller crack was modeled using the finite element alternating method in which an elliptical crack of aspect ratio A1/A2 = 1.33 and centered at the inner diameter of the dissimilar metal weld at the Crack1 location, was grown in depth while keeping the elliptical aspect ratio and the center point the same. The shorter elliptical dimension (A1) represents the crack depth through the thickness while the term (A2) represents the half crack length. The graph shows comparable stress intensity factors calculated with both of these methods despite the difference in crack size. Reference [13] compares K_I values calculated via the crack

closure integral method and the finite element alternating method for cracks in residual stress fields. The comparisons were also quite good.

One can see that the stress intensity factor is zero at the inner diameter and gets higher through the thickness until its value drops off again to zero at 40 percent of the way through the wall thickness of the pipe. The K value begins to increase again at about 70 percent of the way through the pipe for this geometry and location.

Since Equation 5 for crack growth rate is linear with the stress intensity factor, the equation predicts that the crack growth would be zero after the crack reaches 40 percent of the wall thickness in this stress field made up of weld residual stresses and operating temperature and pressure.

To put the crack growth rate values into understandable terms, they were converted into units of years to grow through remaining thickness at a particular depth. For this geometry and loading case, the initiated crack at the inner diameter has a stress intensity factor of zero indicating that additional loading would be required to initiate a stress corrosion crack. At its peak stress intensity factor at 31 percent of the way through the thickness, K = 5.6 MPa-$m^{½}$ (5.1 ksi-$in^{½}$) and it would take 124 years to grow such a crack through the remaining thickness. However, from 40 percent of the way through thickness to 70 percent of the way through the wall, the crack arrests and will not grow through the thickness. If artificially forced to grow further, the stress intensity factor at 75 percent of the way through the wall thickness is K = 8.9 MPa-$m^{½}$ (8.1 (ksi-$in^{½}$) and the crack growth rate predicts it would take 20 years for the crack to grow through the remaining wall thickness.

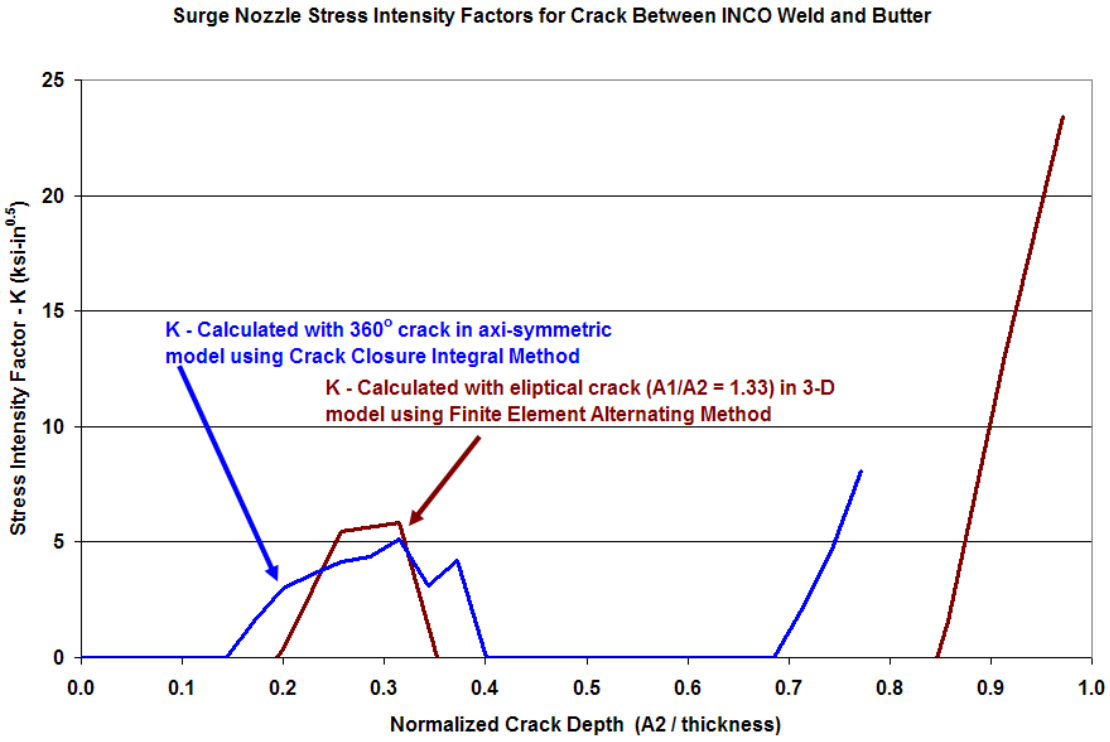

Figure 116 Surge Nozzle Crack1 Stress Intensity Factors before Applying the FSWOL

The second crack scenario subjects this existing crack to the FSWOL and then applies the operating pressure and temperature.

Figure 117 shows the axial stress in the surge nozzle geometry after welding is complete (top figure), after Crack1 is introduced 75 percent through the thickness (middle figure), and after the FSWOL has been completed and a 100 percent deep through-wall crack has been introduced (bottom figure). The figure shows an exaggerated (100x) displacement plot of the crack profile before operating pressure and temperature are applied. One can see the difference between the crack profiles in this case, and in the case in which operating pressure and temperature are applied. In this case, the crack shows some shearing at the inner diameter, but very little axial opening. The crack tip is opened at the outer diameter of the original pipe wall for the case where the through-wall crack has been repaired with a FSWOL (bottom figure in Figure 54).

After application of the FSWOL, the inner diameter is put in compression and the crack mouth is forced closed. The crack tip which is now at 100 percent through the original wall thickness is put into a more tensile field and is opened more by the FSWOL. Figure 118 compares the axial stresses at room temperature and pressure to those at operating pressure and temperature. The inner diameter compression is reduced by operating loads, but the compression stresses remain, and the crack mouth remains closed.

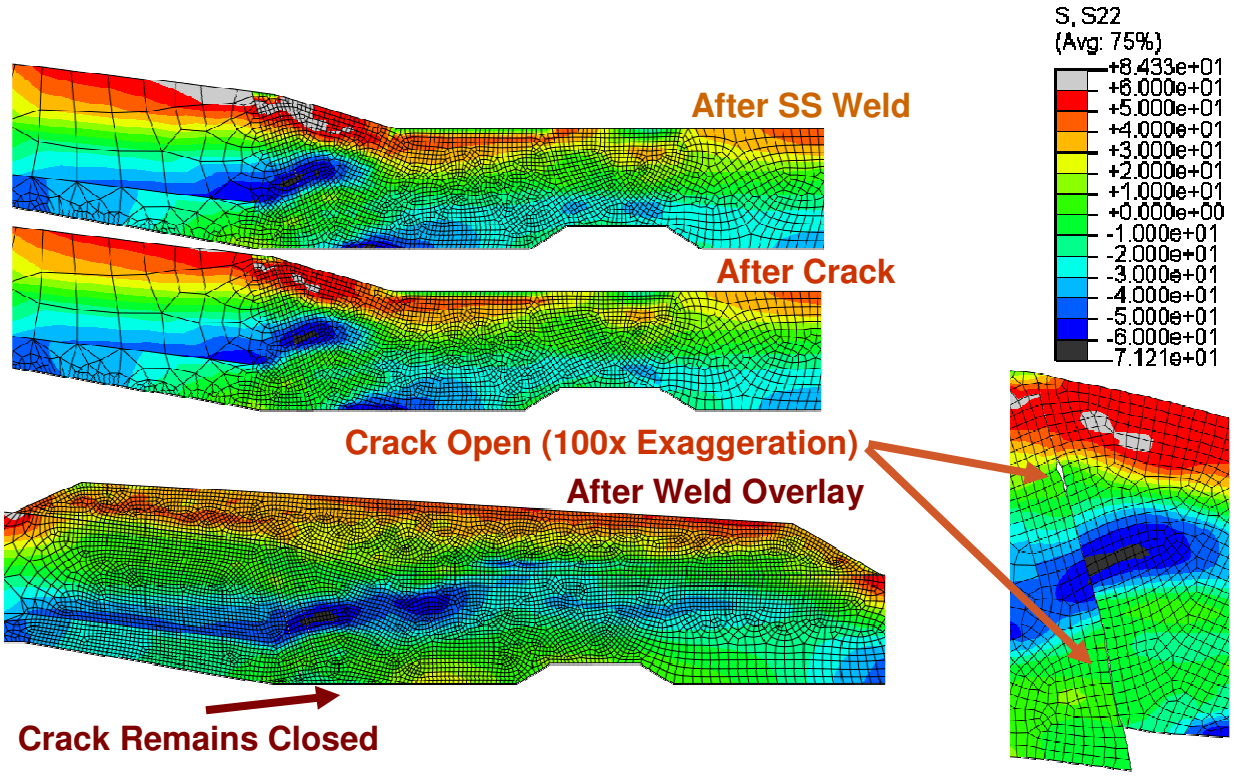

Figure 117 Surge Nozzle Axial Stresses after the Crack1 and after the FSWOL is Applied

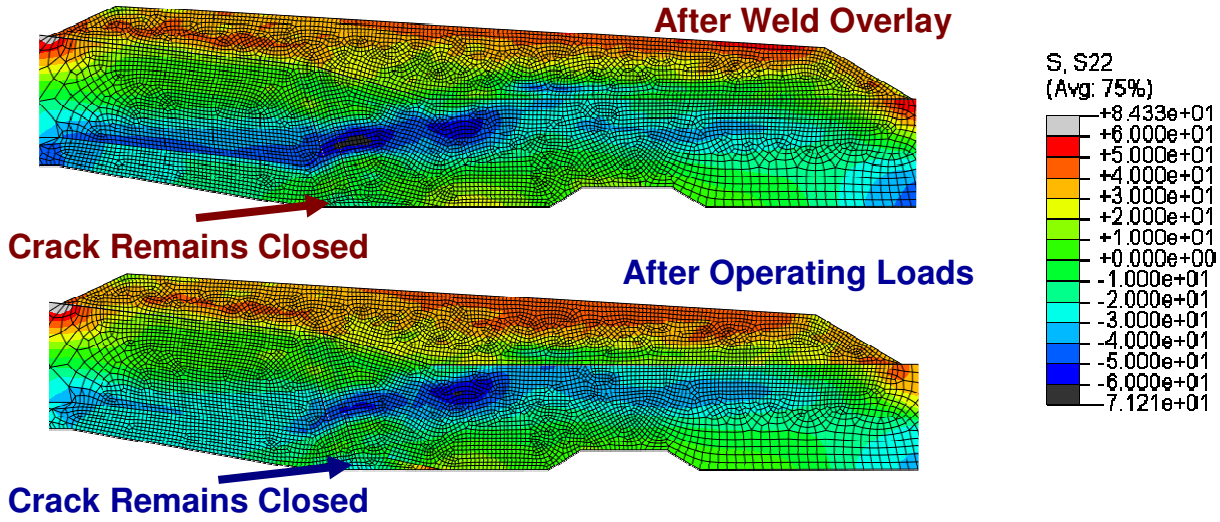

Figure 118 Surge Nozzle Axial Stresses after Crack1 in Introduced and the FSWOL is Applied; with and without Operating Loads

Figure 119 shows the crack opening displacement predicted for the surge nozzle 360 degree circumferential crack before and after applying the FSWOL, and then with operating pressure and temperature applied. The graph shows that the untreated crack (no FSWOL) is closed at the inner diameter, and would open very slightly to a depth of approximately 15 mm (0.6 inches) and then would be closed from that point until it reaches a depth of approximately 28 mm (1.1 inches) where it would be again only be slightly opened. After the FSWOL has been applied, the crack mouth along the inside surface is forced closed further, and the crack tip is not forced open more than that of the untreated pipe even if the crack tip was allowed to grow to 100 percent of the way through the original pipe thickness. When operating pressure and temperature are applied, the crack is forced more into compression on the inner diameter, and the crack tip is forced to open 83 percent more than without operating pressure and temperature.

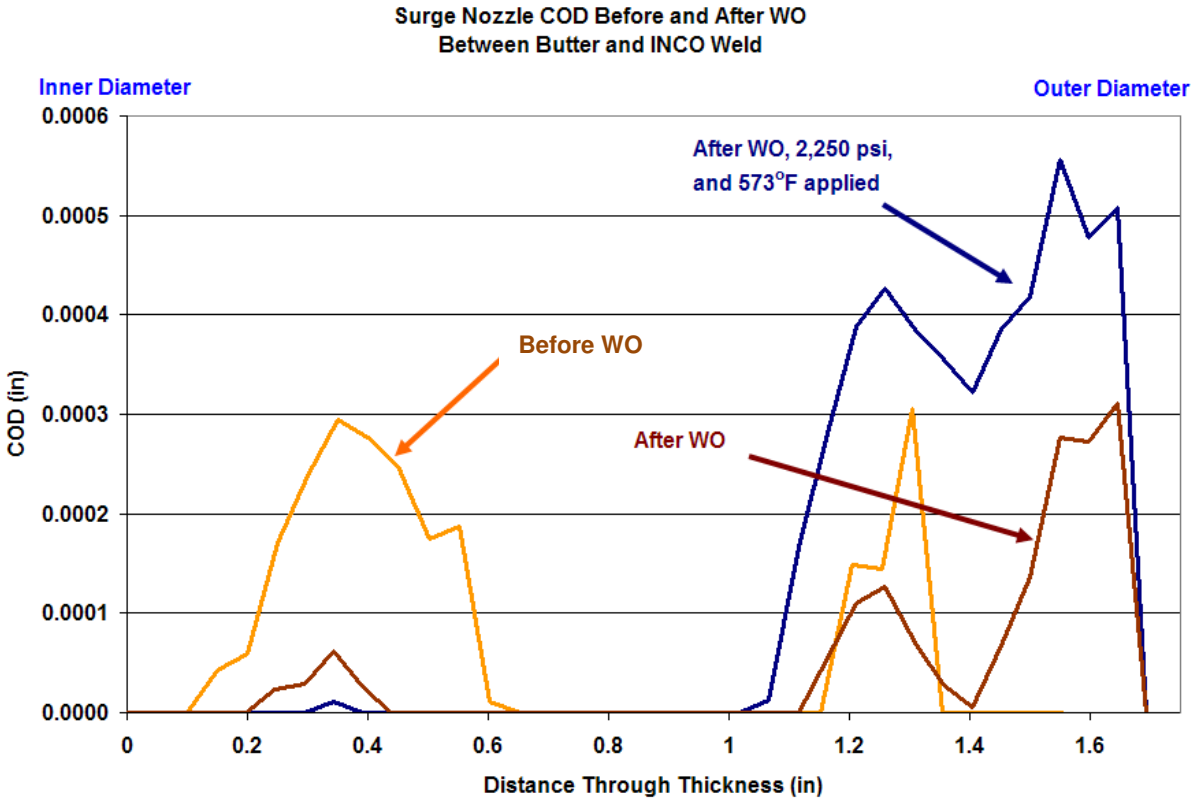

Figure 119 Surge Nozzle Crack1 Crack Opening Displacements before and after Applying the FSWOL and before and after Applying the Operating Temperature and Pressure

The results for the final scenario for the Crack1 location are shown in Figure 120. The FSWOL was applied pre-emptively to an uncracked pipe, and then operating pressure and temperature were applied. For this scenario, a crack was then introduced and forced to grow through the mitigated (post-FSWOL) weld residual stress field. This figure shows that the crack remains closed for the first 60 percent of the thickness and then is forced open beyond this point by the FSWOL as a result of the increased axial tension stresses toward the outer diameter of the pipe due to the application of the FSWOL.

Figure 121 shows a summary stress intensity factor plot which shows the results for all three scenarios. The blue curve is the same as that shown in Figure 116 and shows the stress intensity factor at operating pressure and temperature for an untreated crack (no FSWOL) that grows to 75 percent of the wall thickness. The orange diamond indicates the stress intensity factor of a 75 percent deep through wall crack for this untreated case (no FSWOL). The red square indicates the stress intensity factor for a 100 percent through wall crack after FSWOL has been applied to it. The crack growth rate equation predicts that the 75 percent through wall crack would grow through the remaining wall thickness in 20 years if left untreated by the FSWOL. Conversely, if the pipe were treated, the K value of the 75 percent deep crack would decrease considerably to 3.5 MPa-$m^{½}$ (3.21 ksi-$in^{½}$) and would be predicted to grow through the remainder of the original wall in 86 years. The green line on the graph shows the stress intensity factor calculated for the case in which the FSWOL is applied pre-emptively to an uncracked pipe and then after applying the FSWOL a crack is introduced and forced to grow. The stress intensity factor (K) remains zero until approximately 65 percent through the wall thickness and then increases but to a value that is lower than that of a 75 percent deep crack in the untreated pipe.

All results for the surge nozzle geometry where the crack is located between the butter and main weld indicate that a circumferential crack in an untreated surge nozzle should not grow beyond a third of the wall thickness before being stopped by the compressive weld residual stresses in the structure. In the very unlikely event that a crack is formed beyond this depth to beyond 60 percent of the wall thickness, it would not be made worse by the FSWOL. A crack at 75 percent of the way through the wall thickness would have its stress intensity factor cut in half by the FSWOL, and even if the crack were 100 percent of the way through the original pipe, the FSWOL does not increase the stress intensity factor beyond that which was found for a crack 75 percent of the way through the wall on an untreated pipe.

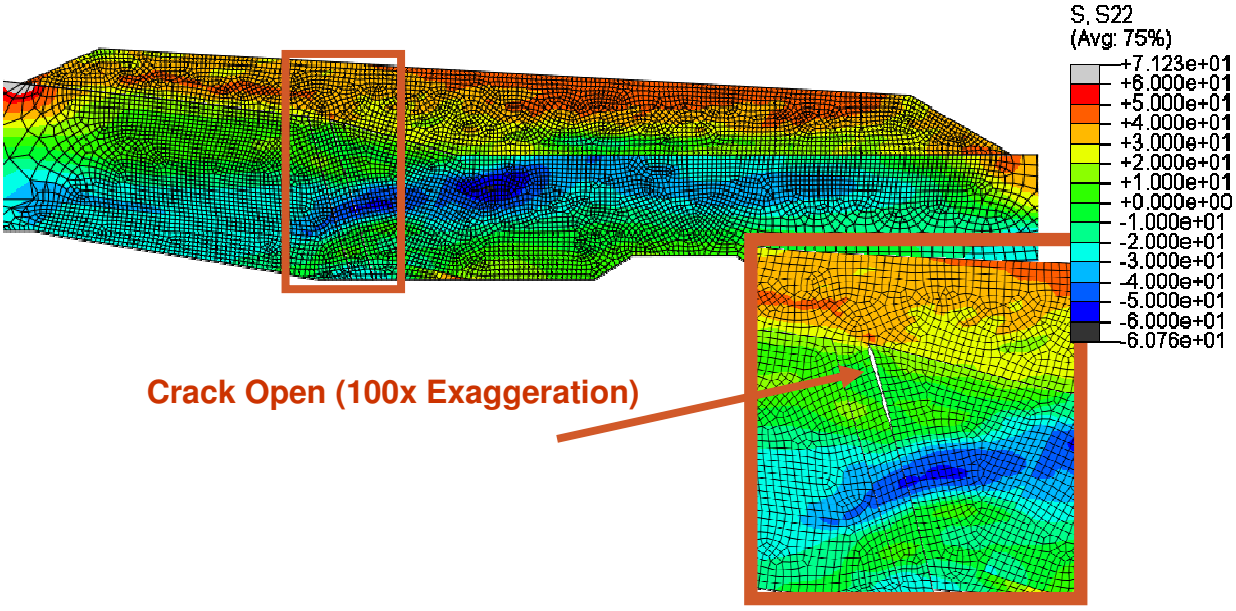

Figure 120 Surge Nozzle Axial Stresses after Crack1 is Introduced and Forced to Grow after Applying the FSWOL and the Operating Loads

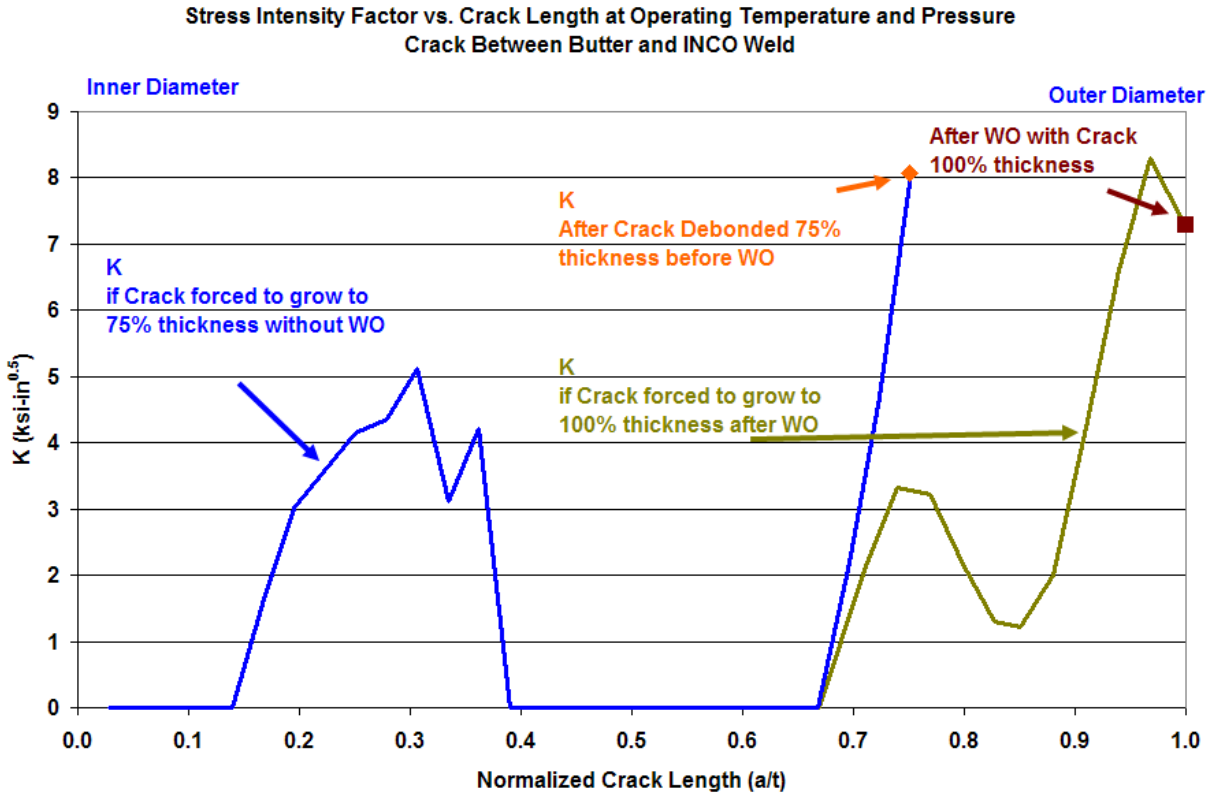

Figure 121 Surge Nozzle Crack1 Stress Intensity Factors for all Cases

4.2.2 Surge Nozzle – Crack2

The same three crack growth scenarios were examined for a crack between the A508 carbon steel nozzle material and the butter layer. This will be noted as crack location 2 (Crack2) as shown in Figure 122.

In the first scenario, the crack is forced to grow to 75 percent of the way through the thickness and then operating temperature and pressure are applied with no FSWOL. Figure 123 shows the axial stress in the surge nozzle after the crack was forced to grow and the operating loads were applied. The exaggerated displacement plot shows that the crack would open at the inner diameter and then close by itself somewhere in the middle of the thickness. Again, it is unlikely that the crack would grow beyond the zone where it is forced closed by the welding residual stresses without external forces well beyond normal operating loads. Some useful information can be gathered from the stress intensity factors as calculated by Equation 4 and the predicted crack growth rates as calculated by Equation 5. As was the case for the previous examples, the crack growth rate will be given in terms of years required for the crack to grow through the remaining thickness assuming that the crack growth remains constant through the remaining thickness.

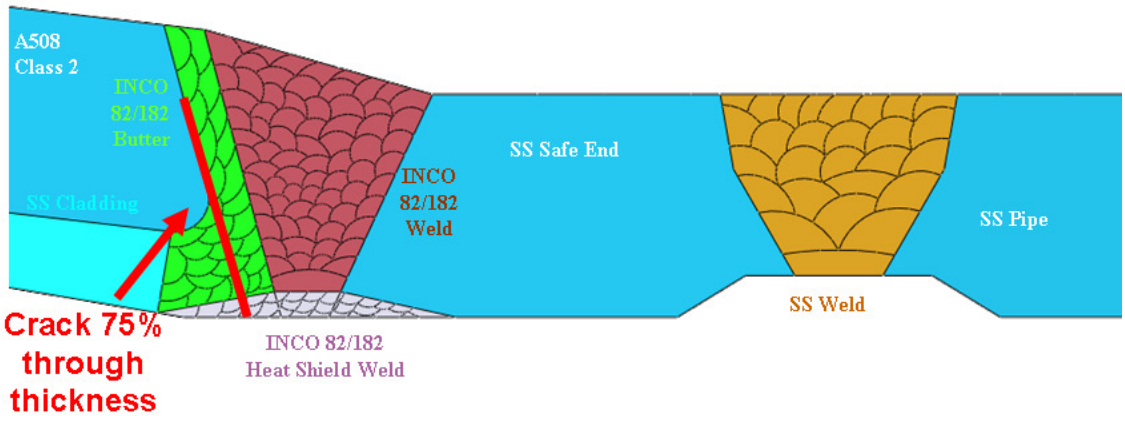

Figure 122 Surge Nozzle Crack through A508/Butter Interface (Crack2)

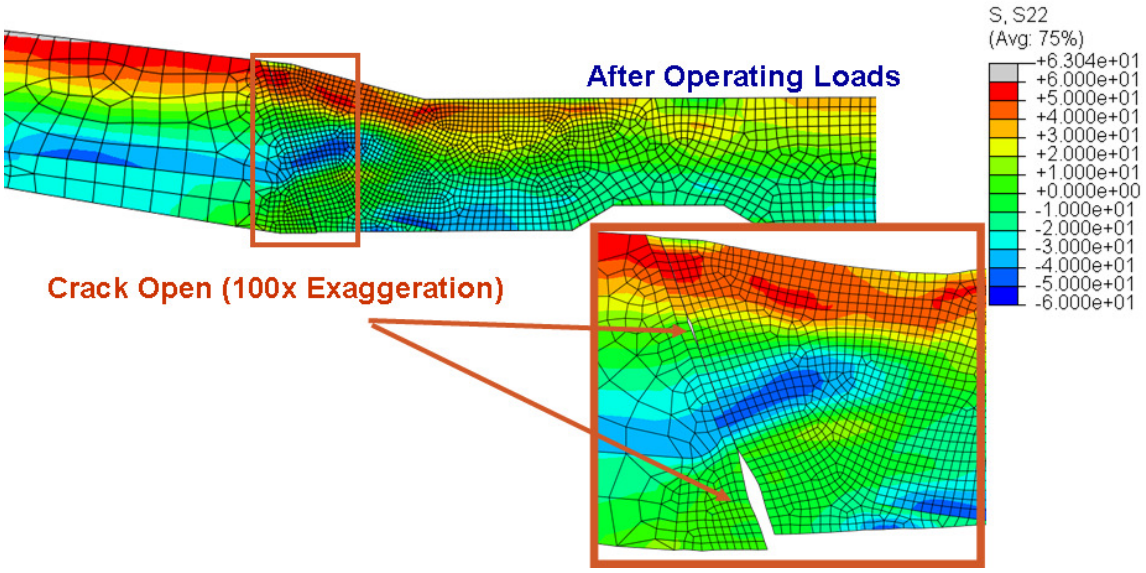

Figure 123 Surge Nozzle Axial Stresses with Crack2 before Applying the FSWOL

Figure 124 shows the stress intensity factor in (ksi-in ^{½}) units for the Crack2 location in the surge nozzle geometry. The stress intensity factor is used to calculate the crack growth rate due to PWSCC. One can see that the stress intensity factor is zero at the inner diameter and gets higher through the thickness until its value drops off to zero at about a third of the way through the original wall thickness of the pipe. This result is similar to that found for the Crack1 location.

Since Equation 5 for the crack growth rate is linear with the stress intensity factor, the equation predicts that the crack growth would be zero after the crack reaches 35 percent of the wall thickness in this stress field which results from the weld residual stresses and the operating temperature and pressure induced stresses.

For this geometry and loading case, the initiated crack at the inner diameter has a stress intensity factor of zero and would require additional loading to initiate a crack using the criterion developed for Equation 5. At its peak stress intensity factor at 22 percent of the way through the thickness, K = 8.9 MPa-m^{½} (8.1 ksi-

in $^{1/2}$), the time required for the crack to grow through the remaining thickness is 69 years. Once the crack reaches a third of the way through the wall, the crack arrests and will not grow through the thickness. If artificially forced to grow, the crack would start to open again at 70 percent through wall. At 75 percent through wall, K = 6.6 MPa-m$^{1/2}$ (6.0 ksi-in $^{1/2}$), the crack would be predicted to grow through the remaining wall thickness in 34 years.

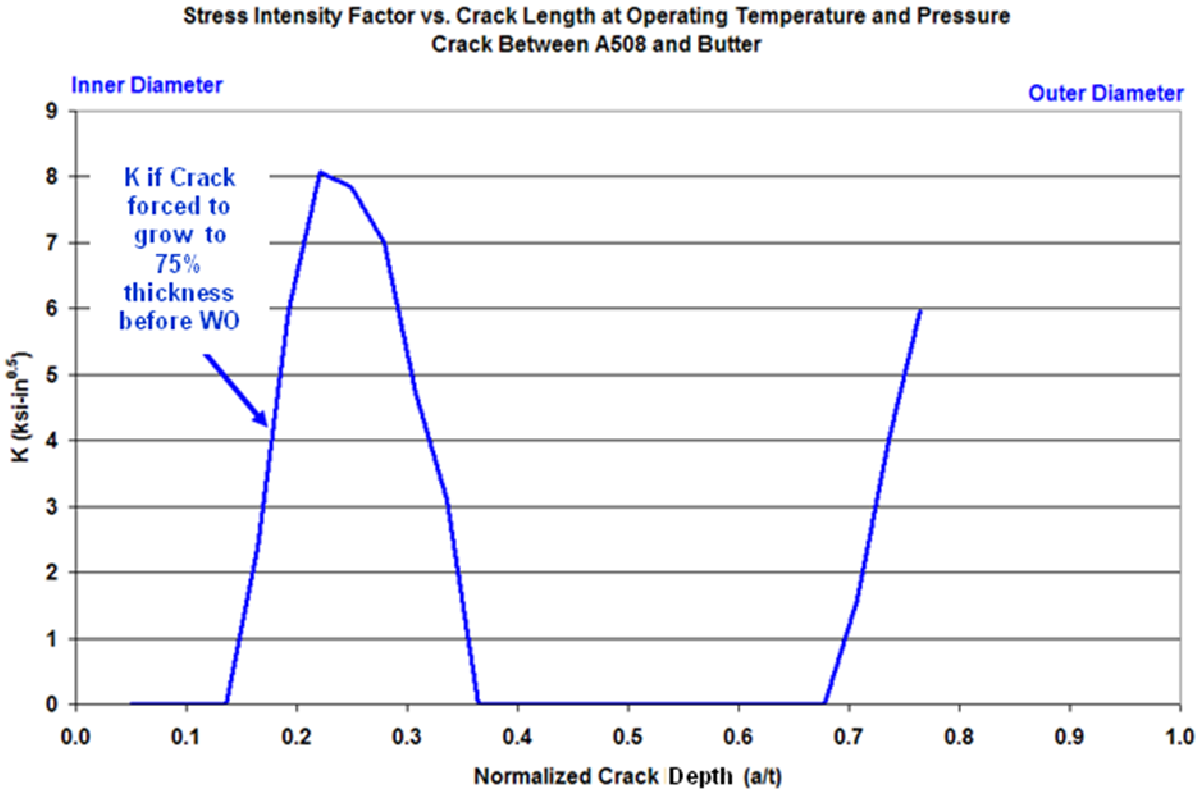

Figure 124 Surge Nozzle Crack2 Stress Intensity Factors before Applying the FSWOL

The second crack scenario studied subjects this crack to the FSWOL and then applies the operating pressure and temperature.

Figure 125 shows the axial stress in the surge nozzle geometry after welding is complete, after the Crack2 is introduced 75 percent through the thickness and after a FSWOL has been applied over a through-wall crack (100 percent deep) in a DMW. The figure shows an exaggerated (100x) displacement plot of the mitigated (post-FSWOL) through-wall crack profile before operating pressure and temperature are applied.

After application of the FSWOL, the inner diameter is put in compression and the crack mouth is forced closed. The crack tip which is at 100 percent through the original pipe thickness is not put into a more tensile field and is not opened more by the FSWOL application despite the fact that the crack is allowed to grow from 75 percent of the original wall thickness to 100 percent the original wall thickness. Figure 126 compares the axial stresses at room temperature and pressure (post-FSWOL) to those at operating

pressure and temperature (post-FSWOL). The inner diameter compression is reduced by the operating loads, but the compression stresses remain, and the crack mouth remains closed on the inside surface.

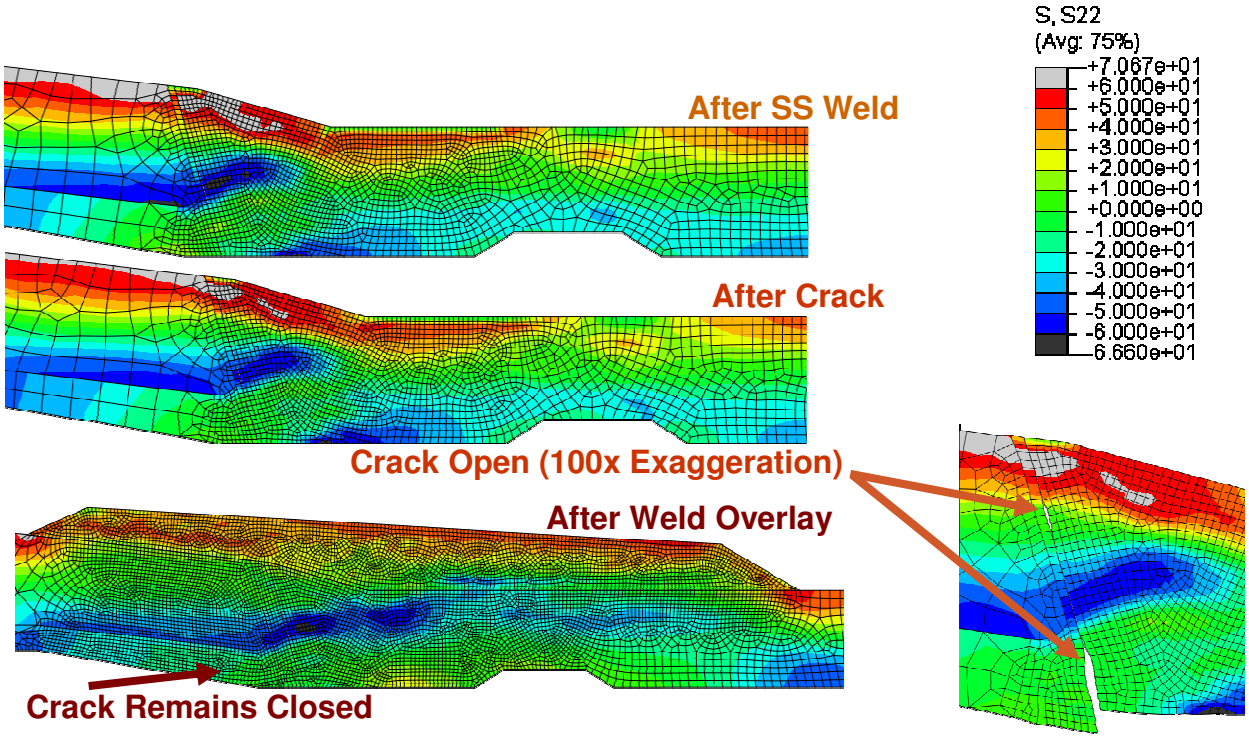

Figure 125 Surge Nozzle Axial Stresses after Crack2 and after Applying the FSWOL

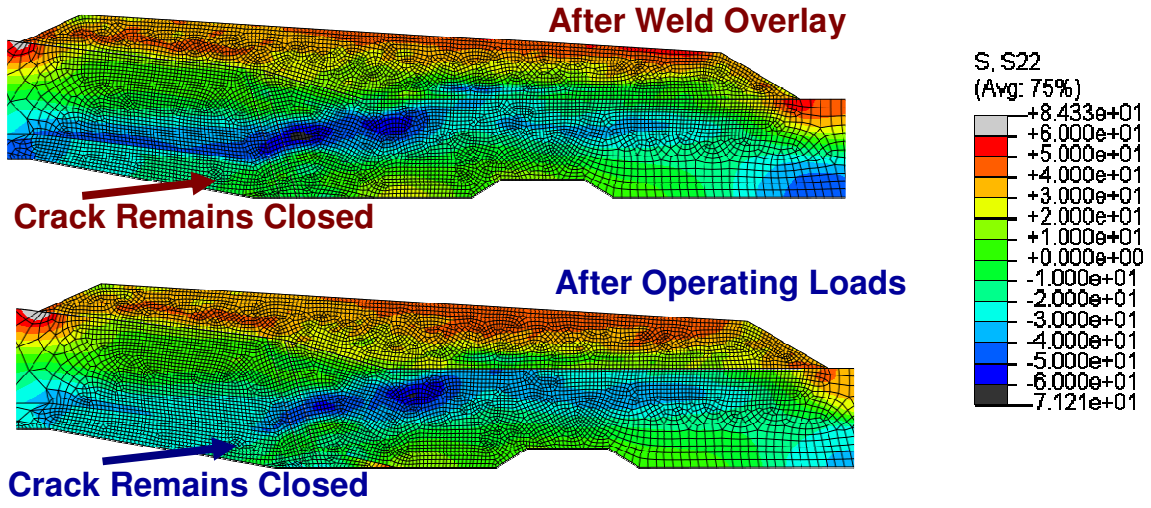

Figure 126 Surge Nozzle Axial Stresses after Crack2 FSWOL and Operating Loads

Figure 127 shows the crack opening displacement predicted for the surge nozzle 360 degree circumferential crack before and after applying the FSWOL, and then with operating pressure and temperature applied. The graph shows that the crack would open to about one third of the thickness due to welding residual stresses and would then be closed for the remainder of the cracked surface until it reached the area of the crack tip beyond 60 percent through the thickness where it opens again. After the FSWOL has been applied, the crack mouth on the inside surface is forced closed, and the crack tip is not forced further open despite the additional crack depth examined. When operating pressure and temperature are applied, the crack profile closes further at the inner diameter and opens to about twice the unloaded value in the outer third of the wall thickness.

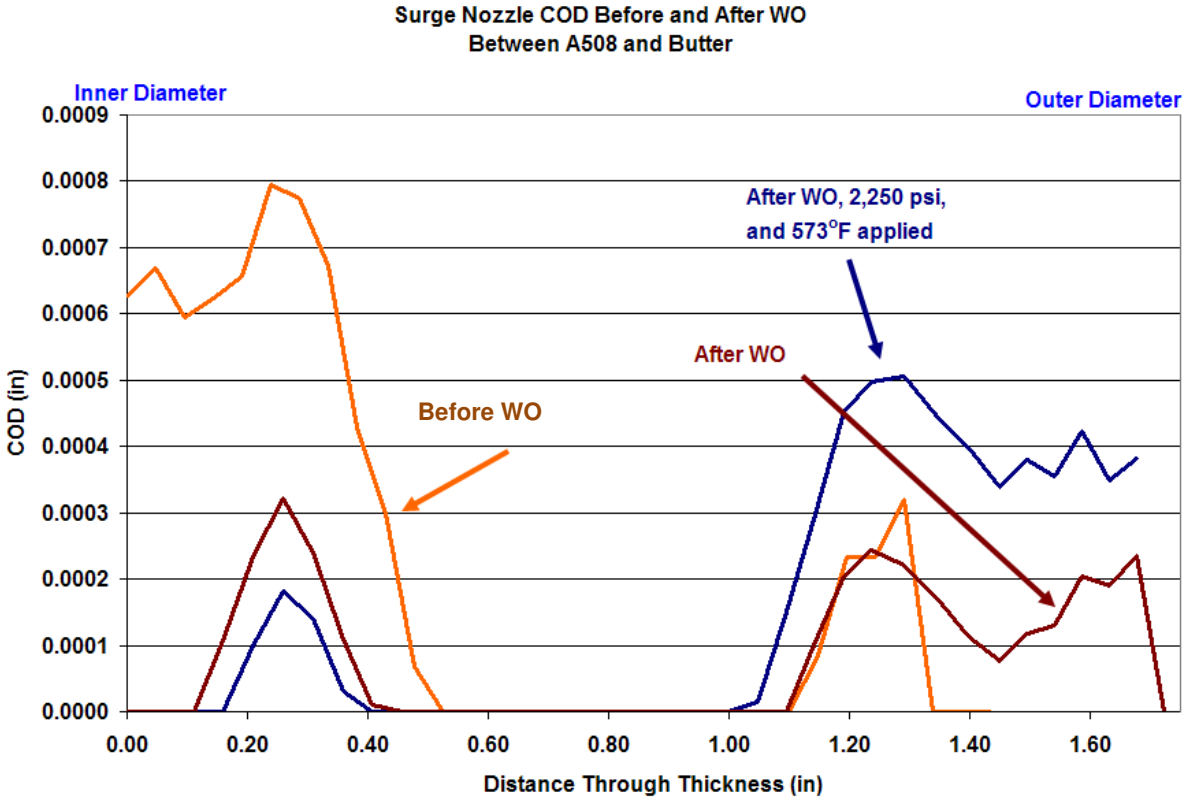

Figure 127 Surge Nozzle Crack2 Crack Opening Displacements before and after FSWOL

The results for the final scenario for the Crack2 location are shown in Figure 128. The FSWOL was applied pre-emptively to an uncracked pipe, and then the operating pressure and temperature were applied. For this scenario, a crack was introduced and forced to grow in this mitigated (post-FSWOL) weld residual stress field. This figure shows that the crack remains firmly closed for the inner 60 percent of the thickness and then opens beyond this point as a result of the increased axial tension stresses toward the outer diameter of the pipe.

Figure 129 shows a summary stress intensity factor plot which shows the results for all three scenarios. The blue curve is the same as that shown in Figure 124 and shows the stress intensity factor at operating pressure and temperature for an untreated crack (no FSWOL) that is grown to 75 percent of the wall thickness. The fact that the blue curve goes to zero at 33 percent through the wall thickness and stays there until 70 percent through wall, indicates that the crack would not naturally progress into this region. The stress intensity factor at the forced crack tip at 75 percent of the way through the thickness is K = 8.7

MPa-m^{½} (7.9 ksi-in ^{½}). This is indicated by the location of the orange diamond. The red square indicates the stress intensity factor for a 100 percent through wall crack after FSWOL has been applied to it. The crack growth rate equation shows that the untreated (no-FSWOL) 75 percent deep through wall crack would be predicted to grow through the remaining wall thickness in 34 years. The K-value for the assumed 75 percent deep treated crack (post-FSWOL) would be 5.6 MPa-m^{½} (5.1 ksi-in ^{½}) and would be predicted to grow through the remaining wall in 43 years. The green line on the graph shows the stress intensity factor calculated for the case in which the FSWOL is applied pre-emptively to an uncracked pipe and then a crack is subsequently introduced and forced to grow in this mitigated (post-FSWOL) stress field. The stress intensity factor remains zero until approximately 65 percent through the wall thickness and then increases, but to a value that is near or lower to that of the untreated pipe (no FSWOL).

All results indicate that a circumferential crack in an untreated surge nozzle would not grow beyond a third of the wall thickness before being stopped by the compressive weld residual stresses in the structure. In the very unlikely event that a crack is formed beyond this depth to beyond 60 percent of the wall thickness, it would be made better by the FSWOL. Other than this unlikely scenario, the FSWOL should prevent new cracks from forming, and should close existing cracks that are less than 60 percent through wall.

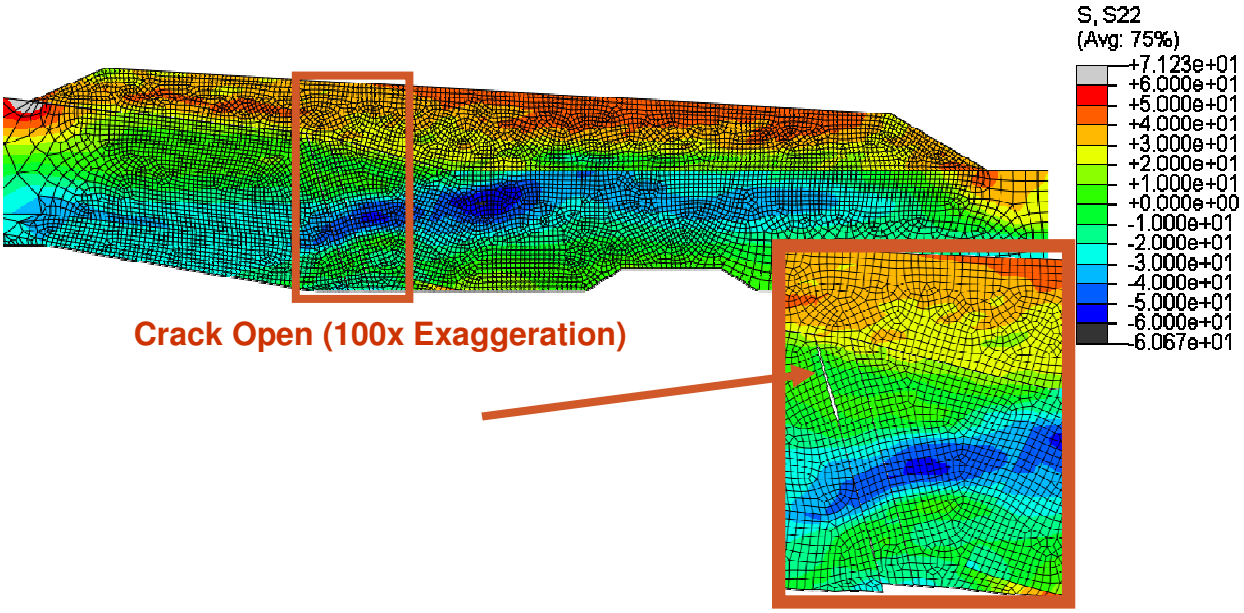

Figure 128 Surge Nozzle Axial Stresses after Crack2 Forced to Grow after Applying the FSWOL and Operating Loads

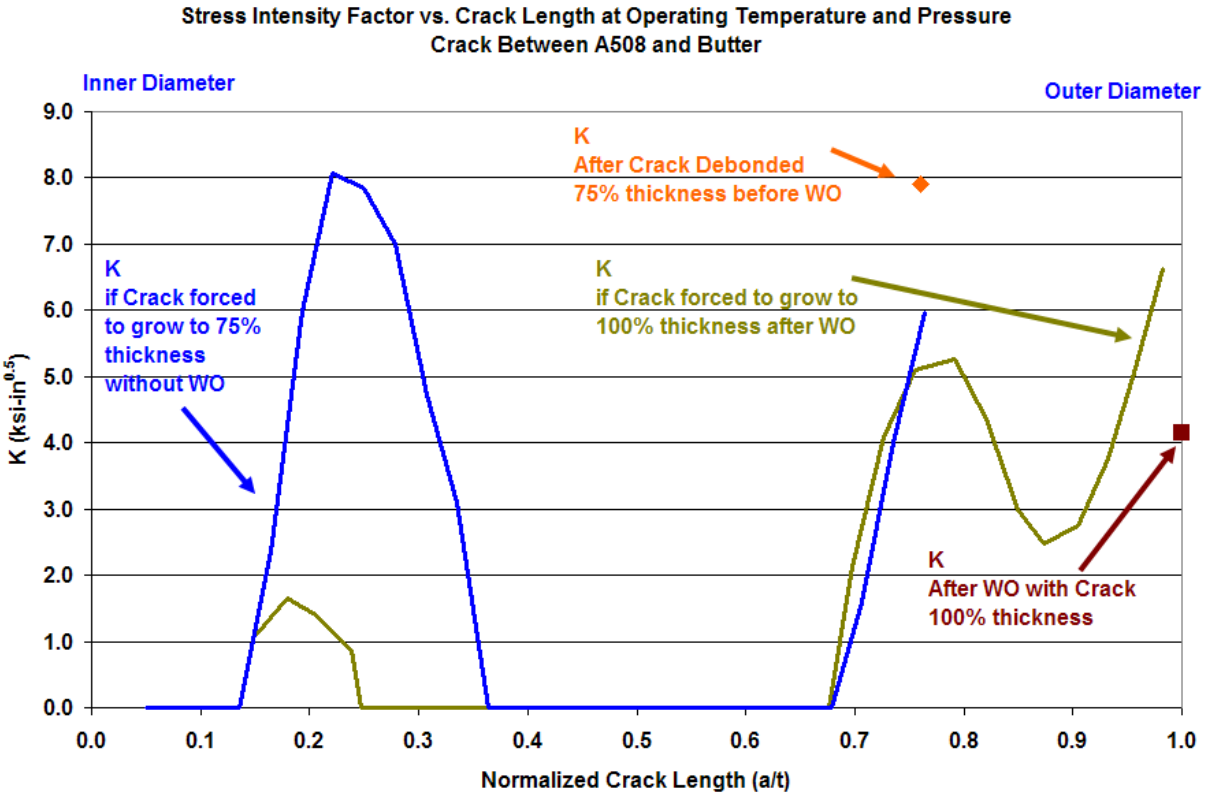

Figure 129 Surge Nozzle Crack2 Stress Intensity Factors for all Cases

4.2.3 Safety Nozzle – Crack1

As with the surge nozzle results, the first three cases examined for the safety nozzle geometry have the simulated crack located at the interface between the butter layer and the dissimilar metal weld as shown in Figure 130. The same three scenarios will be considered for the safety nozzle as were for the surge nozzle.

In the first scenario, the crack is forced to grow to 75 percent of the way through the thickness and then the operating temperature and pressure are applied with no FSWOL. Figure 131 shows the axial stress in the safety nozzle after the crack was forced to grow and operating loads were applied. The exaggerated displacement plot shows that the crack would open only slightly at the inner diameter and then close by itself somewhere near the middle of the thickness, and then open again once it reached the tensile stress field toward the outer diameter of the pipe. It is unlikely that the crack would grow beyond the zone where it is forced closed by the welding residual stresses without external forces well beyond the normal operating loads. Useful information can be gathered from this model by examining the stress intensity factors as calculated by Equation 4 and the predicted crack growth rates as calculated by Equation 5. The crack growth rate equation gives a very small number so this rate was converted into a more easily graspable number of years required to grow the crack through the remaining thickness of the pipe at the currently predicted crack growth rates, i.e., by assuming that the crack growth remains constant through the remaining thickness.

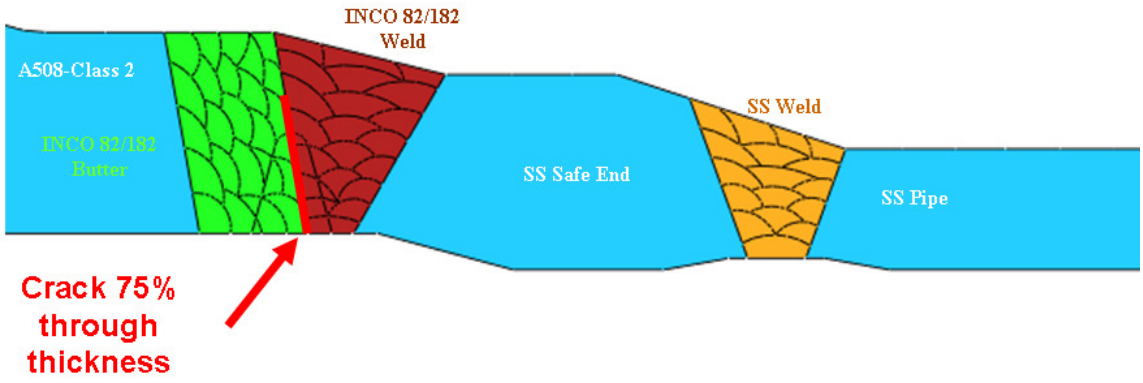

Figure 130 Safety Nozzle Crack through Butter/Weld Interface (Crack1)

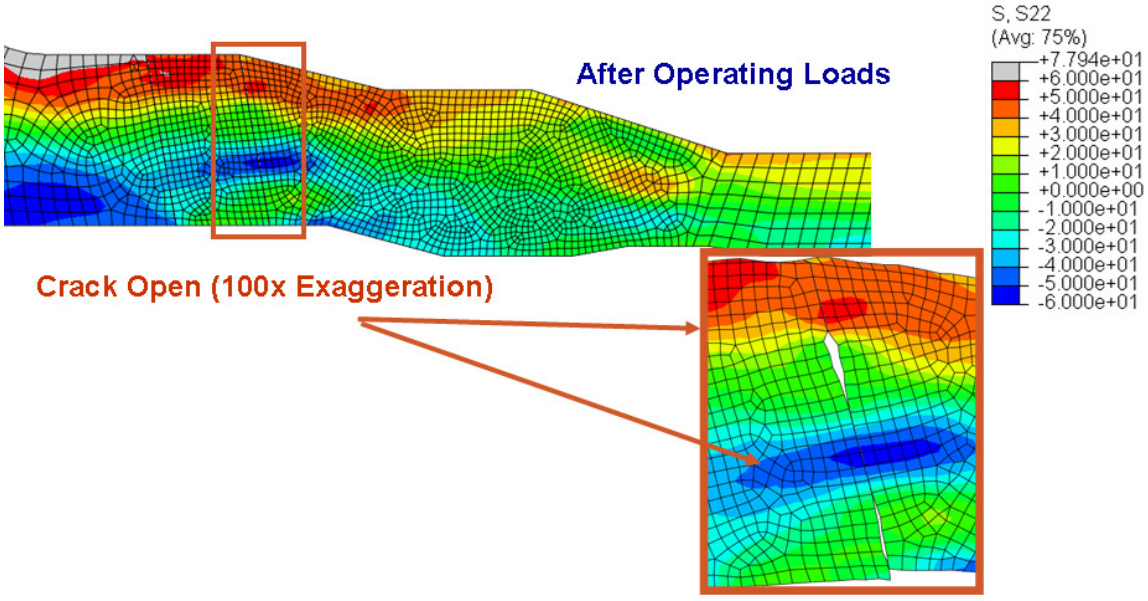

Figure 131 Safety Nozzle Axial Stresses with Crack before Applying the FSWOL

Figure 132 shows the stress intensity factor in (ksi-in ^{½}) units for the Crack1 location in the safety nozzle geometry. The stress intensity factor is used to calculate the crack growth rate due to PWSCC. One can see that the stress intensity factor is zero at the inner diameter and gets higher through the thickness until its value drops off again to zero about a third of the way through the wall thickness of the pipe. The value begins to increase again at about 60 percent of the way through the pipe for this geometry and location.

To put the crack growth rate values into more understandable terms, they were converted into units of (years to grow through remaining thickness) at a particular depth. For this geometry and loading case, the initiated crack at the inner diameter has a stress intensity factor of zero indicating that additional loading would be required to initiate a stress corrosion crack. At its peak stress intensity factor at 25 percent of the way through the thickness, K = 2.79 MPa-m^{½} (2.54 ksi-in ^{½}), it would be predicted to take 296 years to grow the crack through the remaining thickness. From 33 percent of the way through to 60 percent of the way through the wall, the crack arrests and will not grow through the thickness. If artificially forced to grow further, the stress intensity factor at 75 percent of the way through the wall thickness is 14.2

MPa-m$^{1/2}$ (12.9 ksi-in $^{1/2}$) and the crack growth rate predicts it would take 7 years to grow the crack through the remaining wall thickness.

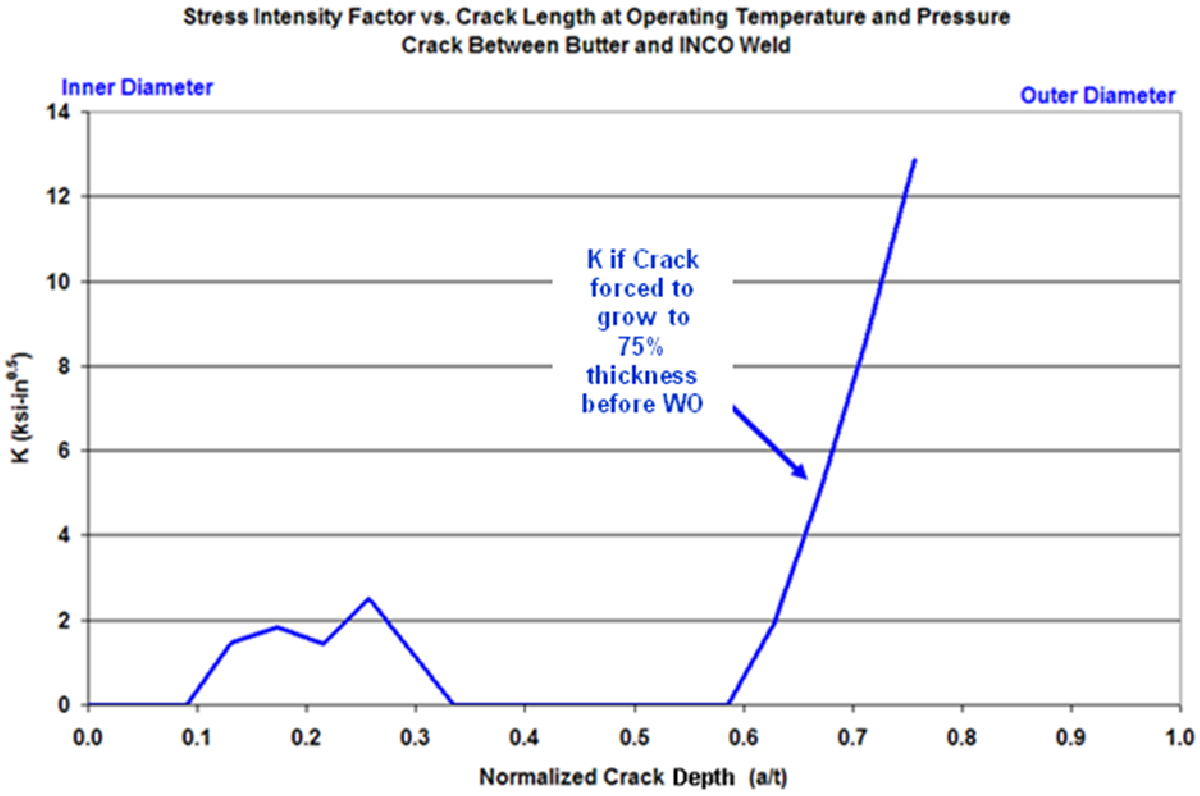

Figure 132 Safety Nozzle Crack1 Stress Intensity Factors before FSWOL

The second crack scenario studied subjects this crack to the FSWOL and then applies the operating pressure and temperature. Figure 133 shows the axial stress in the safety nozzle geometry after welding is complete, after the Crack1 is introduced 100 percent through the original pipe thickness and after the FSWOL has been applied. The figure shows an exaggerated (100x) displacement plot of the crack profile before the operating pressure and temperature are applied. One can see the difference between the crack profile in this case, and in the case in which operating pressure and temperature are applied. In this case, the crack shows some shearing at the inner diameter, but no axial opening. The crack tip is opened at 75 percent through the original pipe wall thickness.

After application of the FSWOL, the inner diameter is put into compression and the crack mouth is forced closed. The axial tension stress at the crack tip which is 100 percent through the original thickness is reduced by the application of the FSWOL. Figure 134 compares the axial stresses at room temperature and pressure to those at operating temperature and pressure. The inner diameter compression is reduced by operating loads, but the compression stresses remain, and the crack mouth on the inside surface remains closed.

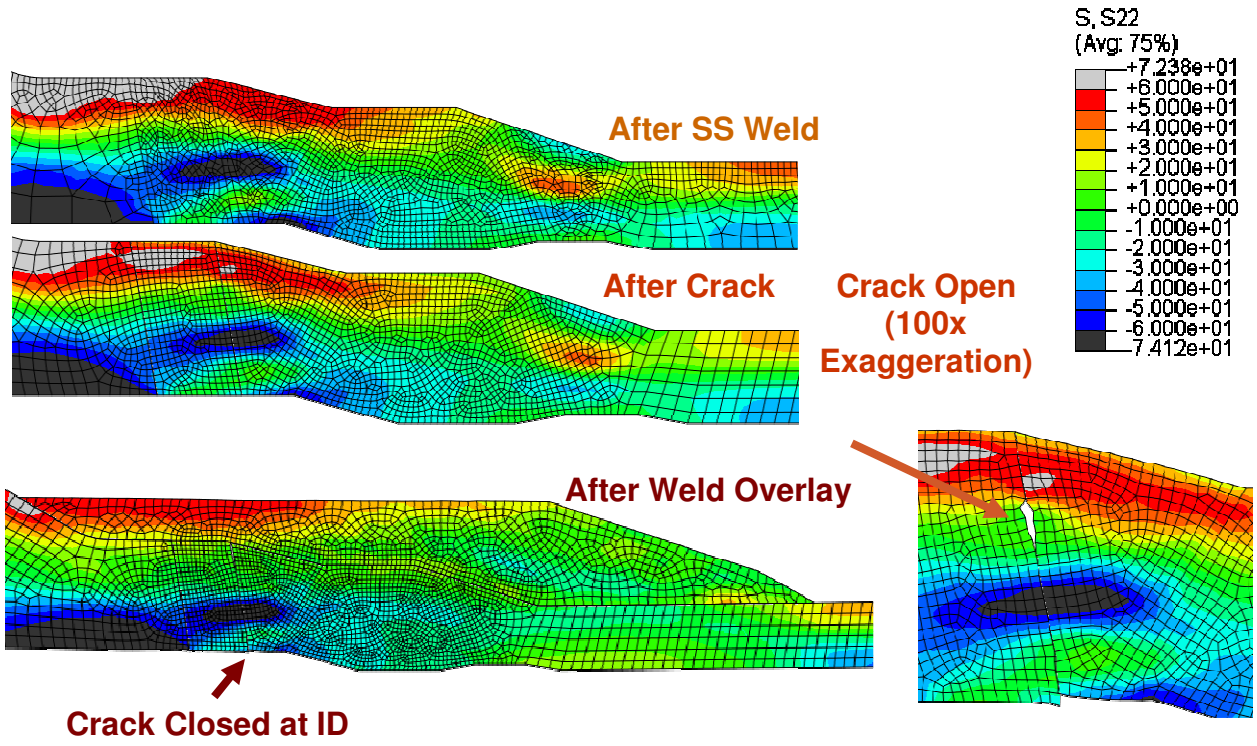

Figure 133 Safety Nozzle Axial Stresses After Crack1 and After Application of the FSWOL

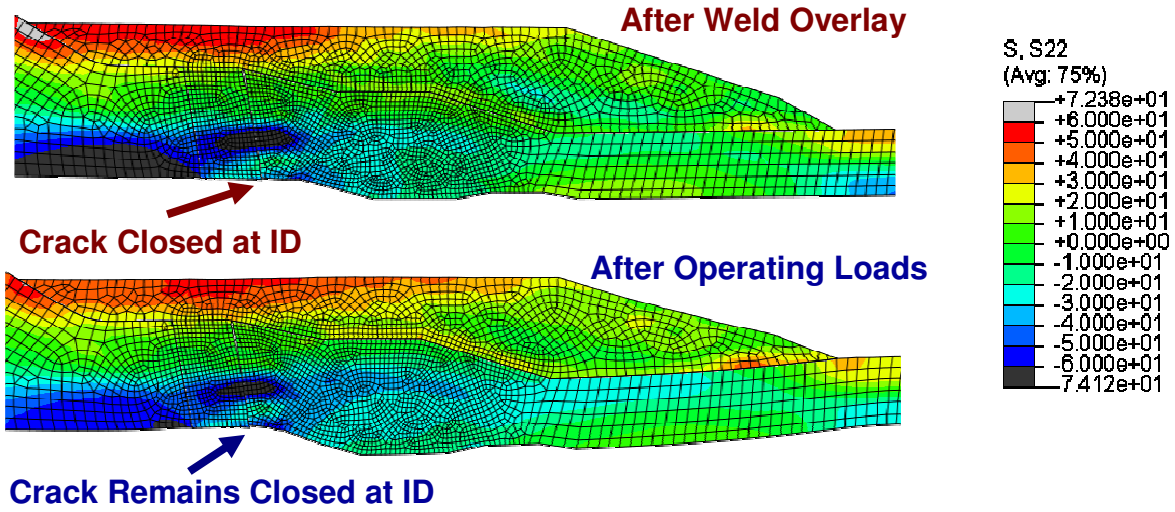

Figure 134 Comparison of the Safety Nozzle Axial Stresses after Introducing Crack1 after Applying the FSWOL both Before and After Applying the Operating Loads

Figure 135 shows the crack opening displacement predicted for the 360 degree circumferential crack in the safety nozzle at the Crack1 location before and after the application of the FSWOL, and after applying the operating pressure and temperature. The graph shows that the untreated crack (no FSWOL) is closed at the inner diameter, and would open from 60 percent to75 percent through the wall thickness. After the FSWOL has been applied, the crack tip is forced open less even though the hypothetical crack is deeper at 100 percent of the way through the original pipe wall thickness. When operating pressure and temperature are applied, the crack profile remains the same, and increases in value only slightly, and the crack tip opening displacement remains less than the case of a 75 percent of the wall thickness deep crack before the application of the FSWOL.

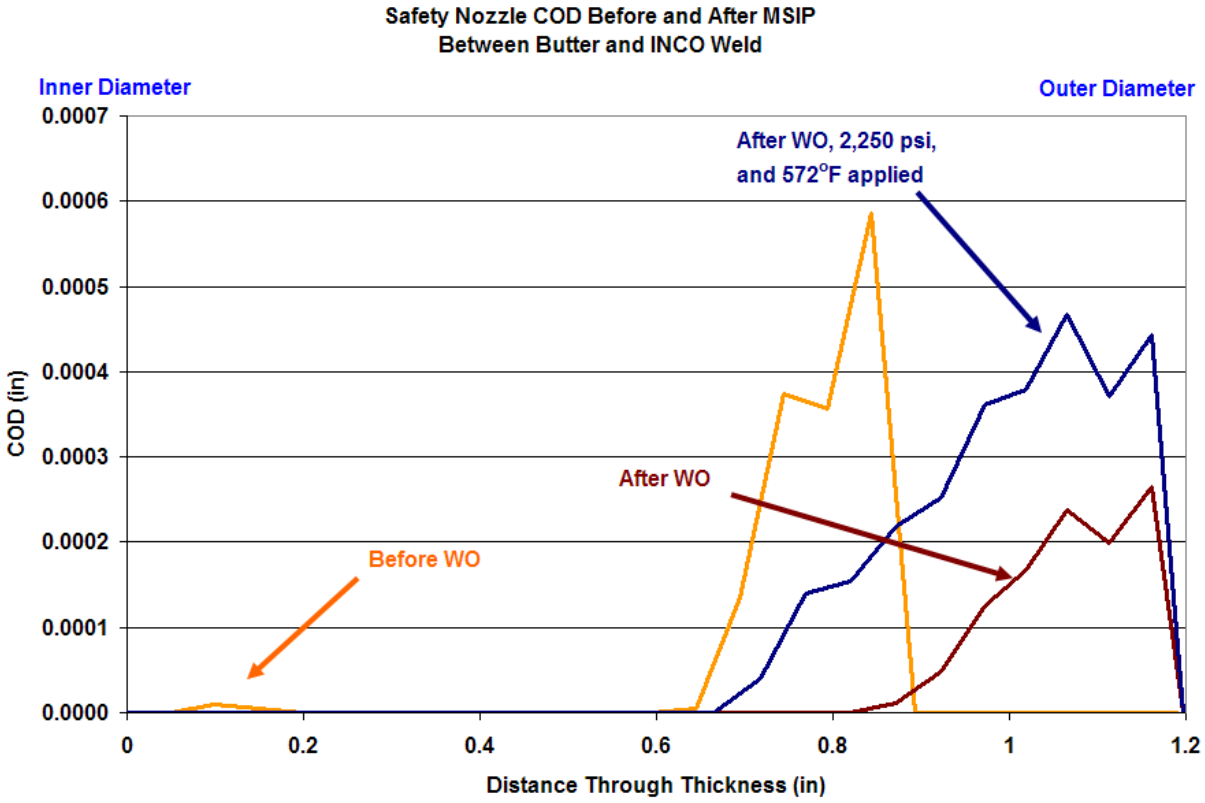

Figure 135 Safety Nozzle Crack1 Crack Opening Displacements before and after Applying the FSWOL

The results from the final scenario for the Crack1 location are shown in Figure 136. The FSWOL was applied pre-emptively to an uncracked pipe, and then the operating pressure and temperature were applied. In this state, a crack was introduced and forced to grow through the mitigated (post-FSWOL) weld residual stress field. This figure shows that the crack remains firmly closed for the first 60 percent of the thickness and then is forced to open beyond this point by the increased axial tension stresses toward the outer diameter of the pipe.

Figure 137 shows a summary stress intensity factor plot for crack growth before and after the application of the FSWOL. The blue curve is the same as that shown in Figure 132 and shows the stress intensity factor at operating pressure and temperature for a crack that grows to 75 percent of the wall thickness prior to the application of the FSWOL. The green line on the graph shows the stress intensity factor calculated for the case in which the FSWOL is applied pre-emptively to an uncracked pipe and then a crack is subsequently introduced and forced to grow through the mitigated (post-FSWOL) stress field.

The stress intensity factor remains zero until beyond 70 percent through the wall thickness and then increases but to a value that is lower than that of the untreated pipe. The crack growth rate equation shows that the 75 percent through wall untreated crack that would be predicted to grow through the remaining wall thickness in 7 years. The K value for the FSWOL treated crack would be 8.2 MPa-$m^{1/2}$ (7.43 ksi-$in^{1/2}$) and would be predicted to grow through the remaining weld overlay material in 30 years.

All results indicate that a circumferential crack in an untreated safety nozzle would most likely not grow beyond a third of the wall thickness before being stopped by the compressive weld residual stresses in the structure. In the very unlikely event that a crack is formed beyond this depth to beyond 60 percent of the wall thickness, the situation would be made better by the FSWOL. The FSWOL will prevent new cracks from forming, and will close existing cracks that are less than 60 percent through wall.

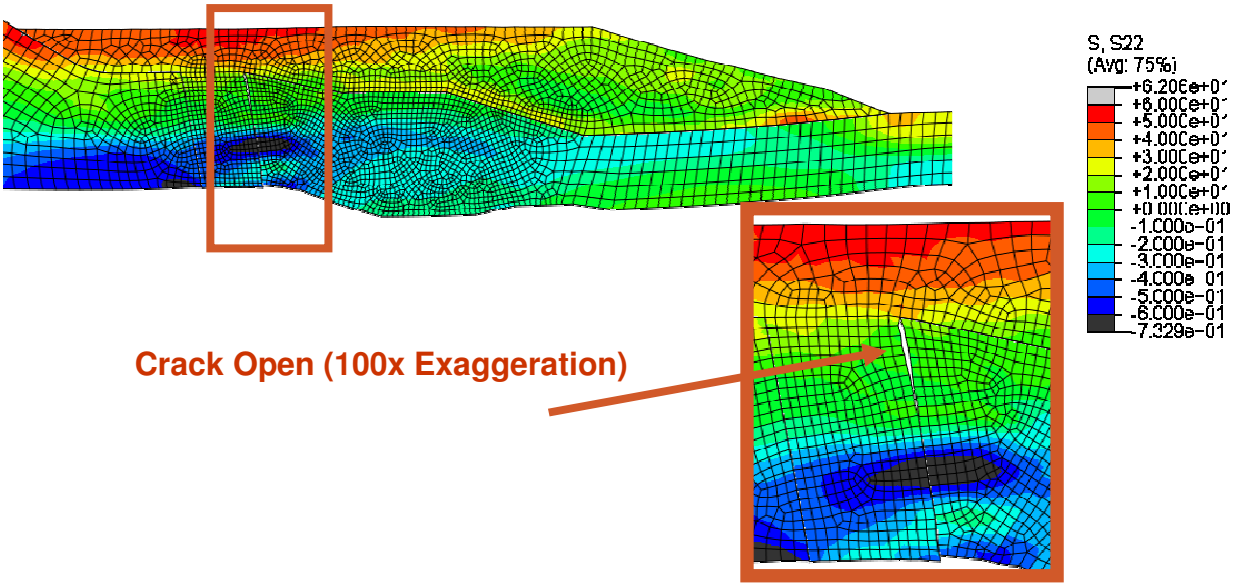

Figure 136 Safety Nozzle Axial Stresses after Crack1 is Introduced and Forced to Grow after Applying the FSWOL and Operating Loads

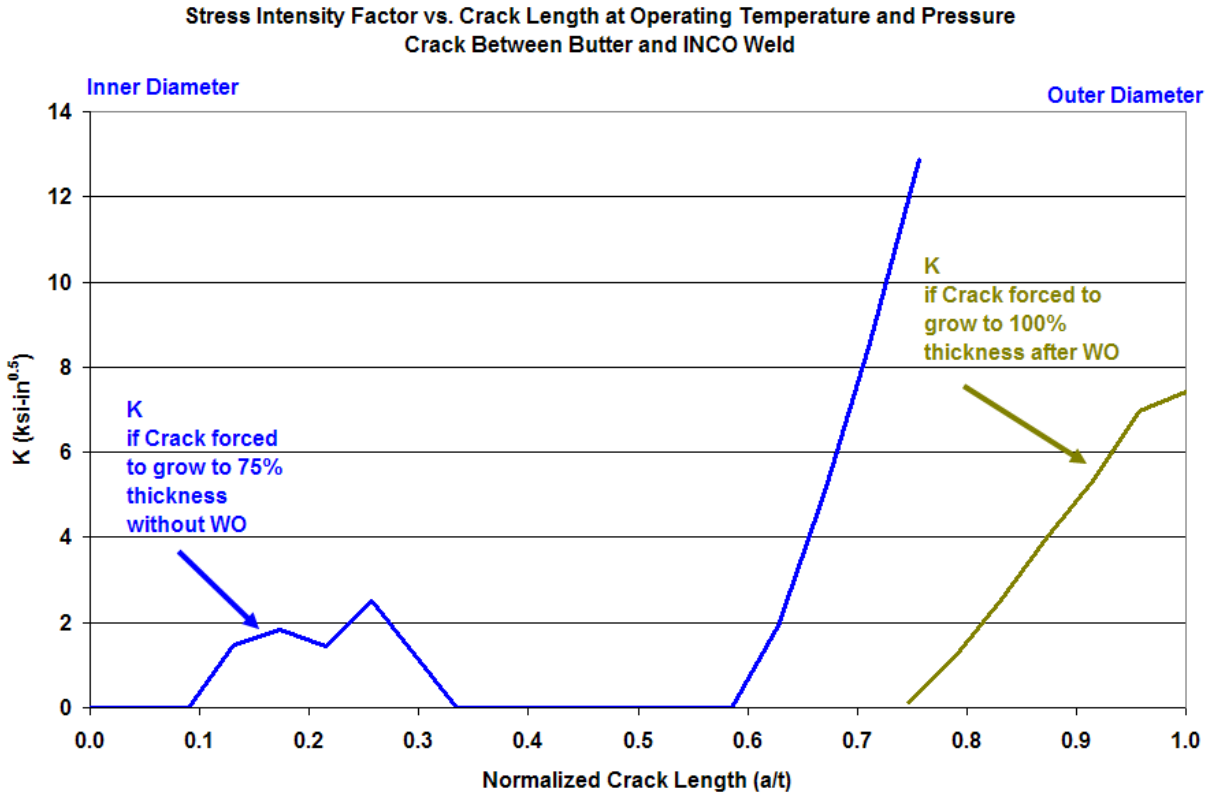

Figure 137 Safety Nozzle Crack1 Stress Intensity Factors for all Cases

4.2.7 Safety Nozzle – Crack2

The same three crack growth scenarios were examined for a crack between the A508 carbon steel nozzle material and the butter layer. This will be noted as crack location 2 (Crack2) as shown in Figure 138.

In the first case, the crack is forced to grow to 75 percent of the way through the thickness and then the operating temperature and pressure are applied with no FSWOL. Figure 139 shows the axial stress in the safety nozzle after the crack was forced to grow and operating loads were applied. The exaggerated displacement plot shows that the crack would remain closed at the inner diameter with some shearing and would not open again until past the middle of the wall thickness. Again, it is unlikely that the crack would grow beyond the zone where it is forced closed by the welding residual stresses without external forces well beyond normal operating loads. Some useful information can be gathered from the stress intensity factor as calculated by Equation 4 and the predicted crack growth rate as calculated by Equation 5. As done in the previous examples, the crack growth rate will be given in terms of years required to grow the crack through the remaining thickness if the current growth rate was maintained, i.e., by assuming that the crack growth rate remains constant through the thickness.

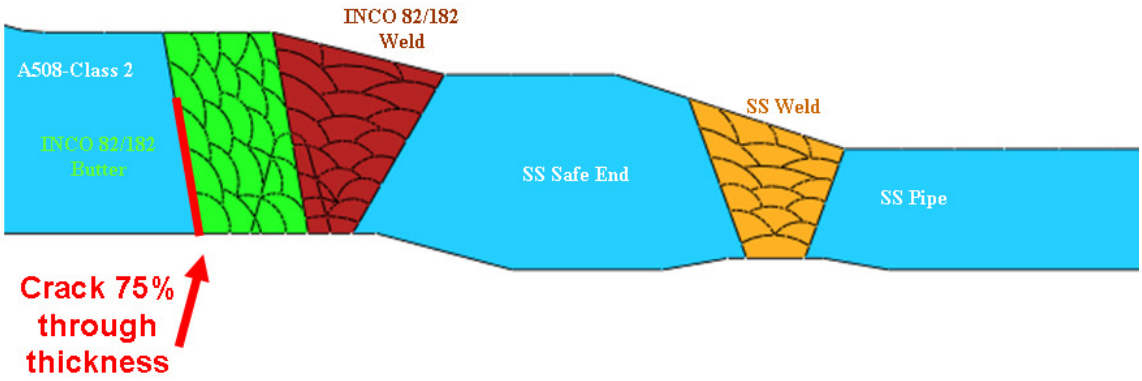

Figure 138 Safety Nozzle Crack through A508/Butter Interface (Crack2)

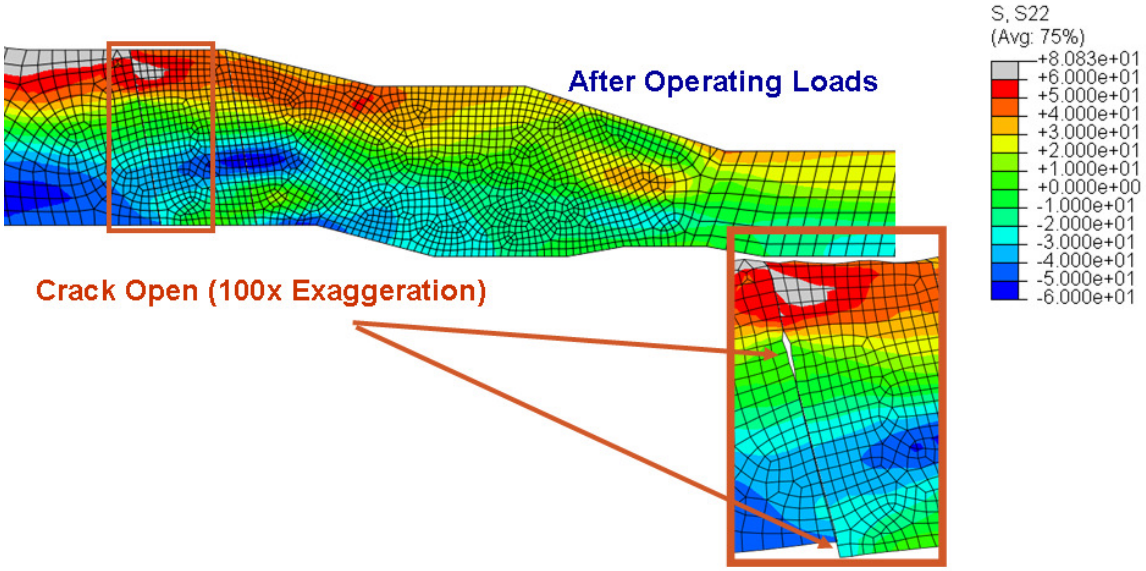

Figure 139 Safety Nozzle Axial Stresses with Crack2 before Applying the FSWOL

Figure 140 shows the stress intensity factor in (ksi-in ^{½}) units for the Crack2 location in the safety nozzle geometry. The stress intensity factor is used to calculate the crack growth rate due to PWSCC. One can see that the stress intensity factor is zero at the inner diameter and remains there until the untreated crack (no FSWOL) grows to a depth of more than 60 percent of the wall thickness. It then increases almost linearly until a depth of 75 percent through thickness.

To put the crack growth rate values into understandable terms, they were converted into units of (years to grow through remaining thickness) at a particular depth. For this geometry and loading case, the initiated crack at the inner diameter has a stress intensity factor of zero and would require additional loading to initiate a crack using the criterion developed for Equation 4. The stress intensity factor at 75 percent of the way through the thickness, K = 11.6 MPa-m^{½} (10.6 ksi-in ^{½}), would require 10 years to grow the crack through the remaining wall thickness, assuming that the crack growth rate remains constant through the remaining thickness.

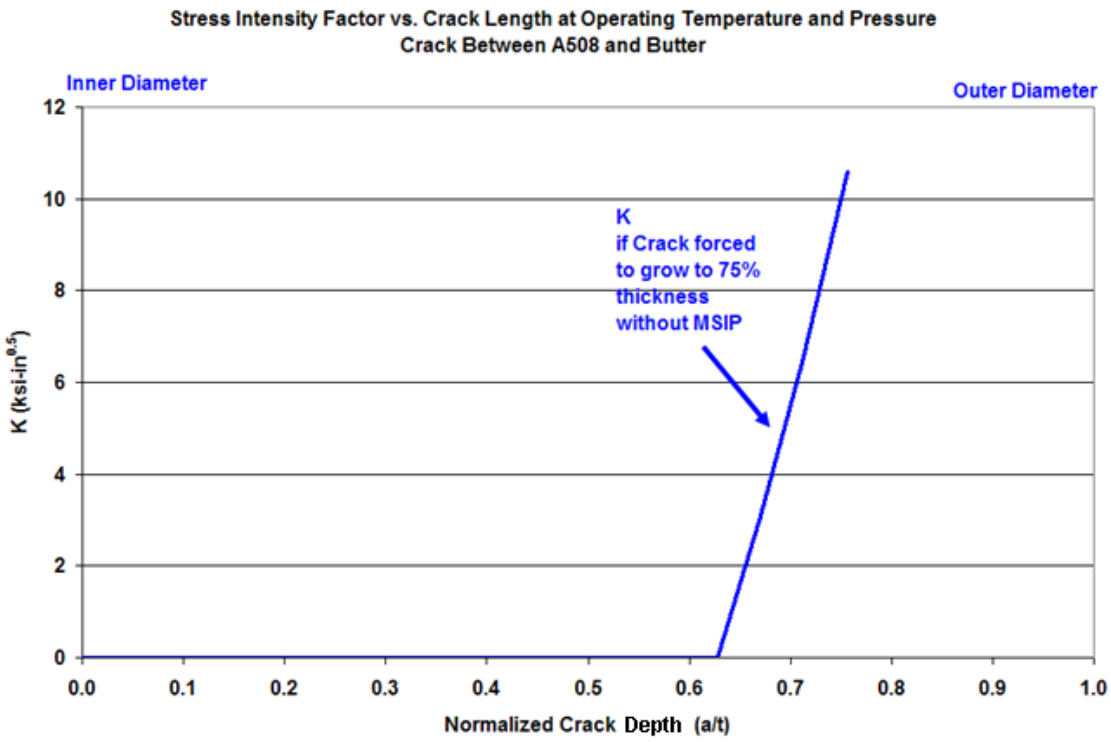

Figure 140 Safety Nozzle Crack2 Stress Intensity Factors before Applying the FSWOL

The second crack scenario studied subjects this crack to the FSWOL and then applies the operating pressure and temperature. Figure 141 shows the axial stress in the safety nozzle geometry after welding is complete, after the Crack2 is introduced 100 percent through the original wall thickness and after the FSWOL has been performed. The figure shows an exaggerated (100x) displacement plot of the crack profile before operating pressure and temperature are applied.

After application of the FSWOL, the inner diameter is put in compression and the crack mouth is closed. The crack tip which is at 100 percent through the original pipe thickness is put into a more tensile field and is opened by the application of the FSWOL. Figure 142 compares the axial stresses at room temperature and pressure to those at operating pressure and temperature. The inner diameter compression is reduced by the operating loads, but the compression stresses remain, and the crack mouth remains closed.

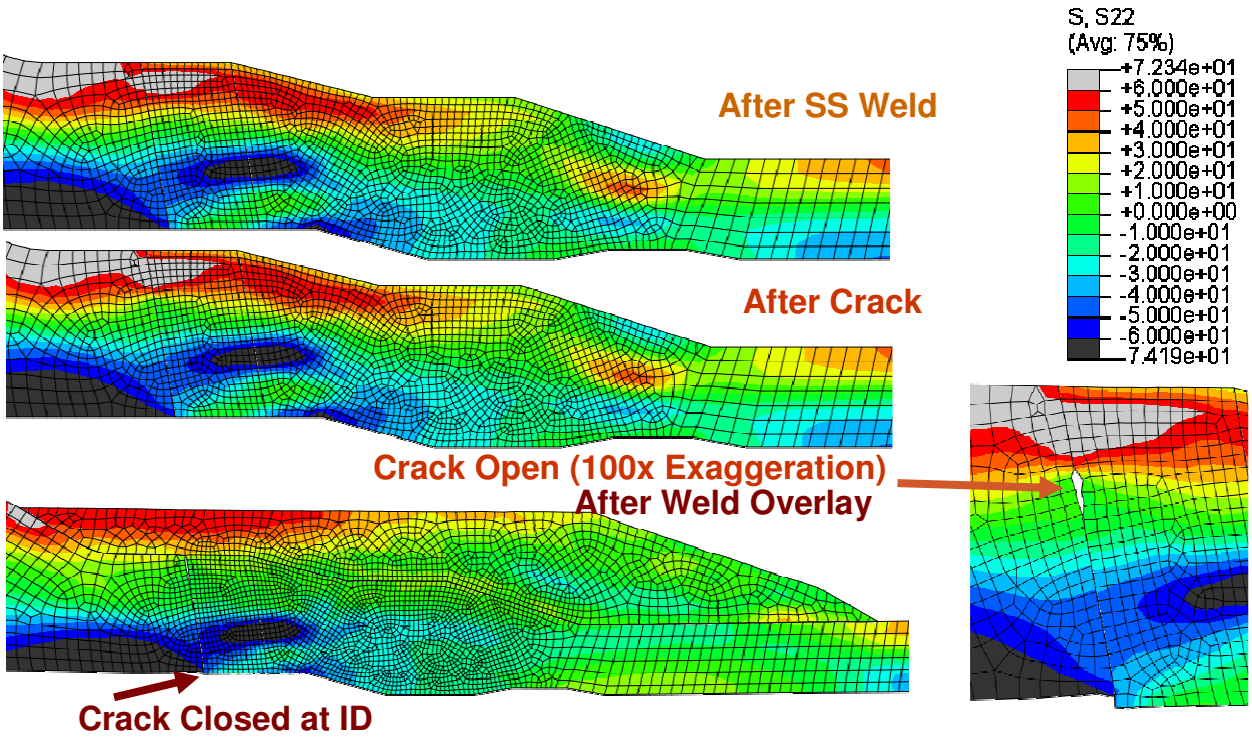

Figure 141 Safety Nozzle Axial Stresses after Crack2 and after Applying the FSWOL

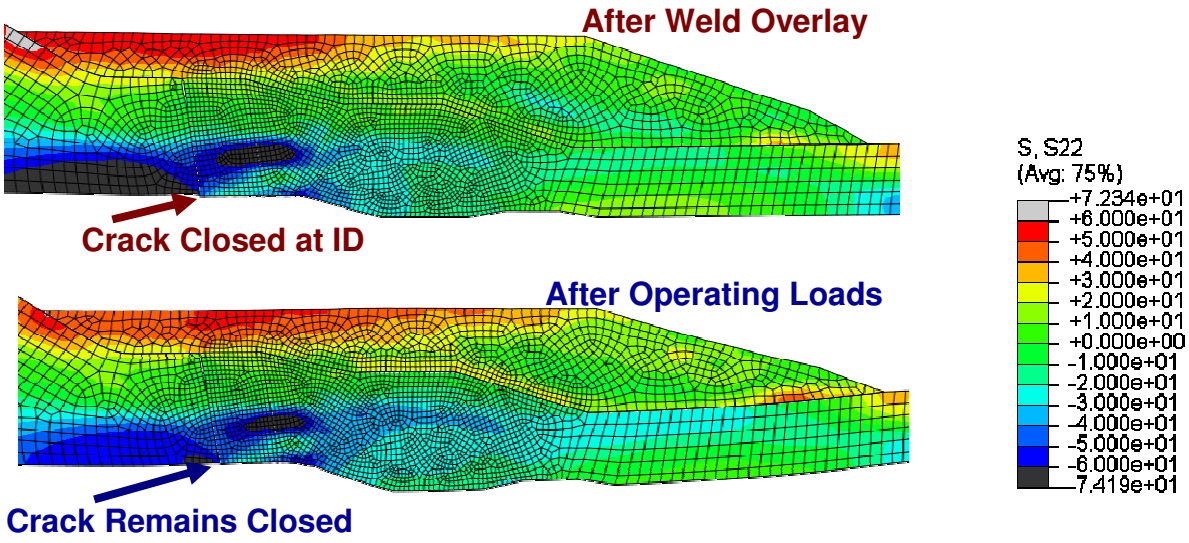

Figure 142 Comparison of the Safety Nozzle Axial Stresses after Introducing Crack2 after Applying the FSWOL, both before and after Applying the Operating Loads

Figure 143 shows the crack opening displacement predicted for the safety nozzle with a 360 degree circumferential crack before and after the application of the FSWOL, and then with operating pressure and temperature applied. The graph shows that the untreated crack (no FSWOL) would remain closed until a crack depth of approximately 15 mm (0.6 inches) and then would open near the crack tip. After the FSWOL has been applied, the crack mouth is forced more tightly closed, and the crack tip is forced open slightly less than without the FSWOL even though the crack has now been forced to progress from 75 percent of the original thickness to 100 percent of the original thickness. When operating pressure and temperature are applied, the crack tip opening displacement remains the same as that for the 75 percent crack before the FSWOL is applied.

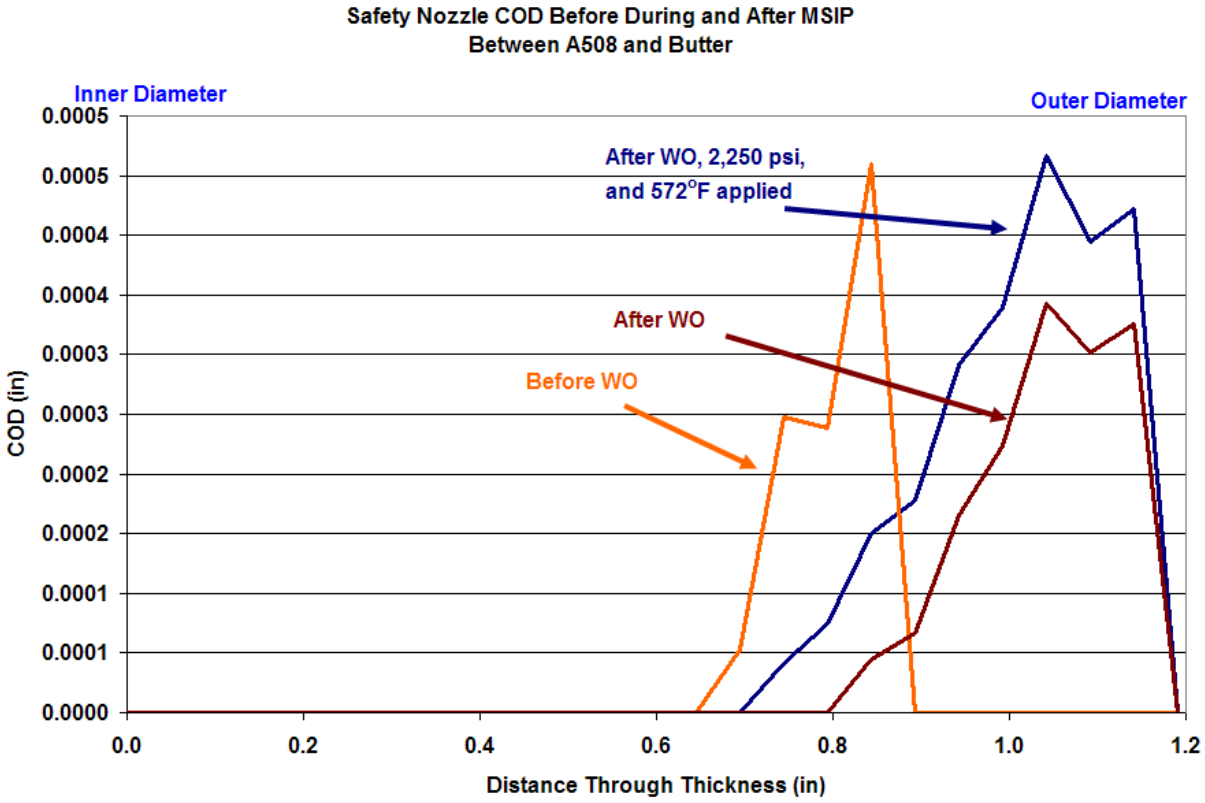

Figure 143 Safety Nozzle Crack2 Crack Opening Displacements before and after Applying the FSWOL

The final scenario for the Crack2 location is shown in Figure 144. The FSWOL was applied pre-emptively to an uncracked pipe, and then operating pressure and temperature were applied. In this state, a crack was introduced and forced to grow in the weld residual stress field after the application of the FSWOL. This figure shows that the crack is closed for the first 60 percent of the thickness and then is forced open beyond this point by the axial tension stresses toward the outer diameter of the pipe. The outer diameter pipe axial stress is slightly reduced by the application of the FSWOL.

Figure 145 shows a summary stress intensity factor plot which shows the results for the case in which a crack was forced to grow at operating conditions before applying the FSWOL and for another case where the crack is forced to grow at operating pressure and temperature after applying the FSWOL. The results are very similar to those of the Crack1 analysis for this geometry. The blue curve is the same as that shown in Figure 140 and shows the stress intensity factor at operating pressure and temperature for an untreated crack (no FSWOL) that is forced to grow to 75 percent of the wall thickness. The fact that the blue curve remains at zero until 60 percent through wall, indicates that the crack would not grow as a result of only the weld residual stresses. The stress intensity factor at the untreated crack tip at 75 percent of the way through the thickness is 11.6 MPa-m^{½} (10.6 ksi-in ^{½}) which would lead to a crack growth rate that would cause the crack to grow through the remaining pipe thickness in 10 years assuming that the crack growth rate remains constant.

The green line on the graph shows the stress intensity factor calculated for the case in which the FSWOL is applied pre-emptively to an uncracked pipe and then a crack is introduced and forced to grow through the mitigated (post-FSWOL) residual stress field. The crack stress intensity factor would be zero for the inner 75 percent of the pipe wall thickness for the case where a crack is introduced and forced to grow in the mitigated (post-FSWOL) residual stress field and would increase to 6.7 MPa-m^{½} (6.1 ksi-in ^{½}) once it reached the outer diameter of the original pipe wall thickness (100 percent deep crack). It would take 40 years for this 100 percent deep crack to grow through the overlay assuming that the crack growth rate remained constant and the crack growth rate for the overlay material (Alloy 52M) was comparable to that of the DMW (Alloy 82/182). This is known not to be the case in that the Alloy 52M is more resistant to PWSCC than the Alloy 82/182. Thus, the time required to grow this crack through the remaining overlay material should be greater than 40 years.

All results indicate that a circumferential crack in an untreated safety nozzle would not grow because of the compressive weld residual stresses in the structure. The FSWOL will prevent new cracks from forming, and will close existing cracks that are less than 60 percent through wall, and reduce the stress intensity factor for cracks that are deeper than this.

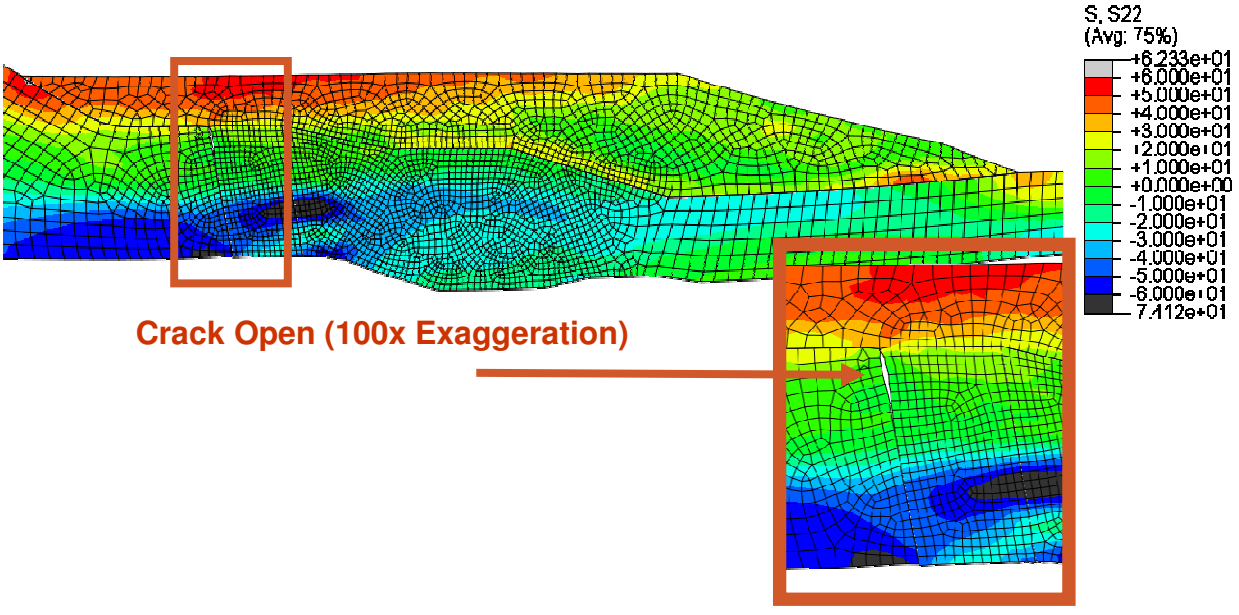

Figure 144 Safety Nozzle Axial Stresses after Crack2 is Introduced and Forced to Grow after Applying the FSWOL and the Operating Loads

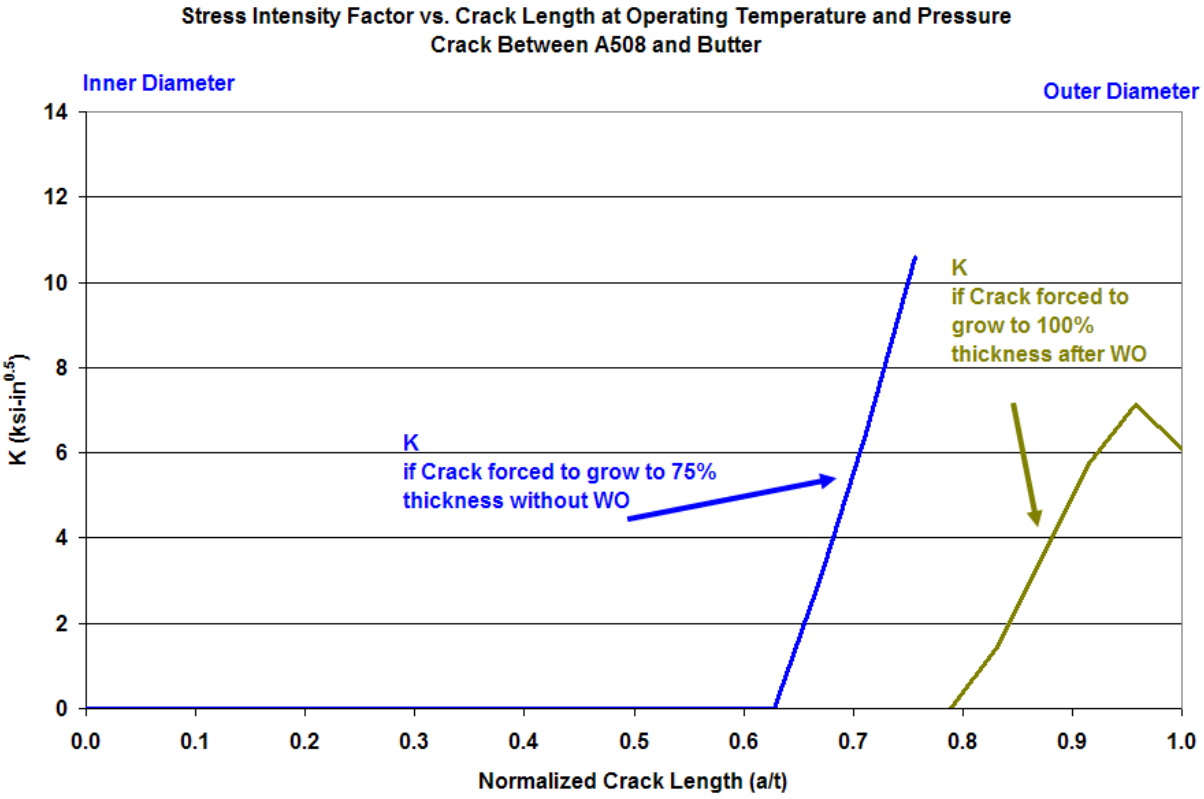

Figure 145 Safety Nozzle Crack2 Stress Intensity Factors for all Cases

5. DISCUSSION OF RESULTS

The scope and objective of this study was to investigate the effectiveness of weld overlays as a mitigation strategy for PWSCC in the PWRs. The primary focus was on the effectiveness of FSWOLs, although OWOLs were also evaluated. Of specific concern is the question as to whether the technical basis for weld overlays as a mitigation strategy for PWSCC is sufficient.

As part of this study 2-D, axi-symmetric weld residual stress analyses using the ABAQUS finite element code were conducted. In modeling the welds, the application of the butter to the ferritic material was modeled along with the post weld heat treatment (PWHT) of the butter material. In addition, the weld root passes at the inside surface were ground out and re-welded as part of the analyses to simulate this common practice in the field. This full-circumference grind out/re-welding resulted in a residual stress field similar to that for a full 360 degree inside surface repair weld. For the two cold leg geometries considered, more extensive repair welds, 25 and 50 percent of the wall thickness in depth were also considered.

Four dissimilar metal weld pipe/nozzle geometries were considered as part of this effort: (1) a large diameter cold leg/reactor pressure vessel nozzle weld, (2) a large diameter cold leg/reactor coolant pump outlet nozzle weld, (3) a medium diameter pressurizer surge nozzle weld, and (4) a small diameter pressurizer safety nozzle weld. In each case the weld residual stresses, both before and after the application of the weld overlay, were estimated in order to evaluate the effectiveness of the weld overlay as a mitigation strategy for PWSCC in PWRs. As part of these assessments, cracks were introduced into the weld butter region in order to determine how the weld overlay affects the crack opening displacements and stress intensity factors (K), and ultimately the crack growth of a crack in this region.

Both hoop and axial weld residual stresses were estimated. However, the primary focus was on the axial stresses which cause circumferential crack initiation and growth. The hoop stresses were thought to be of less concern since the axial cracks which are driven by the hoop stresses are thought to be limited in length to the width of the circumferential girth weld in seamless pipe typically used in nuclear power plants. Due to their limited length, any axial cracks should leak, and not rupture. Even so, the hoop stress results are of some interest, especially for the cold leg. For the cold leg/RPV nozzle weld (see Figure 49), the pre-FSWOL hoop stresses are tensile through the entire wall thickness. As a result, contrary to the axial stress results to be discussed next where there are significant areas of compression through the wall thickness, the hoop stress results, at least for the cold leg/RPV nozzle case, indicate that one might expect an axial crack to grow completely through the wall thickness. This finding is supported by field experience, e.g., the axial through wall crack growth at the hot leg/RPV nozzle DMW at V. C. Summer. (Note, the V. C. Summer cracking was probably further exacerbated by the extensive repairs at these welds.) From Figure 49 one also sees that the OWOL significantly reduced these hoop stresses for the cold leg/RPV nozzle weld by introducing a compressive residual stress field in the hoop direction for the inner 50 percent of the wall thickness. This OWOL-induced compressive stress field should help to mitigate the possibility of axial through-wall crack growth. For the surge nozzle and safety nozzle cases (Figure 25 and Figure 38, respectively), the pre-overlay hoop stresses are lower through the thickness (especially at the inside surface) such that one would not expect significant axial crack growth in these cases, either before or after the application of the weld overlay.

The axial weld residual stress results were plotted both through the thickness and along the length of the pipe (spanning the weld) on the inside surface. As can be seen in the plots of the stress along the inside surface, the high stress location at the inside surface tended to be in the buttered region along the butter/ferritic steel interface.

In examining the axial stress results for the four geometries considered, one sees a similarity in the results. One sees high tensile stresses at the inside surface of the weld which tend to be somewhat mitigated by the presence of the secondary stainless steel weld, for those cases where the secondary

stainless steel weld was close to the DMW. For example, in examining the surge nozzle axial stresses in Figure 23, the inside surface axial stresses near the butter/ferritic steel interface after fabricating the inconel dissimilar metal weld, which joins the ferritic nozzle to the stainless steel safe end, are approximately 550 MPa (80 ksi) tensile. Then, after fabricating the secondary stainless steel weld joining the stainless steel safe end to the stainless steel pipe, the axial stress at the inside surface at this location drops to 140 MPa (20 ksi) tensile. This is similar to the results for the pressurizer safety nozzle geometry, see Figure 36. Furthermore, the inside surface of the entire safe end for both the surge and spray nozzles are in compression after fabricating the secondary stainless steel weld. This is important for those cases where the safe end is fabricated from Alloy 600 material which is susceptible to PWSCC. Conversely, in examining Figure 57 for the cold leg/RCP outlet nozzle geometry, the secondary stainless steel weld, which was approximately 400 mm (16 inches) removed from the DMW, had almost no effect on the weld residual stresses at the DMW.

The FSWOL further reduces the weld residual stresses. Again for the surge nozzle (Figure 23), the FSWOL reduces the inside surface axial stresses near the butter/ferritic steel interface from 140 MPa (20 ksi) tension (post secondary stainless steel weld) to about 35 MPa (5 ksi) tension (after FSWOL). For the safety nozzle (see Figure 36), the FSWOL reduces the inside surface axial stresses in the buttered region from zero (pre-FSWOL) to 140 MPa (20 ksi) compression (post-FSWOL). For the cold leg/RPV nozzle weld (Figure 47) the effect was less. The OWOL only reduced the inside surface axial stresses at the butter/ferritic steel interface from 70 MPa (10 ksi) tension to 35 MPa (5 ksi) tension. For the cold leg/RCP outlet nozzle weld the effect of the weld overlay was more pronounced (Figure 57). The FSWOL lowered the inside surface axial stresses at the butter/ferritic steel interface from nearly 480 MPa (70 ksi) tension (post secondary stainless steel weld) to 200 MPa (30 ksi) tension (post FSWOL) while the OWOL reduced the stresses at this location to approximately 70 MPa (10 ksi) tension (post OWOL). These post overlay inside surface axial stresses along the length of the DMW were further reduced into compression with the application of the operating temperature and pressure, see Figure 62.

The results for the analyses where circumferential cracks were introduced were also consistent for the two geometries considered (surge and safety nozzle geometries). In each case the stress intensity factors (K) after applying the FSWOL were less than what they would have been if no FSWOL had been applied. Contrast this to what was found in the prior study on the MSIP, where the results demonstrate that if a deep crack (i.e., greater than approximately 60 percent of the wall thickness) existed in the weld prior to the application of the MSIP, the MSIP made matters worse. For the case of these deep pre-existing cracks, the MSIP increased the stress intensity factors (K), such that the time required for the crack to grow through the remaining wall thickness of the treated weld (post-MSIP) is very short (estimated to be on the order of a few years or less). Conversely, for the untreated case (no MSIP applied), the time required to grow these 75 percent deep cracks through the remaining wall thickness was estimated to be on the order of decades or longer.

This finding that the FSWOL improves the weld residual stress field for the case of very deep pre-existing cracks (> ~60 percent of the wall thickness) lends credence to the lack of a requirement for a pre-overlay through thickness examination using ultrasonics in the pertinent ASME Code Cases (N-504-4 and N-740-2). The only pre-overlay inspections required are surface examinations using liquid penetrant. (This is in contrast to inspection requirements for MSIP in Code Case N-770 which does stipulate a through-thickness examination prior to implementing a MSIP in almost all cases. Code Case N-770 does grant an exception to this pre-MSIP inspection for the cold leg/reactor pressure vessel welds.) The one concern with the lack of a requirement for a pre-overlay inspection is that pre-existing cracks may be more difficult to detect after the application of the overlay due to the fact that the compressive stresses caused by the overlay may force the crack faces to close upon themselves, therefore reducing their ultrasonic specular and tip responses, see Figure 125 for the surge nozzle and Figure 141 for the safety nozzle. This is a similar concern to that previously expressed for the MSIP. Prior NDE studies have shown that crack responses that were evident by ultrasonic testing prior to MSIP were significantly reduced, and in some

cases, not detectable, after MSIP. The question then becomes will the compressive stresses caused by the FSWOL affect the NDE response in the same manner. In the coming months a series of FSWOL/NDE mockup studies will be conducted during which this issue will be examined. One potential advantage that the FSWOL may have in this regard is that the post-overlay surface geometry may enhance the quality of the ultrasonic inspection post FSWOL.

In addition to possibly enhancing the quality of the ultrasonic inspection and improving the inside surface residual stress field, a FSWOL also adds an element of structural reinforcement to the DMW. Prior full-scale pipe experiments conducted at Battelle for the NRC for which through-wall cracked pipe sections were repaired with weld overlays clearly demonstrated this contention. In addition, the addition of the Alloy 52M material over top the DMW adds a layer of crack resistant material (i.e., resistant to PWSCC) to the pressure boundary.

A series of sensitivity analyses were conducted. As part of these analyses the effect of the FSWOL weld sequence (left to right versus right to left), the effect of the secondary stainless steel safe end weld, the effect of overlay thickness, and the effect of the ID repair depth were considered. The major findings from these sensitivity analyses were:

- The effect of weld sequencing, i.e., left-to-right versus right-to-left weld deposition had a minimal effect on the resultant weld residual stresses (Figure 69 and Figure 70). However, the resultant weld residual stresses for the case where two weld heads were used (Figure 73 and Figure 74) were higher than when a single head was used, as is typically the case.
- The secondary stainless steel weld had a significant effect on the axial weld residual stresses at the DMW. The secondary stainless steel weld tends to add an element of radial constraint to the adjacent dissimilar metal weld which reduces the axial stresses on the inside surface of the dissimilar metal weld. (Note, the hoop stresses remain tensile through much of the wall thickness, see Figure 25.) In fact, for the safety nozzle geometry considered, the FSWOL was found to be of limited benefit from a weld residual stress perspective since the presence of the secondary stainless steel weld for this small diameter safety nozzle geometry created a situation where the inside surface axial stresses were already compressive throughout the region of the dissimilar metal weld before the application of the FSWOL (see Figure 36). However, in those cases where there was no secondary stainless steel weld, such as the hot leg geometry at V. C. Summer, or where the secondary stainless steel weld was not in close proximity to the DMW, such as the cold leg/RCP outlet nozzle weld evaluated herein, the sensitivity analyses conducted as part of this effort indicated that the FSWOL would cause the DMW residual stresses to be as compressive as were the post-FSWOL stresses for those cases where there was a secondary stainless steel weld in close proximity to the DMW. As such, while the FSWOL is still effective, it is of most benefit in those cases where no secondary weld existed (e.g., for the V. C. Summer hot leg geometry) in that the pre-FSWOL stress state was already lower, i.e., compressive or less tensile, for the case where there is a secondary stainless steel weld in close proximity.
- In looking at the results for the repair size sensitivity analyses, it was found that peak stresses were comparable for each of the repair sizes considered, i.e., 0, 25, and 50 percent of the wall thickness. However, the extent of the affected area was much more pronounced for the deeper repairs. For the deeper repairs, the axial extent of the tensile stresses along the ID surface (Figure 106) and the through thickness extent of those stresses (remain tensile for more of the wall thickness, see Figure 107) were both much more pronounced.
- The effect of overlay thickness was also considered. For the surge nozzle geometry considered the number of weld overlay passes had a minimal effect on the through thickness axial stresses near the weld centerline, see Figure 77. There was some effect on the ID axial stresses at the butter/ferritic steel interface, i.e., more layers of weld overlay resulted in a greater reduction in stress, see Figure 78, but that effect tended to saturate after about 3 layers of overlay. For the hoop stress case, Figure 80 and Figure 81, the effect was more pronounced with each successive

layer further reducing the stresses. For the cold leg/RPV nozzle, there was a similar effect as found for the surge nozzle in that both the ID stress along the length of the nozzle as well as the through-thickness stresses near the weld centerline tended to reach a point of saturation, where further layers of overlay resulted in a minimal change in stress, after about half the layers of the FSWOL were deposited, see Figure 91and Figure 92. For the cold leg/RCP outlet nozzle geometry, this saturation effect was even more pronounced. For this geometry the OWOL induced axial stresses were even more compressive in the vicinity of the DMW than they were for the FSWOL case, see Figure 95.

6. CONCLUSIONS

In conclusion, based upon the evaluations conducted, the FSWOL appears to be an effective method to reduce inside surface weld residual tension stresses which can lead to PWSCC in dissimilar metal welds in PWR piping systems. The process was found to be most beneficial for the larger diameter cold leg/RCP outlet nozzle geometry considered where there was no pre-existing benefit from the secondary stainless steel safe end weld. Also, the process was found to be more beneficial for the intermediate diameter pressurizer surge line nozzle than the smaller diameter safety nozzle geometry considered. For the safety nozzle geometry considered, the FSWOL was found to be of limited benefit from a weld residual stress perspective since the presence of the secondary stainless steel weld for the small diameter safety nozzle geometry created a situation where the inside surface axial stresses were already compressive throughout the region of the dissimilar metal weld before the application of the FSWOL. Note, even though the weld overlay provided limited benefit to this safety nozzle geometry from a stress reduction perspective, it was still beneficial since it adds additional structural reinforcement and additional layers of crack resistant material (Alloy 52M) over top the DMW. In addition, it was found that if a deep crack were present prior to the application of the FSWOL, the overlay would act to lower the stress intensity factor of that crack, thus increasing the time required for that crack to potentially grow through the remaining wall thickness. This was contrary to what was found during the MSIP study previously conducted.

It is important to note that changes in weld sequencing in the field from that which was analyzed can negate any claimed weld residual stress benefit predicted for the weld overlay. Several sensitivity studies were conducted to evaluate the effect of weld overlay weld sequencing on the resulting weld residual stress field. Some sequence changes evaluated created large changes in the resulting weld residual stress field. In designing a full structural weld overlay or an optimized weld overlay for a certain geometry it is crucial that the design that is evaluated and approved is the design that is actually created in the field.

Finally, the results for the geometries considered herein tend to indicate that the OWOL design can be an effective mitigation strategy for dealing with PWSCC in PWRs. For the cases considered herein, i.e., the cold leg/RCP outlet nozzle geometry, the stresses post-OWOL application were at, or in some cases, below those for the post-FSWOL application, see Figure 95 and Figure 96. Note, it must be emphasized that this conclusion is based solely on our assessment of this one geometry, i.e., the cold leg/RCP outlet nozzle geometry considered herein. If other licensees chose to apply optimized weld overlays to other geometries, additional confirmatory analyses will be needed to assess the effectiveness of the OWOL design for those applications.

7. REFERENCES

[1] Fredette, Lee, Scott, Paul, "Evaluation of the Mechanical Stress Improvement Process (MSIP) as a Midigation Strategy for Primary Water Stress Corrosion Cracking in Pressurized Water Reactors," US Nuclear Regulatory Commission Report, ML092990646, September, 2009.

[2] King, C., Frederick, G., 2005, "Non-Proprietary Version, Materials Reliability Program: Technical Basis for Preemptive Weld Overlays for Alloy 82/182 Butt Welds in PWRs (MRP-169)," EPRI Report Number 1012843, Electric Power Research Institute, Palo Alto, CA.

[3] Childs, W., J., 1991, "Justification for Extended Weld-Overlay Design Life (NP-7109-D)," EPRI Research Project T303-1, Electric Power Research Institute, Palo Alto, CA.

[4] Scott, P., M., 1987, "Assessment of Design Basis for Load-Carrying Capacity of Weld-Overlay Repairs," NUREG/CR-4877, Battelle Report Number 2150, Division of Engineering Safety, Office of Nuclear Reactor Regulation, U.S. Nuclear Regulatory Commission, Washington D.C.

[5] ASME Code Case N-504-4, Alternative Rules for Repair of Classes 1, 2, and 3 Austenitic Stainless Steel Piping, Section XI, Division I, July 2006.

[6] ASME Code Case N-754, Optimized Structural Dissimilar Metal Weld Overlay for Mitigation of Class 1, 2, and 3 Items, Section XI, Division I, January 2009.

[7] ABAQUS, V6.7-1, 2007, Dassault Systèmes, Providence, RI.

[8] Barber, T. E., Brust, F. W., Mishler, H. w., 1981, "Controlling Residual Stresses by Heat Sink Welding," EPRI Report Number NP-2159-LD, Electric Power Research Institute, Palo Alto, CA.

[9] "Crystal River, Unit 3, Relief Request #08-001-RR, Revision 1, 60-Day Response, Summary of Analysis Calculations," NRC ADAMS Accession Number ML081410058, NRC.gov, May 15, 2008.

[10] Anderson, T. L., 2005, Fracture Mechanics, Fundamentals and Applications, 3rd Edition, CRC Press, Boca Raton, Florida, pg 43.

[11] Krueger, Ronald, 2002, "The Virtual Crack Closure Technique: History, Approach and Application," NASA/ CR-2002-211628, NASA Langley Research Center, Hampton, Virginia.

[12] Rybicki, E. F., and Kanninen, M. F., 1977, "A finite element calculation of stress intensity factors by a modified crack closure integral," Engineering Fracture Mechanics, ***9****(4), pp 931-938.*

[13] Zhang, J., Dong, P., Brust, F.W., Shack, W. J., Mayfield, M., McNeil, M., 2000, "Modeling of Weld Residual Stresses in Core Shroud Structures", International Journal for Nuclear Engineering and Design, 195, pp. 171-187

[14] King, C., 2005 "Non-Proprietary Version, Materials Reliability Program: Primary System Piping Butt Weld Inspection and Evaluation Guideline (MRP-139NP)," EPRI Report Number 1010087, Electric Power Research Institute, Palo Alto, CA.

[15] Miteva R., Taylor, N.G., 2006, " General Review of Dissimilar Metal Welds in Piping Systems of Pressurized Water Reactors, Including WWER Designs," EUR 22469 EN, European Commission Joint Research Centre Network for Evaluating Structural Components, Luxembourg, Netherlands.